PREPARATION, PROPERTIES AND PHOTOCATALYTIC ACTIVITY OF SOME DOPED AND UNDOPED METAL OXIDE NANOMATERIALS

THESIS

SUBMITTED TO

BABASAHEB BHIMRAO AMBEDKAR UNIVERSITY
(A CENTRAL UNIVERSITY)
LUCKNOW

BABASAHEB BHIMRAO AMBEDKAR UNIVERSITY
LUCKNOW
प्रज्ञा शील करुणा
ESTABLISHED 1996

FOR THE DEGREE OF

Doctor of Philosophy

IN

APPLIED CHEMISTRY

Submitted by

Azad Kumar

(M.Sc., M.Phil., CSIR-NET)
Enrollment No. 916/13

Under the Supervision of

Prof. Gajanan Pandey

DEPARTMENT OF APPLIED CHEMISTRY
SCHOOL FOR PHYSICAL SCIENCES
BABASAHEB BHIMRAO AMBEDKAR UNIVERSITY
VIDYA VIHAR, RAE BARELI ROAD, LUCKNOW-226 025

2018

DECLARATION

I hereby declare that the thesis entitled **"PREPARATION, PROPERTIES AND PHOTOCATALYTIC ACTIVITY OF SOME DOPED AND UNDOPED METAL OXIDE NANOMATERIALS"** has been prepared by me under the supervision of Prof. Gajanan Pandey, Department of Applied Chemistry, School for Physical Sciences, Babasaheb Bhimrao Ambedkar University, Lucknow. No part of this thesis has formed the basis for the award of any degree, diploma or fellowship previously. Further, I declare that the material embodied in the present work is based on original research work and the indebtedness to others has been duly acknowledged at relevant places.

Azad Kumar

Azad Kumar
Department of Applied Chemistry,
School for Physical Sciences,
Babasaheb Bhimrao Ambedkar University,
Vidya Vihar, Raebarelli Road, Lucknow-226
025 Date: 23 February 2018
Place: Lucknow

CERTIFICATE

This is to certify that the thesis entitled **"PREPARATION, PROPERTIES AND PHOTOCATALYTIC ACTIVITY OF SOME DOPED AND UNDOPED METAL OXIDE NANOMATERIALS"** submitted by **Azad Kumar, M.Sc., M.Phil. (CSIR-NET)** is an original research work and has not been previously submitted in part or full for the award of any other degree or diploma to this or any other university.

The thesis submitted to the Babasaheb Bhimrao Ambedkar University, Lucknow, India satisfies all the requirements as stipulated in the **Doctor of Philosophy (Ph.D.)** regulations-1999 as amended in 2018/2010/2013 and it is fit for submission and evaluation for the award of Doctor of Philosophy of the University.

Date: 22/02/2018

Supervisor

Head of the Department

23.2.18

PREFACE

Photocatalysed processes have grown in importance mainly due to their widespread applications in energy conversion, pollution abatement and the synthesis of new materials. Researchers are using photocatalysts for oxidative degradation of various non-biodegradable wastes. Fundamentally, photocatalysis deals with reactions which are initiated by electronically excited molecules generated by absorption of suitable radiation in the visible or near ultraviolet region. One of the most widely investigated and convenient class of photocatalysts is of metal oxide semiconductors. Thus, in practical terms chemical reactions occurring in presence of semiconducting materials and light are known as photocatalytic reactions. Semiconductors, with suitable band gaps, can act as quantum collectors of light energy. Illuminating a semiconductor material with photons of desired energy (i.e. $h\nu \geq$ the band gap of semiconductor) can cause a number of photocatalytic reactions.

Titanium dioxide (TiO_2), commonly known as Titania, is one of the most commonly used photocatalysts. Because of its high oxidative power, stability, and non-toxicity, it promises a broad range of uses as a photocatalysts. Advantage of using TiO_2 as photo-catalyst are: (a) using TiO_2, the process occurs under ambient conditions.(b) using TiO_2, the oxidation of the substrate to CO_2 is complete in most cases and (c) it is comparatively inexpensive and remains quite stable in contact with different substrate.

The major source of environmental pollution is the wastewater effluent of textile industries. The textile industries are using the very large amount of chemically stable dyes which are causing water pollution. Several investigations reported that about 12% of dyes used in textile industries in each year. During the manufacturing and processing 20% dyes are lost in environment such as Rose Bengal, Caramine, Rhodamine, Indigo Red, Thymol blue, Red 120, Eriochrome Black-T (EBT), Methylene Blue [2, 3]. Textile industries effluents contain colored pigments which is causing carcinogenic effect on human being and also causing serious impact on aquatic life.

The treatment of such pollutants can be achieved by heterogeneous photocatalysis due to its efficiency and low cost as well as to the fact that it allows complete degradation of pollutants to carbon dioxide and inorganic acids.

Titanium dioxide TiO_2 is a most important nanomaterials which has attracted a great attention due to its unique properties. Titanium dioxide TiO_2 have excellent merits in solar energy transferring and photocatalysis of poison compounds in environment. The chemical inertness and the non-toxicity of TiO_2 have also made it a superior photocatalyst. Titania has a large band gap (3.20 ev for anatase TiO_2) and therefore, only a small fraction of solar light can be absorbed. Many attempts have been made to sensitize titanium dioxide to the whole visible region, such as doping with transition metals, transition metal ions, non-metal atoms and organic materials. Introduction of dopant allows Titania to absorb in the visible region but this does not necessarily mean that the doped catalyst has a better photocatalytic activity.

ACKNOWLEDGEMENT

I am highly indebted and wish to express my deep sense of gratitude to my supervisor, **Prof. Gajanan Pandey**, for instilling in me the thrill of research and intricacies of Chemistry by his constant involvement at every stage of my work. He has motivated and provided me his valuable technical expertise, guidance and incessant inspiration to sustain the tempo of my work. I do not hesitate to state that without his help it would not have been possible for me to complete the research work.

I express my deepest sense of respect and regard to **Prof. Kaman Singh** (Dean of SPS) Applied Chemistry, School of Physical Sciences, BBAU Lucknow, for his invaluable support and encouragement and other faculty members **Dr. Jyoti Pandey, Dr. Shailesh Kumar, Dr. Preeti Gupta, Dr. Jawaharlal** and **Dr. Alok Singh.**

I am also thankful to all guest faculty of department of applied chemistry, **Sanjay Gautam, Saurabh Yadav, Pushyamitra Mishra, Manisha Gautam, Dr. Hardesh Maurya** and **Reena Singh** for their timely help and encouragement.

I am also thankful to all colleagues **Abhishek Verma** for their timely help and encouragement. I am also thankful to all research scholars **Ajay Kumar, Gaurav Hitkari, Sandhya Singh, Ravindra Kumar, Dr. Rakesh Sonker, Ashok Kumar, Sumit Kumar, Gulam Abbas** for providing moral support, encouragement, and consultation during the research work.

It is my immense pleasure to thank my dearest friend **Sudhakar Pushkar, Manoj Kumar, Deepak Kumar** and **Vinit Raj** for his help, support and valuable suggestion throughout my Ph.D. duration.

I am extremely grateful to University Instrumentation center office staff specially **Mukesh Kumar** USIC, BBAU, Lucknow for providing EDX, SEM and FTIR facility.

I am thankful to **Prof. R.A. Singh** (Head) Department of Chemistry, Banaras Hindu University, Varanasi granting me the permission and needed assistance for experimental tryout and sample analysis.

I also express my thanks to **Vivek Kumar Singh** for supporting me in conducting the experiment.

I express my sincere thanks and grateful to **Pradeep Singh**, IIT BHU provides facility to photodegradation and characterization of the samples.

I am also thankfully to **Pankaj Kumar**, IIT Roorki provides facility to characterizes the my samples

Thanks are due to the supporting staff of Department of Applied Chemistry especially **Sarvesh Gupta, Pankaj Singh, Anuj Kumar Saini, Santosh Mishra** and **Om Awasthi** for all the assistance provided by them during the entire research work.

I find no way to express in word my deep gratitude and profound reverence to my Parents, **Mr. Dhani Ram** and **Mrs. Kamla Devi** and all my relatives. This undertaking would not have even been contemplated, let alone be completed, without their prayers, their blessings, their encouragement and the confidence they have showed in me. I recollect all the moments, they have shared with me all these years and waited patiently to see my research this destination in life.

It is my immense pleasure to thank my dearest wife **Mrs. Varsha Kabir** for his help, support and valuable suggestion throughout my Ph.D. duration.

Person who needs special mention here are my brothers **Trimohan Singh, Mukesh Kumar, Jayantesh Kumar** and my sister **Anjali Kumari.** They have boosted my moral at critical moments during this study. Their forbearance and loving care facilitated the completion of my research work. All the credit goes to them for what I am today and I am indebted to them.

Azad Kumar


Dedicated to
My
Parents

Abstract

Titanium dioxide (TiO_2), commonly known as Titania, is one of the most commonly used photocatalysts. Because of its high oxidative power, stability, and non-toxicity, it promises a broad range of uses as a photocatalysts. Advantages of using TiO2 as photo-catalyst are:

(a) Using TiO_2, the process occurs under ambient conditions.

(b) Using TiO_2, the oxidation of the substrate to CO_2 is complete in most cases and

(c) It is comparatively inexpensive and remains quite stable in contact with different substrate.

TiO_2 has also played a leading role in the active research for the utilization of solar energy. The TiO_2 based, dye sensitized, photo-electrochemical cells are receiving a great deal of attention as a possible candidate for converting solar energy into electricity on a large scale. Titanium dioxide's photocatalytic characteristics are greatly enhanced due to the advent of nanotechnology. At nano-scale, not only the surface area of titanium dioxide particle increases dramatically but also it exhibits other effects on optical properties and size quantization. An increased rate in photocatalytic reaction is observed as the redox potential increases and the size decreases. In some cases energy from any ambient light source can be used effectively as the energy source of photo catalysis instead of UV light.

Photo catalyst of solarcoat not only have all the advantages of the traditional photocatalyst, but also can disinfect, purify air and eliminate harmful substance in the condition of visible light . Therefore, it has incomparable technology and quality advantages of fighting against pollution indoors and outdoors. The strong functions of solar coat photocatalysis will completely eliminate odours of newly-decorated houses and enable people to get rid of the danger caused by epidemic disease. Solar coat of photocatalyst has been widely applied in all kinds of fields and highly affirmed & appraised. The theory of photocatalyst: with the irradiation of light, the TiO_2 on the surface of the ultra strong photocatalyst of solarcoat will take photocatalytic reaction the same as photosynthesis which can produce free radical and ozone with strong function of oxidization. And it can oxidize and decompose various organic compounds and some minerals.

A detailed study of the synthesis, characterization and photocatalytic activity of titania based nanocomposites have been carried out and presented in the thesis. The organization of whole thesis is given below:

Chapter 1: Introduction and Literature Review

Chapter 2: Photocatalytic degradation of Eriochrome Black-T by the Ni:TiO_2 Nanocomposites

Chapter 3: Photocatalytic Activity of Co:TiO_2 Nanocomposites and their Application in Photodegradation of Acetic Acid

Chapter 4: The photocatalytic degradation of Methyl Green in presence of Visible light using $Ni_{0.10}$:$La_{0.05}$:TiO_2 nanocomposites as catalyst.

Chapter 5: Photocatalytic degradation of Rose Bengal and Thymol Blue dye under visible light by TiO_2/PAni/GO nanocomposites

Chapter 6: Photocatalytic degradation of Victoria Blue and Rose Bengal dye in visible light by prepared TiO_2/PPy/GO nanocomposite.

Chapter 7: Preparation and Photocatalytic activity of Co:La:TiO_2 nanocomposites for the degradation of Methyl Blue in Visible light

Chapter 8: Conclusion and Scope of Further Research Work

The study will broadly follow the scheme as given above. The summary of research work carried out is as follows:

In the first chapter, general introduction about the subject, historical background, theories, applications, literature review and objectives of the present study has been presented.

In the second chapter, TiO_2 and Ni:TiO_2 nanoparticles (NPs) were prepared and their photocatalytic activity was measured against Eriochrome Black T (EBT). The Photo-degradation of Eriochrome Black T was investigated at different condition of concentration and pH in presence of TiO_2 and Ni:TiO_2. The prepared nanoparticles of photocatalyst are characterized by XRD, SEM, EDX, UV-Vis and BET. The photocatalyst activity was measured by varying pH and concentration of dye solution. Kinetics study of photodegradation was found first order kinetics. The photocatalytic activity of Titania has been enhanced by the doping of Ni.

In the third chapter, TiO_2 and Co-TiO_2 nanoparticles (NPs) were prepared and their photocatalytic activity was measured against Acetic Acid.The prepared material was subjected to XRD analysis which gives the rutile and Anatase both phases were present in the prepared sample. It is found that, in samples sintered at 400 ^{0}C both Anatase and rutile phases were presented and rutile phase was more dominant, while in samples without sintered the exclusive formation of polycrystalline Anatase and rutile phase separately was occurred. Applying the Scherrer's calculations through which particle size was found 35 and 80 nm in case of Cobalt titania and pure titania respectively. The prepared sample of titania and Cobalt titania were subjected to photocatalytic degradation of acetic acid was done. The degradation of acetic acid occurs efficiently. The prominent degradation was found in case of Acetic acid in the presence of nanocomposites Co-TiO_2.

In the fourth chapter, the photodegradation of Methyl green dye has been done in presence of prepared $Ni_{0.10}$:$La_{0.05}$:TiO_2 nanocomposites. The nanocomposites of $Ni_{0.10}$:$La_{0.05}$:TiO_2 was prepared by the solution impregnation method. The characterization of Synthesized TiO_2 and $Ni_{0.10}$:$La_{0.05}$:TiO_2 nanocomposites were done by X-Ray Diffractometer, SEM, TEM, UV- Vis, FT-IR, Band gap energy and BET. The photocatalytic degradation of Methyl Green has been done in presence of TiO_2 and $Ni_{0.10}$:$La_{0.05}$:TiO_2 nanocomposites. The presence of anatase and rutile phase in the nanocomposites has been confirmed by XRD analysis. The photocatalysts particle was found in nanodiamension in morphology. The surface area was observed 34.72 and 96.58 m^2/g for the TiO_2 and $Ni_{0.10}$:$La_{0.05}$:TiO_2 nanocomposites. The band gap energy was observed 3.2 and 3.0 eV for the TiO_2 and $Ni_{0.10}$:$La_{0.05}$:TiO_2 nanocomposites. The photocatalytic degradation behaviour of photocatalysts was investigated by considering different parameters such as effect of concentration, effect of amount of photocatalyst, effect of pH, effect of temperature, adsorption and kinetics. The 90-98 % photodegradation of Methyl Green has been found at 7 pH, 25 ppm concentration of dye, 800 mg/L amount of photocatalyst and 50 min illumination of visible light in presence of $Ni_{0.10}$:$La_{0.05}$:TiO_2 while 10-18 % in presence of neat TiO_2 . The photodegradation of Methyl Green was following the first order kinetics.

In the fifth chapter, Nanocomposites of TiO_2, TiO_2/PAni and TiO_2/PAni/GO were prepared by in situ oxidation polymerization method. The prepared TiO_2, TiO_2/PAni and

TiO_2/PAni/GO Nanocomposites were characterized by the XRD, SEM, TEM, BET, UV-Vis, FTIR, Band gap energy and Photolumiscence. The XRD confirmed the presence of Anatase and rutile phase in the prepared photocatalysts. The average particle size was found 68, 15 and 12 nm for TiO_2, TiO_2/PAni and TiO_2/PAni/GO respectively. The SEM and TEM images also confirmed the formation of nanocomposites in the range of ~ 100 nm. The surface area 37.52, 76.68 and 96.24 m^2/g were observed for TiO_2, TiO_2/PAni and TiO_2/PAni/GO Nanocomposites respectively. The Band gap energy of TiO_2, TiO_2/PAni and TiO_2/PAni/GO were calculated by talc plot and obtained 3.0, 2.86 and 1.76 eV respectively. The Photocatalytic degradation of Rose Bengal dye was done at different condition viz concentration of dye, time of illumination, pH and dose of photocatalyst. The maximum photodegradation were found at neutral pH, 6.25 ppm concentration of dye solution, 800 mg/L amount of photocatalyst and 120 min irradiation of visible light. Kinetics of photodegradation was investigated for Rose Bengal dye and found first order kinetics. The coating of PAni and GO were enhanced the photocatalytic activity of Titania. Hence TiO_2/PAni and TiO_2/PAni/GO are the efficient photocatalyst for the degradation of Rose Bengal B dye than pure TiO_2.

In the sixth chapter, describes a proficient method for synthesis of TiO_2/PPy and TiO_2/PPy/GO nanocomposites. These nanocomposites were prepared by one-step *in situ* deposition oxidative polymerization of pyrrole hydrochloride using Ammonium per sulphate (APS) as an oxidant in the presence of ultra fine grade powder of TiO_2 nanoparticles cooled in an ice bath. The obtained nanocomposites were characterized by XRD, TEM, SEM, UV-Vis, FTIR, techniques. The obtained results showed that TiO_2 nanoparticles have been encapsulated by PPy with a strong effect on the morphology of TiO_2/PPy and TiO_2/PPy/GO nanocomposites. The Photocatalytic degradation of Rose Bengal and Victoria blue dye was done at different condition viz concentration of dye, time of illumination, pH and dose of photocatalyst. The maximum photodegradation were found at 7 pH, 20 ppm concentration of Victoria blue and 25 ppm of Rose Bengal dye solution, 800 mg/L for VB and 1600 mg/L for RB amount of photocatalyst and 120 min irradiation of visible light. Kinetics of photodegradation was investigated for Victoria blue and Rose Bengal dye and found first order kinetics. The coating of PPy and GO were enhanced the photocatalytic activity of Titania. Hence

TiO_2/PPy and TiO_2/PPy/GO are the efficient photocatalyst for the degradation of Rose Bengal and Victoria Blue dye than pure TiO_2.

In the seventh chapter, prepared the nanocomposites of Co:La:TiO_2 by the wet chemical method. Synthesized TiO_2 and Co:La:TiO_2 were characterized by X-Ray Diffractometer, SEM,TEM, UV- vis, FT-IR, Band gap energy and BET. The TiO_2 and Co:La:TiO_2 were used as photocatalyst for the degradation of Methyl Blue. The XRD pattern confirmed the presence of anatase and rutile phase in the catalyst. The particle size was estimated by the Scherrer's and found 68 and 32 nm for TiO_2 and Co:La:TiO_2 respectively. The particle morphology of the photocatalysts was found in nanodiamension. The surface area of the photocatalysts were found 37.52 and 106.68 m^2/g for TiO_2 and Co:La.TiO_2 respectively . The band gap energy of TiO_2 and Co:La.TiO_2 were 3.2 and 3.0 eV. The FT-IR spectra of Co:La:TiO_2 were recorded and found Co bonded with Titania. The photodegradation of Methyl Blue has been found maximum at 5 pH, 25 ppm concentration of dye, 800 mg/L amount of photocatalyst and 180 min illumination of visible light. The photodegradation was following the first order kinetics.

In the eighth chapter, conclusion and some important results of all chapters have been discussed and also describe the future trends.

TABLE OF CONTENTS

CHAPTER-1

Introduction and Literature review

Titanium dioxide (TiO_2), commonly known as Titania, is one of the most commonly used photocatalysts. Because of its high oxidative power, stability, and non-toxicity, it promises a broad range of uses as a photocatalysts. Advantage of using TiO_2 as photo-catalyst are: (a) using TiO_2, the process occurs under ambient conditions.(b) using TiO_2, the oxidation of the substrate to CO_2 is complete in most cases and (c) it is comparatively inexpensive and remains quite stable in contact with different substrate. TiO_2 has also played a leading role in the active research for the utilization of solar energy. The TiO_2 based, dye sensitized, photo-electrochemical cells are receiving a great deal of attention as a possible candidate for converting solar energy into electricity on a large scale.

1.1. Nanotechnology

Nanotechnology is the novel science and art of manipulating matter at the atomic or molecular scale. More important, it is about the structure and the ability of molecular compounds to work. The nanomaterials research is needed to extend manufacturing techniques. It is a synergy approach of top-down with bottom-up processes [1-2].

When matter is as small as 1 to 100 nanometres, many of its characteristics will easily change and have many unique characteristics both different from macro-matters and single atoms due to the quanta effect, regional confinement of matter, and huge surface or interface effects [3]. The main objective of nanotechnology is to manufacture products of special functions with new physical and chemical properties by making atoms, molecules, and matters presenting their features directly in the length of a nanometer.

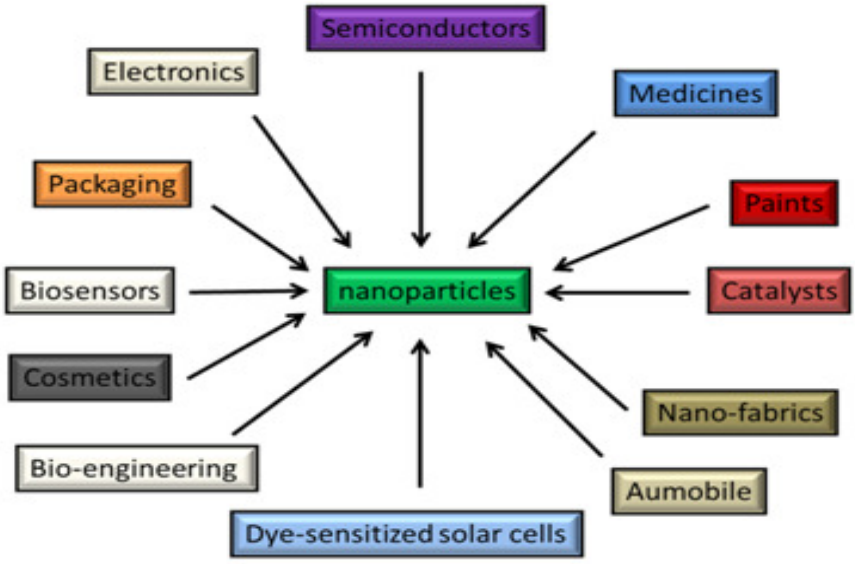

Fig.1.1. Uses of the nanoparticles

In the recent years, a new branch of research has arisen, broadly called to as "nanoscale science and technology" [4-5]. Usually, nanotechnology can be understood as a technology of design, fabrication, and applications of nanostructures and nanomaterials, as well as a fundamental understanding of physical properties and

phenomena of nanomaterials and nanostructures. Nanomaterials, compared to bulk materials, have the scales ranging from individual atoms or molecules to submicron dimensions at least in one dimension.

Nanomaterials and nanotechnology have found very important applications in physical, chemical and biological systems [6-7]. Lots of inventions and discoveries has been done during last few decade for the fabrication of nano-objects. For the development of new nanostructured materials, process and phenomena at the nanoscale, as well as the development of new experimental and theoretical techniques for research providing the lot of opportunities. Nano materials can be made up with unique nanostructures and properties [8-9].

The ability of scientists to manipulate matter virtually atom by atom has been supported by the development of new instruments and approaches that allow the investigation of material properties Nanotechnology with a resolution close to the atomic level. Such new tools have allowed the extensive understanding of the unusual physical and chemical properties characterizing matter at the nanometer scale opening up the way to the use of nanomaterials in a wide variety of applications involving material science, engineering, physics, chemistry and biology [10-11].

Nanoscale semiconductor materials typically show behaviour which is intermediate between that of a macroscopic solid and that of an atomic or molecular system. Consider, for instance, the case of an inorganic crystal composed of very few atoms. By simple intuitive reasoning, it can be perceived that its properties will not be the same as those of a single atom, while also being different from those of a bulk solid [12].

In order to rationalize (and predict) the physical properties of nanoscale materials, such as their electrical and thermal conductivities, or their absorption and emission spectra, their energy level structure needs first to be determined. Many properties specific to nanosized materials are related to the type of motion the charge carriers (electrons and holes) are allowed to execute when they are forced to dwell in confined structures. The unusual characteristics of these systems can only be explained by the laws of quantum mechanics [13], the behaviour of the particles inside them

being obtainable by solving the related Schrödinger equation. For low-dimensional systems, the calculation of the energy structure is traditionally carried out using two main approaches. An approach, which is more elaborate but also more powerful to derive a detailed description of the electronic band Nanotechnology structure in a low-dimensional solid, represents the general physics of a solid when its dimensions shrink one by one down to a few nanometres. The behaviour of carriers in a bulk solid can be described satisfactorily by the model of the "free-electron gas" [14]. The electrons are considered to be delocalized in the solid and thus not bound to individual atoms. Another assumption is made, that the interactions between the electrons and the crystal potential can be neglected at a first approximation. Whenever the size of the solid becomes comparable to the De Broglie wavelength associated with the particles that interact with it, a free carrier confined in this structure will behave as a particle in a potential box. The solutions of the Schrödinger equation are standing waves confined in the potential well, and the energies associated with two distinct wave functions are, in general, different and discontinuous. The particle energies cannot take on any arbitrary value and the system exhibits a discrete energy level spectrum [15-16]. Regarding the forms of materials, nanomaterials are classified as zero-, one-, and two-dimensional nanostructures. Zero-dimensional nanostructures, also named as nanoparticles, include single crystal, polycrystalline and amorphous particles with all possible morphologies, such as spheres, cubes and platelets [17].

In general, the characteristic dimension of the particles is one hundred nanometres or less. They can be named as zero-dimensional nanostructures. If the nanoparticles are single crystallite, they are often referred to as nanocrystals. When the characteristic dimension Nanotechnology 12 of the nanoparticles is small enough and quantum effects are observed, quantum dots are the common term used to describe such nanoparticles. One-dimensional (1D) nanostructures include whiskers, fibres or fibrils, nanowires, and nanorods. In many cases, nanotubules and nanocables are also considered one-dimensional structures. Although whiskers and nanorods are in general considered to have smaller length to thickness ratio (aspect ratio) than fibres and nanowires, the definition is a little arbitrary. Therefore, for clarity, nanostructures with

large aspect ratio are addressed as "nanofibres", albeit they have been termed whisker, rod, fibre, or wire elsewhere. Thin films are two-dimensional nanostructures, which have been a subject of intensive study for almost a century, and for which many methods have been developed and improved [18-19].

1.2. Novel photocatalyst

Photocatalysts play an important role for the photodegradation of harmful organic compounds in the atmospheric air, such as formaldehyde, chlorinated hydrocarbons, dioxins, dyes, acids, pesticides and the like, or harmful organic materials present in daily life water, various types of household effluents and industrial effluents to clean the environment. Titanium dioxide is widely used as this photocatalyst in respect of the most stable one with almost no toxicity against living organisms. When this titanium dioxide is exposed to near UV radiation around 380 nm, an electron in the filled band is excited to the conduction band to cause charge separation. The resultant charge site serves as a source to generate a hydroxyl radical or a superoxide anion which decomposes environmental pollutants, such as organic halides and nitrogen oxides, by its strong oxidizing action [20].

However, titanium dioxide is photocatalytically active only in a wavelength range around 380 nm, and not photocatalytically active in other wavelength ranges, and therefore naturally subject to a limited range of applications. For that purpose, photocatalysts have been proposed, such as a composite of titanium dioxide and an inorganic porous material, e.g., activated carbon, high-silica zeolite, silica gel, sepiolite, bentonite, magnesium sulfate and others; a visible light-sensitive photocatalyst comprising a titanium dioxide film having a very thin layer of N-doped TiO_2 formed on the surface layer; a photocatalytic composition comprising a visible light-sensitive photocatalyst and a photocatalyst having a specific surface area larger than the said visible light-sensitive photocatalyst and the like [21]. Furthermore, alternative photocatalysts free of titanium dioxide have been proposed, such as a composite photocatalyst for hydrogen generation comprising cadmium sulfide and a sulfide of a different metal. A semiconductor photocatalyst having semiconductor

particles encapsulated with a polymer a photocatalyst comprising layered composite metal oxide including interlayer cadmium sulfide and the like. However, none of the photocatalysts can provide so high a conversion rate as to be feasible [22].

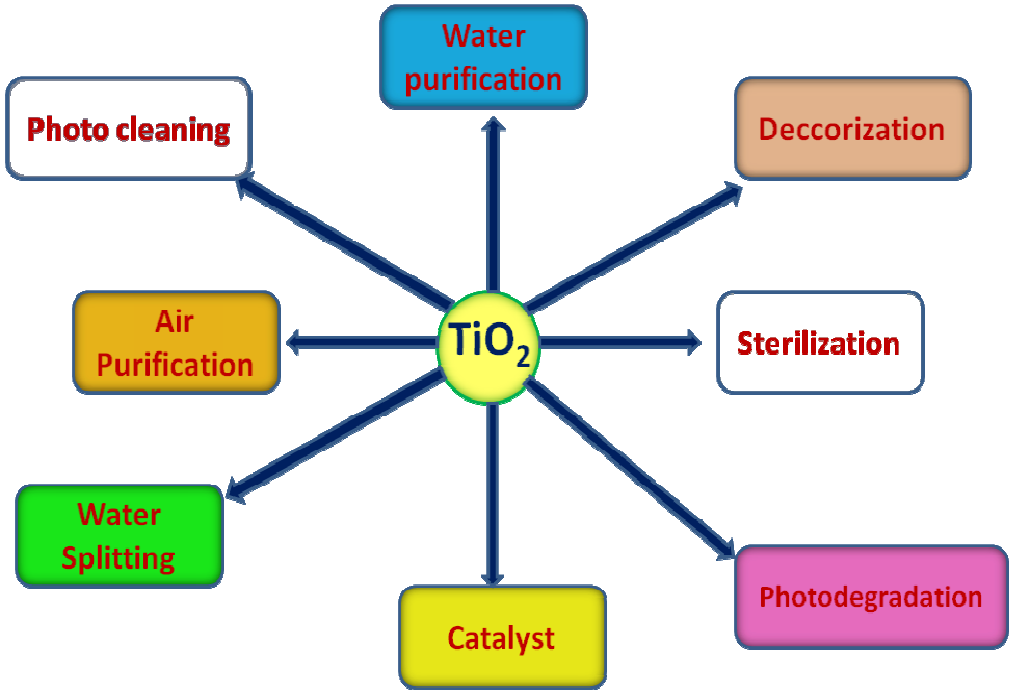

Fig.1.2. Uses of Titania

1.3. Discovery of photocatalysis

Akira Fujishima (1972) discovered the photocatalytic properties of titanium dioxide the process on the surface of the titanium dioxide were called the Honda-Fujishima effect [23].

Titanium dioxide has potential for use in energy production: as a photocatalyst:

It can carry out hydrolysis; i.e., break water into hydrogen and oxygen. Where the hydrogen collected and can be used as a fuel. The efficiency of this process can be greatly improved by doping carbon in oxide.

Research shows that using these nanoparticles form pixels of a screen, where they generate electricity when transparent under the influence of light. If subjected to

electricity, on the other hand, the nanoparticles blacken, forming the basic characteristics of a LCD screen. According to creator Zoran Radivojevic, Nokia has already built a functional 200-by-200-pixel monochromatic screen which is energetically self-sufficient.

In 1995 Fujishima and his group at the Research Institute of Toto Ltd. discovered the super hydrophilicity phenomenon for titanium dioxide coated glass exposed to sun light. This resulted in the development of self-cleaning glass and anti-fogging coatings. TiO_2 incorporated into outdoor building materials, such as paving stones in noxer blocks or paints can substantially reduce concentrations of airborne pollutants such as volatile organic compounds and nitrogen oxides [23].

In photocatalysis process, light is absorbed by an adsorbed substrate. Today, semiconductors are usually selected as photocatalysts, because semiconductors have a narrow gap between the valence and conduction bands. In order to proved photocatalysis, the semiconductors need to absorbed energy equal to or more than its energy gap. This movement of electrons forms e^-/h^+ or negatively charged electron/positively charged hole pairs. The hole can oxidize donor molecules. In photogenerated catalysis, the photocatalytic activity (PCA) depends on the ability of the catalyst to create electron–hole pairs, which generate free radicals able to undergo secondary reactions [24].

Photocatalysts Advantages of using TiO_2 as photo-catalyst are:

(a) High oxidizing power, stability, and non-toxicity.

(b) Using TiO_2, the process occurs under ambient conditions.

(c) Using TiO_2, the oxidation of the substrate to CO_2 is complete in most cases

(d) It is comparatively inexpensive and remains quite stable in contact with different substrate.

1.4. Photocatalytic Reactions

Photocatalysed processes have grown in importance mainly due to their widespread applications in energy conversion, pollution abatement and the synthesis

of new materials [25]. Researchers are using photocatalysts for oxidative degradation of various non-biodegradable wastes. Fundamentally, photocatalysis deals with reactions which are initiated by electronically excited molecules generated by absorption of suitable radiation in the visible or near ultraviolet region. One of the most widely investigated and convenient class of photocatalysts is of metal oxide semiconductors [26]. Thus, in practical terms, chemical reactions occurring in presence of semiconducting materials and light are known as photocatalytic reactions. Semiconductors, with suitable band gaps, can act as quantum collectors of light energy. Illuminating a semiconductor material with photons of desired energy (i.e. hν ≥ the band gap of semiconductor) can cause a number of photocatalytic reactions.

Photocatalytic reactions are broadly classified as:

(a) Homogenous photocatalysis:-

in which phtocatalyst (semiconductor) and substrate exist in the same phase and

(b) Heterogenous photocatalysis:-

where photocatalyst and the substrate exist in different phases.

Most materials can be categorized as conductors, insulators, and semiconductors.

Semiconductors are mainly of two types:

(i) **n-type semiconductor:-** The n-type semiconductors are those, which shows conductivity due to the flow of majority electrons,

(ii) **p-type semiconductors :-** p-type semiconductors shows conductivity due to the presence of positively charged majority holes.

The energy gap (band gap) between valence band (highest occupied molecular orbital, HOMO) and conduction band (lowest unoccupied molecular orbital, LUMO) in a semiconductor is such that these materials behave as a conductor under certain conditions i.e., on exposure to light or at high temperature [27-28].

1.5. Mechanism of Photocatalysis

When photocatalyst titanium dioxide (TiO_2) absorbs Ultraviolet (UV)* radiation from sunlight or illuminated light source, it will produce pairs of electrons

and holes. The electron of the valence band of titanium dioxide becomes excited when illuminated by light. The excess energy of this excited electron promoted the electron to the conduction band of titanium dioxide, therefore, creating the negative-electron (e-) and positive-hole (h+) pair [29]. This stage is referred as the semiconductor's 'photo-excitation' state. The energy difference between the valence band and the conduction band is known as the 'Band Gap. TiO_2 is known to be a semiconductor having a large band gap of 3.2 eV, which corresponds to wavelengths shorter than 387 nm [30].

In order to narrow this band gap to achieve a visible light activity, either the LUMO (lowest unoccupied molecular orbital) level of the conduction band can be lowered or alternatively the HOMO (highest occupied molecular orbital) level of the valence band can be raised [31]. Both methods are useful only for verification of band gap narrowing effects. TiO_2 is a semiconductor which turns to a high-energy state by receiving light energy and releases electrons from its illuminated surface.

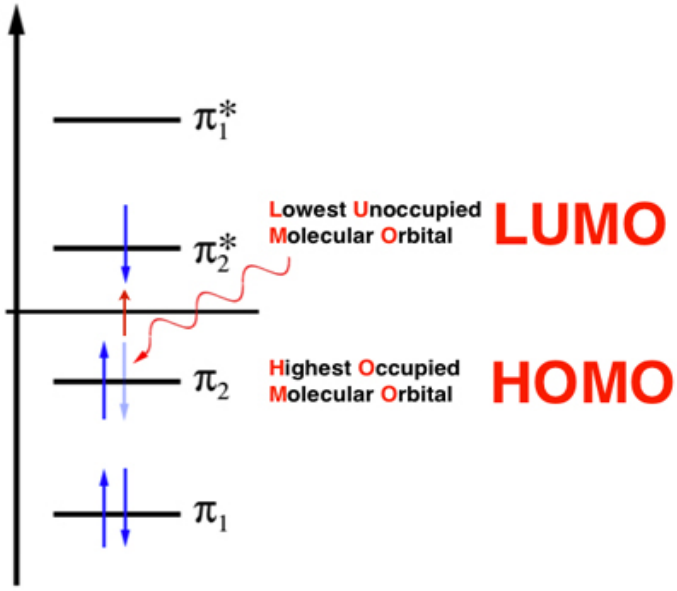

Fig.1.3. structure of photocatalyst with HOMO and LUMO

If the energy received at this stage is high enough, electrons that were initially located in the so-called ‘valence band’ all jump up to the ‘conduction band’[32]. Thus,

the energy that makes electrons jump up is provided by light, and this light energy is believed to be the energy of the light's wavelengths. Therefore, calculating from the height that the electrons have to jump up, this light should have the same wavelength as ultraviolet light.

$$E = hv \quad \text{.....,,,,..(1)}$$

Where E : energy **h :** Plank's constant **v:** frequency

$$v = c / \lambda \quad \text{……...(2)}$$

where c: light speed λ : wavelength, Therefore,

$$E = hc / \lambda \text{……..(3)}$$

Here, E is titanium dioxide 3.2 eV (3.2 eV = $3.2 \times 1.6 \times 10^{-19}$ J), and if you substitute the determinate values $c := 3.0 \times 10^{8}$ m/s, $h := 6.63 \times 10^{-34}$ Js,

It is obvious that the necessary wavelength is approx. 380 nm, which indicates that the light needed to activate photocatalyst is ultraviolet light. Band gap narrowing by raising the HOMO level is carried out by anion doping into TiO_2 lattice, resulting in hybridization of Ti 3d with N 2p orbital. The results of theoretical calculations prove the usefulness of anion doping such as N and S to raise the HOMO level or to form a new sub band right over the HOMO level of TiO_2 [33-34].

The positive-hole of titanium dioxide breaks apart the water molecule to form hydrogen gas and hydroxyl radical. The negative-electron reacts with oxygen molecule to form super oxide anion. This cycle continues when light is available. There are three steps of photocatalysis:

1) Light absorption following excitation of electrons from the valence band of TiO_2 to the conduction band to form electron/hole pairs.

2) Migration of electron/hole pairs thus formed to the TiO_2 surface.

3) Initiation of redox reactions to form active species such as hydroxyl radicals and superoxide ions, in some cases, intermediate products has been identified and reaction mechanisms have been proposed.

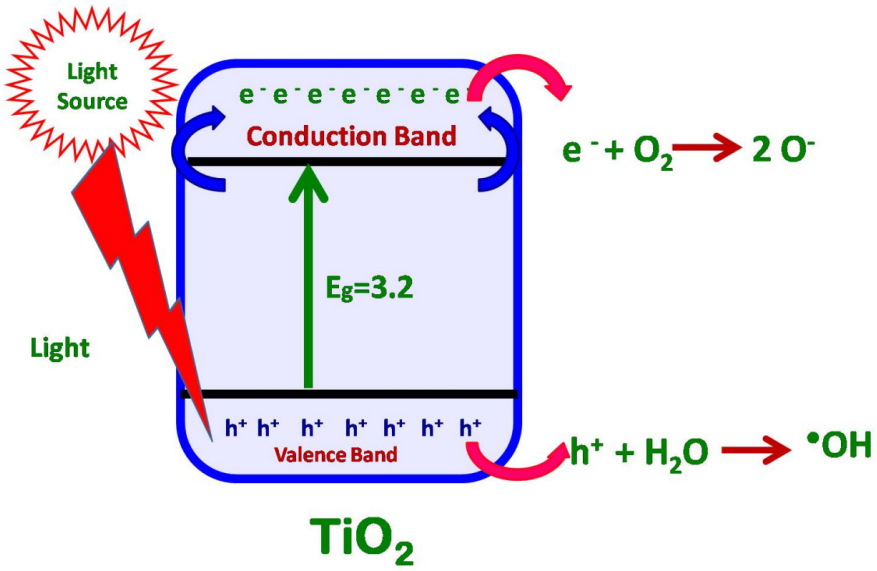

Fig.1.4. Mechanism of photocatalysis

The generation of photocatalytically induced hole electron pairs has been reported as the primary step of the above-mentioned mechanisms [35]. When light irradiates the surface of TiO_2, the absorption of a photon with the energy higher than the band gap energy leads to the formation of conduction band excess electron and valence band hole. The electron can form with oxygen a superoxide radical O^- [36].

1.6. Different theories of photocatalysis

Exist on the transformation of the positive hole from which the most important ones are the $^{\bullet}OH$ free radical theory and direct oxidation theory.

1.6.1 -$^{\bullet}$OH free radical theory

According to the $^{\bullet}OH$ free radical theory, the hole is transformed into a hydroxyl radical through the reaction with water on the TiO_2 surface. This highly active oxidant takes part in the oxidation of a series of organic compounds. Several authors tried to prove this theory by detecting intermediate species and products of

oxidation. Mills and Jishun (1998) [37] reported the hydroxylated product at photo mineralization of 4-chlorophenol in an oxygen-saturated solution where 4-chlorocatechol was expected to be formed by oxidation with $^{\bullet}OH$ free radical.

1.6.2 The direct oxidation theory

This theory suggests the oxidation of substrates directly by positive holes. Several indirect proofs were given for this theory. Richard et al (1997) [38] found that the production of hydroquinone by the photocatalytic transformation of 4-hydroxybenzyl alcohol was little affected in the presence of $^{\bullet}OH$ free radical quencher. In two other studies, extra absorption bands observed by time-resolved diffuse reflectance spectroscopy were assigned to the cationic radicals of photocatalytically oxidized compounds. All the above-mentioned studies were performed in aqueous solutions using microscale techniques but little attention has been paid to gaseous substrates. This publication, therefore, focuses on the photocatalytic oxidation of gaseous ethanol using a macroscale method that should provide the discrimination of mechanisms based on the two theories. A special reaction cell with small clearance was designed to diminish the dispersion influence and assure the experimental accuracy. Moreover, the formation and degradation of an intermediate, acetaldehyde, was also studied, which should help in the elucidation of the mechanism of ethanol photocatalytic oxidation [39].

1.7. Titanium dioxide

Titanium dioxide TiO_2 is a most important nanomaterial which has attracted a great attention due to its unique properties. Titanium dioxide TiO_2 have excellent merits in solar energy transferring and photocatalysis of poison compounds in environment. Further, the strong oxidizing power of the photogenerated holes, the chemical inertness, and the non-toxicity of TiO_2 has also made it a superior photocatalyst. The properties of Titania showing in table 1. Because of its lack of oxygen, Titanium dioxide is usually an *n* type semiconductor.

Table.1.1. Properties of Titania

Property	**Matric**
Density	4.23g/cm^3
Melting point	1855^o C
Boiling point	2500-3000˚C
Molecular weight	79.8658 g/mol
Solubility	hot sulfuric acid
Binding energy	459.3 eV
Band Gap Energy	3.2

1.8. Different Phase Structures of TiO_2

TiO_2 is found in 3 major crystalline forms namely anatase, rutile and brookite. Some other TiO_2 forms exists like the collumbite, hollandite, ramsdellite but these mentioned forms do not occur in nature but rather synthesized by high pressure treatment of anatase and rutile. Brookite is not practically advantageous for it is only stable at low temperatures. Rutile is the primary source of TiO_2 and the most stable form of it. Rutile TiO_2 and anatase TiO_2 have different characteristics and uses and is usually the two forms of TiO_2 compared [40].

Titanium dioxide that is used as the photocatalyst is mainly anatase-type crystal structure. There are 3 kinds crystal structure of titanium dioxide. Generally, the physical/chemical properties of a material may be quite different for their various phase structures. The phase structure of TiO_2 is one of the important factors determining its photocatalytic performance. TiO_2 has generally three polymorphs in nature, including anatase, rutile and brookite phase of TiO_2 (b). All three types of TiO_2 consist of TiO_6 octahedra, but differ in the distortion of the octahedron units and share edges and corners in different manners (Figure 1). For anatase, octahedral arranging in zigzag chains along (221) share four edges; in rutile, octahedra share only two edges and connect in linear chains parallel to (001), while in brookite both corners and edges are connected. These differences in lattice structures cause different mass densities and electronic band structures in different phase forms of TiO_2 [42].

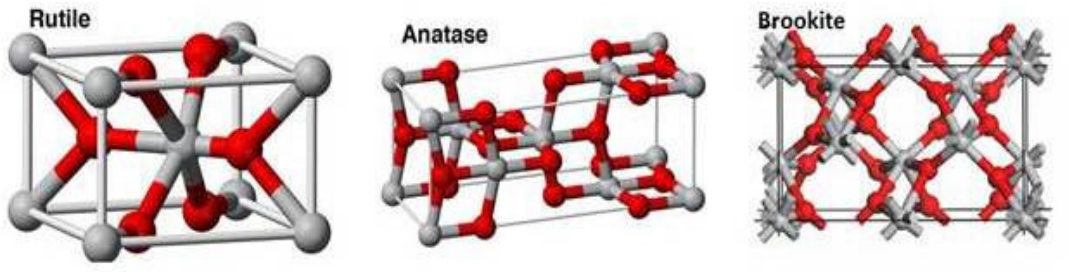

Fig.1.5. Structure of different crystal structure of titanium dioxide. [https://pavemaintenance. wikispaces.com/TiO_2+Photocatalys+-+Shannon [41]]

Thermodynamically, rutile is the most stable phase, while anatase and brookite are the metastable ones. Rutile can be normally obtained after annealing the other three polymorphs at elevated temperatures. The phase transformation of TiO_2 anatase nanoparticles actually starts from the interfaces between the agglomerated anatase particles, leading to a bulk phase transformation. Therefore, this process is usually accompanied by the growth of the particle size. Furthermore, the defect sites on the surface of anatase particles are proposed to play an important role in the phase transformation process. If the defect sites are blocked by some additives, the phase transformation can be efficiently retarded [42]. In addition, the mechanism of anatase to rutile phase transformation largely depends on the particle size of the initial anatase. The different mechanisms of rutile nucleation were proposed as follows. The phase transformation from brookite to rutile undergoes brookite → anatase → rutile transition, and a quasi-$H_2Ti_3O_7$ structure can be observed in the phase transformation from brookite to anatase by UV Raman spectroscopy [43]. The three polymorphs of TiO_2 have been applied in various fields on the basis of their different physical/chemical properties. The most extensively conducted research on TiO_2 still lies in using it as solar energy conversion materials, which is mainly investigated on anatase and rutile.

1.9. Photocatalytic activity of Titania Forms

The photocatalytic activities of these different forms of TiO_2 are quite different. Taking anatase and rutile of the most frequently studied photocatalysts of TiO_2 as examples, the differences in lattice structures of anatase and rutile TiO_2 cause

different densities and electronic band structures, leading to different band gaps (for bulk materials: anatase 3.20 eV corresponding to 384 nm and rutile 3.02 eV corresponding to 410 nm). This makes anatase have a slightly higher redox driving force than rutile, although the range of the light absorption by the former is slightly less than that by the latter. Anatase also has much higher surface area than rutile, leading to enhanced adsorption capability and even generation of much more active sites (such as oxygen vacancies). Furthermore, although rutile has better charge carrier mobility due to its higher crystallinity than anatase, the latter can generate more efficient charge separation due to the existence of more oxygen vacancies. Because of these advantages of anatase, it usually shows much higher photocatalytic activity than rutile [44].

1.10. Limitations of TiO_2 as Photocatalyst

TiO_2 because of its many desirable properties, such as high activity, chemical stability, robustness against photo-corrosion, low toxicity, no secondary pollution, low cost and water insolubility under most conditions; has proved to be the most suitable candidate for photocatalysis than various other semiconductor materials, such as ZnO, ZnS, Fe_2O_3, CdS and ZnS [45]. However, there are some limitations in using TiO_2 as photocatalyst for practical applications, which includes [46].

Limitations of TiO_2 using as photocatalyst

(i) Large band gap of TiO_2,

(ii) Low quantum yield of TiO_2,

(iii) Low photon utilization efficiency,

(iv) Narrow spectrum of light, UV is the most responsive range

(v) Separation of TiO_2 from the treated water is very difficult and energy consumptive

(vi) Direct Electron–Hole Recombination

1.10.1. Direct Electron–Hole Recombination

In heterogeneous photocatalysis, no in-situ direct observation of recombination has been reported because recombination generally proceeds with liberation of heat, and detection of heat is not easy. Although one of our photoacoustic spectroscopic

studies on photocatalysis showed liberation of heat during photocatalytic reaction on titanium(IV) oxide (Titania) particles [47], the detected heat was attributable to heat of exothermic chemical reaction, not heat liberated by e^-–h^+ recombination. Of course, photoemission by recombination may occur for photocatalysts of direct-transition semiconductors, though such photoemission is not always observed, and, even if it is observed, recombination with undetectable non-radiative deactivation may occur in parallel. An alternative way for detecting e– h+ recombination is pump–probe spectroscopy using ultrafast laser pulses.

Since addition of sacrificial electron acceptors or donors, which may trap e– and h+ respectively, did not show appreciable influence on the decay, they concluded that the decay reflects e––h+ recombination and proposed second-order kinetics for the recombination. This seems reasonable considering the high density of photons in a femtosecond pump pulse to produce multiple pairs of e– and h+, not a single e––h+ pair, to undergo recombination with second-order kinetics. The second-order recombination-rate constants with physical and structural properties of various Titania photocatalysts [48]. However, there is no assurance that similar recombination also occurs in practical photocatalytic reaction systems, where the light intensity is markedly lower than that of femtosecond laser pulses to result in creation of only one or a few e––h+ pairs in one photocatalyst particle. It has been suggested that the rate obeys first-order kinetics, not a second-order one, for such mutual recombination induced by low-intensity laser pulses. The low-intensity laser measurements may reproduce the practical photocatalytic reaction system under irradiation with continuous light sources such as light from a mercury or xenon arc lamp. However, the low-intensity laser measurements were performed in transmission mode using transparent thin films of a photocatalyst, not diffuse-reflection mode using powder or a suspension of a photocatalyst, *i.e.*, only nanometer-sized particles could be used as a sample, and decay kinetics of the recombination in sub micrometer-sized particles could not be examined. Thus, the dilemma in excitation-light intensity in direct measurement of recombination kinetics remains [49].

1.10.2. Donor Levels in an *n*-Type Semiconductor

It had been believed that lattice defects in crystalline photocatalyst particles are responsible for e−–h+ recombination when the author started working in this field in the 1980's; the defects work as a recombination center, though no direct observation of the recombination had been performed, as described in the preceding section. This might be because it is convenient to attribute lower and higher activities of photocatalysts to enhanced and inhibited e−–h+ recombination, respectively, and to attribute the recombination to ambiguous but plausible recombination centers. However, one of the most significant problems might be the misconception that the recombination center must be "crystal lattice defects". Most photocatalysts, e.g., Titania (VI) oxide, is categorized as n-type semiconductor [50].

It is known that metal oxides tend to release oxygen, leaving electrons in the lattice, and this may be an origin of the n-type semiconductor property of metal oxides. Actually, Titania in the form of powder or a single crystal turns black or blue-black when heated under reduced atmosphere due to the release of oxygen (O_2) and resulting formation of reduced titanium species, *i.e.*, trivalent titanium cation (Ti^{3+}) [51]. In an electrochemical sense, this phenomenon corresponds to the formation of electron-filled donor levels located below the CB to give an n-type semiconducting property; Fermi level is located between the CB bottom and those donor levels. When such an n-type semiconductor is immersed, or in contact in an electrolyte solution, electrons in the donor levels go out to the electrolyte since the donor level in an *n*-type semiconductor may be more cathodic than the electrode potential of electrolyte solutions. This flow of electrons in the donor level to an electrolyte results in the formation of a so-called Schottky-type barrier [52] at the interface to prohibit electron flow from an electrolyte to an electrode, *i.e.*, potential slope due to an electron-deficient so-called depletion layer is built in a semiconductor.

1.11. Methods of Improvement of photocatalytic activity

The visible light photoactivity of metal-doped TiO_2 can be explained by a new energy level produced in the band gap of TiO_2 by the dispersion of metal nanoparticles in the TiO_2 matrix. The electron can be excited from the defect state to the TiO_2

conduction band by photon with energy equals *hv* [53]. Additional benefit of transition metal doping is the improved trapping of electrons to inhibit electron-hole recombination during irradiation. Decrease of charge carriers recombination results in enhanced photoactivity.

There are three modification mechanism of TiO_2.

(1) Band gap narrowing;

(2) Impurity energy levels; and

(3) Oxygen vacancies.

1.11.1. Band gap narrowing:

Asashi, *et al.* [54] investigated that N 2p state hybrids with O 2p states in anatase TiO_2 doped with nitrogen because their energies are very close, and thus the band gap of N-TiO_2 is narrowed and able to absorb visible light.

1.11.2. Impurity energy level:

Irie, *et al.* [55] reported that TiO_2 oxygen sites substituted by nitrogen atom form isolated impurity energy levels above the valence band. Irradiation with UV light excites electrons in both the VB and the impurity energy levels, but illumination with visible light only excites electrons in the impurity energy level.

1.11.3. Oxygen vacancies:

Ihara, *et al.* [56] reported that oxygen-deficient sites formed in the grain boundaries are important to emerge vis-activity and nitrogen doped in part of oxygen-deficient sites are important as a blocker for reoxidation.

1.11.4. Charge separation

Efficient charge separation is the most important factor that determines the photocatalytic activities. Various strategies could be applied for improving charge separation efficiency. For example, preparation of semiconductor photocatalysts at high temperatures may lead to high crystallinity that diminishes the formation of charge recombination defect sites. Construction of various kinds of nanostructures

such as nanowires (belts) [57] and nanosheets [58] may also facilitate charge transportation and promote charge separation efficiency. As compared to zero dimensional nanoparticles, one-dimensional nanostructures exhibit better photocatalytic activity because they have better charge mobility and can reduce the charge recombination. Furthermore, creation of "junctions" with built-in electric fields or chemical potential differences is also an effective strategy for improving charge separation efficiency. The surface catalytic reaction is a successive step of charge separation. In principle, a photocatalytic reaction consists of two half reactions, reduction reaction, and oxidation reaction. The electrons in CB may initiate the reduction reaction, and the reduction capability is determined by the position of CB; the holes in the VB involve the oxidation reaction, and the oxidation capability is determined by the position of VB. For the water splitting reaction, the position of CB of a semiconductor photocatalyst should be more negative than the redox potential of H^+/H_2 (0 V vs NHE, pH = 7), while the energy level of VB should be more positive than the redox potential of O_2/H_2O (1.23 V vs NHE, pH = 7). Sometimes, some particular surface sites of a semiconductor can act as the active centers themselves, especially for oxidation reaction on the surface of metal oxide semiconductors. However, in most cases, efficient photocatalytic reactions proceed only after loading noble metal and oxide cocatalysts on semiconductors [59-60].

1.12. Band Gap energy of Titania

Aqueous suspensions of the samples were used for the UV absorption studies. The blue shift that is observed in the absorption spectra with the decrease in particle size has been reported earlier [61]. The bandgap of the materials calculated from the extrapolation of the absorption edge onto the energy axis is 3.2 eV and this is well reported. Firstly, to establish the type of band-to-band transition in these synthesized particles, the absorption data were fitted to equations for both indirect and direct bandgap transitions. Fig. 7 shows the $(\alpha E_{phot})^2$ versus E_{phot} for a direct transition, where α is the absorption coefficient and Ephot is the photon energy, Ephot = (1239/λ) eV, where λ is the wavelength in nanometers.

The value of E_{phot} extrapolated to $\alpha = 0$ gives an absorption energy, which corresponds to a bandgap E_g. For direct bandgap semiconductors, electronic transition from the valence band to the conduction band is electrical dipole allowed and the electronic absorption, as well as emission, is usually strong [62]. For indirect bandgap semiconductors, the valence band to the conduction band electronic transition is electrical dipole forbidden and the transition is phonon assisted, i.e., both energy and momentum of the electron–hole pair are changed in the transition.

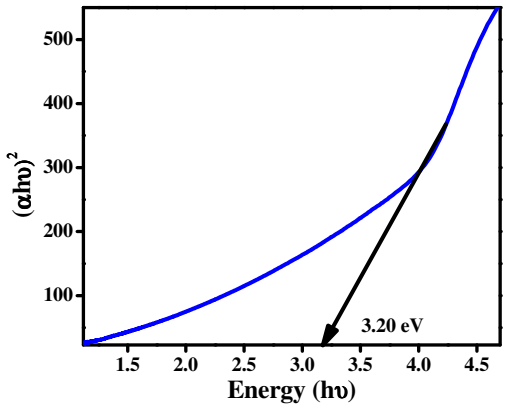

Fig.1.6. Direct Band Gap determination

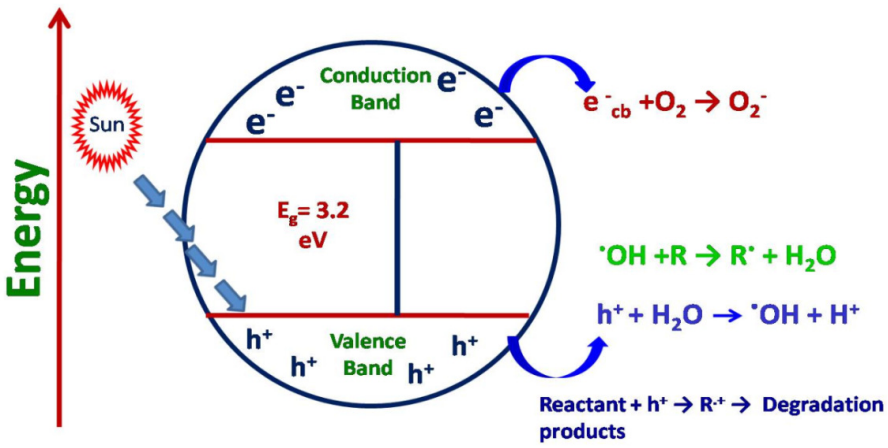

Fig.1.7. Band Gap Energy of Titania

Both their absorption and emission are weaker compared to those of direct bandgap semiconductors since they involve a change in momentum. Hence a direct

bandgap transition would result in a more efficient absorption of solar energy and therefore much better photovoltaic devices. Hence, any indication in this direction would direct towards a more favourable material for the applications envisaged. Similar observations were made on Si nanocrystals where the quantum confinement causes a kinetic enhancement of the luminescence quantum yield, as well as an increase of the bandgap. Among the possible semiconductors, TiO_2, or Titanium Dioxide, (E_g = 3.2 eV) is most extensively used because it has many advantages. It is inert and resistant to corrosion, and it requires little post-processing, making it inexpensive. Finally, it can react under mild-operating conditions.

1.13. Bandgap Reduction Engineering.

1.13.1. Doping with Cations.

In the band structure of TiO_2, O 2p orbitals contribute to the filled VB, while Ti 3d, 4s, 4p orbitals contribute to the unoccupied CB. The lower position of CB is dominated by Ti 3d orbitals [63]. Upon doping with other cations in replacement of Ti, an impurity level could be introduced in the forbidden band. This intermediate energy level can act as either an electron acceptor or a donor, which allows TiO_2 to absorb visible light. Until now, many investigations have been made in the preparation of visible light-responsive TiO_2 by cation doping [64]. The photocatalytic H_2O splitting reaction on Cr^{3+}-doped TiO_2 nanoparticles in the visible light region (400–550 nm). The visible light absorption was attributed to the photoexcited transition of Cr^{3+} 3d electrons into the CB of TiO_2. Prepared Fe^{3+}-doped Titania by hydrothermal treatment can be split the water into a 2:1 stoichiometric ratio of H_2 and O_2 under visible light irradiation.

Niishiro et al. [65] reported that TiO_2 doped with Ni^{2+} can produce H_2 from aqueous methanol solution under visible light irradiation ($\lambda > 420$ nm).

When codoped with Nb^{5+}, the absorption intensity of TiO_2 can be obviously increased in the visible region. It is proposed that codoping of two cations with different charges can increase the stability of the photocatalyst due to the charge balancing effect [66]. Sun et al.[67] reported that the Fe and Ni codoped TiO_2 nanoparticles prepared through alcohol-thermal method can give a H_2 evolution rate of

361.64 μmol h^{-1} $gcat^{-1}$ in ethanol aqueous solution under visible light ($\lambda > 400$ nm). The high H_2 evolution activity was ascribed to the efficient separation of photoinduced electrons and holes by the codoping method, as evidenced by the photoluminescence spectroscopy. Wu et al.[68] reported that a Co^{2+}-doped TiO_2 had a long-term stability for H_2 production, and the presence of CoOx species on the surface of TiO_2 was crucial for the stability. The enhancement of H_2 production activity on Bi doped TiO_2 was ascribed to its lower overpotential as compared to the undoped TiO_2 [69].

1.13.2. Doping with Anions.

Anion doping is another approach to extend the light absorption of TiO_2 into the visible region. Unlike cation doping, anion doping could hardly affect the CB band of TiO_2, which is made up of Ti 3d, 4s, and 4p orbitals. It usually reconstructs the VB and shifts it upward to narrow the bandgap of TiO_2. Asahi and co-workers [70] preferred anion doping rather than cation doping by considering that cation doping would lead to instability of the material and require an expensive ion implantation facility. Furthermore, cation doping usually leads to quite localized d states deep in the bandgap of TiO_2 acting as the recombination centers of charge carriers. It can be seen that N is the most suitable doping element as its p orbitals contribute to VB by mixing with O 2p orbitals, which can narrow the bandgap of TiO_2 by shifting the VB upward. However, there is also an argument that extension of the light absorption into the visible region by N doping is not due to bandgap narrowing. Instead, N doping may introduce local states and oxygen vacancies inside the band gap of TiO_2, which is the cause of the visible light absorption [71].

1.14. Photocatalytic Reactions on TiO_2

Semiconductor is a kind of material with electrical conductivity between conductor (such as metals) and insulator (such as ceramic). The conductivity of a semiconductor usually increases with the increase of the temperature, which is opposite to that of a metal [72]. The unique electronic property of a semiconductor is characterized by its valence band (VB) and conduction band (CB). The VB of a semiconductor is formed by the interaction of the highest occupied molecular orbital

(HOMO), while the CB is formed by the interaction of the lowest unoccupied molecular orbital (LUMO). There is no electron state between the top of the VB and the bottom of CB. The energy range between CB and VB is called forbidden bandgap (also called energy gap or bandgap), which is usually denoted as Eg. The band structure, including the bandgap and the positions of VB and CB, is one of the important properties for a semiconductor photocatalyst because it determines the light absorption property as well as the redox capability of a semiconductor. As shown in Figure 1.8, the photocatalytic reaction initiates from the generation of electron–hole pairs upon light irradiation. When a semiconductor photocatalyst absorbs photons with energy equal to or greater than its Eg, the electrons in VB will be excited to CB, leaving the holes in VB [73].

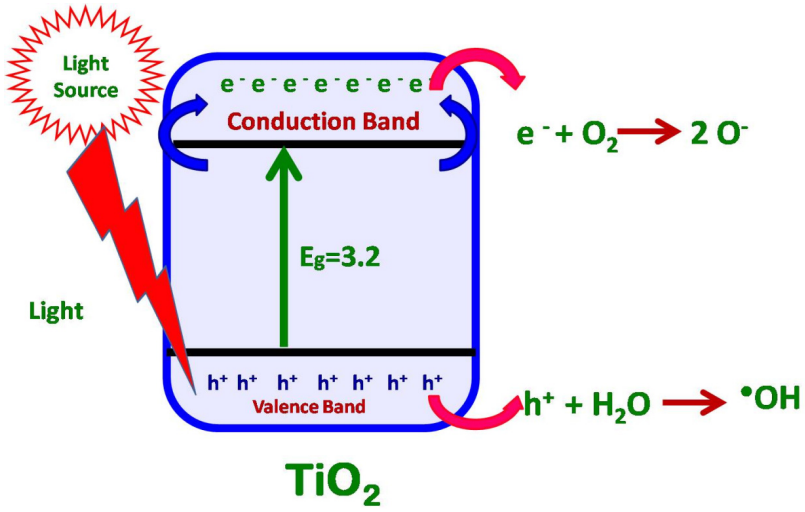

Fig.1.8. Formation of e^- h^+ pair on the surface of semiconductor

This electron–hole pair generation process in TiO_2 can be expressed as follows:

$$TiO_2 + h\nu \rightarrow h^+ + e^- \quad \text{.....(4)}$$

These photogenerated electron–hole pairs may further be involved in the following four possible processes:

(i) Successfully migrate to the surface of semiconductor;

(ii) Captured by the defect sites in bulk and/or

(iii) Captured on the surface region of semiconductor; and

(iii) Recombine and release the energy in the form of heat or photon.

The last two processes are generally viewed as deactivation processes because the photogenerated electrons and holes do not contribute to the photocatalytic reaction. Only the photogenerated charges that reached to the surface of semiconductor could be available for photocatalytic reactions [74]. The defect sites in the bulk and on the surface of semiconductor may serve as the recombination centers for the photogenerated electrons and holes, which will decrease the efficiency of the photocatalytic reaction [75].

Titanium dioxide's photocatalytic characteristics are greatly enhanced due to the advent of nanotechnology. At nano-scale, not only the surface area of titanium dioxide particle increases dramatically but also it exhibits other effects on optical properties and size quantization. An increased rate in photocatalytic reaction is observed as the redox potential increases and the size decreases. In some cases, energy from any ambient light source can be used effectively as the energy source of photo catalysis instead of UV light [76].

Photo catalyst of solarcoat not only have all the advantages of the traditional photocatalyst but also can disinfect, purify air and eliminate harmful substance in the condition of visible light .therefore, it has incomparable technology and quality advantages of fighting against pollution indoors and outdoors. The strong functions of solar coat photocatalysis will completely eliminate odours of newly-decorated houses and enable people to get rid of the danger caused by epidemic disease. Solar coat of photocatalyst has been widely applied in all kinds of fields and highly affirmed & appraised. The theory of photocatalyst: with the irradiation of light, the TiO_2 on the surface of the ultra strong photocatalyst of solarcoat will take photocatalytic reaction the same as photosynthesis which can produce free radical and ozone with strong function of oxidization. And it can oxidize and decompose various organic compounds and some minerals [77].

Titanium dioxide, particularly in the anatase form, is a photocatalyst under ultraviolet light. Recently it has been found that titanium dioxide when spiked with nitrogen ions or doped with metal oxide like tungsten trioxide, is also a photocatalyst under visible and UV light. The strong oxidative potential of the positive holes

oxidizes water to create hydroxyl radicals. It can also oxidize oxygen or organic materials directly. Titanium dioxide is thus added to paints, cements, windows, tiles, or other products for sterilizing, deodorizing and anti-fouling properties and is also used as a hydrolysis catalyst. It is also used in the Graetzel cell, a type of chemical solar cell [78].

1.15. Energy structure of titanium oxide and photoeffect

In a compound semiconductor consisting of different atoms, the valence band, and conduction band formation processes are complicated, but the principles involved are the same. For example, it is known that the valence band of titanium oxide is comprised of the 2p orbital of oxygen (O), while the conduction band is made up of the 3d orbital of titanium (Ti) [79]. In a semiconductor with a large band gap, electrons in the valence band cannot jump up to the conduction band. However, if energy is applied externally, electrons in the valence band can rise (this is referred to as "excitation") to the conduction band. Consequently, as many electron holes (holes left behind by the electrons moving up to the conduction band) as the number of excited electrons are created in the valence band [80]. This is equivalent to the movement of electrons from the bonding orbital to the antibonding orbital. In other words, the photoexcited state of a semiconductor is generally unstable and can easily break down. Titanium oxide, on the other hand, remains stable even when it is photoexcited. This is one of the reasons that titanium oxide makes an excellent photocatalyst.

The following three factors pertaining to the band structure of semiconductors have the greatest effect on photocatalytic reactions:

(1) Band gap energy

(2) Position of the lowest point in the conduction band

(3) Position of the highest point in the valence band

In photocatalytic reactions, the band gap energy principally determines which light wavelength is most effective, and the position of the highest point in the valence band is the main determinant of oxidative decomposing power of photocatalyst [81].

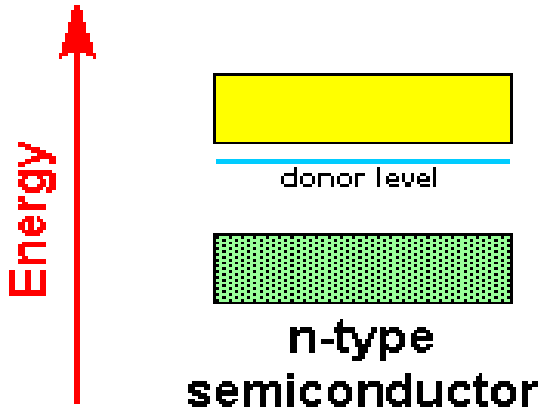

Fig.1.9. Structure of n type semiconductor

1.16. Photocatalyst Nanotechnology

This report defines a nanocatalyst as a substance or material with catalytic properties that has at least one nanoscale dimension, either externally or in terms of its internal structures. The report covers substances with catalytic properties that may not have nanoscale dimensions, but which have been nano engineered in order to enhance their catalytic activity [82].

Photocatalysis refers to the chemical reaction that occurs when light strikes a chemical compound that is light sensitive, such as titanium oxide. When light strikes titanium dioxide, a chemical reaction will be started in the immediate region and cause the breakdown of organic toxins, odours, and more. Over the past several years, a variety of methods have been developed to synthesize TiO_2 materials in a form of nanostructures such as nanoparticles, nanowhiskers, nanowires, and nanobelts. TiO_2 nanotubes have been fabricated by pressure impregnating of a nanoporous template with titanium isopropoxide and then oxidative decomposing the reagent at 500 °C. Although, the specific area of these nanostructures was usually high enough to meet the requirements of most applications. The chemical approaches require high annealing temperatures and have further problems arising of residual impurities incorporation from organic precursors and blends. On the other hand fabrication of

nanostructures by physical approaches involves specific patterning of the deposited material, which are time consuming processes [83].

A photocatalyst is a substance that increases the rate of a chemical reaction by reducing the required activation energy, but which is left unchanged by the reaction. In addition to speeding up certain chemical reactions, catalysts also can be used to alter the temperature at which various reactions take place and thus make them feasible. Nanocatalyst represent the convergence of catalysts, a mature technology, with a new one, nanotechnology [84]. Catalysts systematically have been used at least since the beginning of the industrial age, and today their use is widespread in industries such as petrochemicals and pharmaceuticals. In a sense, all catalysis is nanoscale, since it involves chemical reactions at the nanoscale. The several report provides an understanding of developments in nanocatalyst technology and applications that will influence the future size and structure of the material for these unique substances. Oxidation of organic contaminants using magnetic particles that are coated with titanium dioxide nanoparticles and agitated using a magnetic field while being exposed to UV light [85].

1.17. Thin-film Photocatalyst

Titanium dioxide (TiO_2) is a harmless substance widely applied in various fields such as cosmetics, toothpaste, extenders for medicines, and coating. For these uses, TiO_2 is usually supplied in the form of powder. But in order to use TiO_2 as an effective photo-catalyst for the 5 functions, powder is not an appropriate form, for it may be blown off by wind or washed out by water, and when used to purify water, it has to be separated from the water. Thus, a method to fix the powder has long been considered [86].

It is easy to fix powdery $TiO_2$with a binder, but if an organic binder is used, the photo-catalytic reaction will destroy the binder itself. Inorganic binder is not influenced by photo-catalytic reaction, but only the powder exposed on the surface can work effectively despite the total amount of powder contained in the binder.

Photo-catalytic thin-film has been developed that can cover all surface only with TiO_2, instead of using powder TiO_2. This method, called the Sol-Gel method, uses titanium alkoxide as a starting material. It is hydrolyzed to obtain sol, and the sol is applied to coat substrate through such coating methods as the dip-coating method, to form a film. At this stage, the film is not the film of TiO_2. So, the sol is sintered along with the substrate to be crystallized, and thus the film of titanium dioxide is formed. Photocatalytic oxidation reactions with titanium dioxide induced by the photogenerated hole-electron pairs have been investigated extensively. Complete photocatalytic mineralization of many organic pollutants has been of considerable interest [87].

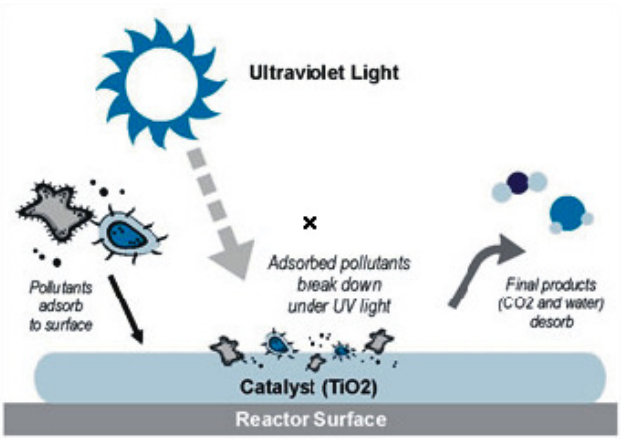

Fig.1.10. Thin film photocatalysis

The use of Titanium Dioxide (TiO_2) ultra fine particulates as coating for concrete pavement have received considerable attention in recent years as these coatings can trap and absorb organic and inorganic air pollutants by a photocatalytic process.. The use of titanium dioxide coating has a positive effect on four main environmental categories: acidification, eutrophication, criteria air pollutants, and smog formation. However, during production phases and due to the consumption of fossil energy, titanium dioxide causes an increase in global warming, fossil fuel depletion, water intake, ozone depletion, and impacts on human health. Based on the overall environmental performance of this product, life cycle assessment shows that

titanium dioxide coating has an overall negative score of -0.70 indicating that the addition of this surface layer will have an overall positive effect on the environment [88].

1.18. TiO_2 Nanocomposites

Noble metals such as Ag, Au, Pt, Pb and Pd etc are deposited on a TiO_2 surface to enhance photocatalytic activity. These noble metals act as an electron trap promoting interfacial charge transfer processes in the composites. Utilization of solar energy needs the material's band gap matching with the highest intensity of solar radiation which is around 500–700 nm which is equivalent to band gap in the region of 1–2 eV. In addition, for the photocatalyst application the semiconductor should be chemically and photochemical stable in acidic and alkaline media. Unfortunately all semiconductors of band gap in the region of 1–2 eV are unstable chemically and photochemically in acidic or alkaline media; whereas large semiconductors like TiO_2, ZnO etc, are stable in alkaline or acidic media but due to their large band gap (~3 eV) covers only about 4% of solar radiation. Thus, though these materials are good but their solar conversion efficiency is very low. Therefore, there is a need to develop some technique to make low band gap material stable in acidic or alkaline media. Considering this requirement, Sharon and his group developed a mathematical model which can be used to predict the mixture of two large band gap materials such that their effective band gap is small [89-90].

1.19. Synthesis methods of TiO_2 Nanoparticles

Since the physicochemical properties such as size, shape, morphology and composition of the Titanium oxide is very important for the photocatalytic performance, it is important to control them; thus there is a need for employing the synthetic procedure, which can contribute towards the development of desired properties of the photocatalyst. Moreover, the Titanium oxides should be ecologically affable and prepared by economically viable inexpensive method. Various routes have been tried for this purpose; some of them which are suitable for synthesis of Titanium dioxide and its composites are discussed below.

1.19.1. Sol-Gel Method

The sol-gel method was developed in the 1960s, for preparing materials with a variety of shapes, porous structures, thin fibers, dense powders and thin films. Sol-gel process involves the transition of a system from a liquid solution (Sol) to a solid gel phase (Gel). A sol consists of a liquid with colloidal particles which are not dissolved, but do not agglomerate or sediment. A sol is a stable dispersion of colloidal particles or polymers in a solvent. Whereas, gel consists of a three dimensional continuous network, which encloses a liquid phase, in a colloidal gel, the network is built from agglomeration of colloidal particles. In a polymer gel the particles have a polymeric substructure made by aggregates of sub-colloidal particles. Generally, the sol particles may interact by Van der Waals forces or hydrogen bonds. A gel may also be formed from linking polymer chains. In most gel systems used for materials synthesis, the interactions are of a covalent nature and the gel process is irreversible. The gelation process may be reversible if other interactions are involved. In a nut shell sol-gel process can be described as "Formation of an oxide network through polycondensation reactions of a molecular precursor in a liquid". In a typical sol-gel process, TiO_2 nanoparticles are formed by hydrolysis and polycondensation (de-hydration and de-alcoholation) reactions of Titanium alkoxide, to form oxopolymers, which are then transformed into an oxide network. The structure and properties of metal oxides is strongly dependent on the rate of hydrolysis and poly-condensation. The factors responsible for the formation of metal oxides are: reactivity of metal alkoxide, water to alkoxide ratio, pH ofreaction medium, and nature of solvent and additives and reaction temperature. Ibrahim and Sreekantan [91] in the XRD analysis of TiO_2 found that pH affects size and degree of crystallinity. Moreover, they also observed that high acidity favours formation of rutile phase, while low acidity favours anatase phase formation.

1.19.2. Sol Method

The sol method refers to the non-hydrolytic sol-gel processes and usually involves the reaction of Titanium chloride with a variety of different oxygen donor molecules like a metal alkoxide or organic ether [92].

1.19.3. Hydrothermal Method

Hydrothermal processing can be defined as any heterogeneous reaction in the presence of aqueous solvents or mineralizers under high pressure and temperature conditions to dissolve and recrystallize (recover) materials that are relatively insoluble under ordinary conditions [93]. The process involves use of a solvent under high temperature (typically between 100 ºC and 1000 ºC) and also high pressure (typically between 1 *atm* and 10,000 *atm*) that facilitates the interaction of precursors during synthesis. If water is used as a solvent, the method is called as hydrothermal synthesis.

1.19.4. Micelle and Inverse Micelle Method

Micelles are composed of surfactants. Surfactants normally contain a hydrophilic head and a hydrophobic chain, and these amphiphilic molecules can self-assemble into a rich variety of organized structures in solution, such as normal and reverse micelles. Aggregates of surfactant molecules dispersed in a liquid colloid are called micelles, when the surfactant concentration exceeds the critical micelle concentration. Reverse micelles are globular aggregates formed by the self assembly of surfactants in apolar solvents, whereas normal micelles are globular aggregates formed by the self-assembly of surfactants in water [94].

1.19.5. Solvothermal Method

The solvothermal method is similar to the hydrothermal method. The only difference is the solvent used. In solvothermal method solvent used is non-aqueous. Since a variety of organic solvents with high boiling points can be chosen, the temperature can be elevated much higher than that in the hydrothermal method. This method has better control than hydrothermal method for the size and shape distributions and the crystallinity of the TiO_2 nanoparticles. This method had been found to be a versatile method for the synthesis of a variety of nanoparticles with narrow size distribution and dispersity [95-96]. The solvothermal synthesis method is used for preparing nano size metals, semiconductors, ceramics, and polymers using solvent under moderate to high pressure. If water is used as the solvent, the method is called “hydrothermal synthesis”. The synthesis under hydrothermal conditions is

usually performed below the supercritical temperature of water (374 ºC). Among all the methods discussed above, the sol-gel method is the simplest, economic and effective method and can produce high purity products [97].

1.20. Synthesis of Titania based nanocomposites

The various Titania based nanocomposites have been prepared by the doping of cation, anion, nobel metal, mettaloid, non-metals. The different nanocomposites of Titania have been prepared by the addition of different metal which is showing below in detail.

1.20.1. Addition of Nobel metals

Addition of noble metals is another approach for the modifying photocatalysts. Noble metals including Pt, Ag, Au, Pd, Ni, Rh, and Cu have been reported to be very effective at enhancing photocatalysis by TiO_2 [98-99]. Because the Fermi levels of these noble metals are lower than that of TiO_2, photoexcited electrons can be transferred from the conduction band of TiO_2 to metal particles deposited on the surface of TiO_2, while photogenerated holes in the valence band remain on TiO_2. This greatly reduces the possibility of electron-hole recombination, resulting in efficient separation and higher photocatalytic activity. Numerous studies have found that the properties of these kinds of composites depend strongly on the size of the metal particle, dispersion, and composition. When the size of the metal particles is less than 2.0 nm, the composites display exceptional catalytic behaviour [100]. It has been suggested that too high a concentration of metal particles reduces photon absorption by TiO_2 and allows the metal particles to become electron-hole recombination centres, resulting in lower efficiency [101].

1.20.2. Doping with metalloids

Xu *et al*. [102] prepared TiO_2 photocatalyst that was active under visible light by doping with boron using sodium boro hydride at 55°C under hydrothermal conditions. Compared with pure TiO_2, the doped sample exhibited stronger absorption in the visible region and also showed a larger surface area. The photocatalytic activity was evaluated by measuring the degradation of Reactive Brilliant Red and4-

chlorophenol under irradiation with visible light. The photocatalytic activities of the samples showed the following order: B-doped TiO_2 (hydrothermal method) > B-dopedTiO_2 (sol-gel method) > pure TiO_2> Degussa P25. The same group also prepared B-doped TiO_2 hollow spheres [103] using hydrothermally prepared carbon spheres as a template. The photocatalytic activity of these TiO_2 spheres was determined by degrading Reactive Brilliant Red under visible light irradiation. It was revealed that the photocatalytic activity of the hollow TiO_2 spheres was almost 22 times greater than that of Degussa P25.

1.20.3. Doping with anions

Many studies have been devoted to the development of TiO_2 that is responsive to visible light by doping it with various anions [104] as a substitute for oxygen in theTiO_2 lattice. For these anion-doped TiO_2 photocatalysts, the mixing of the p states of the doped anion (N, S or C) with the O 2p states shifts the valence band edge upwards, narrowing the band gap energy of TiO_2. Unlike metal cations, anions are less likely to form recombination centers and therefore, are more effective at enhancing the photocatalytic activity of TiO_2 [105].

Asahi *et al.* [106] calculated the electronic band structures of TiO_2 containing different substitutional dopants including C, N, F, P and S. Substitutional doping with N narrowed the band gap most significantly because its p state mixed with the O 2p states. In addition, molecular dopants like NO and N_2 gave rise to bonding states below the O 2p valence band and anti bonding states deep in the band gap (N*i* and N*i*+s) that were well screened and hardly interacted with the band states of TiO_2. Diwald *et al.* [107] incorporated nitrogen monoanions into single crystals of TiO_2 by sputtering with N^{2+}/Ar^{+} mixtures and subsequent annealing to 627°C under ultrahigh vacuum conditions. This modified catalyst exhibited an unexpected blue shift in the O_2 photo desorption compared with that of undoped crystals of TiO_2. Ao *et al.*[108] prepared N-doped TiO_2 hollow spheres by a one-photo hydro thermal method using urea as precursor of nitrogen. The photocatalytic activity of the spheres was determined by degrading Reactive Brilliant Red dye X-3B under irradiation with

visible light and showed higher photocatalytic activity than undoped TiO_2 hollow spheres and commercial Degussa P25.

Dong *et al.* [109] synthesized N-doped TiO_2 nanotube array by annealing anodized TiO_2 nano tubes with ammonia at 500°C. The array exhibited enhanced photocatalytic efficiency for the photocatalytic degradation of methyl orange under visible light irradiation compared with undoped nano tubes because nitrogen doping narrowed the band gap of the nano tubes. Yu *et al.* [110] found that F-doped TiO_2 exhibited higher photocatalytic activity for the oxidation of acetone into CO_2 than undoped TiO_2. Sakthivel and Kisch [111] showed that C-doped TiO_2 was five times more active than N-doped TiO_2 toward the degradation of 4-chlorophenol by artificial light ($\lambda \geq 455$ nm). Park *et al.* [112] reported that TiO_2–xCx nano tube arrays exhibit much higher photocurrent densities and more efficient water splitting under irradiation with visible light than pure TiO_2 nano tube arrays.

1.20.4. Codoping

Codoping of TiO_2 may be used as an effective way to improve charge separation. Yang *et al.* [113] reported that mono crystalline TiO_2 codoped with optimal concentration sof Eu^{3+} and Fe^{3+} (1% Fe^{3+} and 0.5% Eu^{3+}) showed significantly enhanced photocatalytic activity compared with undoped TiO_2. Fe^{3+} serves as a hole trap and Eu^{3+} as an electron trap, increasing the rates of anodic and the cathodic processes *via* improved interfacial charge transfer.

Song *et al.* [114] prepared (Cu, N)-codoped TiO_2 nano particles and investigated the influence of the amounts of Cu and N codoped into TiO_2 on the photocatalytic activity. Codoping of TiO_2 with N and Cu extended absorption upto 590 nm and gave higher photocatalytic activity than pure TiO_2 or Cu-doped TiO_2 for the photocatalytic degradation of xylenol orange, thus revealing a potential application in degrading organic pollutants. Xu *et al.* [115] synthesized (Ce, C)-codoped TiO_2 using a modified sol-gel method under mild conditions. The photocatalytic activity of (Ce, C)-codoped TiO_2 for degradation of Reactive Brilliant Red X-3B under visible light was significantly improved compared with that of C-doped TiO_2, undoped TiO_2, and Degussa P25 because cerium doping slowed the radiative recombination of

photogenerated electrons and holes in TiO_2. Shen *et al.* [116] prepared a (N, Ce)-codoped TiO_2 photocatalyst by the sol-gel route that could degrade nitrobenzene under irradiation with visible light. Nitrogen atoms were incorporated into the TiO_2 crystal structure and narrowed the band gap energy. The dopant cerium atoms existed in the form of Ce_2O_3 and were dispersed on the surface of TiO_2. The improvement in the photocatalytic activity was ascribed to the synergistic effects of nitrogen and cerium codoping. Yang *et al.* [117] codoped TiO_2 with metallic silver and vanadium oxide using a one-step sol-gel solvothermal method in the presence of a triblock copolymer surfactant (P123). The resulting Ag/V-TiO_2 three-component junction system exhibited the highest photocatalytic activity for the degradation of Rhodamine B and Coomassie Brilliant Blue G-250 under both visible and UV light exceeding that of Degussa P25, pure TiO_2, singly-doped TiO_2(Ag/TiO_2 or V-TiO_2).

1.20.5. Coupled/composite TiO_2

It is possible to create coupled colloidal structures, in which illumination of one semiconductor produces a response in the other semiconductor at the interface between them. Coupled semiconductor photocatalysts exhibit very high photocatalytic activity for both gas and liquid phase reactions by increasing the charge separation and extending the energy range of photo excitation. The geometry of particles, surface texture, and particle size play a significant role in inter particle electron transfer. Appropriate placement of the individual semiconductors and optimal thickness of the covering semiconductor are crucial for efficient charge separation.

There has been much interest in coupling different semiconductor particles with TiO_2, with coupled samples such as TiO_2-CdS, Bi_2S_3-TiO_2, TiO_2-WO_3, TiO_2-SnO_2, TiO_2-MoO_3, and TiO_2-Fe_2O_3 being reported [118–121]. The coupled structure that has received the most attention is that consisting of CdS and TiO_2 colloidal particles. It is possible to irradiate CdS with light of lower energy than that needed to electronically excite TiO_2 particles, so the photogenerated electron can be injected from CdS to TiO_2 while hole remains in CdS. The electron transfer from CdS to TiO_2 increases the charge separation and the efficiency of the photocatalytic process. The separated electron and hole are then free to undergo electron transfer with adsorbates

on the surface of the catalyst. Methyl viologen was almost completely reduced using coupled CdS/TiO_2 as a photocatalyst under irradiation with visible light [122]. Bi_2S_3 nano particles with a direct band gap of 1.28 eV area good material for the photosensitization of nanocrystallineTiO_2. The conduction band of Bi_2S_3 nano particles is less anodic than the conduction band of TiO_2 and the valence band is more cathodic than the valence band of TiO_2 [123], enhancing electron injection from the excited state of Bi_2S_3 into TiO_2.

Bessekhouad *et al*. [124] proposed a Bi_2S_3/TiO_2 junction prepared by precipitation of different concentrations of Bi_2S_3 onto TiO_2. Bi_2S_3 absorbed a large portion of visible light and when the junction contained 10 wt% Bi_2S_3, the absorbance started at 800 nm. The coupled system WO_3/TiO_2 has been used as a photocatalyst for decades. Both the upper edge of the valence band and the lower edge of the conduction band of WO_3 are lower than those of TiO_2. WO_3 can be excited by illumination with visible light and the photogenerated holes can transfer from WO_3 to TiO_2.

Song *et al.* [125] observed that loading of WO_3 on the TiO_2 surface improved the decomposition of 1,4-dichlorobenzenein aqueous solution by up to 5.9 times compared with pureTiO_2. Because the standard reduction potential between W (VI) and W(V) is only –0.03 V, it was deduced that electrons in the conduction band of TiO_2 could be easily accepted by WO_3. The electrons in WO_3 would then be transferred to the oxygen molecules adsorbed on the surface of TiO_2.

The coupled system SnO_2/TiO_2, where TiO_2 plays the role of photo sensitizer for SnO_2, also attracts much interest. Pure SnO_2 shows little catalytic activity compared withTiO_2-based photocatalysts because the band gap of SnO_2 (3.5–3.8 eV) is not sufficient to initiate photocatalytic reactions, even after UV illumination. The work function and electron affinity of TiO_2 are both around 4.2 eV while the work function of SnO_2 is around 4.4 eV and its electron affinity is about 0.5 eV larger than that of TiO_2. The Fermi energy level of TiO_2 is higher than that of SnO_2 because of its smaller work function so electron transfer occurs from the conduction band of TiO_2 to the

conduction band of SnO_2 and hole transfer occurs from the valence band of SnO_2 to the valence band of TiO_2 [126].

Vinod Gopal *et al.*[127] reported that the rate of photocatalytic degradation of several textile azo dyes increased by 10 times using an SnO_2/TiO_2 composite system as a result of improved charge separation.

1.21. Advantages of TiO_2 Composites

Additionally, TiO_2 composite structures can create and tune other properties such as mid-band-gap electronic states which can alter charge migration or produce a red shift in the absorption spectrum. Further, formation of heterojunctions between TiO_2 and other materials can yield visible light absorption by the added material with charge separation facilitated by the TiO_2. The two main polymorphs of TiO_2 which show the highest photoactivity are the anatase and rutile phases, which have typically reported band-gap values of 3.2 and 3.0 eV, respectively. Although the band gap of rutile is narrower, the anatase phase is typically considered more favourable as it has a higher reduction potential and a slower rate of recombination of electron–hole pairs [128-130]. However, commercial P25 is one of the most commonly used mixed phase TiO_2 composites. This mixed phase material allows for utilization of visible light wavelengths through excitation of the rutile phase while also containing benefits of anatase TiO_2, such as a decreased recombination rate of charge carriers. The initial mechanism for this enhancement was ambiguous; however, utilizing electron paramagnetic resonance (EPR).

Hurum et al. [131] studied the fate of photogenerated charge carriers in order to shed light on the mechanism. They found that electrons which were photogenerated by the rutile component were transferred to a previously proposed electron trap site in the anatase lattice which lies 0.8 eV below the anatase conduction band. Further, this is situated lower than the rutile conduction band. A decrease in electron–hole recombination is achieved since the photogenerated holes remain within the rutile component and the electrons are spatially separated into the anatase component. It was later determined that the photogenerated holes are preferentially trapped on the surfaces, whereas electrons become trapped within the lattice. As such surface electron

trap sites increase the recombination rate, which indicates that a composite with a second material which is either a hole or an electron sink can further increase catalytic efficiency [132-133].

Beyond the use of mixed phase TiO_2, composites with non-TiO_2 materials are a very promising means to extend the usefulness of anatase into the visible wavelengths. Alternatively, for composites consisting of the rutile phase, inclusion of higher work function materials can yield slower charge carrier recombination. Other methods to decrease charge carrier recombination include increasing crystallinity, which can be done by high-temperature calcination, addition of dopants, or specific synthetic protocols [134]. Additionally, defects, which can serve as charge carrier traps and reduce the recombination of photogenerated electron−hole pairs, can also be either induced or stabilized by formation of a composite. Composites which can help to tune the grain size have also been shown, such as metal oxide sol−gel precursors which can form composites with TiO_2 and inhibit crystallinity [135].

In addition to the improvement of photocatalysis, composite structures can yield other benefits. Such advantages include the ability to tune the surface properties, i.e., acidity/basicity or open coordination sites, of the resultant materials, which is of importance to the adsorption of molecules, a critical factor relevant to catalysis, separation, and further modification. Numerous mixed metal oxide/TiO_2 composites are beneficial for stabilization of thermal catalysts where reactions such as high-temperature NO_x reduction are improved. Composites such as core−shell materials are also beneficial toward the stabilization of nanoparticles against phenomena such as sintering or aggregation. Further, composites can be of great use to create highly porous materials, hollow shells, or hierarchical structures by templating methods [136].

1.22. Polymer composites with Titania

1.22.1. Polyaniline/Titania nanocomposites

In recent years, the composites of conductive polymers and inorganic particles have been the focus of a great deal of research due to their potential applications in chemical sensing, catalysis, energy storage, solar cells, and medical diagnosis [137].

However, the application of this new type of materials as adsorbent in wastewater treatment, especially in the removal of dyes from printing and dyeing wastewater, is seldom reported. Polyaniline (PANI) has attracted considerable attention for its low cost, simple synthesis, excellent electrical conductivity, thermal stability, antioxidant properties, and so on [138]. The unique reversible electrochemical activity, large specific surface area, good stability, and doping–dedoping reversibility, etc., make the adsorption and desorption of ions on PANI possible by simple acid and alkali treatment. The use of polyaniline as adsorbent for dye removal has been reported recently [139]. However, PANI, as a significant conductive polymer material with low mass density, is hard to be settled, which restricts the application as the adsorbent for the difficulty of recovery.

1.22.2. Titania composites with Graphene and Graphene Oxide

Graphene with many extraordinary properties such as high electron mobility and surface area has been investigated broadly with respect to composites with TiO_2 over the past decade. Similar to the case of carbon nanotubes, the higher work function of graphene (~4.9–5.2 eV) with respect to on the surface of amine-functionalized amorphous TiO_2 microspheres. TiO_2 allows for an increase in charge separation by electron injection into the graphene sheets. Chemical utilization of graphene has been established through reduction of graphene oxide (graphitic oxide, GO) sheets, which are commonly synthesized by the Hummers method or a modification methods [140]. Reduction is done by number of means such as by hydrothermal/solvothermal treatment or, more frequently, in situ with TiO_2 deposition. One recent study by Zhu et al.[141] simultaneously formed the graphene/TiO_2 composite and reduced the GO sheets by utilizing $TiCl_3$ as the reductant for GO and precursor for TiO_2. Concurrent reduction of GO and crystallization of TiO_2 is one of the optimal methods as it provides good contact between the two materials with well-crystallized morphology. It must be noted that reduction is not always carried out in prior reports, and many claimed graphene/TiO_2 composites are in reality graphene oxide/ TiO_2. These graphene/TiO_2 composites have shown applications in the construction of DSSCs, Li^+ battery applications, and enhanced photocatalysis [142-144].

One simple composite reported by Zhang et al. [145] consisted of graphene oxide mixed with P25. The components were mixed and held at 120 °C for 3 h in water−ethanol mixture within a Teflon-sealed autoclave to achieve both reduction of the GO and deposition on P25. This P25−graphene (P25−GR) composite showed improved photoactivity for degradation of methylene blue under both UV and visible light irradiation, as compared to bare P25, and a slight improvement when compared to a P25−carbon nanotube composite.

These composites were then hydrothermally treated to reduce the GO, followed by calcination under argon at 400 °C. The composite structure after the negatively charged graphene oxide is wrapped on the positively charged TiO_2. At this stage, the graphene oxide has been reduced to graphene and the TiO_2 has crystallized to anatase phase. Samples showed improved photocatalytic activity compared to a two-step method where GO was coated on precalcined anatase microspheres and then subsequently reduced, indicating that the order of preparation was critical. Degradation of MB by visible light is improved photocatalytic activity of the composite as compared to P25, bare anatase particles [146].

1.23. Factors influencing the photocatalytic degradation

The oxidation rates and efficiency of the photocatalytic system are highly dependent on a number of operational parameters that govern the photodegradation of the organic molecule [147]. This section will briefly discuss the significance of each operational parameter.

1.23. 1. Effect of dye concentration

The quantity of the dye adsorbed on the surface of the photocatalyst is of foremost importance since only this amount contributes to photocatalytic process and not the one in the bulk of the solution. The extent of dye adsorption depends on the initial dye concentration. The initial concentration of dye in a given photocatalytic reaction is an important factor which needs to be taken into account. Generally speaking, the percentage degradation decreases with increasing amount of dye concentration, while keeping a fixed amount of catalyst [148]. This can be rationalized

on the basis that as dye concentration increases, more organic substances are adsorbed on the surface of TiO_2, whereas less number of photons are available to reach the catalyst surface and therefore less •OH are formed, thus resulting in less degradation percentage.

1.23.2. Effect of catalyst amount

Dye degradation is also influenced by the amount of the photocatalyst and aggregation of catalyst particles in high amounts of catalyst. The dye degradation increases with increasing catalyst concentration, which is characteristic of heterogeneous photocatalysis [148]. The increase in catalyst amount actually increases the number of active sites on the photocatalyst surface thus causing an increase in the number of •OH radicals which can take part in actual discoloration of dye solution. Beyond a certain limit of catalyst amount, the solution becomes turbid and thus blocks UV radiation for the reaction to proceed and therefore percentage degradation starts decreasing [149].

1.23.3. Effect of pH

Photodegradation efficiency of dyes is affected by the pH of the solution. The variation of solution pH changes the surface charge of TiO_2 particles and shifts the potentials of catalytic reactions. As a result, the adsorption of dye on the surface is altered thereby causing a change in the reaction rate. Under acidic or alkaline condition the surface of Titania can be protonated or deprotonated respectively according to the following reactions [150]:

$$\mathbf{TiOH + H^+ \rightarrow TiOH_2^+} \quad \text{……………………………………}(5)$$

$$\mathbf{TiOH + OH^- \rightarrow TiO^- + H_2O} \quad \text{……………………………..}(6)$$

Thus Titania surface remains positively charged in acidic medium and negatively charged in alkaline medium. Titanium dioxide is reported to have higher oxidizing activity at lower pH, but excess H^+ can decrease reaction rate. TiO_2 behaves as a strong Lewis acid due to the surface positive charge. The anionic dye, on the other hand, is a fused polynuclear aromatic compound with an extensive π electron conjugation which can easily form a stable complex by donating electrons to the

vacant d orbital of titanium. In other words, the anionic dye acts as a strong Lewis base and can easily adsorb on the positively charged catalyst surface. This favours the adsorption of the dye under acidic conditions, while in the alkaline conditions this complexation process is not favoured presumably because of competitive adsorption by hydroxyl groups and the dye molecule in addition to the Coulombic repulsion due to the negatively charged catalyst with the dye molecule [151].

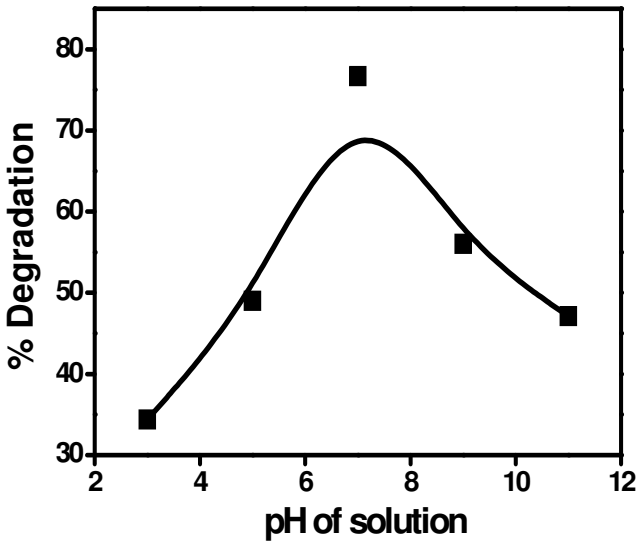

Fig.1.11. Effect of pH of solution on photodegradation

The extent of dye adsorption depends on the initial dye concentration, nature of the dye, surface area of photocatalyst and pH of the solution. The pH determines the surface charge of the photocatalyst. Adsorption of the dye is minimum when the pH of the solution is at the isoelectric point (point of zero charge). The surface of the photocatalyst is positively charged below isoelectric point and carries a negative charge above it. Depending on the nature of dye that needs to be adsorbed on the surface of a photocatalyst, the adsorption can be low or high in acidic and basic media. At low pH, reduction by electrons in conduction band plays a very important role in the degradation of dyes due to the reductive cleavage of azo bonds [152–153]. Acid Orange 7 (an anionic dye) has shown to degrade more at pH 3 [154]. The rationale behind this is that at low pH values, more H+ are available for adsorption to mask the surface of the catalyst thus preventing the photoexcitation of semiconductor particles,

thereby reducing the generation of free radicals. In alkaline solutions, •OH radicals are easier to be generated by oxidizing more hydroxide ions available on TiO2 surface, thus the efficiency of the process is increased [155]. Similar results have been reported in the photocatalysed degradation of diazo and triazo dyes [156]. Fig. 1.11 shows the trend in % degradation of azo dye at different pH values.

1.23.4. Size and structure of the photocatalyst

Surface morphology such as particle size and agglomerate size is an important factor to be considered in photocatalytic degradation process because there is a direct relationship between organic compounds and surface coverage of the photocatalyst [157]. The number of photon striking the photocatalyst controls the rate of reaction which signifies that the reaction takes place only in the absorbed phase of the photocatalyst [158]. A number of different forms of TiO_2 have been synthesized to achieve the desired characteristics of the photocatalyst [159]. For the degradation of various organic compound such as pesticides and dyes, the efficacy of these photocatalysts has generally been reported in the order of Degussa P25 > UV100 > PC500 >TTP [160-161].

1.23.5. Surface area

Surface morphology of TiO_2 is a crucial factor in its use as photocatalyst, as all the chemical events take place at the surface, its enlargement has been attempted, usually by using very fine particles, either suspended in solvents or made into a porous film. Nanostructured materials with the crystallite/grain size below 20 nm are of great research interest mainly due to the fact that their physical properties may be markedly different from the bulk counter parts. This has also opened up avenues for their applications as photocatalyst in numerous areas. Significant alteration reported in properties, viz., porosity, band gap and effective surface area of metal oxide semiconductors, when these are obtained in nanodimensions has drawn the attention of researchers working in the area of heterogeneous photocatalysis [162]. The surface area of materials increases with increasing the fragmentation of particle. The surface

area of material is showing in Fig.1.12 showing. The breakdown of particle in several small particles is increase the surface area of materials.

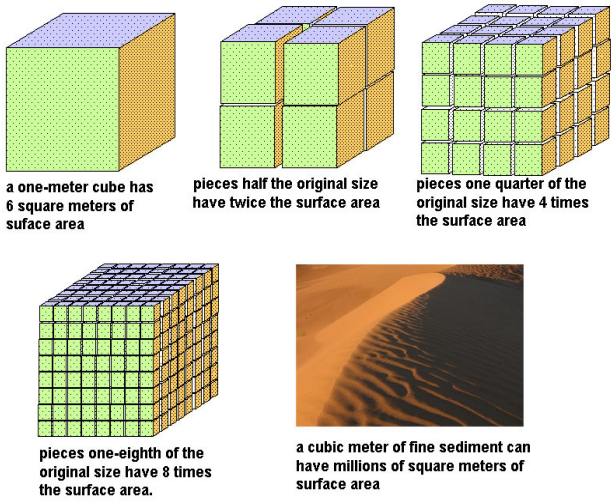

Fig.1.12. Effect of surface area

1.23.6. Reaction temperature

An increase in reaction temperature generally results in increased photocatalytic activity however reaction temperature >80 ^{o}C promotes the recombination of charge carriers and disfavour the adsorption of organic compounds on the Titania surface [163]. A reaction temperature below 80^{o}C favours the adsorption whereas further reduction of reaction temperature to 0^{o}C results in an increase in the apparent activation energy [164]. Therefore temperature range between 20-80^{o}C has been regard as the desired temperature for effective photomineralization of organic content.

1.23.7. Concentration and nature of pollutants

The rate of photocatalytic degradation of certain pollutant depends on its nature, concentration and other existing compounds in water matrix. A number of studies have reported the dependency of the TiO_2 reaction rate on the concentration of contaminants in water [165]. High concentration of pollutants in water saturates the TiO_2 surface and hence reduces the photonic efficiency and deactivation of the

photocatalyst [166]. In addition to the concentration of pollutants, the chemical structure of the target compound also influences the degradation performance of the photocatalytic reactor. For example, 4-chlorophenol requires prolonged irradiation time due to its transformation to intermediates compared with oxalic acid that transforms directly to carbon dioxide and water, i.e., complete mineralization [167].

Furthermore, if the nature of the target water contaminants is such that they adhere effectively to the photocatalyst surface the process would be more effective in removing such compounds from the solution. The photocatalytic degradation of aromatics is highly dependent on the substituent group [168]. The organic substrates with electron withdrawing nature (benzoic acid, nitrobenzene) strongly adhere to the photocatalyst and therefore are more susceptible to direct oxidation compared with the electron donating groups [169].

1.23.8. Inorganic ions

Various inorganic ions such as magnesium, iron, zinc, copper, bicarbonate, phosphate, nitrate, sulfate and chloride present in wastewater can affect the photocatalytic degradation rate of the organic pollutants because they can be adsorbed onto the surface of TiO_2 [170]. Photocatalytic deactivation has been reported whether photocatalyst is used in slurry or fixed-bed configuration which is related to the strong inhibition from the inorganic ions on the surface of the TiO_2 [171]. A number of studies have been conducted on the effect of inorganic ions (anions and cations) on TiO_2 photocatalytic degradation [172]. Some of the cations such as copper ions and phosphate have been reported to decrease the photodegradation efficiency if they are present at certain concentrations whereas calcium, magnesium, and zinc have little effect on the photodegradation of organic compounds which is associated to the fact that these cations have are at their maximum oxidation states that results in their inability to have any inhibitory effect on the degradation process [173].

The inorganic anions such as nitrate, chlorides, carbonates, and sulphates are also known to inhibit the surface activity of the photocatalyst. The presence of salts diminishes the colloidal stability, increases mass transfer and reduces the surface contact between the pollutant and the photocatalyst [174]. Other than fouling of the

TiO_2 surface certain anions such as chlorides, carbonates, phosphate, and sulphates also scavenge both the hole and the hydroxyl radicals [175]. The mechanism of hole and radical scavenging by chloride has been proposed by Matthews and McEnvoy [176] as follows.

$$Cl^- + {}^{\bullet}OH \rightarrow Cl^{\bullet} + OH^- \quad \text{..... (7)}$$

$$Cl^- + h^+ \rightarrow Cl^{\bullet} \quad \text{..... (8)}$$

The inhibitory effect of chloride ions occurs through preferential adsorption displacement mechanism which results in reducing the number of OH- available on the photocatalyst surface [177]. The fouling of photocatalytic surface can be reduced by pre-treatment of water such as with ion exchange resins which have been reported to reduce the fouling and so the cost of treatment [178]. Similarly, the fouling induced by sulphates and phosphates has been reported to be displaced by NaOH, KOH, and $NaHCO_3$ [179]. However, most of studies conducted on the effect of inorganic ions are based on the model compounds and therefore do not necessarily represent their effect in real water matrix where several ions exist. More work concentrating on the effect of complex mixtures of inorganic ions is thus required.

1.23.9. Effect of light intensity and irradiation time

Both light intensity and time of irradiation affect the dye degradation [180]. It has been shown that at low light intensities (0–20 mW/cm2), the rate would increase linearly with increasing light intensity (first order), whereas at intermediate light intensities (25 mW/cm2) the rate would depend on the square root of the light intensity [181]. At high light intensities, the rate is independent of light intensity because at low light intensity reactions involving electron–hole formation are predominant and electron–hole recombination is negligible. On the other hand, when light intensity is increased, the electron–hole pair separation competes with recombination, thereby causing lower effect on the reaction rate. In many literature studies, it has been shown that the dye decolorization initially increases as the light intensity is increased [182]. The reaction rate decreases with irradiation time as it follows the pseudo first-order kinetics and additionally a competition for degradation may occur between the reactant and the intermediate products. The slow kinetics of dye degradation after certain time

limit is mainly attributed to the difficulty in the reaction of short chain aliphatics with •OH radicals, and the short lifetime of photocatalyst because of active sites deactivation by strong by-products deposition [183].

1.23.10. Dissolved oxygen

Oxygen dissolved in solution is commonly employed as an electron acceptor in photocatalysis reaction to assure sufficient electron scavengers present to trap the excited conduction band electron from recombination [184]. The oxygen does not affect the adsorption on the TiO_2 catalyst surface as the reduction reaction takes place at a different location from where oxidation occurs. Dissolved oxygen involves in the stabilization of radical intermediates, mineralization, and direct photocatalytic reactions.

Its presence is also known to induce the cleavage mechanism for aromatic rings in organic pollutants that are present in the water matrices [185].

1.23.11. Effect of dopants on dye degradation

Heterogeneous photocatalysis involving titanium dioxide (TiO_2) appears to be the most promising technology for organic dyes degradation. However one of the major problems in using TiO_2 as a catalyst is the low photo-quantum efficiency which arises from the fast recombination of photogenerated electrons and holes. Moreover, TiO_2 is inactive under visible light due to its wide band gap (3.03 eV for rutile and 3.18 for anatase form). This inherently causes the inability to make use of the vast potential of solar photocatalysis. Various techniques have been employed to make TiO_2 absorb photons of lower energy as well. These techniques include surface modification via organic materials and semiconductor coupling, band gap modification by creating oxygen vacancies and oxygen sub-stoichiometry, by non-metals including co-doping of non-metals and metal doping. Dopants, such as transitional metals have been added to the TiO_2 catalyst to improve its response and also reduce the recombination of photogenerated electrons and photogenerated holes [186–188]. The main objective of doping is to induce a bathochromic shift, i.e., a decrease of the band gap or introduction of intra-band gap states, which results in more visible light

absorption. The effect of metal ion dopants on the photocatalytic activity is a complex problem. The total induced alteration of the photocatalytic activity is made up from the sum of changes which occur in the light absorption capability of the TiO_2 photocatalyst, adsorption capacity of the substrate molecules at the catalyst's surface and interfacial charge transfer rate. Using suitable transitional metals as dopants improves the performances of TiO_2 [189]. This results in the overlap of the conduction band due to Ti (3d) with d levels of the transition metals causing red shift of the band edge of TiO_2. It can thus also allow the light absorption to be widened into the visible region to various extents, depending on the type of the dopant and its concentration. Therefore the photocatalysis on modified TiO_2 can be promoted using visible light. Various transition metals, such as Ni^{2+}, Zn^{2+}, Cr^{3+} and Fe^{3+} can be easily incorporated into the crystal lattice of TiO_2 because of their similar ionic radii (The ionic radii of Ni^{2+}=0.72 Å, Zn^{2+}=0.74 Å, Cr^{3+}= 0.76 Å and Fe^{3+}=0.69 Å are quite similar to that of host Ti^{4+}=0.75 Å ions) [190]. The degradation of dyes is usually faster in mixed systems as compared to single systems, because the oxidation of dyes consumes photo-excited holes promptly and efficiently, thus attenuating electron–hole recombination.

1.24. Application of photocatalysis

1.24. 1. Waste water treatment

A number of important features for the heterogeneous photocatalysis have extended their feasible applications in water treatment, such as;

(1) Ambient operating temperature and pressure.

(2) Complete mineralization of parents and their intermediate compounds without secondary pollution and

(3) Low operating costs.

The fact that the highly reactive oxygen species (ROS) generated as a result of the photo-induced charge separation on TiO_2 surfaces for microbial inactivation and organic mineralization without creating any secondary pollution is well-documented. So far, the application of such TiO_2 catalysts for water treatment is still experiencing a series of technical challenges [191].

Fig.1.13. Waste water treatment by photodegradation

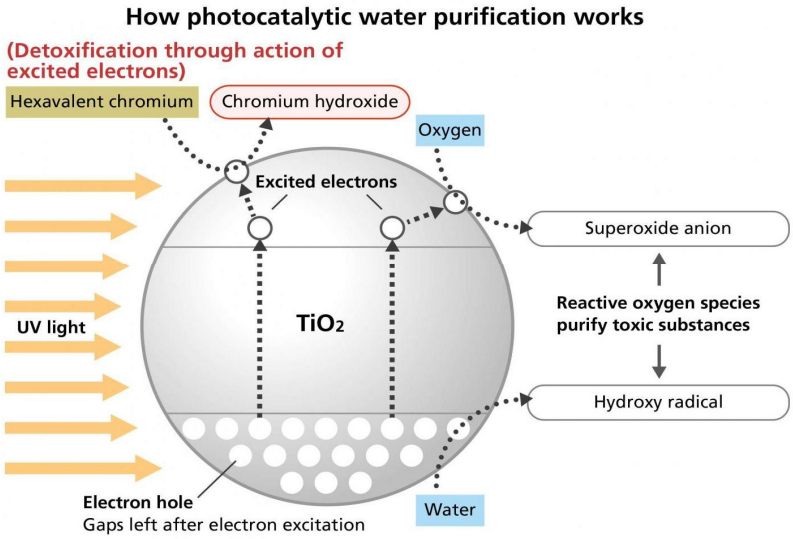

Fig.1.14. Mechanism of water treatment by photodegradation

The post-separation of the semiconductor TiO_2 catalyst after water treatment remains as the major obstacle towards the practicality as an industrial process. The fine particle size of the TiO_2, together with their large surface area-to-volume ratio and surface energy creates a strong tendency for catalyst agglomeration during the

operation. Such particles agglomeration is highly detrimental in views of particles size preservation, surface-area reduction and its reusable lifespan [192]. Other technical challenges include in the catalysts development with broader photoactivity range and its integration with feasible photocatalytic reactor system.

In addition, the understanding of the theory behind the common reactor operational parameters and their interactions is also inadequate and presents a difficult task for process optimization. A number of commonly made mistakes in studying kinetic modelling on either the photomineralization or photo-disinfection have also been seen over the years. A short outlines of the feasible application of photocatalytic water technology via life cycle interpretation and the possible future challenges are also recommended [193].

1.24.2. Sensing Properties of Titanium Oxide

When gas absorbs onto the TiO_2 surface, it could release electrons into TiO_2, leading to the increase or decrease of resistance of TiO_2 materials, the typical sensing mechanism of TiO_2-based gas sensor. Furthermore, the conductivity property can be modified by doping other elements (especially metal elements) into TiO_2 materials. By controlling the doping pattern, such as doping dosage and heating temperature, the n-type TiO_2 materials can be transformed to p-type [194]. Different from n-type, the resistance of p-type TiO_2 will increase when contacting gases. On the other hand, TiO_2 is an excellent photocatalyst for two structural properties: first, the valence band of TiO_2 is quite deep; second, the photon generated holes tend to locate on the surface of materials, which makes it easy to be harvested by free electrons from outside, that is, working as an oxidant agent.

It has inherent surface band bending that forms spontaneously in a deep region with a steep potential [195]. Thus, its surface hole trapping dominates because spatial charge separation is achieved by the photogenerated holes transfer toward the surface of the particle via the strong upward band bending. However, in the rutile phase, the bulk recombination of electrons and holes inevitably occurs, and only the holes close to the surface are trapped and transferred to the surface. These advantages make Anatase phase the most competitive candidate for COD sensor because of its good

electron transfer capability and chemical stability. Furthermore, the photovoltaic property of TiO_2 under UV illumination makes the sensors self-clean the contamination, resulting in a long life span [196].

TiO_2 nanomaterials are basically biocompatible and environmentally friendly and have been frequently proposed as a prospective interface for the immobilization of biomolecules [197] which is another important aspect for TiO_2 materials. Moreover, titanium forms coordination bonds with the amine and carboxyl groups of enzymes and maintains the enzyme's biocatalytic activity [198]. In addition, due to the electron accepting character of TiO_2 as discussed above, the electrons produced by the reaction between biomolecules and analyte can be harvested by TiO_2. The injected electrons can be transferred to the outer circuit, which can be used to detect the reaction. With all aforementioned merits, TiO_2 is one of the most competitive candidates for biosensor. Because a particular sensing purpose can only be achieved with a specific TiO_2 property, the types of TiO_2 phase, composition, and nanostructures feature are decisive factors for sensor performance [199].

1.24.3. Sensing Electrode of TiO_2 Nanomaterials

It is commonly recognized that nanostructured TiO_2 is more favourable for sensor applications due to their advantages of larger surface area and better electron transition. In the past decade, TiO_2 nanotube arrays (NTs) obtained from electrochemical oxidation reaction of a metallic titanium substrate are the most popular nanostructure. In a typical process, TiO_2 NTs can be prepared by anodization of titanium foil in the F-containing electrolyte at a constant anodization potential [200]. The geometry of TiO_2 NTs could be varied according to the anodization voltage, duration, and electrolyte composition. Various technical alloys can also be anodized to fabricate nanotube layers using the same approach as for Ti. TiO_2 nanotubes can be prepared using a liquid-phase deposition (LPD) method [201].

1.24.4. Water Splitting on TiO_2- Based Photocatalysts.

Gra□tzel and co-workers intensively investigated a bifunctional colloidal TiO_2 loaded with Pt and RuO_2 [202-203]. The H_2 generation quantum yield in the overall

water splitting reaction was up to 30% at 310 nm. In this system, Pt is the H_2 evolution site, while RuO_2 is the O_2 evolution site. By using $Ru(bpy)_3^{2+}$ or Rhodamine B as a sensitizer, overall water splitting reaction was realized under visible light irradiation. Some modified TiO_2, such as chromium-doped TiO_2 [204] and boron oxides modified TiO_2 were also found to exhibit overall water splitting activity but with rather low efficiencies.

1.24.5. Photocatalytic sterilization

TiO_2 photocatalysts can be used to kill bacteria and, therefore, self-sterilizing surfaces can be prepared. The first work of this type was carried out with *E. coli* suspensions [205]. A typical experiment involves placing 150 ml of an *E. coli* suspension, containing cells on an illuminated TiO_2 coated glass plate (1mWcm−2 UV light) [206]. Under these conditions, there were no surviving cells after only 1 h of illumination. By contrast, after 4 h under UV illumination without a TiO_2 film, only 50% of the cells were killed.

1.24.6. Photocatalytic cancer treatment

Cancer treatment is one of the most important topics that are associated with photocatalysis. While surgical, radiological, immunological, thermo therapeutic, and chemotherapeutic treatments have been developed and are contributing to patient treatment, cancer has remained the top cause of death in Japan since 1980. As far back as the mid-1980s, we were interested in using the strong oxidizing power of illuminated TiO_2 to kill tumor cells [207]. In the first experiments a polarized, illuminated TiO_2 film electrode, and an illuminated TiO_2 colloidal suspension was also found to be effective in killing HeLe cells. A series of studies followed, in which we examined various experimental conditions, including the effect of superoxide dismutase, which enhances the effect, due to the production of peroxide. In addition, it was found possible to selectively kill a single cancer cell using a polarized, illuminated TiO_2 microelectrode [208].

1.25. Objectives of the present work

In view of tremendous properties and applications of TiO_2 and TiO_2 based materials author is enthusiastic to further extends to undertake a detailed systematic investigation on the photocatalysed oxidative degradation of some target substrates (dyes) using Titania nanocomposites as photocatalyst. The proposed study would also attempt to evaluate the kinetic and thermodynamic parameters of the photodegradation process. The main objectives of the study use as under:

[1]. Synthesis of Titania nanoparticle by wet-chemical methods (sol-gel and solution impregnation).

[2]. Doping of different metals (Cu, Ni, Co, and La) was done in Titania by chemical methods.

[3]. Synthesis of PAni was done by chemical oxidation.

[4]. Synthesis of PAni/TiO_2 nanocomposites was done by chemical oxidation method.

[5]. Synthesis of PAni/TiO_2/GO nanocomposites was done by chemical oxidation method.

[6]. Synthesis of Polypyrrole/TiO_2 nanocomposites was done by wet chemical methods.

[7]. Synthesis of Polypyrrole/TiO_2/GO nanocomposites was done by wet chemical methods.

[8]. Characterization of the prepared samples of photocatalyst nanocomposites has been done. XRD analysis, BET, SEM, TEM, FTIR, UV-Vis, Fluorescence spectroscopy and band gap energy.

[9]. Photocatalytic degradation of carboxylic acids, viz., oxalic acid, citric acid, tartaric acid and acetic acid in the presence of photocatalyst and illumination.

[10]. Photocatalytic degradation of dyes (viz., methyl red, Methyl blue, Methyl orange, Victoria blue, Rose bengal, Thymol blue, and Eriochrome Black T) have been done.

[11]. Estimation and computation of kinetic and thermodynamic properties for degradation processes.

References

[1]. W. Dudefoi, A. Villares, S. Peyron, C. Moreau, B. Cathala, 10.1016/j.ifset. 2017.09.007, Available online 15 September (2017).

[2]. Y. Badr, M.G Abd El-Wahed, M.A. Mahmoud, J. of Hazardous Materials, 154, 1-3, (2008), 245-253

[3]. F. Cao, G.J. Oskam., S. Meyer, and P.C. Searson, J. Phy.Chem.B, 100, (1996) 17021.

[4]. G.L. Hornyak, A.K. Rao, Chapter 2: Fundamentals of Nanoscience Nanoscience in Dermatology, (2016), 15-29

[5]. D. Beydoun and R. Amal J. Phys. Chem. B, 104 (18), (2000), 4387–4396.

[6]. R. I. Bickley, G. Munuera, and F. S. Stone, J. Catal31, (1973), 398

[7]. G.L. Hornyak, H.F. Tibbals, and J. J. Moore, Fundamentals of Nanotechnology, ISBN 9781420048032, (2008)

[8]. A. Akyol, M. Bayramoglu, Chemical Engineering and Processing: Process Intensification, 47, 12, (2008), 2150-2156

[9]. H.F. Tibbals, G.L. Hornyak, J. Dutta, Introduction to Nanoscience and Nanotechnology, ISBN 9781420047790

[10]. M.F. Ashby, Nanomaterials, nanotechnologies and design, ISBN: 9780080941530, (2009),

[11]. S.C. Ameta, P.B. Punjabi, P. Rao, and B. Singhle, J. Indian Chem Soc., 77, (2000), 157-160.

[12]. L. Armelao, Barreca.D, Bertapelle.M, Balttaro.G, Sada.C, and Tondello.E, thin solid films, 442, (2003), 48.

[13]. G.D. Arora, (2000), Crystallography and Crystal Structure, Ist edition, Sarup, and Sons: New Delhi, India.

[14]. G. Cao, Nanostructures & nanomaterials, ISBN: 978-981-4324-55-7, (2004)

[15]. V.M. Aroutiounian, V.M. Arakelyan, G.E. Shahnazaryan, G.M. Stepanyan, J.A. Turner, O.Khaselev, Int. J. Hydrogen Energy, 27, (2002), 33.

[16]. D.R. Askland, The Science and Engineering of Materials, Third Edition, London, Chapman & Hall, 854, (1996).

[17]. B. Balamurugan, B.R. Mehta, Thin solid films, 396, (2001), 90.

[18]. C.G. Silva, W. Wang, J.L. Faria, J. of Photochemistry and Photobiology A: Chemistry, 181, (2006), 314-324.

[19]. C. Chen, X. Li, W. Ma, J. Zhao, H. Hidaka, N. Serpone, J. Phys. Chem. B 106, (2002), 318–324.

[20]. C. Xu, R. Killmeyer, M. L. Gray, S.U.M. KhanApplied Catalysis B: Environmental, 64, 3-4, (2006), 312-317

[21]. L.C. Chen. Y.C. Ho. W.S. Guo. C.M. Huang. and Pan.T.C, Electrochimica Acta, 54, (2009), 3884-3891.

[22]. B. Damardji. H. Khalaf, L. Duclaux, and B. David, Applied Clay Science, 44, (2009), 201-205.

[23]. A. Fujishima, Nature 238, (1972), 37.

[24]. G. A. Epling, C. Lin, Chemosphere, 46, 6, (2002), 937-944

[25]. G. A. Epling, C. Lin, Chemosphere, 46, 4, (2002), 561-570

[26]. M. Gratzel, Research opportunities in Photochemical science, Dept. of Energy, 34 (6), (1996), 1221-1230, USA.

[27]. F. Han., M. Srinivasan., D. Rajarathnam, and R. Naidu, Applied Catalysis A: General, 359, (2009), 25-40

[28]. M.M. Haque, M. Muneer, J. of Hazardous Materials, 145, 1-2, (2007), 51-57

[29]. http://www.mchnanosolutions.com/mechanism.html

[30]. H. Lachheb, E. Puzenat, A. Houas, M. Ksibi, E. Elaloui, C. Guillard, J.M. Herrmann, Applied Catalysis B: Environmental, 39, 1, (2002), 75-90

[31]. http://diposit.ub.edu/dspace/bitstream/2445/55763/1/TFG_QU%20Broch%2c%20Mireia.pdf

[32]. H. Jia, Z. Zheng, H. Zhao, L. Zhang, and Z. Zou, Materials Research Bulletin, 44, (2009), 1312-1316.

[33]. K.S. Go, S.R. Son, S.D. Kim, Int. J. of Hydrogen Energy, 33 21, (2008), 5986-5995

[34]. http://www.mchnanosolutions.com/mechanism.html

[35]. M. Kaneko, and I. Okura, (2002), Photocatalysis: Science and Technology (Springer, Berlin, 2002).

[36]. C. Karunakaran, and R. Dhanalakshmi, Solar Energy Materials and Solar Cells, 92, (2008), 1315-1321.

[37]. A. Mills, M. McGrady, J. Wang, and J. Hepburn, International Journal of Photoenergy, Article ID 504945, (2008), 6 pages

[38]. C. Richard, F. Bosquet, J.F. Pilichowski, Journal of Photochemistry and Photobiology A: Chemistry, 108, 1, (1997), 45-49

[39]. R. Khan, and T.J. Kim, J. of Hazardous Materials, 163, (2009), 1179-1184.

[40]. J.M. Herrmann, Catalysis Today, 53, (1999), 115-129

[41]. https://pavemaintenance. wikispaces.com/TiO_2+Photocatalys+-+Shannon

[42]. H.P. Klug, L.E. Alexander, X-ray Diffraction Procedures for Polycrystalline and Amorphous Materials, New York, Wiley (1974).

[43]. A. Li Bassi, D. Cattaneo, V. Russo, and C. E. Bottani, Journal of Applied Physics 98, (2005), 074305

[44]. M. Muruganandham, M. Swaminathan, Solar Energy Materials and Solar Cells, 81, 4, (2004), 439-457.

[45]. A. O. Ibhadon and P. Fitzpatrick, Catalysts 3, (2013), 189-218.

[46]. C.Y. Kuo, and H.Y. Lin., J. of Hazardous Materials, 165, (2009), 1243-1247

[47]. B. Xiang, Y. Li, C.H. Pham, F. Paesani and W. Xiong, Science Advances (2017): 3, e1701508

[48]. A. Vilan, D. Cahen, M. Case, Chem. Rev. 117, (2017), 4624–4666.

[49]. A. L. Ayzner, S. C. Doan, B. T. De Villers, B. J. Schwartz, J. Phys. Chem. Lett. 3, (2012), 2281–2287.

[50]. F. Deng, L. Min, X. Luo, S. Wu, & S. Luo, Nanoscale, 5, (2013), 8703–8710.

[51]. D. Guan, Q. Yu, C. Xu, C. Tang, L. Zhou, D. Zhao, L. Mai, Nano Research, 10, (2017),4351–4359.

[52]. J. Tersoff, Phys. Rev. B 32, (1985), 6968(R),

[53]. J.H. Koh, J.T. Park, D.K. Roh, J.A. Seo, and J.H. Kim, A: Physicochemical and Engineering Aspects, 329, (2008), 51-57.

[54]. R. Asahi, T. Morikawa, T. Ohwaki, K. Aoki, Y. Taga. Science , 293, (2001), 269-271.

[55]. H. Irie, Y. Watanabe, K. Hashimoto, J Phys Chem B: 4, (2003), 5483-5486.

[56]. T. Ihara, M. Miyoshi, Y. Triyama, O. Marsumato, S. Sugihara, Appl Catal B, 42, (2003), 403-409.

[57]. A. Zaleska, Recent Patents on Engineering 2, (2008), 157-164.

[58]. K. Takeshita, A.Yamakata, T. Ishibashi, H. Onishu, K. Nishijima, T. Ohno, J. Photochem Photobiol 177, (2006), 269-275.

[59]. J.C. Colmenares, Y.J. Xu, Heterogeneous Photocatalysis: From Fundamentals to Green Applications, ISBN 978-3-662-48719-8

[60]. M. Mrowetz, E. Selli, J. of Photochemistry and Photobiology A: Chem. 162, 1, (2004), 89-95

[61]. J.W. Shi, S.H. Chen., S.M. Wang, P. Wu, G.H. Xu., J. of Molecular Catalysis A: Chemical, 303, (2009), 141-147.

[62]. R. Amadelli, A. Molinari, I. Vitali, L. Samiolo, G.M. Mura, A. Maldotti, Catalysis Today, 101, 3-4, (2005), 397-405

[63]. A. Zdravkov, J. Kudryashova, A. Kanaev, A. Povolotskiy, Materials Chemistry and Physics, 160, 2015, 73-79

[64]. T. Ohno, T. Mitsui, M. Matsumura, Chem Lett, 32 (2003), 364-365.

[65]. R. Niishiro, H. Katoa and A. Kudo, Phys. Chem. Chem. Phys., 7, (2005), 2241–2245.

[66]. J. Lu, H. Jin, Y. Dai, K. Yang, and B. Huang, Int. J. of Photoenergy , Article ID 928503, 8 pages, (2012), doi:10.1155/2012/928503

[67]. T. Sun, J. Fan, E. Liu, L. Liu, Y. Wang, H. Dai, Y. Yang, W. Hou, X. Hu, Z. Jiang, Powder Technology 228, (2012), 210–218.

[68]. Y. Wu, G. Lu, S. Li. J Photochem Photobiol A Chem (2006), 181:263e7

[69]. Y. Wu, G. Lu, and Shuben, J. Phys. Chem. C, , 113 (22), (2009), 9950–9955

[70]. R. Asahi, T. Morikawa, T. Ohwaki, K. Aoki, and Y. Taga, Science, 293, (2001), 269–275,

[71]. H.M. Yates, M.G. Nolan, D.W. Sheel, and M.E. Pemble, J. of Photochemistry and Photobiology A: Chemistry, 179, (2006), 213–223,

[72]. M.R. Hoffmann, S.T. Martin, W. Choi, and W. Detlef, Chem. Rev. 95, (1995), 69-96.

[73]. K. Hashimoto, H. Irie, A. Fujishima, J. Appl. Phys. 44, (2005), 8269–8285.

[74]. J. Peral, X. Domenech, D.F. Ollis, J. Chem. Technol. Biotechnol. 70, (1997), 117–140.

[75]. X. Chen, S. S. Mao, Chem. Rev. 107, (2007), 2891–2959.

[76]. L. Cavigli, F. Bogani, A. Vinattieri, V. Faso, G. Baldi, J. Appl. Phys., 106, (2009), 053516

[77]. M.M. Mohamed, I. Othman and R.M. Mohamed., J. of Photochemistry and Photobiology A: Chemistry, 191, (2007), 153-161.

[78]. Li.F, Jiang.Y, Xia.M, Sun.M, Xueand.B, and Ren. X, (2009), J. of Hazardous Materials, 165, 1219-1223

[79]. R. Li, W. Chen, and W. Wang, Separation and Purification Tech.,66, (2009), 171-176.

[80]. Y. Liu, X. Chen, J. Li and, C. Burda, Chemosphere, 61, (2005), 11-18.

[81]. A. Mills, W. Jishun, J. of Photochemistry and Photobiology A: Chem. 118, (1998), 53-63.

[82]. M.M. Mohamed, I. Othman, and R.M. Mohamed, J. of Photochemistry and Photobiology A: Chemistry, 191, (2007), 153-161.

[83]. M. Muruganandham, N. Sobana, M. Swaminathan, J. of Hazardous Materials, 137, 3, (2006), 1371-1376

[84]. L. L. Lifongo, D. J. Bowden, P. Brimblecombe, Chemosphere 55, (2004), 67–476

[85]. A.N. Okte, O. Yılmaz Applied Catalysis A: General, 354, 1-2, (2009), 132-142

[86]. H. Ohsaki, Y. Tachibana, A. Mitsui, T. Kamiyama, Y. Hayashi, Thin Solid Films 392, (2001), 169.

[87]. B. Neppolian, S. Sakthivel, B. Arabindoo, M. Palanichamy, V. Murugesan, Surface Science and Catalysis, 113, (1998), 329-335

[88]. T. Takahashi, K. Prabakar, T. Nezuka, T. Yamazaki, T. Nakashima, Y. Kubota, Fujishima A. J. Vac. Sci. Technol. A 24, (2006), 1161.

[89]. L. Straka, H. Kawakami, J. Romu, R. Ilola, R. Mahlberg, M. Heikkila and H. Hanninen, Thin Solid Films, 517, (2009), 3797-3805.

[90]. S. Kaur, V. Singh, J. of Hazardous Materials, 141, 1, (2007), 230-236

[91]. M.S. Lee, S.S. Hong, M. Mohseni, J Molecular Catal A 242, (2005), 135-140.

[92]. J.C. Wu, C.H. Chen. J Photochem Photobiol A 163, (2004), 509-515.

[93]. H. Hayashi, and Y. Hakuta, Materials 3, (2010), 3794-3817.

[94]. R. Abazari, A.R. Mahjoub and S. Sanati, RSC Adv., 4, (2014), 56406-56414

[95]. C. Li, R. Li, C. Fu, X. Song, M. Gu, Rare Metals 30, (2011), 544.

[96]. S.Yin, Y. Aita, M. Komatsu, J.S.Wang, Q. Tang, and T. Sato, J. Mater. Chem., 15, (2005), 674.

[97]. A. Fujishima, Nature 238, (1972), 37.

[98]. M.R. Hoffmann, S.T. Martin, W. Choi, D.W. Bahnemann Chem. Rev. 95, (1995), 69–96.

[99]. A.L. Linsebigler, G.Q. Lu, J.T. Yates, Chem. Rev. 95, (1995), 735.

[100]. K. Pirkanniemi, M. Sillanpä, Chemosphere, 48, 10, (2002), 1047-1060

[101]. M. M. Byranvand, A. N. Kharat, L. Fatholahib, Z. M. Beiranvand, JNS 3, (2013), 1-9

[102]. J. Xu, Y. Ao, M. Chen, D. Fu, J. of Alloys and Comps 484(1-2), (2009), 73-79.

[103]. C. Richard, F. Bosquet, J.F. Pilichowski, J. of Photochemistry and Photobiology A: Chem.108, (1997), 45—49

[104]. L.G. Devi and R. Kavitha, Applied Catalysis B: Environmental 140–141, (2013), 559-587

[105]. N. Nomura, T. Tagawa, and S. Goto, Reaction Kinetics and Catalysis Letters, 63, (1998), 9-13

[106]. R. Asahi, T. Morikawa, T. Ohwaki, Science, 293, (2001), 269–271

[107]. O. Diwald, T.L. Thompson, E.G. Goralski, J Phys Chem B,108, (2004), 52–57.

[108]. Y. Ao, J. Xu, S. Zhang, Appl Surf Sci, 256, (2010), 2754–2758.

[109]. L. Dong, G.X. Cao, Y. Ma, Trans Nonferrous Met Soc China, 19, (2009), 1583–1587

[110]. J.C. Yu, J.G. Yu, W.K. Ho, Chem Mater, 14, (2002), 3808–3816

[111]. S. Sakthivel, H. Kisch, Angrew Chem Int Ed, 42, (2003), 4908–4911

[112]. J. H. Park, S. Kim, A. J. Bard, Nano Lett, 6, (2006), 24–28

[113]. P. Yang, C. Lu, Hua N, Mater Lett, 57, (2002),794–801.

[114]. K. Song, J. Zhou, J. Bao, J Am Ceram Soc, 91, (2008), 1369-1371.

[115]. J. Xu, Y. Ao, D. Fu, Appl Surf Sci, 256, (2009), 884–888.

[116]. X. Z. Shen, Z.C. Liu, S.M. Xie, J Hazard Mater, 162, (2009), 1193–1198

[117]. X. Yang, F. Ma, K. Li, J Hazard Materer, 175, (2010), 429–438

[118]. Y. Bessekhouad, D. Robert, J. V. Weber, J. Photochem Photobiol A Chem, 163, (2004), 569–580

[119]. K. Y. Song, M .K. Park, Y .T. Kwon, Chem. Mater, 13, (2001), 2349–2355

[120]. J.C. Colmenares, M.A. Aramendia, A. Marinas, J.M. Marinas, F.J. Urbano, Appl. Catal. A: Gen. 306, (2006), 120–127.

[121]. X. Zhang, L. Lei, J. Zhang, Separ Purif Tech, 66, (2009), 417–421

[122]. A. Kumar, A. K. Jain, J. Mol. Catal. A Chemical, 165, (2001), 265–273.

[123]. Nayak B B, Acharya H N, Mitra G B, Thin Solid Film, 105, (1983), 17–24.

[124]. A. Kumar, G. Pandey, Int. J. for Research in Applied Science & Engineering Technology, 6, (2018), 339-350

[125]. K. Y. Song, M. K. Park, Y. T. Kwon, Chem Mater, 13, (2001), 2349–2355

[126]. K.I. Zamaraev, M.I. Khramov, V.N. Parmon, Cat. Rev. Sci. Eng. 36, (1994), 617.

[127]. K. Vinodgopal, I. Bedja, P. V. Kamat, Chem. Mater, 8, (1996), 2180–2187

[128]. C. Sahoo, A.K. Gupta, Anjali Pal, Desalination, 181 1-3, (2005), 91-100

[129]. F. Shiraishi, and C. Kawanishi, J. Phys. Chem., A 108, (2004), 10491.

[130]. M. Saquib, M. Muneer, Dyes and Pigments, 56, 1, (2003), 37-49

[131]. D. C. Hurum, A. G. Agrios, K. A. Gray, T. Rajh, M. C. Thurnauer, J. Phys. Chem. B 107, (2003), 4545.

[132]. S. Leytner, J. T. Hupp, Chem. Phys. Lett. 330, (2000), 231.

[133]. V. Rajendran, A.V.G. Devi, M. Azooz, F. H. El-Batal, J. Non-Cryst. Solids 353, (2007), 77.

[134]. K. H. Kim, F. A. Hummel, J. Am. Ceram. Soc. 43, (1960), 611.

[135]. G. Izquierdo, A. R. West, Mater. Res. Bull. 15, (1980), 1655.

[136]. N.R. Smith, P.A. Leighton, W.G. Leighton, J. Am. Chem. Soc. 61, (1939), 2299–2301.

[137]. L.A. Gu, J.Y. Wang, R. Qi, X.Y. Wang, P. Xu, X.J. Han, Journal of Molecular Catalysis A – Chemical 357, (2012), 19–25.

[138]. X.W. Li, G.C. Wang, X.X. Li, D.M. Lu, Applied Surface Science 229, (2004), 395–401.

[139]. W. Feng, E.H. Sun, A. Fujii, H.C. Wu, K. Niihara, K. Yoshino, Bulletin of the Chemical Society of Japan 73, (2000), 2627–2633.

[140]. M. Okano, K. Itoh, A. Fujishima, & K. Honda, Journal of the Electrochemical Society, 134, (1987), 837–841.

[141]. Y. Zhu, S. Murali, W. Cai, X. Li, J. W. Suk, J. R. Potts, and R. S. Ruoff, Adv. Mater., 22, (2010), 3906–3924.

[142]. C. N. R. Rao, A. K. Sood, K. S. Subrahmanyam, and A. Govindaraj, Angew. Chem., Int. Engl., 48, (2009), 7752–7777.

[143]. D. Wei, and Y. Liu, Adv. Mater., 22, (2010), 3225–3241.

[144]. A. K. Geim, Science, 324, (2009), 1530–1534.

[145]. J. Zhang, H. Yang, G. Shen, P. Cheng, J. Zhang, and S. Guo, Chem. Commun., 46, (2010), 1112–1114.

[146]. Q. Huang, ACS Catal., 3, (2013), 1477–1485.

[147]. K. M. Reza, ASW Kurny, F. Gulshan Appl Water Sci 7, (2017), 1569–1578.

[148]. D.F. Ollis, H. Al-Ekabi (Eds), Photocatalytic Purification and Treatment of Water and Air, Elsevier, Amsterdam, (1993).

[149]. I.K. Konstantinou, T.A. Albanis, Appl. Catal. B: Environ. 49, (2004), 1–14.

[150]. S. Xu, Y. Zhu, L. Jiang, & Y. Dan, Water, Air, & Soil Pollution, 213, (2010), 151–159.

[151]. D. Wang, Y. Wang, X. Li, Q. Luo, J. An, & J. Yue, Catalysis Communications, 9, (2008), 1162–1166.

[152]. Y. Park, S. Lee, S. O. Kang, & W. Choi, Chemical Communications, 46, (2010), 2477–2479.

[153]. G. Stewart, M.A. Fox, Res. Chem. Intermediates 21, (1995), 933.

[154]. N. Serpone, Res. Chem. Intermediates, 20, (1994), 953.

[155]. P.V. Kamat, Chem. Rev. 93, (1993), 267.

[156]. M. Saquib, M. Muneer, Dyes Pigments, 56, (2003), 37–49.

[157]. C.C. Chen, C.S. Lu, J. Phys. Chem. C 111, (2007), 13922–13932.

[158]. M.N. Makwana, J. T. Christopher, I. G. Robert, Paul F. McMillan, Materials Science in Semiconductor Processing, 42, (2016), 131-137.

[159]. U.G. Akpan, B.H. Hameed, Journal of Hazardous Materials 170, (2009), 520–529.

[160]. A. Fujishima, X. Zhang, D.A. Tryk, Surf. Sci. Rep. 63, (2008), 515–582.

[161]. B.M. Ng, P.C. Chen, S. Manickam, Applied Catalysis A: General, 433–434, (2012), 75-80.

[162]. A. Kumar, G. Pandey. American J. of Nano Research and Applications, 5, (2017), 40-48, doi: 10.11648/j.nano.20170504.11

[163]. A. Kumar, G. Pandey, Chem Sci J., 8 (2017) 164. doi: 10.4172/2150-3494.1000164.

[164]. A. Kumar, G. Pandey, Desali. and Water Treat., 71, (2017), 406–419.

[165]. S. Mozia, A.W. Morawski, M. Toyoda, M. Inagaki, Desalination 241, (2009) 97–105

[166]. A. Kumar, G. Hitkari, M. Gautam, S. Singh, G. Pandey, IJIRSET 4, I12, (2015), 12721-12731, DOI:10.15680/IJIRSET.2015.0412097

[167]. D.W. Kormann, D. Bahnemann, M.R. Hoffman, Environ Sci Technol 22, (1988), 798–806.

[168]. J. Zhu, Z. Deng, F. Chen, J. Zhang, H. Chen, M. Anpo, J. Huang, L. Zhang, Appl. Catal. B: Environ. 62, (2006), 329–335.

[169]. K. Nakata, A. Fujishima, J. of Photochemistry and Photobiology C: Photochemistry Reviews 13, (2012), 169– 189.

[170]. G. Tian, K. Pan, H. Fu, L. Jing, W. Zhou, J. Hazard. Mater. 166, (2009), 939–944.

[171]. X. Cheng, H. Liu, Q. Chen, J. Li, P. Wang, Electrochim. Acta. 103, (2013), 134–142.

[172]. D.L. Liao, C.A. Badour, B.Q. Liao, J. Photochem. Photobiol. A: Chem. 194, (2008), 11–19.

[173]. H. Lachheb, E. Puzenat, A. Houas, M. Ksibi, E. Elaoui, Appl. Catal. B: Environ. 39, (2002), 75–90.

[174]. A. Fujishima, T.N. Rao, D.A. Tryk, J. Photochem. Photobiol. C: Photochem. Rev. 1, (2000), 1–21.

[175]. R. W.Matthews .S. R. McEvoy, J. of Photoche. and Photobio. A: Chemistry, 66, (1992), 355-366

[176]. Y.M. Slokar, A.M.L. Marechal, Dyes & Pigments 37 (4), (1998), 335–356.

[177]. W. Baran, A. Makowski, W. Wardas, Dyes Pigm. 76, (2008), 226–230.

[178]. K.H. Wang, Y.H. Hsieh, C.H. Wu, C.Y. Chang, Chemosphere 40, (2000), 389–394.

[179]. U.I. Gaya, A.H. Abdullah, J. of Photochem. and Photobio. C: Photochemistry Reviews 9, (2008), 1-12.

[180]. V. Augugliaro, M. Litter, L. Palmisano, J. Soria, J. Photochem. Photobiol. C: Photochem. Rev. 7, (2006), 127-144.

[181]. Pal, R. Kaur, I. S. Grover, J. of Industrial and Engineering Chemistry 33, (2016), 178–184.

[182]. S. Liu, N. Jaffrezic, C. Guillard, Appl. Surf. Sci. 255, (2008), 2704-2709.

[183]. K. Rajeshwar, M.E. Osugi, W. Chanmaneec, C.R. Chenthamarakshan, M.V.B. J. of Photochem. and Photobio. C: Photochemistry Reviews 9, (2008), 171–192

[184]. J.C. Yu, J. Yu, W. Ho, Z. Jiang, L. Zhang, Chem Mater 14, (2002), 3808-3816.

[185]. X. Hong, Z. Wang, W. Cai, Chem Mater 17, (2005), 1548-1552.

[186]. M. N. Chong, B. Jin, C. W.K. Chow, C. Saint, water research 44, (2010), 2997-3027.

[187]. S.K. Kansal, M. Singh, D. Sud, J Hazard Mater 141, (2007), 581–590.

[188]. K. Selvam, M. Muruganandham, I. Muthuvel, M. Swaminathan, J Chem Eng 128, (2007), 51–57.

[189]. W. Baran, A. Makowski, W. Wardas, Chemosphere 53, (2003), 87–95.

[190]. H. Nishikiori, S. Fujiwara, S. Miyagawa, N. Zettsu, K. Teshima, Applied Catalysis B: Environmental, 217, (2017), 241-246,

[191]. A.L. Kretzschmar, M.Manefield, AIMS Environmental science, 2(2), (2015), 122-133

[192]. R.D. Kale and Chet Ram Meena, Advances in Applied Science Research, 3 (5), (2012), 3073-3080.

[193]. Z. Liu, R. Wang, F. Kan and F. Jiang, Asian Journal of Chemistry; 26, 3, (2014), 655-659

[194]. P. Kluson, H. Luskova, O. Solcova, L. Matejova, T. Cajthaml, Materials Letters, 61, Issues 14–15, 2007, 2931-2934

[195]. Shu Yin, Yoshinobu Fujishiro, Jihuai Wu, Minoru Aki, Tsugio Sato, Journal of Materials Processing Technology, 137,2003, 45-48

[196]. P.A. Russo, S. Lima, V. Rebuttini, M. Pillinger, M.G. Willinger, N. Pinna, A.A. Valente, RSC Adv. 3, (2013,) 2595-2603.

[197]. N. Serpone, E. Pelizzetti (Eds.), Photocatalysis: Fundamentals and Applications, Wiley, New York, (1989).

[198]. K.H. Song, M.K. Park, V.T. Kwon., K.W. Lee, W.J. Chang., W.I. Lee, Chem. mater, 13, (2001), 2349.

[199]. M. Toyoda, T. Yano, B. Tryba, S. Mozia, T. Tsumura, and M. Inagaki, Applied Catalysis B: Environmental, 88, (2009), 160-164.

[200]. H.H. Tseng, M.C. Wei, S.F. Hsiung, and C.W. Chiou, Chemical Engineering J.,150, (2009), 160-167

[201]. P. Vinodgopal, K. D.E. Wynkoop, P.V. Kamat, Environ. Sci. Technol. 30, (1996), 1660–1666.

[202]. C. Wang, X. Zhang, H. Liu., X. Li, W. Li, and H. Xu, J. of Hazardous Materials, 163, (2009), 1101-1106.

[203]. Z. Wang, C. Chen, F. Wu, B. Zou, M. Zhao, J. Wang, and C. Feng, J. of Hazardous Materials, 164, (2009), 615-620.

[204]. L. Wei, C. Shifu, Z. Wei, and Z. Sujuan, J. of Hazardous Materials, 164, (2009), 154-160.

[205]. W.Y. Ahn, S.A. Sheeley, T. Rajh, D.M. Cropek, App., Cata., B: Envi., 74, 1-2, (2007), 103-110

[206]. X. Fu, J. Long, X. Wang, D. Y.C. Leung, Z. Ding, L. Wu, Z. Zhang, Z. Li, X. Fu, Int. J. of Hydrogen Energy, 33, 22, (2008), 6484-6491.

[207]. X.H. Qi, Z.H. Wang, Y.Y. Zhuang, Y. Yu, J.l. Li, J. of Hazardous Materials, 118, 1-3, (2005), 219-225

[208]. X.R. Xu, S.X. Li, X.Y. Li, J.D. Gu, F. Chen., X.Z. Li., and H.B. Li., J. of Hazardous Materials, 164, (2009), 527-532.

CHAPTER-2

Photocatalytic degradation of Eriochrome Black-T by the Ni:TiO_2 Nanocomposites

Conventional chemical, biological and adsorption treatments have been applied for the removal of dyes from textile waste water but these processes are insufficient in removing dye contaminants. Photocatalysis is greener approach for the degradation of harmful dye pollutant compounds completely. In the present study TiO_2 and Ni:TiO_2 nanoparticles (NPs) were prepared and their photocatalytic activity was measured against Eriochrome Black T (EBT). The Photo-degradation of Eriochrome Black T was investigated at different condition of concentration and pH in presence of TiO_2 and Ni:TiO_2. The prepared nanoparticles of photocatalyst are characterized by XRD, SEM, EDX, UV-Vis and BET. The photocatalyst activity was measured by varying pH and concentration of dye solution. Kinetics study was also performed in this investigation.

2.1. Introduction

Nowadays water pollution has become a major threat to living organism because large amount of hazardous industrial wastes containing dyes, pigments, pharmaceutical products, industrial chemicals and various organic compounds are dumped into water bodies, causing water polluted. Since these wastes are stable to light, oxidizing agents, and resistant to aerobic digestion, therefore pose serious ecological problems [1-4]. Some investigations reported that approximately 12% of the synthetic textiles dyes use each year, such as Caramine, Indigo Red, Red 120, Rhodamine B, Methylene Blue, Eriochrome Black-T (EBT) [5-8], while 20% of these dyes are lost during manufacturing and processing operations, which enter into water through effluents. While conventionally chemical [9], biological [10] and adsorption [11] treatments have been applied for the removal of dyes from industrial waste water but these processes are insufficient in removing dye contaminants.

Photodegradation is an advanced oxidation process and it has lot of advantages over traditional wastewater treatment techniques such as chemical oxidation [16], activated carbon adsorption [17], biological treatment [18], etc. Activated carbon adsorption method involves the phase transfer of pollutants without decomposition and thus creates another pollution problem. Chemical oxidation method is unable to remove all organic substances and it is suitable for the removal of pollutants at high concentrations. The biological treatments are very slow, dispose large amount of sludge and required strict control of proper pH and temperature [19]. In this regard photocatalytic processes have advantages for the removal of pollutants even at low concentration for industrial waste water [20]. Moreover in photooxidation, complete oxidation of organic pollutants take place within few hours, even at ppb level, without formation of secondary hazardous products using highly active and cheap catalysts which can be used in specially design reactor systems [21].

Titanium dioxide is a widely accepted photocatalyst due to its high oxidation efficiency, non-toxicity, high photo stability, chemical inertness and environmental friendly nature [22-24]. It is a wide band gap (~ 3.2 eV) semiconductor and mineralizes a large range of organic pollutants such as herbicides, dyes, pesticides, phenolic

compounds, tetracycline, sulfamethazine, etc under UV irradiation [25]. In photocatalytic processes the photon with energy, equal to or greater than the energy gap (3.2 eV) is absorbed by TiO_2 particles, therefore holes (h^+) are created in the valence band and electrons (e−) in the conduction band, which diffuses to the surface of TiO_2 and participates in redox reactions of the adsorbed substrates [26].

TiO_2 is a large band gap semiconductor; therefore it is suitable in UV light photodegradation. Since the solar light contains only 5% UV radiation, therefore TiO_2 is not suitable photocatalyst in solar light. Further electron hole recombination is another drawback in TiO_2 mediated photocatalysis. The above drawbacks could be overcome at some extent by doping metal ions in TiO_2 host [27-29]. In the present investigation, Ni doped TiO_2 has been performed in a green synthetic manner and its photocatalysis activity has been performed against Eriochrome black T (EBT).

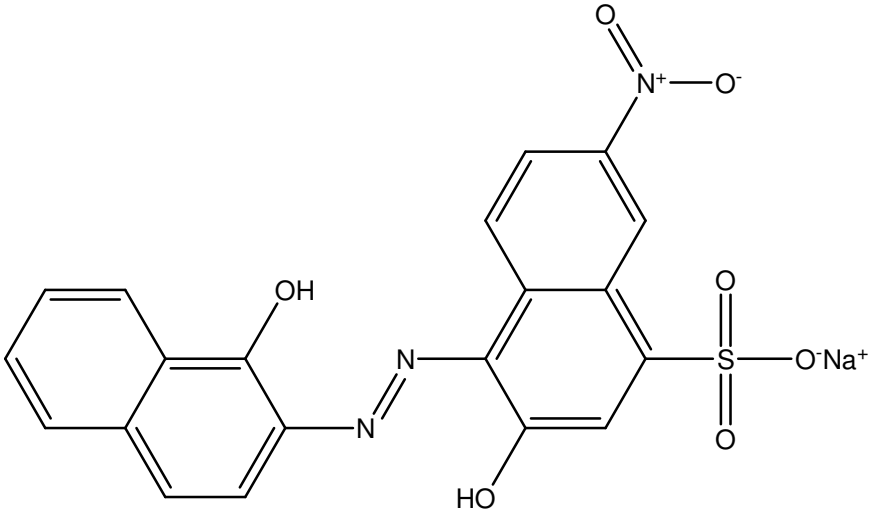

Fig.2.1. Molecular Structure of EBT

2.2. Experimental

2.2.1. Materials

The materials used in this study were purchased from merck. All chemicals used in this investigation viz titanium tetrachloride, sodium hydroxide, ammonia, nitric acid and Eriochrome Black - T dye are analytical grade reagent and used as supplied. Ethyl alcohol and deionised water were used as solvents in this experiment.

2.2.2. Synthesis of TiO_2.

In this method, both $TiCl_4$ solution (200 g/L) and NaOH solutions (64.5 g/L) was added drop wise to water with stirring. When pH of resulting solution reaches to 7, slurry was formed which was filtered. The filter cake of TiO_2 was washed and re-dispersed in water to prepare 1 M of TiO_2 slurry. TiO_2 slurry was added to an aqueous solution of HNO_3 and resulting solution was refluxed for 2 h at 95 ^oC, cooled naturally to room temperature, neutralized with 28 % of aqueous ammonia, filtered, washed with double distilled water and calcined at 400 ^{o} C. The TiO_2 formed as under [30].

$$TiCl_4 + 4NaOH + NH_3 \longrightarrow Ti(OH)_4 + 4NaCl \quad (1)$$

$$Ti(O)_4 \longrightarrow TiO_2 + 2H_2O \quad (2)$$

2.2.3. Synthesis of Ni doped TiO_2 (Ni:TiO_2)

5 g of as prepared TiO_2 was dissolve in 100 ml water: alcohol (ratio 3:1 V/V) mixture. 5 % alcoholic Nickel acetate solution was added drop wise to TiO_2 solution. The dispersion was agitated continuously for 4 h at 80 ^oC. After the treatment, the residue was removed by filtration and sintered for 1 h in presence of air at 400 ^oC, keeping in a silica boat inside muffle furnace. After sintering, slow annealing was done at room temperature. Content was taken out from furnace and stored in closed air tight bottles. The obtained yield of prepared nanocomposites of TiO_2 and Ni:TiO_2 was more than 90% of the expected theoretical yield [31].

$$TiO_2\,(Soln) + Ni(CH_3CO)_2\,(alc\ sol) \longrightarrow Ni{:}TiO_2 \quad (3)$$

2.2.4. Characterization

XRD pattern of above synthesized TiO_2 and Ni:TiO_2 was recorded on X-Ray diffractometer (Bruker AXS D8 Advance System, Germany). The particles morphology of the photocatalysts were studied using scanning electron microscope (JEOL JSMn 6490 LV). The surface area and pore characteristics of the derived photocatalyst were determined by nitrogen adsorption/desorption isotherms at 77 K (boiling point of nitrogen gas at 1atm pressure) using a BET surface area analyzer (BELSORP-max,

Japan). Since the absorption of light by photocatalysts and their band gap average energy are the most crucial step in any photocatalysed reaction, the UV-visible spectra of material was recorded on spectrophotometer (UV 2450 Shimadzu). The FT-IR spectra of the pellets were recorded using a Fourier Transform Infra-Red Spectrometer (FTIR) Thermo Scientific (Nicole 6700). For FTIR study, the Photocatalyst (2 mg) was mixed with 200 mg of KBr and then made pellet.

2.2.5. Photo-degradation of EBT

The photocatalytic activity of as prepared TiO_2 and Ni:TiO_2 materials was evaluated by Photodegradation of EBT(structure shown in Fig.2.1) under visible light which is less than 420 nm using a filter (fluorescent visible lamp, Philips, 500 W) exposure in a photocatalytic chamber. 200 mg photocatalyst was dispersed in 20 ml of solution of EBT dye of different concentration (16.6 x 10^{-5}, 20.0 x 10^{-5}, 25.0 x 10^{-5} 33.3 x 10^{-5} M), in the dark condition for 30 min in order to achieve the adsorption equilibrium. The solution was irradiated continuously by visible light in a photocatalytic chamber. During irradiation, solution was agitated using a magnetic stirrer and air was bubbled into the reaction medium to provide a constant supply of oxygen. After desired time interval, an aliquot of solution was isolated, centrifuged and its absorbance was measured on UV-Visible spectrophotometer to calculate the percentage degradation. The photocatalytic degradation efficiency was calculated using the following equation [33-35].

$$(\%)\mathbf{Degradation} = \frac{\mathbf{Ao-A}}{\mathbf{Ao}}\mathbf{x\ 100} \qquad \textbf{(4)}$$

Where Ao the initial absorbance of the dye solution and A is the absorbance after irradiation at particular time.

2.2.6. GC-MS analysis

In order to observe the products of photocatalytic experiment GC-MS analysis (Gas chromatography-Mass spectroscope, Shimadzu, GC-2010 and GC-MS-QP 2010 plus, using RTX-5Sil-MS column (30 m × 0.25 mm × 0.25 μm). was carried out. In a typical experiment, 5 ml of EBT solution was collected after 180 min of UV-light

exposure in presence of catalyst. The solutions were centrifuged (5000-8000 rpm), filtered through cellulose filter (0.22 μm) and extracted in three successive quantities (5 ml) of ethyl acetate. The ethyl acetate extract carry samples were passed through sodium sulphate (anhyd.), evaporated to dryness over rota-evaporator, and their traces removed over gentle stream of N_2 gas. Residue thus obtained redissolve in methanol (GC grade) and analyzed. Helium was used as a carrier gas with a flow of 1ml/min through capillary column. Injector was maintained at 240 °C, while transfer line was kept at 260 °C and 1 μl of the sample was injected. Oven was programmed at 60 °C to 300 °C @ 6 °C/min rise of temperature

2.3. Results & discussion

2.3.1. Powder x-ray diffraction analysis of TiO_2 and Ni:TiO_2

The XRD pattern of as prepared TiO_2 and Ni:TiO_2 nanoparticles are depicted in Fig.2.2 (a) and (b). In the XRD pattern of TiO_2, the major peaks observed at 2θ value 25.2, 37.2, 48.3 and 55.4º are corresponds to anatase phase whereas the peaks at 26.9, 28.2, 42.6 and 54.2 indicate the presence of rutile phase. In the XRD pattern of Ni:TiO_2 the intensity of some peaks has been changed with compared to TiO_2. This is due to change in crystallinity, grain fragmentization, and partial amorphization. The observed X-Ray diffractogram of samples were analyzed further to estimate average grain size in the sample using Scherrer's equation [32].

$$T = \frac{K\lambda}{\beta \cos\theta} \qquad \textbf{(5)}$$

Where, T is the mean size of the ordered (crystalline) domains, which may be smaller or equal to the grain size, K is a dimensionless shape factor, with a value close to unity. The shape factor has a typical value of about 0.9 but varies with the actual shape of the crystallite, λ is the X-ray wavelength, β is the line broadening at half the maximum intensity (FWHM), (in radians) and θ is the Bragg angle. The particle size of TiO_2 and Ni:TiO_2 was calculated as 72 and 16 nm respectively using above equation.

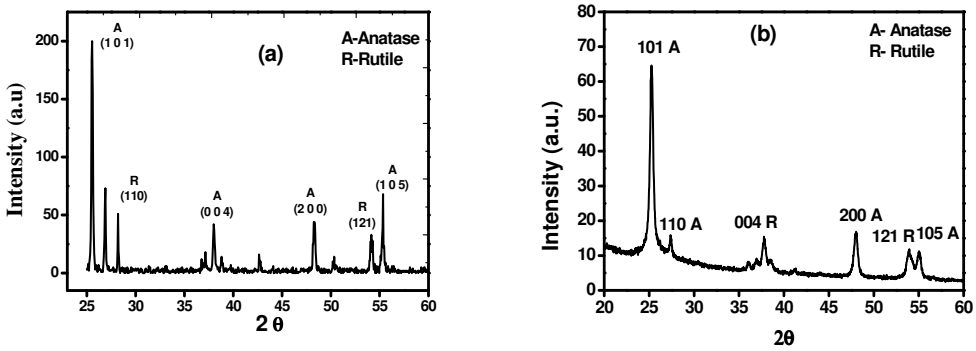

Fig.2.2. Observed XRD pattern of (a) TiO_2 (b) Ni-TiO_2

2.3.2. Scanning electron microscope (SEM)

The morphology of the samples was investigated by scanning electron microscopy analysis. Fig.2.3 clearly shows that both the prepared samples are obtained as agglomerate in nanometric dimension. The doping of Ni^{2+} ion indicates that the particle size reduces due the penetration of nickel in the lattice of titanium dioxide.

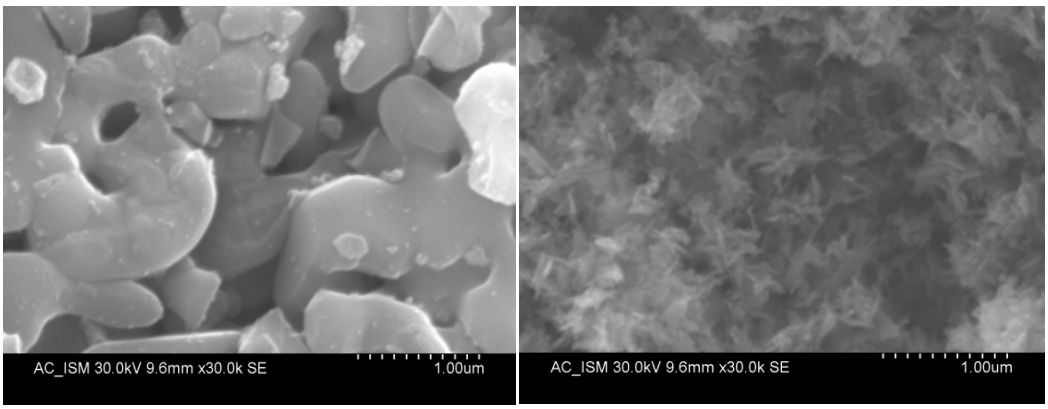

Fig.2.3. Observed SEM pattern of TiO_2 and Ni:TiO_2

2.3.3 Transmission Electron Microscopy (TEM)

TEM analysis of materials was used to examine the crystallite/particle size, morphology. The prepared TiO_2 powders consist of both spherical and semi spherical shape, on the contrary, the particles of Ni:TiO_2 have mostly spherical morphology. It can be estimated that the particle size of TiO_2 and Ni:TiO_2 powders in Figure 2.4 (a) and 2.4 (b) are in the nanoscale with the grain size less than 100 nm.

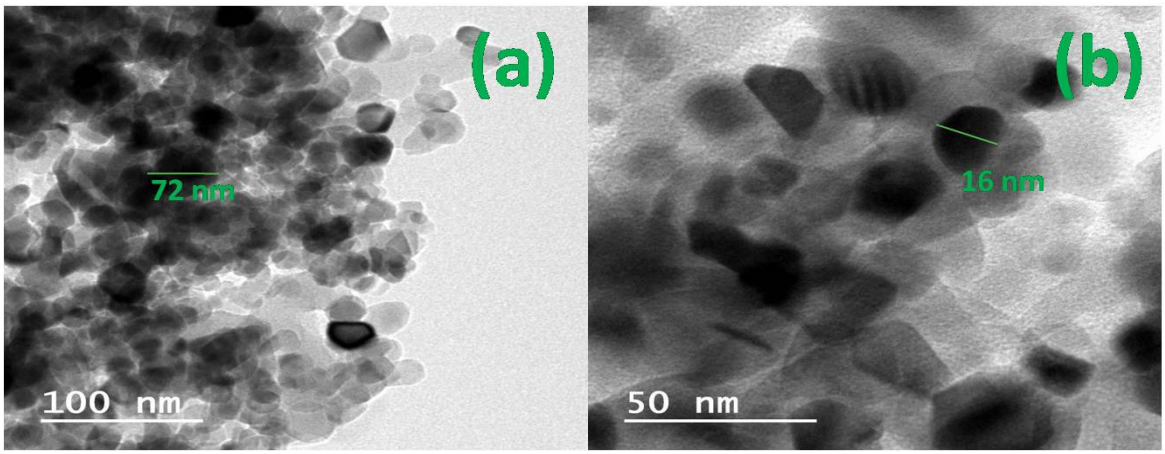

Fig.2.4. Observed TEM pattern of (a) TiO_2 (b) Ni:TiO_2

2.3.4. Surface area analysis (BET)

The specific surface area, pore volume and average pore size of the TiO_2 and Ni:TiO_2 photocatalyst were determined by N_2 adsorption technique using BET. Fig.2.5 shows adsorptions desorption and BJH plot and Table.2.1 summarizes their physical properties. The TiO_2 modified by Ni^{2+} incorporation during thermal treatment, lead to a marked increase of the BET surface areas, average pore radius and pore volume. Doping with 5% Ni, the crystallite size was decreased and the surface area value increased. These results suggest that Ni doping effectively inhibits TiO_2 grain growth probably by staying at grain boundaries thereby decreasing the crystallite size and increasing the surface area. The decrease in grain growth can also be attributed to the formation of Ni–O–Ti bonds in the doped powders, which inhibits the growth of the TiO_2 crystals.

Table.2.1. BET data of TiO_2 and Ni:TiO_2

Sample	Surface area (m^2/g)	Pore volume (cm^3/g)	Pore radius (nm)
TiO_2	2.1522	10.132×10^{-3}	1.21
Ni:TiO_2	46.685	9.5124×10^{-2}	1.64

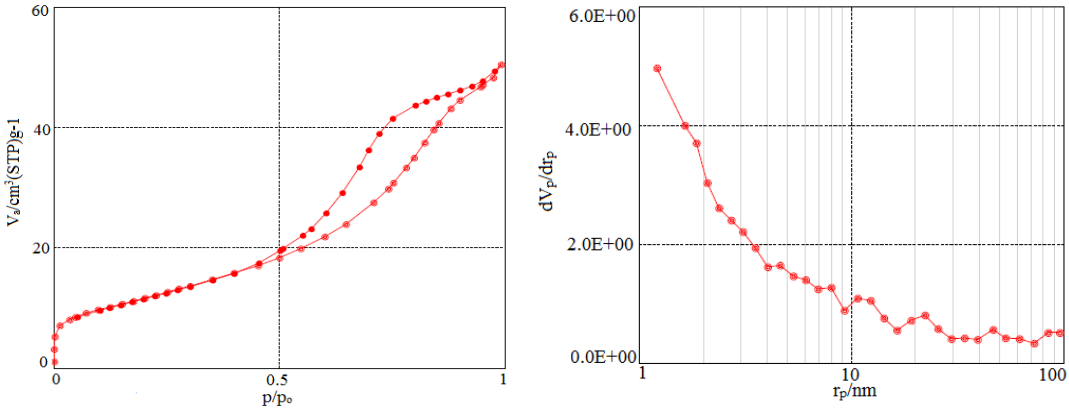

Fig.2.5. (a) adsorption desorption plot of Ni:TiO_2 (b) BJH plot of Ni:TiO_2

2.3.5. UV-Vis spectra

Aqueous suspensions of the samples were used for the UV absorption studies. The absorption spectrum of TiO_2 consists of a single broad intense absorption between 250 to 300 nm due to the charge-transfer from the valence band to the conduction band [36]. The undoped TiO_2 showed absorbance in the shorter wavelength region while Ni:TiO_2 result showed slight red shift in the absorption edge. The doping of Ni ions into TiO_2 could shift optical absorption edge from UV to visible range, but no prominent change in TiO_2 band gap was observed [37-38].

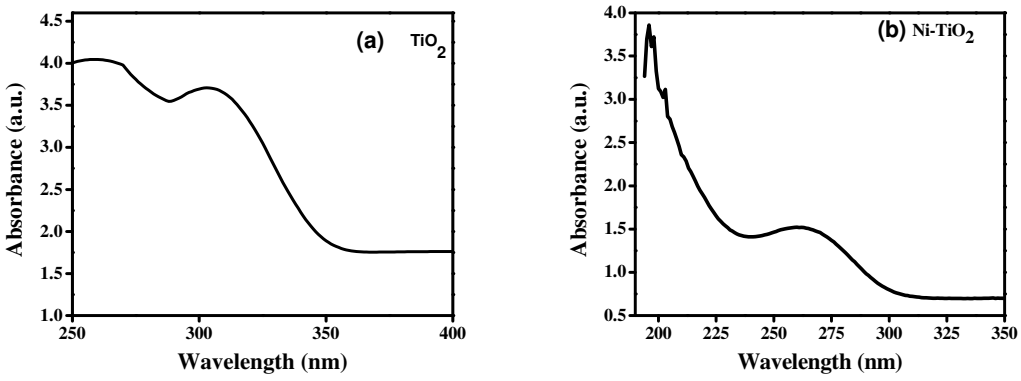

Fig.2.6. UV- spectra of (a) TiO_2 (b) Ni-TiO_2

2.3.6. Band gap energy determination

The band gap of samples was calculated by extrapolation of the $(\alpha h\nu)^2$ versus $h\nu$ plots, where α is the absorption coefficient and $h\nu$ is the photon energy, $h\nu = (1239/\lambda)$

eV. The value of *hv* extrapolated to $\alpha = 0$ gives an absorption energy, which corresponds to a band gap (*E*g). Graph yields an *E*g value of 3.2 eV for TiO_2 and 3.0 for Ni:TiO_2 shown in Fig.2.7 [39]. The slight decrease in band gap energy in case of Ni:TiO_2, is due to formation of sub-band level between valence band and conduction band caused doping of Ni^{2+} in TiO_2 host.

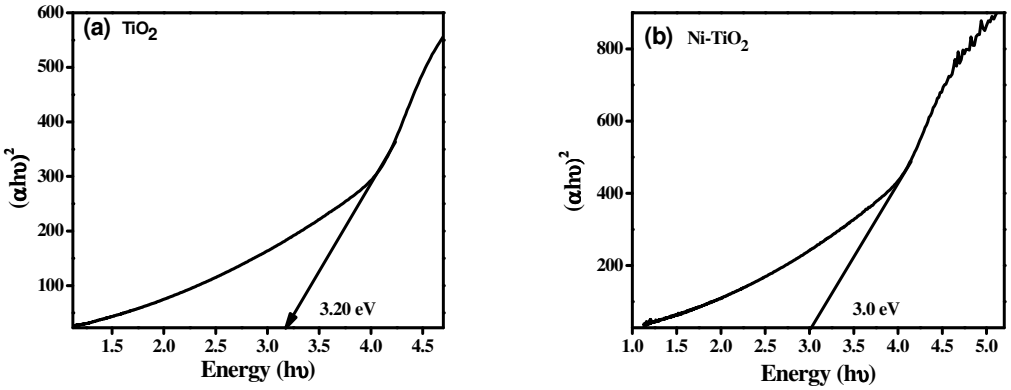

Fig.2.7. Band gap energy of (a) TiO_2 (b) Ni:TiO_2

2.3.7. FT-IR spectroscopy

FT-IR spectra of undoped and 5% Ni doped TiO_2 samples (Fig.2.8) show peaks corresponding to stretching vibrations of the O-H and bending vibrations of the adsorbed water molecules around 3350-3450 cm^{-1} and 1620-1635 cm^{-1}, respectively. The broad intense band below 820, 804, 592 and 456 cm^{-1} is due to Ti-O-Ti vibrations. The shift to the higher wave numbers and sharpening of the Ti-O-Ti band may be due to decrease in size of the catalyst nanoparticles. In addition, the surface hydroxyl groups in TiO_2 increased with the increasing of Ni loading, which is confirmed by increase in intensity of the corresponding peaks. The FT-IR spectra of Ni:TiO_2 show strong band at 1075 cm^{-1}, corresponds to the vibration of Ni–O bond and confirms the penetration of nickel in Titania [40].

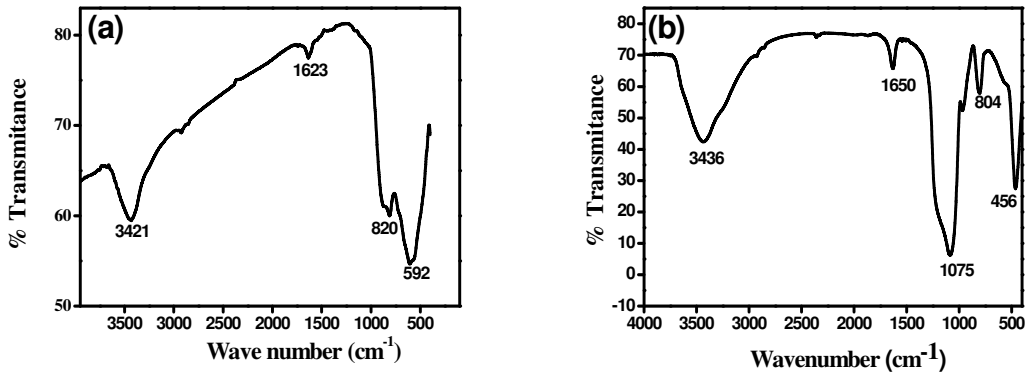

Fig.2.8. FT-IR spectra of (a) TiO_2 (b) Ni:TiO_2

2.4. Photo-degradation of EBT

The photocatalytic degradation of EBT has been studied in the presence of TiO_2 and Ni:TiO_2 nanoparticles Different concentration solutions of dye was prepared in 3:2 (V/V) ratio of water and alcohol. The known amount of photocatalyst 0.2 g was dispersed in the 20 ml dye solution and the reaction mixture was irradiated with visible light with constant stirring on magnetic stirrer. After different time interval, an aliquot of solution was separated, centrifuged and absorption was recorded spectrophotometrically. The results obtained for the degradation of EBT are shown in Fig.2.9. As obvious from the graph, the % removal of dye decreases with increase in concentration. Further, the photocatalytic efficiency of TiO_2 increases by doping Ni^{2+} ion in TiO_2 host. The Photodegradation efficiency of Ni:TiO_2 is greater than bare TiO_2 [41-42].

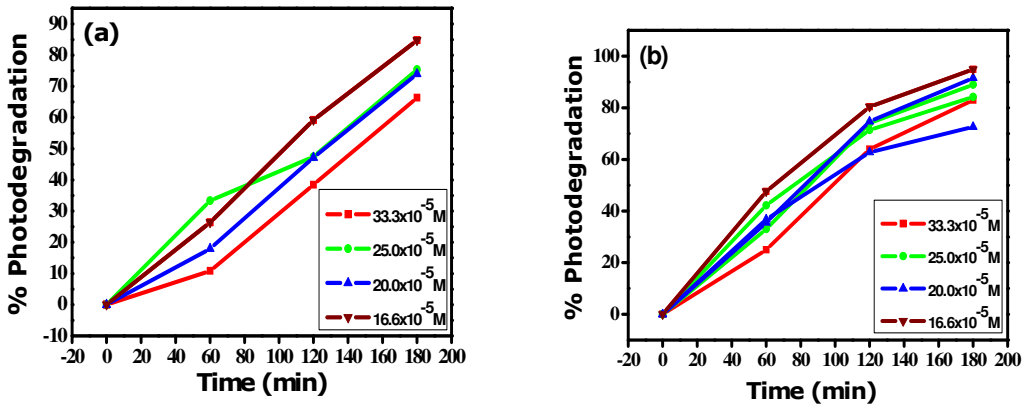

Fig.2.9. Photodegradation of EBT at different concentration (a) TiO_2 and (b) Ni:TiO_2

2.4.1. Effect of dye concentration

The effect of dye concentration on photocatalytic degradation was studied in presence of TiO_2 and Ni:TiO_2 materials, keeping the amount of catalyst constant. Known concentration of dye solution was prepared in water: alcohol (3:2, V: V) ratio. The known amount of photocatalyst (0.2 g) was dispersed in the different concentration of dye (33.3 x 10^{-5}, 25.0 x $10^{-5,}$ 20.0 x 10^{-5} and 16.6 x 10^{-5} M) and reaction mixtures were irradiated by visible light. The effect of photocatalytic degradation with time was measured and result is shown in Fig.2.9. When the concentration of solution increased, the number of dye molecule also increased therefore the effective number of photon penetrating the dye reached at the catalyst surface also reduced, owing to hindrance in the path of light, thereby reducing the reactive hydroxyl and superoxide radicals and decreasing the % degradation [44].

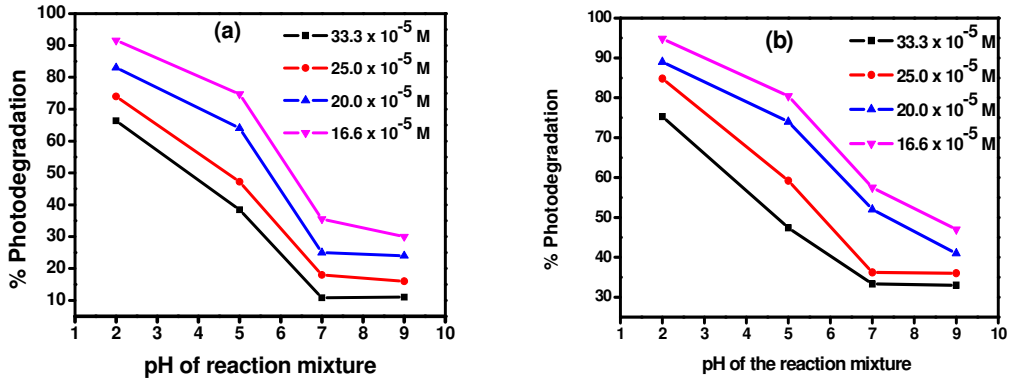

Fig.2.10. Effect of pH on Photodegradation of EBT at various concentrations (a) TiO_2 (b) Ni:TiO_2

2.4.2. Effect of pH

The photodegradation reaction was also carried out under varying pH conditions from (2 to 9), by addition of H_2SO_4 and NaOH, keeping other parameters same. The results (Fig.2.10) show that degradation of dye is highest in acidic medium (at pH = 2) while it decrease with increase in pH and ultimately becomes constant after pH 7. This implies that acidic condition is favourable for formation of the reactive intermediate hydroxyl radicals. This further helps in enhancing the reaction rate. On the other hand

in neutral condition the formation of reactive intermediate is relatively less favourable and hence not feasible [45].

2.4.3. Effect of photocatalyst

It is clear from the results shown in Fig.2.6 that both TiO_2 and Ni:TiO_2 are effective photocatalyst for degradation of EBT dye, however Ni:TiO_2 seems to be more effective photocatalyst for degradation of EBT.

2.4.4 Effect of dose of photocatalyst on photodegradation of EBT

The effect of photocatalyst dose on the photodegradation of EBT was studied by applying te different concentration (200mg/L, 100mg/L and 50mg/L) of the photocatalyst shown in Fig.2.11. The Degradation rate of EBT was found to increase by increasing the dose of photocatalyst from 50 mg/L to 200mg/L. this is due to the no active site increased. When the Ni is incorporated in TiO_2, the band gap energy is decreased which enhanced the photo efficiency, the surface area of photocatalyst also increased the efficiency of photocatalyst.

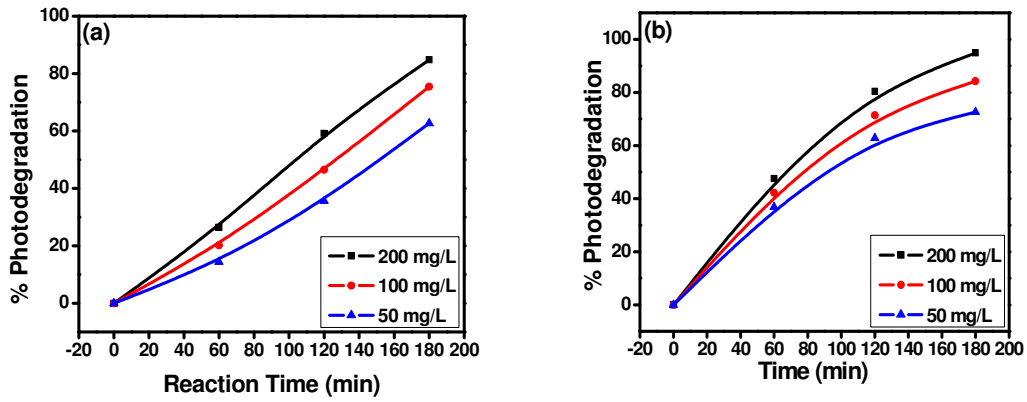

Fig.2.11. Effect of Dose on Photodegradation of EBT (a) TiO_2 (b) Ni:TiO2

2.4.5. Recyclability of Photocatalyst

The photocatalyst and EBT mixture was agitated, illuminated with visible light and after desired time, the mixture was centrifuge to remove the photocatalyst. The obtained photocatalyst was washed three times with distilled water and kept in oven for 24 h at 60 ^{o}C and reused for the degradation of EBT. The photodegradation of EBT by

the recyclized Photocatalyst are showing in Fig. 2.12 (a) and 2.12 (b). The result shows that the recyclized photocatalyst efficiency is decreased probably due to the loss of some active sites and decrease of collection efficiency of photon.

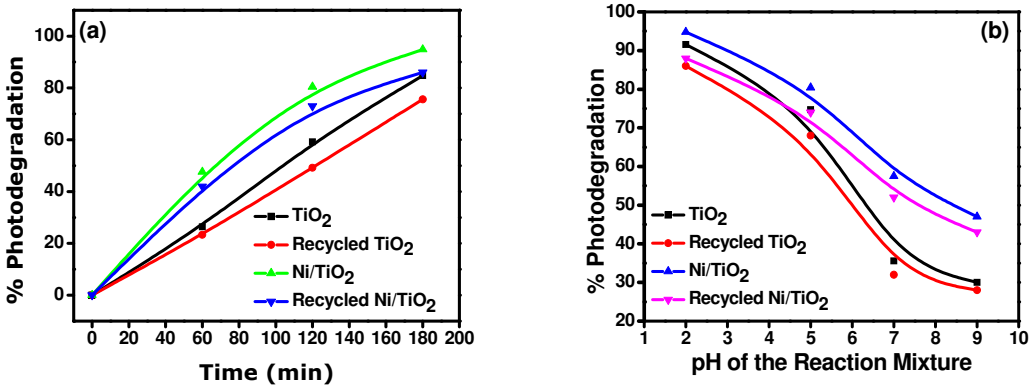

Fig.2.12. Photodegradation of EBT by recyclable Photocatalyst (a) photodegradation with time (b) photodegradation at different pH

2.4.6. GC-MS of EBT photodegradation products

The photodegradation of the EBT takes place by irradiating under visible-light in the presence of bare TiO_2 and Nickel doped Titania nanocomposite. The photodegraded products of photodegradation of EBT have been determined by GC-MS analysis (Fig. 2.14 and 2.16). It has been found that MS chromatograph (Fig.2.13 and 2.15) and correspondingly mass chromatographs of EBT (after 2 h of irradiation) in the presence of bare TiO_2 and Ni:TiO_2 are almost similar, except in their respective intensities (Fig. 2.13 and 2.15). Among the number of degraded products of EBT, seven products formed in the photodegradation, shown in mass chromatograph (Fig. 2.14 and 2.16) have been identified, as listed in Table.2.2. The mechanism for the photodegradation of EBT using titania nanocomposites is believed to take place by the photo produced e- and h+, that results into formation of highly oxidative species such as hydroxyl and superoxide radicals, which on reaction with EBT results into its decomposition to smaller molecules.

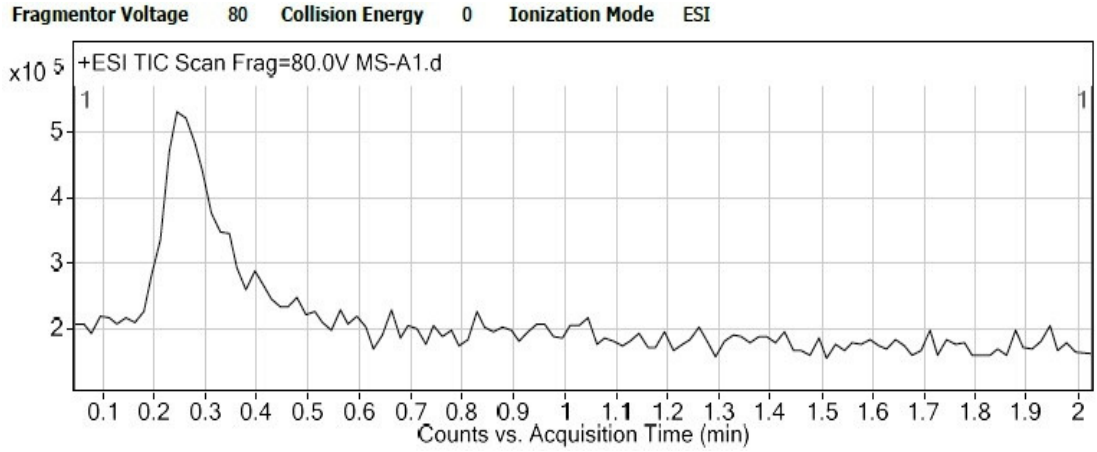

Fig.2.13. GC chromatogram of EBT in presence of Titania

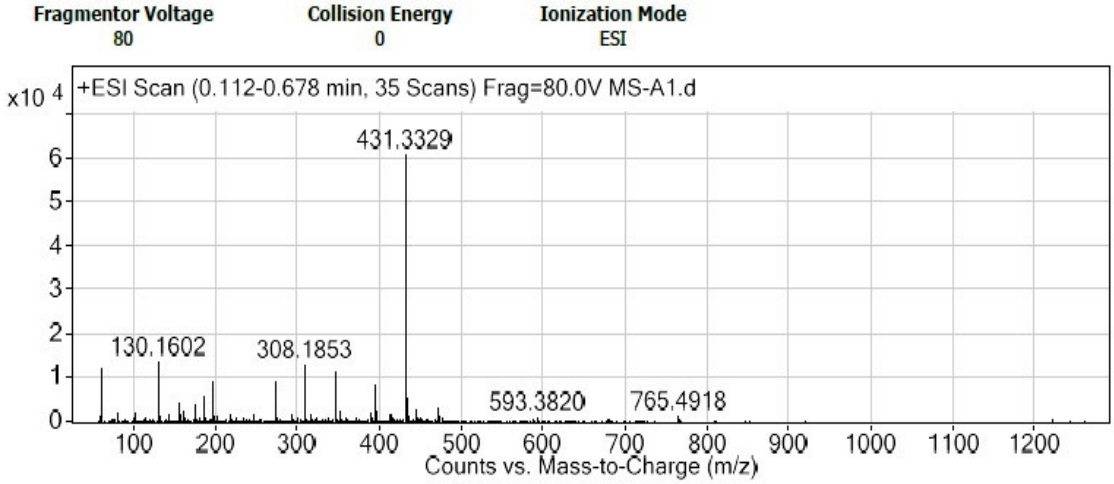

Fig.2.14. Mass spectra of EBT photodegradation in presence of Titania

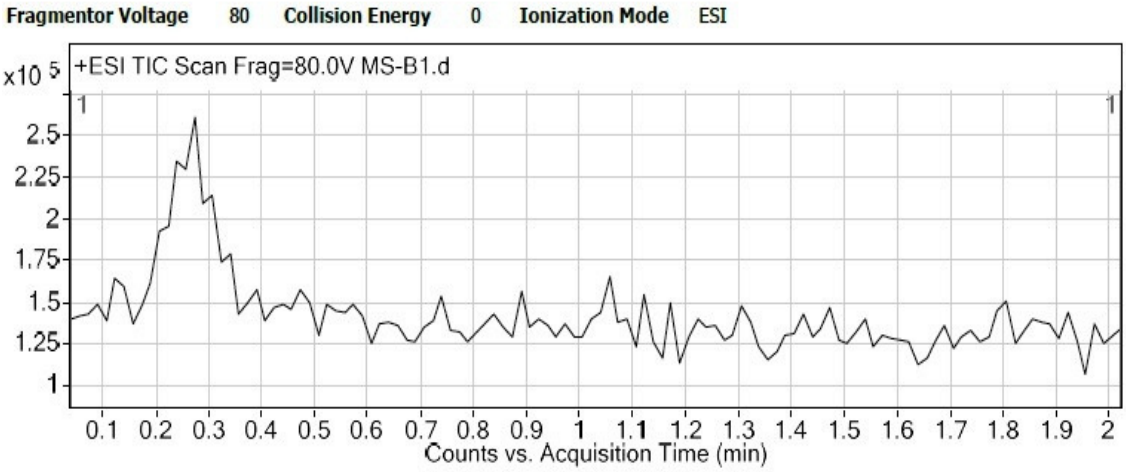

Fig.2.15. GC chromatogram of EBT in presence of Ni:TiO_2

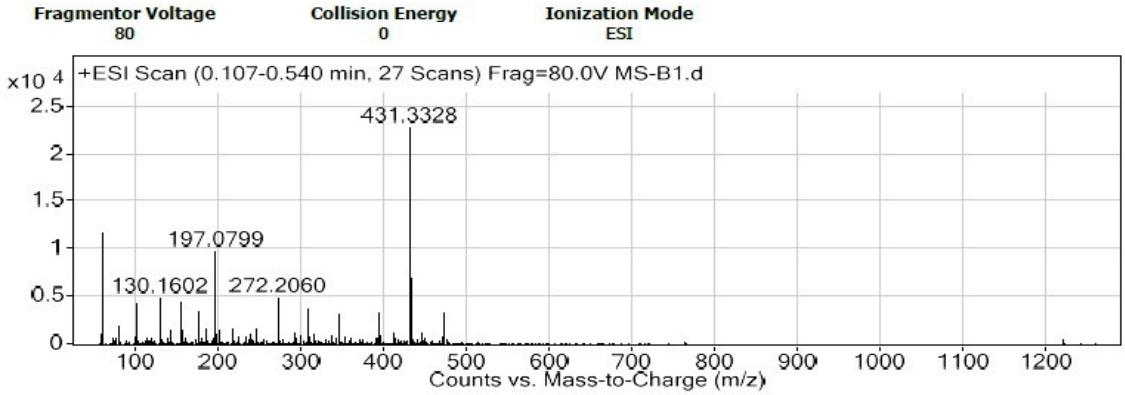

Fig.2.16. Mass spectra of EBT photodegradation in presence of Ni:TiO_2

Table 2.2. Intermediate photoproducts formed during Eriochrome black-T degradation by Ni:TiO_2 after 2 h Visible light irradiation.

S.No	IUPAC Name of compound	MS (m/z)
1-	3-Hydroxy-7-nitroso-1,8 adihydronaphthalene-1-sulfonoperoxoic acid	272,
2-	2-(6-(hydroxymethyl)-4-nitrocyclohexa-2,4-dienylidene)ethanol	197
3-	2-Hydrazinylnaphthalen-1-ol-	175
4-	2-Diazenylnaphthalen-1-ol	155,
5-	4-Formylbenzonitrile	131
6-	1-Ethynylbenzene	102
7-	Methyl formate	60

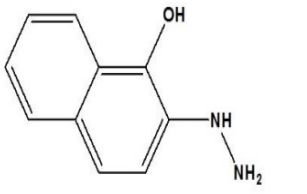

4-formylbenzonitrile, 131

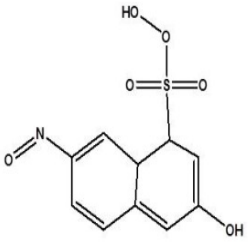

3-hydroxy-7-nitroso-1,8 a dihydro naphthalene-1-sulfonoperoxoic acid, 272

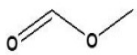

Methyl Formate 60

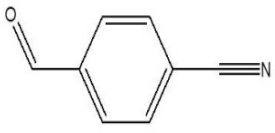

2-hydrazinylnaphthalen-1-ol, 175

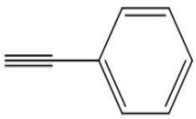

1-ethynylbenzene, 102

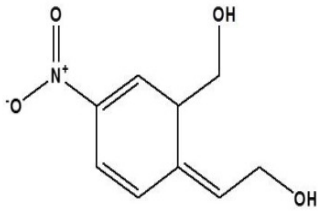

(Z)-2-(6-(hydroxymethyl)-4-nitro cyclohexa-2,4-dienylidene)ethanol

2.4.7. Lowering of electron-hole recombination

Photoluminescence spectra have been used to examine the mobility of the charge carriers to the surface as well as the recombination process involved by the electron-hole pairs in semiconductor particles. PL emission results from the radiative recombination of excited electrons and holes. In other words, it is a critical necessity of a good photocatalyst to have minimum electron-hole recombination. To study the recombination of charge carriers, PL studies of synthesized materials have been undertaken. PL emission intensity is directly related to recombination of excited electrons and holes. Fig. 2.17 shows the photoluminescence spectra of synthesized photocatalysts. In the PL spectra, the intensity of TiO_2 is higher than Ni:TiO_2 indicating rate of recombination of e^-- h^+ is higher in TiO_2 than that of Ni:TiO_2.The weak PL intensity of Ni:TiO_2 may arise due to the impregnation of Ni in Titania lattice, which for sub band level in band gap region of TiO_2. This delays the electrons- holes recombination process and hence utilized in the redox, reaction leading to improved photocatalytic activity.

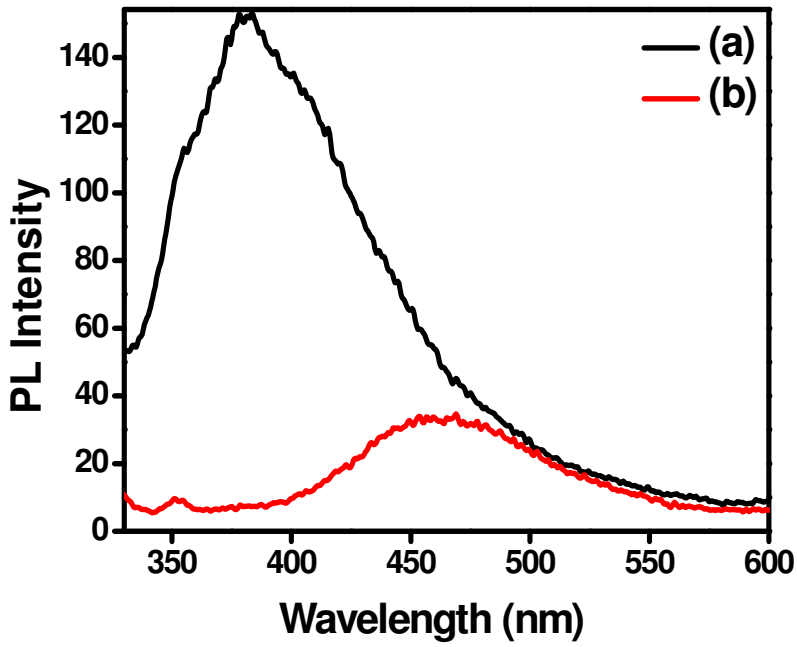

Fig.2.17. Photolumiscence Spectra of (a) TiO_2 (b) Ni:TiO_2

2.4.8. Hydroxyl radical formation

As hydroxyl radical performs the key role for the decomposition of the organic pollutants, it is necessary to investigate the amount of hydroxyl radicals produced by each photocatalyst. In this study terephthalic acid (TA) has been used as a probe reagent to evaluate •OH radical present in the photoreaction pathway. Fig. 2.18 shows the PL spectra of TiO_2 and Ni:TiO_2 recorded EBT solution in presence of 10^{-3}M Terephthalic solution. OH, radical attack Terephthalic, forming 2- hydroxyl terephthalic acid (TAOH) which gives a fluorescence signal at 426 nm. The fluorescent intensity is linearly related to the number of hydroxyl radicals formed by the photocatalysts. Higher the generation of hydroxyl radical, more will be yield of TAOH and hence more intense will be the fluorescence peak. The spectra show that the intensity of peak indicating in presence of Ni:TiO_2 higher generation of more number of hydroxyl radicals compared to TiO_2.

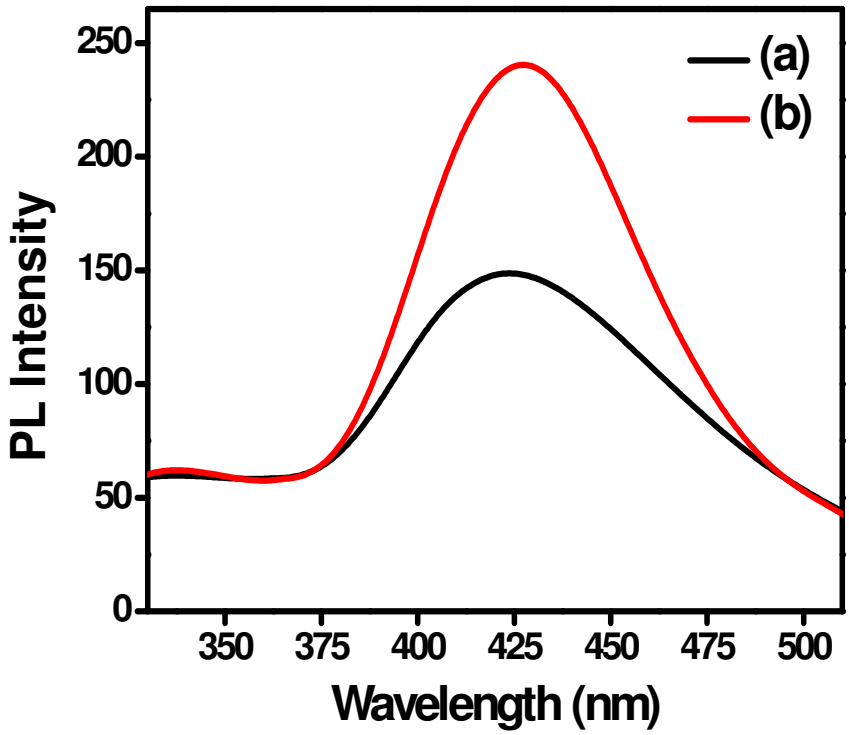

Fig.2.18. PL spectra of photocatalysed EBT solution in presence of terephthalic acid (0.001M) (a) TiO_2 (b) Ni:TiO_2

2.5. Mechanism of photooxidation process

The acceleration of a chemical transformation by light in presence of a catalyst is called photocatalysis. The catalyst may accelerate the photoreaction by interaction with the substrate in its ground or excited state and/or with a primary photoproduct, depending upon the mechanism of the photoreaction remaining unaltered at the end of each catalytic cycle. Heterogeneous photocatalysis is a process in which two active phases, solid and liquid are present. The solid phase is a catalyst, usually a semiconductor. The molecular orbital of semiconductors has a band structure. The bands of interest in photocatalysis are the populated valence band (VB) and it's largely vacant conduction band (CB), which is commonly characterized by band gap energy (E_{bg}). The semiconductors may be photoexcited to form electron-donor sites (reducing sites) and electron-acceptor sites (oxidising sites), providing great scope for redox reaction. When the semiconductor is illuminated with light (hυ) of greater energy than that of the band gap, an electron is promoted from the VB to the CB leaving a positive hole (h^+) in the valence band and an electron (e^-) in the conduction band as illustrated in Fig. 2.19

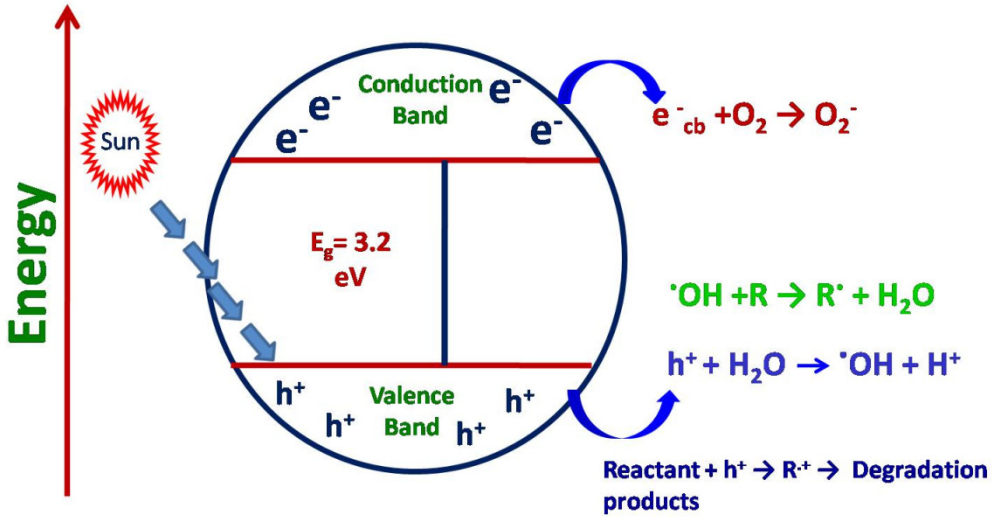

Fig.2.19. Mechanism of Photodegradation of Titania and formation of Free radical.

If charge separation is maintained, the electron and hole may migrate to the catalyst surface where they participate in redox reactions with sorbed species.

Specially, h^+_{vb} may react with surface-bound H_2O or OH^- to produce the hydroxyl radical and e^-_{cb} is picked up by oxygen to generate superoxide radical anion (O_2^-), as indicated in the following equations 6-8;

Absorption of efficient photons by titania ($h\upsilon \geq E_{bg} = 3.2$ ev)

$$TiO_2 + h\upsilon \rightarrow e_{cb} + h^+_{vb} \quad \textbf{(6)}$$

Formation of superoxide radical anion

$$O_2 + e_{cb} \rightarrow O_2^- \quad \textbf{(7)}$$

Neutralization of OH^- group into OH by the hole

$$(H_2O \square H^+ + OH^-)_{ads} + h^+_{vb} \rightarrow {}^{\bullet}OH + H^+ \quad \textbf{(8)}$$

It has been suggested that the hydroxyl radical ($^{\bullet}OH$) and superoxide radical anions ($O_2^{\cdot -}$) are the primary oxidizing species in the photocatalytic oxidation processes. These oxidative reactions would results in the degradation of the pollutants as shown in the following equations 9-10;

Oxidation of the organic pollutants via successive attack by OH radicals

$$R + {}^{\bullet}OH \rightarrow R^{\cdot} + H_2O \quad \textbf{(9)}$$

or by direct reaction with holes

$$R + h^+ \rightarrow R^{\cdot +} \rightarrow \text{ degradation products} \quad \textbf{(10)}$$

For oxidation reactions to occur, the VB must have a higher oxidation potential than the material under consideration. The redox potential of the VB and the CB for different semiconductors varies between +4.0 and -1.5 volts versus Normal Hydrogen Electrode (NHE) respectively. The VB and CB energies of the TiO_2 are estimated to be +3.1 and -0.1 volts, respectively, which means that its band gap energy is 3.2 eV and therefore absorbs in the near UV light (λ<387 nm). Many organic compounds have a potential above that of the TiO_2 valence band and therefore can be oxidized. In contrast, fewer organic compounds can be reduced since a smaller number of them have a potential below that of the TiO_2 conduction band.

2.6. Adsorption study

The degradation of EBT under visible light irradiation in presence of TiO_2 and Ni:TiO_2 nanoparticles are an example of heterogeneous catalysis. Rate laws in such reactions seldom follow proper law model and hence are inherently more difficult to formulate from the data. It has been widely accepted that heterogeneous catalytic reactions can be analyzed with the help of Langmuir Hinshelwood (LH) Model [46-48], satisfying, the following assumptions (i) there are limited number of adsorption sites on the catalyst and its surface is homogeneous, (ii) only one molecule can be adsorbed on one site and monolayer formation occurs (iii) the absorption reaction is reversible in nature, and (iv) the adsorbed molecules do not react amongst themselves [49-50]. According to LH Model, following three steps take place in the kinetics mechanism [51–52], these steps are of adsorption, surface reaction and desorption of products from the surface.

Step 1: D (Dye) + C (catalyst) $\longleftrightarrow$ D.C (Adsorption)

Step 2: D.C $\longleftrightarrow$ E.C + Other products (Surface reaction)

Step 3: E.C $\longleftrightarrow$ E + C (Desorption)

The Freundlich isotherm [53] is employed, assuming a heterogeneous surface with a non uniform distribution of heat of adsorption over the surface and it may be written as:-

$$q_e = K_F C_e^{\frac{1}{n}} \quad \textbf{(11)}$$

The above equation can be linearized as

$$lnq_e = lnK_F + \frac{1}{n} lnC_e \quad \textbf{(12)}$$

Where q_e (mg/g) is the amount of solute adsorbed per unit weight of adsorbent, C_e (mg/l) is the equilibrium concentration of solute, K_F (mg/g) is the Freundlich constant (which indicate the relative adsorption capacity of the adsorbent) and 1/n is the constant indicate the intensity of adsorption. Since the TiO_2 is covered by both EBT as well as

water molecules (C_{water}) by hydrogen bonding, their competition for the active sites cannot be ignored.

Langmuir adsorption model [54] can be applied to the aqueous solutions of dyes with the help of the following expression:

$$q = \frac{q_t}{q_{\max}} = \frac{K_L C}{1+K_L C+K_{water}+C_{water}} \quad \textbf{(13)}$$

Where q is the fractional sites covered by the dye, q_t is the absorbed quantity of dye at any time, q_{max} shows the maximum quantity of dye that can be adsorbed, K_L is the Langmuir adsorption constant for reactant and K_{water} is the adsorption constant for water. The value of C_{water} >> C, hence C_{water} remains almost same throughout the reaction and the catalyst coverage by water molecules remains almost constant. Thus, we can ignore the quantity K_{water}, C_{water} and rewrite Eq. (13) as:

$$q = \frac{K_L\ C}{1+K_L\ C} \quad \textbf{(14)}$$

The quantity adsorbed at a particular time can also be expressed as:

$$qt = \frac{(Reactor\ Volume\ )*(\boldsymbol{Change}\ in\ concentration)}{Mass\ of\ catalyst} \quad \textbf{(15)}$$

The equilibrium adsorption quantity q_{eq} can be written as:

$$q_e = q_{Max}\left[\frac{K_L C_e}{1+K_L C_e}\right] \quad \textbf{(16)}$$

where Ce is the equilibrium concentration of the EBT. On transforming Eq. (16), a function can be derived as follows:

$$\frac{C_e}{q_e} = \frac{1}{K_L q_{max}} + \frac{C_e}{q_{max}} \quad \textbf{(17)}$$

The intercept on the vertical axis gives $1/K_L q_{max}$ and the reciprocal of slope gives q_{max}.

The graph (Fig.2.20) indicates that the adsorption of EBT dye on the surface of Ni:TiO_2 follows the non linear Freundlich adsorption isotherm. The Freundlich isotherm non linear regression coefficient value was found 0.96 and Langmuir non linear regression coefficient value was found to be 0.91. Therefore the adsorption of dye EBT follows the Freundlich isotherm.

Table.2.3. Adsorption parameters of EBT adsorption

Adsorption equation	Isotherm parameter		R^2(non linear)
Freundlich	K_F	8.457	0.96
	1/n	0.432	
Langmuir	K_L	0.116	0.91
	q_{max}	43.62	

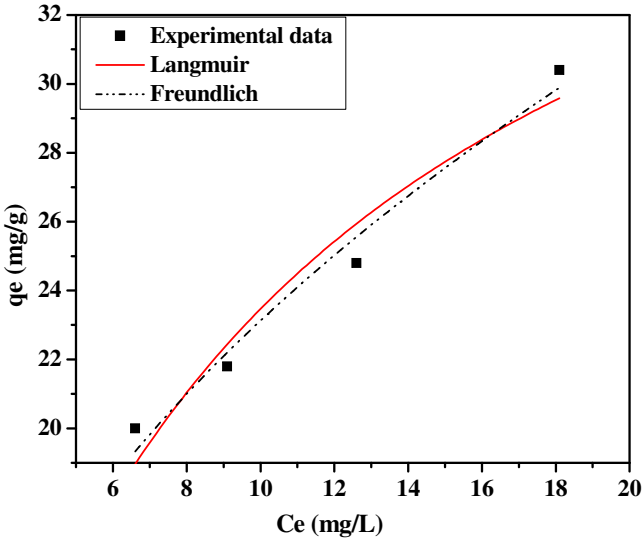

Fig.2.20. Langmuir and Freundlich adsorption isotherm with experimental data for the EBT dye adsorption on Ni:TiO_2

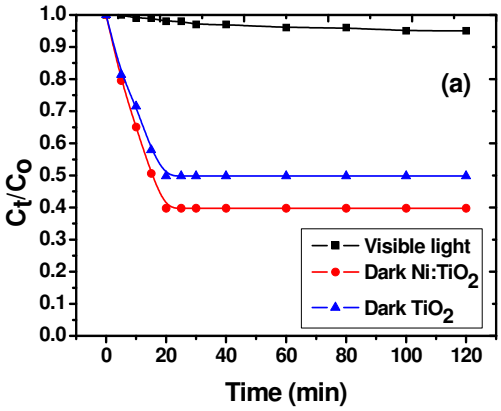

Fig.2.21. Change in concentration under dark with TiO_2, Ni:TiO_2 and in visible light

2.7. Kinetic study of Photocatalytic degradation

For kinetic study of photocatalytic degradation, a control experiment was first carried out under two conditions, vis (i) dye + Visible light (no catalyst) (ii) catalyst+ dye in dark without any irradiation (Fig. 2.22). It can be seen that under dark conditions, the amount of catalyst adsorbed becomes constant after 20 min, where adsorption equilibrium is achieved.

For kinetic study of photodegradation of EBT, the initial concentration of the dyes was varied and the experiments were first conducted in dark for 20 min and then immediately followed by irradiation (Fig. 2.22). The amount of catalyst was kept constant (0.2 g) throughout the experiment.

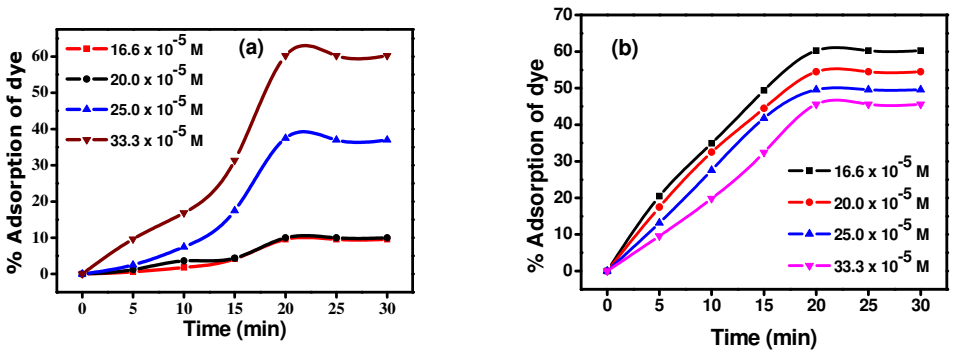

Fig.2.22. % Adsorption under dark condition (a) TiO_2 (b) Ni:TiO_2

Applying the Langmuir Hinshelwood model for determining the oxidation rate of the photocatalysis of dye:

$$Rate\ (r) = -\frac{dC}{dt} = k\theta = \theta = \frac{kK_AC}{1+K_AC} \qquad \textbf{(18)}$$

Where k is the rate constant (mg/L min^{-1}), C is the concentration of dye, K_A is the adsorption constant of the dye (L/mg), and t is the illumination time (min). During the course of reaction, the initial pH, amount of catalyst, and photointensity were kept same. In addition to it, the formation of intermediates may interfere in the rate determination; hence the calculation was done at the beginning of irradiation. The rate expression can be written as:

$$r_o = \frac{kK_AC_o}{1+K_AC_o} \qquad \textbf{(19)}$$

Where r_o is the initial rate of degradation of EBT and C_o is the initial concentration (almost equal to Ceq). When the initial concentration $C_{initial}$ is very small, Co will also be small and Eq. (19) can be simplified as an first-order equation [55-58]:

$$-\frac{dC}{dt} = kK_AC_o = \frac{lnC_o}{C} = kK_At \quad \textbf{(20)}$$

$$C = C_o e^{-k_f photo\, t} \quad \textbf{(21)}$$

Where

$k_{f,\,Photo=}\, k\, k_A$

The value of $k_{f,photo}$ can be determined from the plot of ln C_t/ Co vs. t (Fig.2.23). The slope of the straight line is the value of first order rate constant [59].

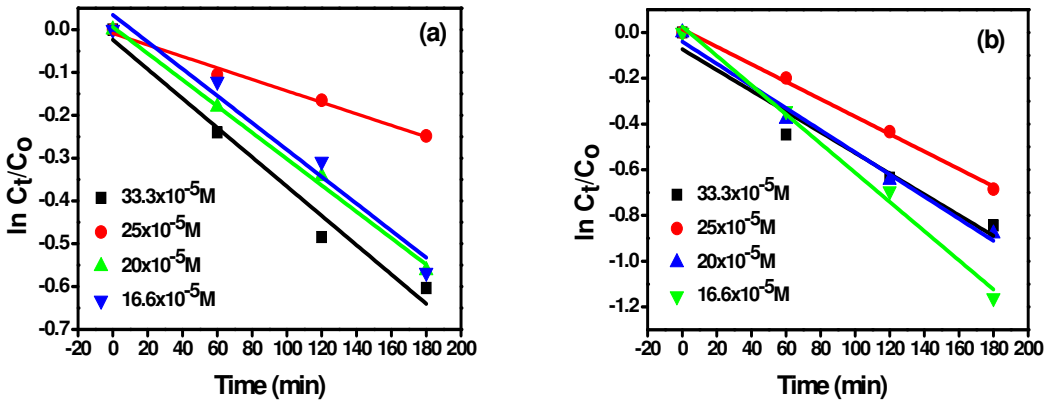

Fig.2.23. Linear first order reaction of Langmuir Hinshelwood kinetics of EBT dye vs. time (a) TiO_2 (b) Ni:TiO_2 (initial concentration were 33.3, 25, 20, 16.6 x 10^{-5} M)

Table.2.4. Value of apparent rate constant at various initial concentrations of dye solution for photocatalysis reaction in presence of TiO_2

Concentration	k(min^{-1})	R^2
33.3x10-5M	-0.00342	0.96852
25.0x10-5M	-0.00304	0.98338
20.0x10-5M	-0.00308	0.99412
16.6x10-5M	-0.00315	0.96074

The value of apparent rate constant at various initial concentrations of dye solution for photocatalysis reaction in presence of TiO_2 and Ni:TiO_2 are shown in Table.2.4 and 2.5.

The rate constant values for the photocatalytic degradation of EBT follow the first order kinetic for the both photocatalyst. In case of TiO_2 the regression (R^2) coefficient values shows large variation and optimum value was obtained at 20.0 x 10^{-5}M concentration of dye and in case of Ni:TiO_2 the regression (R^2) coefficient values was not show variation whose optimum value was obtained at 25.0 x 10^{-5}M concentration of dye. This is confirmed that photocatalytic degradation of EBT follows first order kinetic in presence of TiO_2 and Ni:TiO_2.

Table.2.5.Value of apparent rate constant at various initial concentrations of dye solution for photocatalysis reaction in presence of Ni:TiO_2

Concentration	k(min^{-1})	R^2
33.3x10^{-5}M	-0.004537	0.93066
25.0x10^{-5}M	-0.003821	0.99589
20.0x10^{-5}M	-0.004843	0.98083
16.6x10^{-5}M	-0.006393	0.99086

Conclusion

In the present investigation TiO_2 and Ni:TiO_2 nanoparticles were prepared and their photocatalytic degradation capacity was measured against of Eriochrome Black T under visible light irradiation. Prepared TiO_2 and Ni:TiO_2 nanoparticles were analyzed by XRD, SEM, TEM, UV-Vis, FTIR, BET and Band gap energy. In the XRD pattern of TiO_2 and Ni:TiO_2 nanoparticles, both Anatase, and rutile phases were present. The particle size of TiO_2 and Ni:TiO_2 was calculated as 72 and 16 nanometer respectively using Scherrer's equation. SEM and TEM images of TiO_2 and Ni:TiO_2 nanoparticles were found as agglomerate in nanometric dimension. The doping of Ni^{2+} indicates that the particle size reduces due the penetration of nickel in the lattice of TiO_2. Doping with 5% Ni, the crystallite size was decreased and the surface area value increased. These results suggest that Ni doping effectively inhibits TiO_2 grain growth probably by staying at grain boundaries thereby decreasing the crystallite size and increasing the

surface area. The undoped TiO_2 showed absorbance in the shorter wavelength region while Ni:TiO_2 results showed slight red shift in the absorption edge. The band gap energy *E*g value of TiO_2 and Ni:TiO_2 was found 3.2 and 3.0 eV respectively. The slight decrease in band gap energy in case of Ni:TiO_2, is due to formation of sub-band level between valence band and conduction band due to doping of Ni^{2+} in TiO_2 host. The broad intense band below 820, 804, 592 and 456 cm^{-1} is due to Ti-O-Ti vibrations and Ni:TiO_2 shows strong band at 1075 cm^{-1}, corresponds to the vibration of Ni–O bond and confirms the penetration of nickel in Titania. The Photo-degradation of Eriochrome Black T was investigated at different condition of concentration and pH in presence of TiO_2 and Ni:TiO_2. The effective photo-degradation of Eriochrome Black T was found better in the presence of Ni:TiO_2 as than the pure TiO_2.$^{\bullet}$OH, radicals mediated photocatalytic degradation of EBT was proved by GC-MS. Since TA is readily converted to TAOH in presence of $^{\bullet}$OH radical, the Photolumiscence spectra of photodegraded EBT with TA shows higher Photolumiscence peak correspond to TA in presence of Ni:TiO_2 than TiO_2. Photo-degradation of Eriochrome Black T is follow the pseudo first order kinetics. Complete degradation of Eriochrome Black T was more prominent in 180 min, in the presence of Ni:TiO_2 while it was 90 % in presence of TiO_2 in same condition.

References

[1]. A.A. Ahmad, B.H. Hameed, N. Aziz, J. Hazard. Mater. 141, (2007), 70–76.

[2]. N.Barka, A. Assabbane, A. Nounah, L. Laanab, and Y. Ait-Ichou,Desalination235, (2009), 264-275.

[3]. N. Barka, S.Qourzal, A.Assabbane, Nounah, A. and Ait-Ichou, Y.J. Environ. Sci. 20, (2008), 1268-1272.

[4]. D.V. Bavykin, K.E. Redmond, B.P. Nias, A.N. Kulak, F.C. Walsh, Aust. J. Chem. 63, (2010), 270–275.

[5]. M. I. Franch, J. Peral, X. Domènech, R. F. Howe, J. A. Ayllón, Applied Catalysis B: Environmental, 55, (2005), 105–113.

[6]. W.T Tsai, C.Y Chang, M.C Lin, S.F Chien, H.F Sun, M.F Hsieh, Chemosphere, 45, (2001), 51-58.

[7]. Hiroyuki Kono, Ryo Kusumoto, Journal of Water Process Engineering, 7, (2015), 83-93.

[8]. R. Gong, S. Zhu, D. Zhang, J. Chen, S. Ni, R. Guan, Desalination, 230, (2008), 220-228.

[9]. N. K. Goel, V. Kumar, N. Misra, L. Varshney, Carbohydrate Polymers, 132, (2015), 444-451.

[10]. S. Wijannarong, S. Aroonsrimorakot, P. Thavipoke, C. Kumsopa, S. Sangjan, APCBEE Procedia 5, (2013), 279-282

[11]. H. Laguna, S. Loera, I. A. Ibarra, E. Lima, M. A. Vera, V. L. Azoic, Microporous and Mesoporous Materials, 98, (2007), 234-241

[12]. N. Hirun, V. Tantishaiyakul, W. PichayakornInt. J. of Pharmaceutics, 388, (2010), 196-201.

[13]. H. Song, C. Chen, H. Zhang, J. Huang, J. of Env. Chem. Eng, 4, (2016), 460-467

[14]. K. Chinoune, K. Bentaleb, Z. Bouberka, A. Nadim, U. Maschke, Applied Clay Science, 123, (2016), 64-75.

[15]. E. Rubin, P. Rodriguez, R. Herrero, J.Cremades, I. Barbara and M. E. S. Vicente, J. Chem. Technol. Biotechnol. 80, (2005), 291-298.

[16]. C.L. Porras, A.T. Teran, O.V. Becerra, M.M. Yoshida, M.R. Villalobos, M.G. Guaderrama, J.A.A. Martínez, J. of Allo. and Comp., 647, (2015),627-636

[17]. H. Cai, W. Mu, W. Liu, X. Zhang, Y. Deng, Inorganic Chemistry Communications 51, (2015), 71-74

[18]. O. Jongprateep, R. Puranasamriddhi, J. Palomas,Ceramics International, 41, (2015), S169-S173

[19]. H. Lee, Y.K. Park, S.J. Kim, B.H. Kim, S. C. Jung, Journal of Industrial and Engineering Chemistry, 32, (2015), 259-263

[20]. H. Jia, Z. Zheng, H. Zha., L. Zhang,and Z. Zou, Materials Research Bulletin, 44, (2009), 1312-1316

[21]. M.N. Makwana, J. T. Christopher, I. G. Robert, Paul F. McMillan, Materials Science in Semiconductor Processing, 42, (2016), 131-137

[22]. C. M. Ng, P.C. Chen, S. Manickam, Applied Catalysis A: General, 433–434,(2012), 75-80.

[23]. A. Gnanaprakasam, V.M. Sivakumar, P.L. Sivayogavalli, M. T. Murugan, Ecotoxicology and Environmental Safety, 121, (2015), 121-125

[24]. S. Kaur, V. Singh, Ultrasonics Sonochemistry, 14, (2007), 531-537

[25]. L. Cavigli, F. Bogani, A. Vinattieri, V. Faso, G. Baldi,J. Appl. Phys. 2009, 106, 053516

[26]. S. Liu, N. Jaffrezic, C. Guillard, Appl. Surf. Sci. 255, (2008), 2704-2709.

[27]. M. Scarisoreanu, I. Morjan, R. Alexandrescu, C.T. Fleaca, A. Badoi, E. Dutu, A.M. Niculescu, C. Luculescu, E. Vasile, J. Wang, S. Bouhadoun, N. Herlin-Boime, App. Sur. Sci., 302, (2014), 11-18.

[28]. E. Baran, B. Yazici, Int. J. of Hydrogen Energy, 41, (2016), 2498-2511.

[29]. B. Choudhury, M. Dey,and A. Choudhury, Int. Nano Letters, 3, (2013), 25

[30]. A. E. Gary and C. Lin, Chemosphere, 46, (2002), 937-944.

[31]. M. Toyoda, T. Yano, B. Tryba, S. Mozia, T. Tsumura, and M. Inagaki, Applied Catalysis B: Environmental, 88, (2009), 160-164.

[32]. B. D.Cullity, S. R.Stock, Elements of X-Ray Diffraction, Third Edition, and New Jersey: Prentice-Hall, Inc. (2001).

[33]. R. Byberg, J. Cobb, L.D. Martin, R.W. Thompson, T.A. Camesano, O. Zahraa, M.N. Pons, Environ. Sci. Pollut. Res. 20, (2013), 3570–3581.

[34]. R. Matos, E. Montan, V.Rivero, Environ. Sci. Pollut. Res. 22, (2015), 784–791.

[35]. B. Pal, R. Kaur, I. S. Grover, J. of Ind. and Eng. Chem., 33, (2016), 178-184

[36]. K. Madhusudan Reddy, Sunkara V. Manorama, A. Ramachandra Reddy, Materials Chemistry and Physics 78, (2002), 239–245.

[37]. A. Kumar, G. Hitkari, S. Singh, M. Gautam, G. Pandey Int. J. of Innovative Research in Science, Engineering and Tech. 4, (2015), 12721-12731

[38]. A. Kumar, G. Hitkari, M. Gautam, S. Singh, G. Pandey, Int. Adv. Research J. in Science, Engineering and Tech. 2, (2015), 50-55

[39]. Fujishima, Akira, Nature 238, (1972), 37.

[40]. S.K. Kansal, M. Singh, D. Sud, J. Hazard. Mater. 141, (2007), 581–590

[41]. K. Selvam, M. Muruganandham, I. Muthuvel, M. Swaminathan, J. Chem. Eng. 128, (2007), 51–57

[42]. W. Baran, A. Makowski, W. Wardas, Chemosphere 53, (2003), 87–95

[43]. H. Nishikiori, S. Fujiwara, S. Miyagawa, N. Zettsu, K. Teshima, Applied Catalysis B: Environmental, 217, (2017), 241-246,

[44]. A.L. Kretzschmar, M.Manefield, AIMS Environmental science, 2(2), (2015), 122-133

[45]. R.D. Kale and Chet Ram Meena, Advances in Applied Science Research, 3 (5), (2012), 3073-3080

[46]. R.Q. Cabrera, A. Mills, C. O'Rourke, Applied Catalysis B: Environmental, 150–151, (2014), 338-344

[47]. H. Lachheb, E. Puzenat, A. Houas, M. Ksibi, E. Elaloui, C. Guillard, J.M. Herrmann, Appl. Catal. B: Environ. 39, (2002), 75–90.

[48]. G.A. Epling, C. Lin, Chemosphere 46, (2002), 561–570.

[49]. M.M. Ba-Abbad, A.A.H. Kadhum, A.B. Mohamad, M.S. Takriff, K. Sopian, Int. J. Electrochem. Sci 7, (2012), 4871–4888.

[50]. M. Hema, A.Y. Arasi, P. Tamilselvi, R. Anbarasan,, Chem. Sci. Trans. 2, (2013), 239–245.

[51]. S. Yang, X. Yang, X. Shao, R. Niu, L. Wang, J. Hazard. Mater. 186, (2011), 659–666.

[52]. M. Vautier, C. Guillard, J.M. Herrmann, J. Catal. 201, (2001), 46–59.

[53]. E. Vulliet, J.M. Chovelon, C. Guillard, J.M. Herrmann, J. Photochem. Photobiol. A: Chem. 159, (2003), 71–79.

[54]. N. Guettaı, H.A. Amar, Desalination 185, (2005), 439–448.

[55]. D. Chen, A.K. Ray, Appl. Catal. B: Environ. 23, (1999), 143–157.

[56]. H. Freundlich, J. Phys. Chem. 57, (1907), 385–470.

[57]. I. Langmuir, J. Am. Chem. Soc.40, (1918), 1361–1403.

[58]. R.W. Matthews, J. Catal. 111, (1988), 264–272.

[59]. R. Zepp, D. Crosby D., J. Photochem. Photobiol., A, Lewis Publs., CRC Press, Boca Raton, Florida, Chap. 22, (1994), 317–348.

CHAPTER-3

Photocatalytic Activity of Co:TiO_2 Nanocomposites and their Application in Photodegradation of Acetic Acid

Nanocomposites of Co:TiO_2 were prepared by wet chemical methods. The prepared samples were characterized by XRD, SEM, BET, FTIR and UV-Visible spectra. The XRD analysis confirmed the presence of rutile and anatase both phases were present. It is found that rutile phase was more dominant. Applying the Scherrer's calculations through which particle size was found 35 and 80 nm in case of Co:TiO_2 and pure TiO_2 respectively. SEM image of Co:TiO_2 and TiO_2 were observed and both found in nanodiamension. The photocatalytic degradation of acetic acid was done at different condition of concentration, amount of photocatalyst and type of catalyst. The effective photodegradation of acetic acid were found at low concentration and photodegradation increases with decrease the concentration of acetic acid. The prominent degradation of acetic acid was found in the presence of nanocomposites Co:TiO_2 as compared with TiO_2.

3.1. Introduction

The photocatalytic degradation (PCD) in the presence of UV and oxygen has attracted attention of researchers for remediation of hazardous pollutants in water [1]. The advantages of PCD over conventional treatment techniques are degradation of a broad range of organic pollutants, lower cost, and mild operating conditions [2]. The TiO_2catalyzed PCD of various groups of organic pollutants like alcohols, phenols, carbonyls and carboxylic compounds, aromatics, halocarbons etc. has been reported extensively [3-8].

The removal of several aliphatic carboxylic acids [9-11], as well as aromatic acids such as benzoic acid, polycarboxylic acids, salicylic acid, chlorobenzoic acids, etc. [12-15] from water using TiO2catalyzed PCD, has been reported. Besides this, photocatalytic degradation of the higher aliphatic carboxylic acids such as branched C4 and C5 aliphatic acids using titanium dioxide has also been studied [16].

The present paper focuses on Co:TiO_2 catalyzed PCD of Acetic Acid and studying the influence of various parameters affecting PCD of acetic acids, i.e., molecular structure on the kinetics and mechanistic pathway, effect of initial concentration, pH, temperature, amount of catalyst and type of catalyst[17].

Most of the researchers are working on the photocatalytic degradation of organic compounds such as dyes, pesticides, and aromatic compounds. The photocatalytic reactions for the degradation of trace acids, dyes, and pesticides in water have been used by researchers in recent years. It is the advanced oxidation process [18] to degrade the water contaminants such as acids [19], dyes [20], pesticides [21] and non biodegradable materials [22], which exhibit chemical stability and resistance to biodegradation [23]. Most of the researcher are focused on the use of semiconductor materials as photocatalysts for the removal of organic and inorganic species from aqueous or gas phase [24]. Titanium dioxide (TiO_2) is the cheapest, corrosive resistant photocatalysts [25] and it has high oxidative power, stability, and non-toxicity [26]. The most of the photocatalytic reactions occurs under ambient conditions. Titanium dioxide (TiO_2) photocatalysed reaction, complete oxidation of the substrate into CO_2 in most

cases and it is comparatively inexpensive and remains quite stable in contact with different substrate [27]. Semiconductor photocatalytic oxidation is the best eco-friendly techniques for the removal of trace organic pollutants from waste water.

Wolff et al. [28] have examined the photocatalytic oxidation of Acetic Acid on TiO_2. It has been proposed that hydroxyl radicals ($^{\bullet}OH$) attack acetate ions mainly, at the methyl group.

$$CH_3COOH + {}^{\bullet}OH \rightarrow {}^{\bullet}CH_2COOH + H_2O$$

In the presence of oxygen, the radicals thus formed react quickly with molecular oxygen leading to the formation of CHOCOOH, $HOCH_2COOH$, $HOOCH_2OOCH_2COOH$, HCHO, andCO_2. Direct electrochemical oxidation of acetate results in the well-known Kolbe decarboxylation with the formation of a methyl radical.

3.2. Experimental

3.2.1. Synthesis of TiO_2

25ml of diluted $TiCl_4$ was taken along with 1ml of concentrated H_2SO_4 and diluted to 1 l using double distilled water. Liquor NH_3 was added drop wise to the solution so as to maintain the solution pH in the range of 7–8. The precipitate is filtered and washed free of chloride and ammonium ions. The precipitate is first oven dried at 100 $^{\circ}$C for 12 h and grinded in a mortar. The obtained powder is then calcined at 500 ^{o}C for 4 h in muffle furnace to get TiO_2 [29].

3.2.2. Synthesis of Co:TiO_2

In this study, Co:TiO_2 nanocomposites were prepared by solution impregnation method. TiO_2 powder (4.5g) was dispersed in 100 ml of alcoholic solution of 0.1M cobalt acetate. The dispersion is agitated continuously for 4 hour at 85 ^{o}C temperature. After the heating and agitation, the residue will removed through filtration and was sintered for 3 hour in presence of air at 400 ^{o}C by kipping it in a silica boat inside muffle furnace. After sintering and slow anilling to room temperature, content was taken out from furnace and was used as photocatalyst [30].

3.2.3. Photo-degradation studies

Photocatalysed oxidative degradation reaction of organic substrates is holds lot of potential in pollution abatement as well as in synthetic Organic Chemistry. Although in literature several photocatalyst have been cited for this purpose many of then suffer from one or more disadvantage, particularly with regard to either then being highly expensive and chemically unstable. TiO_2 is well known semiconductor that has also been widely used as photocatalyst. In this study, to investigate the photo-degradation behaviour of a prepared TiO_2 and Co:TiO_2 nanocomposites towards photo-degradation of acetic acid [31-32].

3.3. Result

3.3.1. X-ray diffraction analysis

Phase identification in the samples was attempted by analyzing them using X-Ray Diffractometer (Bruker AXS D8 Advance System, Germany). The obtained X-Ray diffraction patterns of TiO_2 and Co:TiO_2 are shown in Figures 3.1(a) and (b). The observed pattern of peaks, when compared with the standard JCPDS database, suggested that, in synthesized TiO_2, major peaks at 2θ angles 25.5, 37.2, 48.3 and 55.40 correspond to anatase phase, whereas major peaks at 2θ angles 26.9, 28.2, 42.6and 54.2^0 indicate the presence of rutile phase. In case of Co:TiO_2 sample, the observed XRD pattern indicates not only a decrease in the peak intensity, compared to TiO_2 but even the absence of some originally observed TiO_2 peaks.

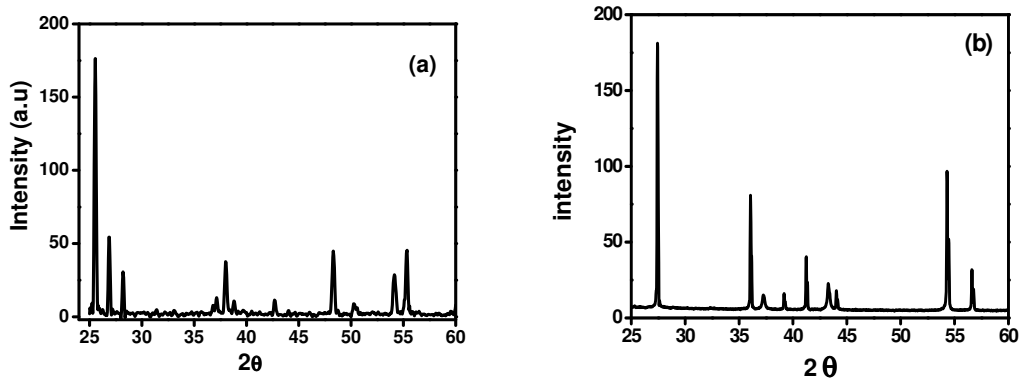

Fig.3.1. Observed XRD pattern of (a) TiO_2 (b) Co:TiO_2

This is, probably, due to the change in the crystallinity, grain fragmentation, and partial amorphization, when the samples were doped by Cobalt acetate [33].

3.3.2. Determination of Average size of Particles/ Grains in samples

Utilizing the observed X-ray diffraction data of samples, Scherrer's calculations were attempted to know the average size of particles/grains in the samples. Although, Scherrer's calculations are only approximate in nature, but definitely provide a first-hand idea of the average size of the particles/ grains in the samples, which may be quite accurate, provided the size of particles/ grains is below 100 nm [34]. The results of Scherrer's calculations are presented in Table 3.1. The results suggest average size of the particles/ grains in the samples lying in nm range.

Table.3.1. Average size of particles/grains in the samples of TiO_2 and Co:TiO_2

Sample	Particle size (nm)
TiO_2	100
Co:TiO_2	35

3.3.3. FT-IR spectroscopy

FT-IR spectra of undoped and 10.0% Co doped TiO_2 samples (Fig.3.2) show peaks corresponding to stretching vibrations of the O-H and bending vibrations of the adsorbed water molecules around 3750 cm^{-1} and 2319 cm^{-1}, respectively. The broad intense band below 497, 604 and 645 cm^{-1} is due to Ti-O-Ti vibrations The shift to the higher wave numbers and sharpening of the Ti-O-Ti band (Fig.3.2) may be due to decrease in size of the catalyst nanoparticles. In addition, the surface hydroxyl groups in TiO_2 increase with the increase of Co loading, which is confirmed by increase in intensity of the corresponding peaks. The FT-IR spectra shows strong band at 757 cm^{-1} corresponds to the vibration of Co–O bond and it is confirm the penetration of Cobalt in Titania [35].

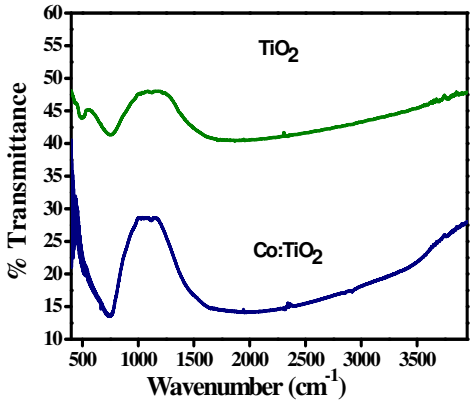

Fig.3.2. FTIR spectra of TiO_2 and Co:TiO_2

3.3.4. UV-Vis spectroscopy

The absorption spectrum of TiO_2 consists of a single broad intense absorption between 250 to 300 nm due to the charge-transfer from the valence band to the conduction band [36]. The undoped TiO_2 showed absorbance in the shorter wavelength region while Co:TiO_2 results showed a blue shift in the absorption onset value in the case of Co added Titania [Fig.3.3].The impregnation of Co ions into TiO_2 could shift its optical absorption edge from UV into visible light range [37]. Aqueous suspensions of the samples were used for the UV absorption studies. The blue shift that is observed in the absorption spectra with the decrease in particle size has been reported earlier [38].The wavelength of Co:TiO_2 has been decreased due to the formation of cobalt oxygen bond.

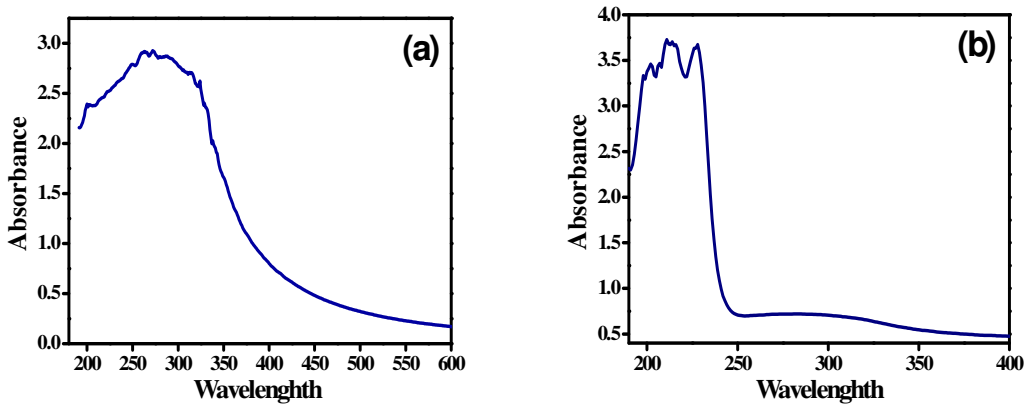

Fig.3.3. UV-Vis spectra of (a) TiO_2 and (b) Co:TiO_2

3.3.5. Scanning Electron Microscopy (SEM)

The morphology of the samples was investigated by scanning electron microscopy and it resumes the most interesting outcomes. Fig 3.4(a) and (b) clearly show that both the prepared samples are obtained agglomerate in nanometric dimension. The doping of cobalt is indicating that the particle size reduce due the penetration of cobalt in the lattice of titanium dioxide.

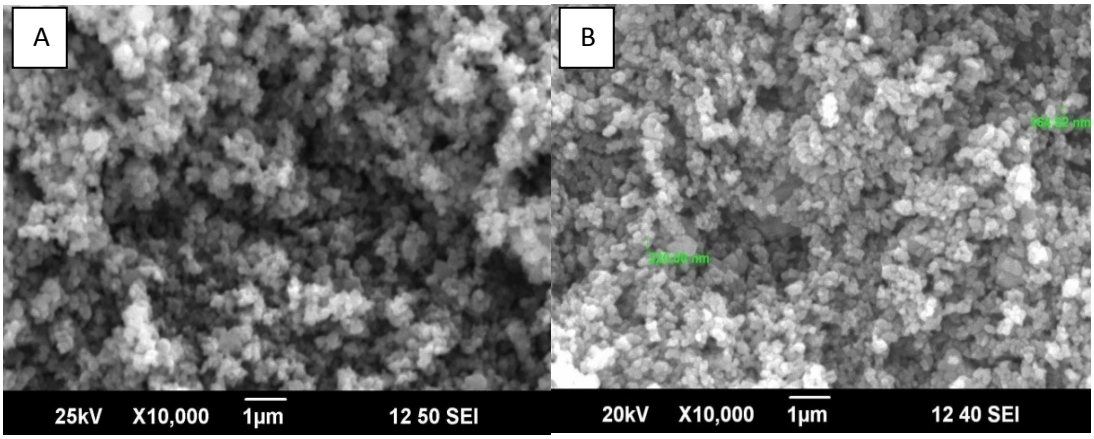

Fig.3.4. Observed SEM image of (A) TiO_2 (B) Co:TiO_2

3.3.6. Surface area analysis (B.E.T)

The specific surface area, pore volume and average pore size of the TiO_2 and Co:TiO_2 as-prepared photocatalyst were characterized by using the N_2 adsorption technique *BET*. Table.3.2 summarizes their physical properties. The TiO_2 modified by Cobalt are fragmentized to some extent during thermal treatment, leading to a marked increase of the *BET* surface areas and the average pore radius size and decreasing of the pore volume [39].

Table.3.2. Phase surface areas, pore volume, average particle sizes of TiO_2 and Co:TiO_2

Sample	Surface area (m^2/g)	Pore volume (cm^3/g)	Pore radius (nm)
TiO_2	6.4	0.018	11
Co:TiO_2	13.2	0.031	6

3.3.7. Photo-degradation of Acetic Acid

In this study, photo-catalytic degradation of Acetic Acid was investigated. The samples of TiO_2 and Co:TiO_2 were used as photocatalyst in the photo-degradation of Acetic acid. 200 mg/10 ml of the photo-catalyst was dispersed in Acetic Acid solution of 10.6×10^{-3} M, 5.3×10^{-3} M, and 2.65×10^{-3}M concentration and the reaction mixture was illuminated with UV–Visible light, while kept under agitation. The results presented in this Section comprise the residual concentrations (10.6×10^{-3}, 5.3×10^{-3}, and 2.65×10^{-3} M) of Acetic Acid in the reaction mixture, measured by titrimetrically against NaOH at different time intervals. The measured values of residual concentration of acids in the reaction mixture at different times of illumination (or reaction time) have been shown in Figures 3.5-3.7. It is clear from the results shown that both TiO_2 and Co:TiO_2 are proving as an effective photo-catalyst for the degradation of acetic acid. However Co:TiO_2 seems to be more effective photo-catalyst as compared to TiO_2, for the degradation of acetic acids [40].

3.3.7.1. Effect of concentration

Effect of acid concentration was investigated at constant temperature and amount of photocatalyst 200mg/10 ml of Acetic Acid solution, the effect of varying amounts of the acid was studied on its rate of its degradation (10.6×10^{-3}, 5.3×10^{-3}, and 2.65×10^{-3} M) as given in Fig.3.5. With increasing concentration of Acetic Acid the rate of degradation was found to decrease. This is because as the number of Acetic Acid molecules increase, the amount of light (quantum of photons) penetrating the Acetic Acid solution to reach the catalyst surface is reduced owing to the hindrance in the path of light. Thereby the formation of the reactive hydroxyl and superoxide radicals is also simultaneously reduced. Thus there should be an optimum value maintained for the catalyst and the Acetic Acid concentration, wherein maximum efficiency of degradation can be achieved.

3.3.7.2. Effect of photocatalyst

It is clear from the results shown in Fig.3.5-3.7 that both TiO_2 and Co:TiO_2 are proving as an effective photo-catalyst for the degradation of Acetic Acid. However Co:TiO_2 seems to be more effective as photo-catalyst for the degradation of Acetic acid. The prominent degradation of Acetic Acid was found in the presence of Co:TiO_2

in comparison to TiO_2. This is due to the large surface area of Co:TiO_2 as compared to TiO_2.

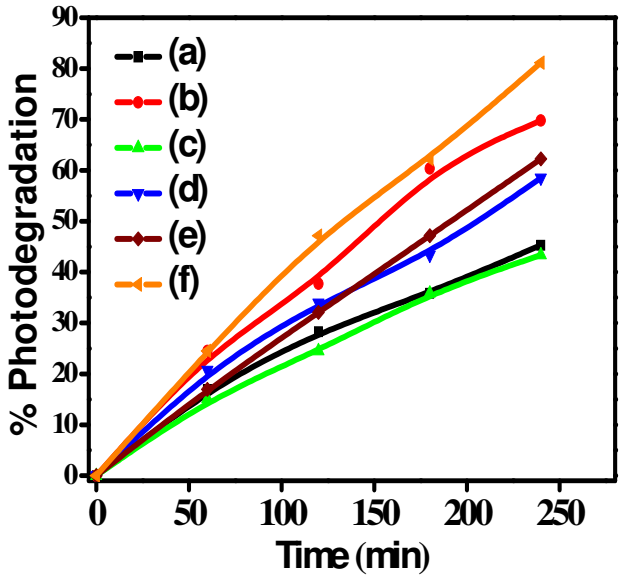

Fig.3.5. Photodegradation at different concentration (a) 10.6 x 10^{-3} M with TiO_2 (b)10.6 x 10^{-3} M with Co:TiO_2 (c) 5.3×10^{-3} M withTiO_2 (d) 5.3×10^{-3} M with Co:TiO_2 (e) 2.65×10^{-3} M with TiO_2 (f) 2.65×10^{-3} M with Co:TiO_2

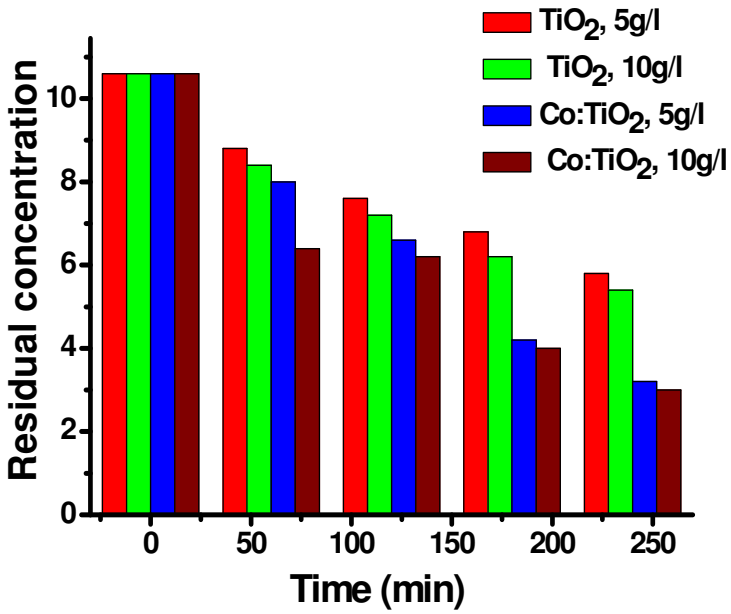

Fig.3.6. Photodegradation at different amount of photocatalyst in presence of TiO_2 and Co:TiO_2 at constant temperature, pH, and concentration.

3.3.7.3. Effect of photocatalyst amount

It is clear from the results shown in Fig. 3.6, that both TiO_2 and Co:TiO_2 are proving as an effective photo-catalyst for the degradation of Acetic Acid. But when the amount of photocatalyst increases the photodegradation of acid also increase. It is observed that Co:TiO_2 is the more effective photocatalyst than TiO_2.

3.3.7.4. Effect of Temperature

The effect of system temperature on photocatalysis has not attracted enough attention. But In present research, it is found that the temperature has a great effect on the photodegradation of Acetic acid. The photocatalytic efficiency can be increased about 2-3 times if the temperature increased from 30 ℃ to 40 ℃ Because the solar energy include UV light, which can be used to activate the photocatalytic course, which is increase the temperature of photocatalytic system. The experiments showed that Acetic Acid cannot be photodegraded if TiO_2 or UV light was not used, indicating that Acetic Acid cannot be pyrolyzed by heating with the heating temperature which was less than 40 ^oC and self degraded by absorbing irradiation. Only when TiO_2 and UV light were both used, the Acetic Acid was efficiently degraded shown in Fig.3.7. The obvious decrease of concentration of Acetic Acid shows that the TiO_2 and Co:TiO_2 can serve as an effective photocatalyst.

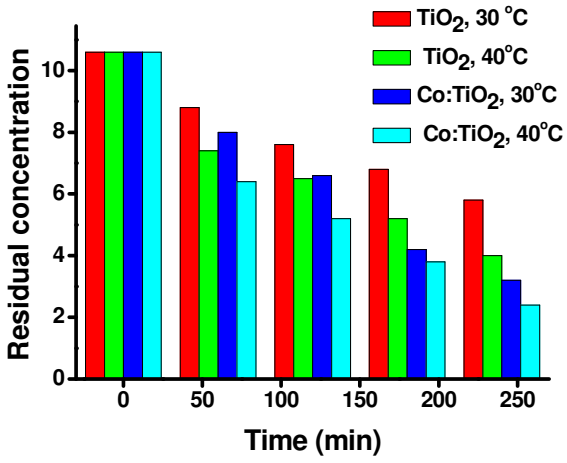

Fig.3.7. Photodegradation at different temperature in presence of TiO_2 and Co:TiO_2 at constant amount of photocatalyst, pH, and concentration.

3.3.7.5. Effect of pH

The photodegradation reaction was also carried out under varying pH conditions from (2 to 7), by adjusting with NaOH, with TiO_2 kept at constant amounts of 200mg in 20 ml of Acetic Acid solutions. The reaction was found to have low rates at neutral ranges of pH. While at lower cases it was found to increase at 4 to 5 pH shown in Fig.3.8. The photodegradation is maximum at 3-4 pH but at 6 pH the photodegradation is rapidly decrease and after increasing pH, the photodegradation slightly increase. This implies that acidic conditions are favourable towards the formation of the reactive intermediates that is hydroxyl radicals is significantly enhanced, which further help in enhancing the reaction rate. On the other hand in neutral medium conditions, the formation of reactive intermediates is relatively less favourable and hence less spontaneous.

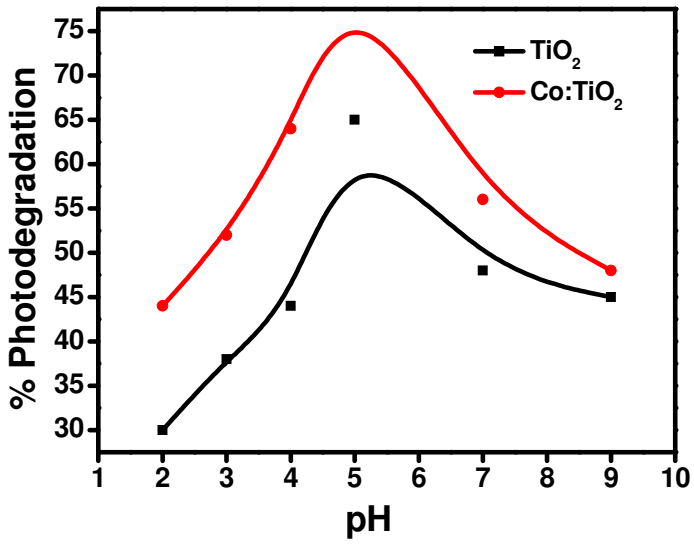

Fig.3.8. Effect of pH on Photodegradation of Acetic Acid in presence TiO_2 and Co:TiO_2.

3.3.8. Kinetics of Acetic Acid Photodegradation

The photocatalytic degradation of various carboxylic acids using titanium dioxide can be generally given by the Langmuir–Hinshelwood kinetics model [41-45]

$$\frac{dC}{dt} = \frac{kKC}{1+kKc} \quad \text{.....(1)}$$

where (dC/dt) is the rate of degradation, k the apparent reaction rate constant, K the adsorption coefficient of the substance to degraded and C concentration of carboxylic acid. In case the concentration of the substances to be degraded exceed the saturation coverage of the TiO_2 surface, i.e. K C >> 1, equation (13) simplifies to a zero-order rate equation.

$$\frac{dC}{dt} = k \quad \text{.....(2)}$$

Some of the carboxylic acids like formic acid, phenoxyacetic acid, 2-chlorobenzoic acid, 3-chlorobenzoic acid and 4- chlorobenzoic acid [46], p-hydroxy benzoic acid [47] follow zeroth kinetic order interpreted by a Langmuir-Hinshelwood mechanism involving a saturation of the adsorption sites. For very low concentration (i.e., K C << 1), the Langmuir-Hinshelwood equation (13) simplifies to a pseudo-first order kinetic law, where k is being the pseudo-first order rate constant.

$$-\ln \frac{C_t}{C_0} = kt \quad \text{.....(3)}$$

where C_0 is the initial concentration of carboxylic acid at time t = 0 and C_t is the concentration of carboxylic acid at reaction time t. The semi-logarithmic plot of [-ln (C_t/C_0)] versus time gives straight line and slope of the straight line gives the value of reaction rate constant, k ($time^{-1}$).

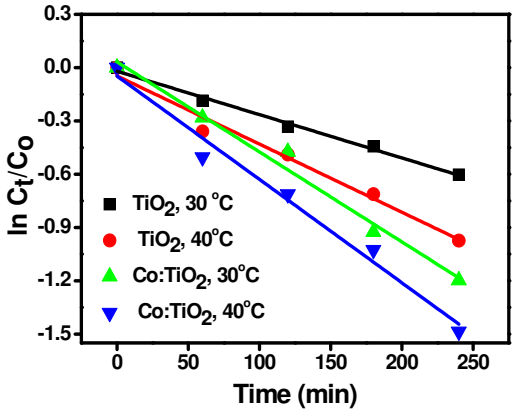

Fig.3.9. Change in concentration of Acetic Acid vs. time with TiO_2 and Co:TiO_2 at 30 and 40 ^oC temperature.

Some of the carboxylic acids like butanoic acid [48], phthalic acid [49], terephthalic acid [50] and oxalic acid [51] are followed pseudo-first order reaction under given experimental conditions.

The rate constant values for the photocatalytic degradation of Acetic Acid follow the first order kinetic. The effect of temperature on rate constant for the TiO_2 and Co:TiO_2 are showing in Fig.3.9 and in Table 3.3. In case of TiO_2 follow first order reaction at 30 and 40 ^oC temperature. The rate constant value has been increase by increased of temperature of reaction from 30 and 40 ^oC. The regression (R^2) coefficient values have been slightly decreased. It means that if we increase the temperature, the linearity slightly decreased. In case of Co:TiO_2 follow first order reaction at 30 and 40 ^oC temperature. The rate constant value has been increase by increased of temperature of reaction from 30 and 40 ^oC. The regression (R^2) coefficient value has been slightly decreased. It means that if we increase the temperature, the linearity slightly decreased. This is confirmed that photocatalytic degradation of Acetic Acid follows first order kinetic in presence of TiO_2 and Co:TiO_2 at different temperature. The effect of concentration of Acetic Acid on photocatalytic degradation has been measured in presence of TiO_2 and Co:TiO_2. Basically, the effect of concentration was measured by the calculation of rate constant of the reaction. The effect of concentration is showing in Fig.3.10 (a) and (b) and Table.3.4.

Table. 3.3. Rate constant and regression coefficient for TiO_2 and Co:TiO_2 at various 30 ^oC and 40 ^oC temperature.

Photocatalyst	Temperature	K (min^{-1})	R^2
TiO_2	(at 30^oC)	-0.00244	0.99120
TiO_2	(at 40^oC)	-0.00384	0.97533
Co:TiO2	(at 30^oC)	-0.00507	0.98032
Co:TiO2	(at 40^oC)	-0.00582	0.97689

The graph was plotted remaining concentration vs. time at different concentration of Acetic Acid (10.6 x10^{-3}M, 5.3 x10^{-3}M, and 2.65 x10^{-3}M). Change in concentration of Acetic Acid vs. time is showing in Fig.3.10 for TiO_2 and Co:TiO_2. In this case, the values of rate constant are increased with decrease of concentration of

acetic acid, it means that if we will decreased the concentration of acetic acid, the rate of photodegradation will increased.

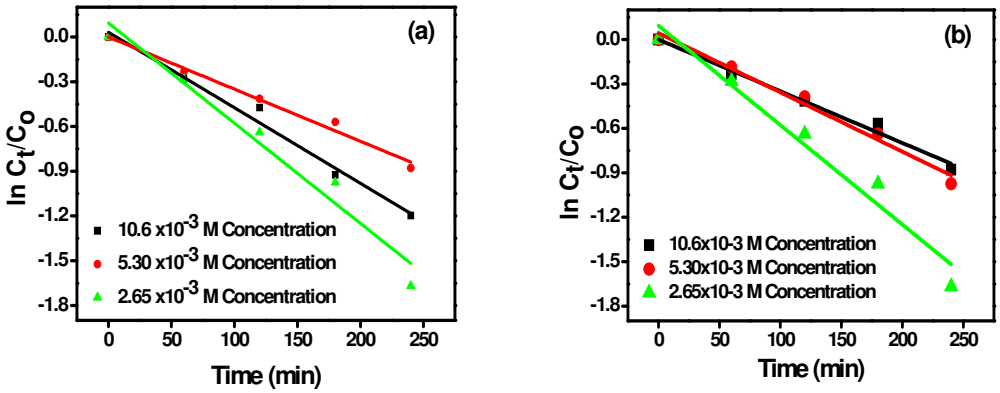

Fig.3.10. Change in concentration of Acetic Acid vs. time for (a) TiO_2 and (b) Co:TiO_2 at 40 ^oC temperature.

This is because the no of molecule per unit volume has been decreased that's why no of photon easily penetrate to the solution of acid and strike on the surface of semiconductor which is generate the electron (e^-) hole (h^+) pair. The generation of electron (e^-) hole (h^+) pair per unit volume will increased and no of reacting molecules of acid decreased with decrease of concentration of acetic acid. Hence the photocatalytic reaction will be fast at low concentration. But at high concentration, the penetration of photon is hindered by the molecules of acid; however, the photon will not reach properly on the surface of semiconductor. Hence the photocatalytic degradation will decrease.

Table. 3.4. Rate constant and regression coefficient for TiO_2 and Co:TiO_2 at various concentration.

TiO_2			Co:TiO_2	
Concentration	K(min^{-1})	R^2	K(min^{-1})	R^2
10.6×10^{-3}M	-0.00244	0.9912	-0.00349	0.98232
5.3×10^{-3}M	-0.00236	0.99665	-0.00400	0.98266
2.65×10^{-3}M	-0.00400	0.97879	-0.00671	0.95461

Conclusion

The prepared material was subjected to XRD analysis which gives the rutile and Anatase both phases were present in the prepared sample. It is found that in samples sintered at 400 ^{0}C both Anatase and rutile phases were presented and rutile phase was more dominant, while in samples without sintered the exclusive formation of polycrystalline Anatase and rutile phase separately was occurred. Applying the Scherrer's calculations through which particle size was found 35 and 80 nm in case of Cobalt Titania and pure Titania respectively. The prepared sample of Titania and cobalt Titania were subjected to photocatalytic degradation of Acetic Acid was done. The degradation of Acetic Acid occurs efficiently. The prominent degradation was found in case of Acetic Acid in the presence of nanocomposites Co:TiO_2.

References

[1]. P.V. Bakre, P.S. Volvoikar, A.A. Vernekar, S.G. Tilve, J. of Colloid and Interface Science, 474, (2016), 58-67

[2]. A. Wang, Y. Teng, X. Hu, L. Wu, Y. Huang, Y. Luo, P. Christie, J. of Haza. Mat., 308, 5 (2016), 199-207

[3]. V. Vinod Kumar, K. Gayathri, Savarimuthu Philip Anthony, Materials Research Bulletin, 76, (2016), 147-154

[4]. Y. Pan, D.C.W. Tsang, Y. Wang, Y. Li, X. Yang, Chem. Engi. J., 297, (2016), 74-96

[5]. L. Mino, A. Zecchina, G. Martra, A. M. Rossi, G. Spoto, Appl. Cat. B: Environmental, 196, (2016), 135-141

[6]. B. Barrocas, C.D. Nunes, M.L. Carvalho, O.C. Monteiro, Applied Surface Science, 385, (2016), 18-27

[7]. Z. Khodami, A.N. Ejhieh, J. of Mole. Cat. A: Chemical, 409, 2015, 59-68

[8]. Narges Arabpour, Alireza Nezamzadeh-Ejhieh, Process Safety and Environmental Protection, 102, (2016), 431-440

[9]. Dwight R. Stoll, Kelly O'Neill, David C. Harmes, Journal of Chromatography A, 1383, (2015), 25-34

[10]. A. kumar, G. Hitkari, S. Singh, M.Gautam, G. Pandey, Int. J.of Innovative Research in Science, Engineering, and Tech. 4, (2015), 12721-12731

[11]. C. Karunakaran, R. Dhanalakshmi, P. Anilkumar, Chemical Engineering Journal, 151, (2009), 46-50

[12]. A. Assabane, Y.A. Ichou, H. Tahiri, C. Guillard, J.M. Herrmann, App. Cata. B: Enviro., 24, (2000), 71-87

[13]. S. Belaidi, T. Sehili, L. Mammeri, K. Djebbar, Journal of Photochemistry and Photobiology A: Chemistry, 237, (2012), 31-37.

[14]. Y. Wang, C.S. Liu, F.B. Li, C.P. Liu, J.B. Liang, Journal of Hazardous Materials, 162, (2009), 716-723

[15]. Y. Zhang, N. Klamerth, M.G. El-Din, Chemical Engineering Journal, 292, (2016), 340-347

[16]. K.D. Dobson, A.J. McQuillan, Spectrochimica Acta Part A: Molecular and Biomolecular Spectroscopy, 55, (1999), 1395-1405

[17]. Q. Lan, M. Cao, Z. Ye, J. Zhu, M. Chen, X. Chen, C. Liu, J. of Photochemistry and Photobiology A: Chemistry, 328, (2016), 198-206

[18]. C. Oliveira, D. L.D. Lima, C.P. Silva, Marta Otero, V.I. Esteves. Chemosphere, 159, (2016), 545-551

[19]. M. L. Škorić, I. Terzić, N. Milosavljević, M. Radetić, Z. Šaponjić, M. Radoičić, M.K. Krušić, European Polymer J. 82, (2016), 57-70

[20]. M.M. Zapata, C. Aristizábal, G. Peñuela, J. of Photochemistry and Photobiology A: Chemistry, 251, (2013), 41-49

[21]. A.B. Baranda, O. Fundazuri, I. M. de Marañón, J. of Photochemistry and Photobiology A: Chemistry, 286, (2014), 29-39

[22]. H. Nakatani, G. Kawajiri, S. Miyagawa, S. Motokucho, Polymer Degradation and Stability, 130, (2016), 135-142

[23]. A. Ramchiary, S.K. Samdarshi, Applied Surface Science, 305, (2014), 33-39

[24]. M. Imran, S. Riaz, S. Naseem, Materials Today: Proceedings, 2, (2015), 5455-5461

[25]. A.J.J. Lennox, P. Bartels, M.M. Pohl, H. Junge, M. Beller, J. of Catalysis, 340, (2016), 177-183

[26]. F. Araiedh, F. Ducos, A. Houas, N. Chaoui, Applied Catalysis B: Environmental, 187, (2016), 350-356

[27]. G. N. Shao, S.M. Imran, S. J. Jeon, M. Engole, N. Abbas, M. S. Haider, S. J. Kang, H. T. Kim, Powder Technology, 258, (2014), 99-109.

[28]. K. Wolff, D. Bockelmann, D. Bahnemann, Proceedings of the IS&T 44th Annual Conference; Levt, B., Ed.; IS&T: Springfield, VA (1991) 259-267.

[29]. M. Hema, A.Y. Arasi, P. Tamilselvi, R. Anbarasan,, Chem. Sci. Trans. 2, (2013), 239–245.

[30]. R.Q. Cabrera, A. Mills, C. O' Rourke, Applied Catalysis B: Environmental, 150–151, (2014), 338-344

[31]. I. Nitoi, P. Oancea, M. Raileanu, M. Crisan, L. Constantin, I.Cristea, J. of Industrial and Engineering Chemistry, 21, (2015), 677-682

[32]. B. D. Collity, S. R. Stock, Elements of X-Ray Diffraction, Third Edition, and New Jersey: Prentice-Hall, Inc. (2001)

[33]. M. Pelaez, P. Falaras, A.G. Kontos, A.A. de la Cruz, K. O'shea, P. S.M. Dunlop, J.A. Byrne, D. D. Dionysiou, Applied Catalysis B: Env, 121–122, (2012), 30-39

[34]. A. Folli, J.Z. Bloh, D.E. Macphee, J. of Electroanalytical Chemistry, In Press, Corrected Proof, Available online 10 November (2015)

[35]. V.C. Anitha, A. N. Banerjee, S. W. Joo, B. K. Min, J. of Industrial and Engineering Chemistry, 29, (2015), 227-237

[36]. A.W. Morawski, E. Kusiak-Nejman, A. Wanag, J. Kapica-Kozar, R.J. Wróbel, B. Ohtani, M. Aksienionek, L. Lipińska, Catalysis Today, In Press, Corrected Proof, Available online 23 June (2016).

[37]. Assabane, Y. A., Ichou, H. Tahiri, C. Guillard, J. M. Hermann, Appl Catal B: Environ 24, (2000), 71-87.

[38]. N. Serpone, J. Martin, S. Horikoshi, H. Hidaka, J Photoch Photobio A 169, (2005), 235- 251.

[39]. T. Sakata, T. Kawai, K. Hashimoto, J Phys Chem 88, (1984), 2344-2350.

[40]. Y. Ine, A. N. Okte, J Photoch Photobio A 96, (1996), 175-180.

[41]. C. S. Turchi, D. F. Ollis, J Catal 11, (1989), 483-496.

[42]. Y. Zang, R. Farnood, Appl Catal B: Environ 57, (2005), 275-282.

[43]. K. Mehrotra, G.S. Yablonsky, A. K. Ray, Chemosphere 60, (2005), 1427-1436.

[44]. A. Mills, C. E. Holland, R. H. Davies, D. Worsley, J. Photoch. Photobio. A 83, (1994), 257-263.

[45]. M. Trillas, J. Peral, X. Domenech, Appl., Catal., B: Environ. 3, (1993), 45-53.

[46]. K. Tanaka, K. Padampole, K., T. Hisanaga, Water Research 34, (2000), 327-333.

[47]. A. Piscopo, D. Robert, J. V. Weber, Appl Catal B: Environ 35, (2001), 117-124.

[48]. A. Kumar, G. Hitkari, M. Gautam, S. Singh, G. Pandey, Int. Adv. Research J. in Science, Engineering, and Tech. 2, (2015), 50-55

CHAPTER-4

The photocatalytic degradation of Methyl Green in presence of Visible light using $Ni_{0.10}$:$La_{0.05}$:TiO_2 nanocomposites as catalyst

In this paper, we have done the photodegradation of Methyl green dye in presence of prepared $Ni_{0.10}$:$La_{0.05}$:TiO_2 nanocomposites. The nanocomposites of $Ni_{0.10}$:$La_{0.05}$:TiO_2 was prepared by the solution impregnation method. The characterization of Synthesized TiO_2 and $Ni_{0.10}$:$La_{0.05}$:TiO_2 nanocomposites were done by X-Ray Diffractometer, SEM, TEM, UV- Vis, FT-IR, Band gap energy and BET. The photocatalytic degradation of Methyl Green has been done in presence of TiO_2 and $Ni_{0.10}$:$La_{0.05}$:TiO_2 nanocomposites. The presence of anatase and rutile phase in the nanocomposites has been confirmed by XRD analysis. The photocatalysts particle was found in nanodiamension in morphology. The surface area was observed 34.72 and 96.58 m^2/g for the TiO_2 and $Ni_{0.10}$:$La_{0.05}$:TiO_2 nanocomposites. The band gap energy was observed 3.2 and 3.0 eV for the TiO_2 and $Ni_{0.10}$:$La_{0.05}$:TiO_2 nanocomposites. The photocatalytic degradation behaviour of photocatalysts was investigated by considering different parameters such as effect of concentration, effect of amount of photocatalyst, effect of pH, effect of temperature, adsorption and kinetics. The 90-98 % photodegradation of Methyl Green has been found at 7 pH, 25 ppm concentration of dye, 800 mg/L amount of photocatalyst and 50 min illumination of visible light in presence of $Ni_{0.10}$:$La_{0.05}$:TiO_2 while 10-18 % in presence of neat TiO_2 . The photodegradation of Methyl Green was following the first order kinetics.

4.1. Introduction

Cationic triphenylmethane dyes have found extensive use as colorants in industry and as antimicrobial agents [1]. Recent reports indicate that they may further serve as targetable sensitizers in the photodestruction of specific cellular components or cells [2-3]. Methyl Green is a basic triphenylmethane type dicationic dye, usually used for staining solutions in medicine and biology [4] and as a photochromophore to sensitize gelatinous films [5]. It has been used to differentiate between deoxyribonucleic acid and ribonucleic acid [6]. The binding of Methyl Green to DNA is probably ionic, as opposed to intercalative, and it remains so stably bound to double stranded DNA that, with its conversion to the colourless carbinol form, it has been used to assess the binding of other molecules to DNA [7-8]. However, great concern has arisen about the thyroid peroxidase-catalyzed oxidation of the triphenylmethane class of dyes because the reactions might form various N-de-alkylated primary and secondary aromatic amines, with structures similar to aromatic amine carcinogens [9].

Dyes are the most resistant compounds and used in various industries. The industrial effluents are causing adverse environmental problems [10-11]. Most of the dyes used in the pigmentation of textiles, leather, paper, ceramics, and food-processing are derived from azo dyes. Dyes are lost with waste water during synthesis and processing [12-13]. This represents a great hazard to human and environmental health due to the toxicity of azo dyes [14]. The treatment of such pollutants can be achieved by heterogeneous photocatalysis due to its efficiency and low cost as well as to the fact that it allows complete degradation of pollutants to carbon dioxide and inorganic acids [15-16].
Titanium dioxide TiO_2 is a most important nano material which has attracted a great attention due to its unique properties [17]. Titanium dioxide TiO_2 have excellent merits in solar energy transferring and photocatalysis of poison compounds in environment. The chemical inertness and the non-toxicity of TiO_2 have also made it a superior photocatalyst [18-19]. Titania has a large band gap (3.20 ev for anatase TiO_2) and therefore, only a small fraction of solar light can be absorbed [20-21]. Many attempts have been made to

sensitize titanium dioxide to the whole visible region, such as impregnation with transition metals [22-23], transition metal ions [24], non-metal atoms [24] and organic materials [25]. Introduction of dopant allows Titania to absorb in the visible region but this does not necessarily mean that the doped catalyst has a better photocatalytic activity [26].

In this study, prepared the nanocomposites of $Ni_{0.10}$:$La_{0.05}$:TiO_2 by the solution impregnation method. Synthesized TiO_2 and $Ni_{0.10}$:$La_{0.05}$:TiO_2 were characterized by X-Ray Diffractometer, SEM, TEM, UV- Vis, FT-IR, Band gap energy and BET. The TiO_2 and $Ni_{0.10}$:$La_{0.05}$:TiO_2 were used as photocatalyst for the degradation of Methyl Green. We have investigated the photocatalytic degradation behaviour of cationic dye molecule from aqueous system onto prepared $Ni_{0.10}$:$La_{0.05}$:TiO_2 nanocomposites by taking methyl green as model molecule (showing in Figure 4.1). The photocatalytic degradation behaviour was investigated by considering different parameters such as effect of concentration, effect of amount of photocatalyst, effect of pH, effect of temperature, adsorption and kinetics.

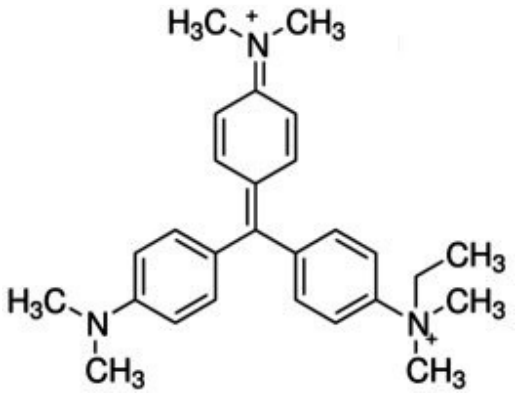

Fig.4.1. Structure of Methyl Green dye

4.2. Methodology

4.2.1 Preparation of the photocatalysts

In this method, 10 ml of $TiCl_4$ solution (1000 mg/l), 2ml of 0.1M Nickel acetate, 1ml of 0.1M Lanthanum nitrate and NaOH solution (64.5 g/l) was added drop wise to water with stirring. After the resulting solution reaches pH to 7, the slurry was filtered, and the filter cake of TiO_2 was washed and redispersed in water to prepare 1 M of TiO_2 slurry. Resulting TiO_2 slurry and an aqueous solution of HNO_3 were refluxed at 95^0C for

2 h, cooled to room temperature and neutralized with 28% of aqueous ammonia. Then, it was filtered, washed and calcined at 400 ^{o}C. The $Ni_{0.10}$:$La_{0.05}$:TiO_2 nanocomposites were prepared by solution impregnation method. In this method suitable quantity of prepared TiO_2 (2 g) was dispersed in alcoholic Nickel acetate 10% (w/v) and lanthanum nitrate 5% (w/v). The dispersion is agitated continuously for 4 hour at 80 ^{o}C temperature. After the treatment the residue was removed through filtration and was sintered for 4 hour in presence of air at 600 ^{o}C by kipping it in a silica crucible inside the muffle furnace. After sintering and slow anilling to room temperature, content was taken out from furnace and was stored in air tight bottles and was used as photocatalyst [27-31].

$$TiCl_4 + 4NaOH \longrightarrow Ti(OH)_4 + 4NaCl \quad (1)$$

$$Ti(OH)_4 \longrightarrow TiO_2 + 2H_2O \quad (2)$$

$$TiO_2 + 10\ \%\ Ni(CH_3COOH)_3 + 5\ \%\ La(NO_3)_3 \longrightarrow Ni_{0.10}:La_{0\cdot05}:TiO_2 \quad (3)$$

4.2.2. Photocatalyst characterization

4.2.1.1. Powder x-ray diffraction analysis (P-XRD)

The physical properties of metal oxide semiconductor nanocomposites that may influence significantly their use as photocatalyst are dependent on nature of crystalline phase present. Thus, phase analysis is an important parameter for this study and the prepared samples were subjected to x-ray diffraction analysis on Powder X-Ray Diffractometer (Bruker AXS D8 Advance System, Germany). The observed X-Ray diffractogram of samples were analyzed further to estimate average grain size in the sample by Scherrer's calculation [32].

$$T = \frac{0.9\,\boldsymbol{\lambda}}{\boldsymbol{\beta}\,\mathbf{Cos}\boldsymbol{\theta}} \quad (4)$$

Where, T is the mean size of the ordered (crystalline) domains, which may be smaller or equal to the grain size, *K* is a dimensionless shape factor, with a value close to unity. The shape factor has a typical value of about 0.9, but varies with the actual shape of the crystallite, λ is the X-ray wavelength, β is the line broadening at half the maximum intensity (FWHM), after subtracting the instrumental line broadening, in radians. This quantity is also sometimes denoted as $\Delta(2\theta)$, θ is the Bragg angle.

4.2.2.2. SEM analysis

The particle morphologies of the photocatalyst were studied using scanning electron microscope. Samples were mounted on aluminum stab with the help of double-sided tape. Mounted stabs were coated with gold palladium prior to analysis using a Polaron sputter coater.

4.2.2.3. TEM analysis

The particle morphologies of the photocatalyst were studied by using Transmission electron microscopy (TEM, JEOL JEM 2011 equipped with LaB6 filament). The TEM images were collected with a 4008 - 2672 pixel CCD camera (Gatan Orius SC1000) coupled with the DIGITAL MICROGRAPH software. Coupled chemical analyses were obtained by an EDX micro- analyzer (PGT IMIX PC).

4.2.2.4. BET surface area analysis

The surface area and pore characteristics of the derived photocatalyst was determined from nitrogen adsorption/desorption isotherms at 77 K (boiling point of nitrogen gas at 1atm pressure) using a BET surface area analyzer (BELSORP-max, Japan).

4.2.2.5. UV visible spectrometer

Since the absorption of light by photocatalyst is the most crucial step in any photocatalysed reaction, and is decided primarily by the band gap energy of material, attempt would also be made to evaluate band gap energy employing a UV spectrometer (UV 2450 Shimadzu).

4.2.2.6. Fourier transforms Infrared spectroscopy (FTIR)

The Photocatalyst (2 mg) was mixed with 200 mg of KBr and then pelleted. The FT-IR spectra of the pellets were recorded using a Fourier Transform Infra-Red Spectrometer (FTIR) Thermo Scientific (Nicole 6700).

4.2.3. Dark adsorption studies

The adsorption studies were performed using aqueous solutions of EBT. For this purpose 20 ml dye solution of different concentrations (25-100 ppm) were magnetically stirred separately in presence of bare and metal impregnated catalysts (0.5g) in dark up to 30 min. Thereafter, the suspensions were collected after regular time intervals (5 min) filtered through cellulose filter and then sample were analyzed by UV-vis spectrophotometer at λmax = 631.5 nm for Methyl Green [33].

4.2.4. Photo-degradation of dyes

In this work, the photo-catalytic degradation of Methyl Green was investigated. A solution of dye in water: alcohol (10:1 V/V) was prepared and in this solution a suitable quantity of photocatalyst (100 to 800 mg/L) was dispersed. The dispersion was subjected to Visible light irradiation (500 W Tungsten Lamp were used for the visible light radiation in a close chamber) for varying duration and after desired irradiation the residual concentration of dye in the solution was determine spectrophotometrically by taken out suitable aliquot of dispersion and removal of photocatalyst by centrifugation. A quantitative estimation of dye concentration spectrometric observation when recorded only at the experimental determines λ max value which is 631.5 nm [34-43]. The % degradation efficiency of Methyl Green dye was calculated by Equation (5).

$$\eta\ \% = \frac{A_O - A_F}{A_O} * \mathbf{100} \qquad (5)$$

4.3. Results

4.3.1. Characterization of Photocatalyst

4.3.1.1. Phase identification by X-ray diffraction analysis

The obtained X-Ray diffraction patterns of TiO_2 and $Ni_{0.10}$:$La_{0.05}$:TiO_2 are shown in Figures 4.2. The observed pattern of peaks, when compared with the standard JCPDS database, suggested that, in prepared TiO_2 sample, major peaks at 2θ = 25.5 □ 37.2, 48.3, and 54.4, which can be indexed to the (101), (004), (200), and (211) crystal facets of anatase TiO_2 (JCPDS File number: 21-1272). Whereas major peaks at 2θ = 26.9º and

28.2º indicate the presence of rutile phase which can indexed to the (110), (121), respectively [32]. In case of $Ni_{0.10}$:$La_{0.05}$:TiO_2 sample, the observed XRD pattern indicates not only a change in the peak intensity, compared to TiO_2, but even the absence of some originally observed TiO_2 peaks [44]. This is, probably, due to the change in the crystallinity and grain fragmentation, when the samples were wet impregnated by Nickel and Lanthanum. Utilizing the observed X-ray diffraction data of samples, Scherrer's calculations were attempted to know the average size of particles/grains in the samples [32]. Although, Scherrer's calculations are only approximate in nature, but definitely provide a first-hand idea of the average size of the crystal in the samples, which may be quite accurate, provided the size of crystal is below 100 nm.

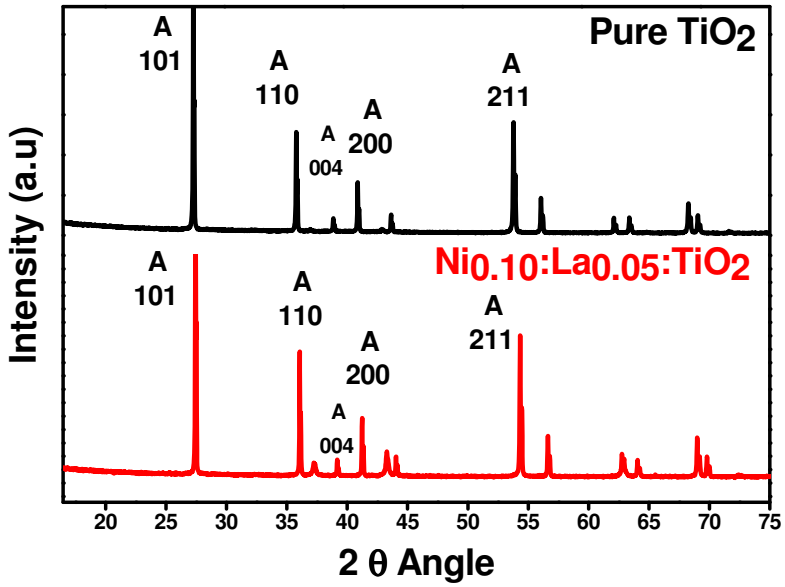

Fig.4.2. Observed XRD pattern TiO_2 and $Ni_{0.10}$:$La_{0.05}$:TiO_2

Table 4.1. Average size of crystal in the samples of TiO_2 and $Ni_{0.10}$:$La_{0.05}$:TiO_2.

Sample	Particle Size (nm)
TiO_2	76
$Ni_{0.10}$:$La_{0.05}$:TiO_2	34

The mean size of TiO_2 and $Ni_{0.10}$:$La_{0.05}$:TiO_2 nanocomposites, calculated by Scherrer's Equation, are about 76 and 34 nm respectively. The results of Scherrer's calculations are presented in Table 1. The results suggest average size of the crystal in the samples lying in nm range. The result is in good agreement with the TEM.

4.3.1.2. UV-Vis spectra

Aqueous suspensions of the samples were used for the UV absorption studies. The absorption spectrum of TiO_2 consists of a single broad intense absorption between 383 nm due to the charge-transfer from the valence band to the conduction band [45]. The undoped TiO_2 showed absorbance in the shorter wavelength region while $Ni_{0.10}$:$La_{0.05}$:TiO_2 result showed slight red shift in the absorption edge. The absorption peak of $Ni_{0.10}$:$La_{0.05}$:TiO_2 was found at 410 nm. It is showing in Figure 4.3. The impregnation of Ni and La ions into TiO_2 could shift optical absorption edge from UV to visible range, but slight change in TiO_2 band gap was observed [46-47].

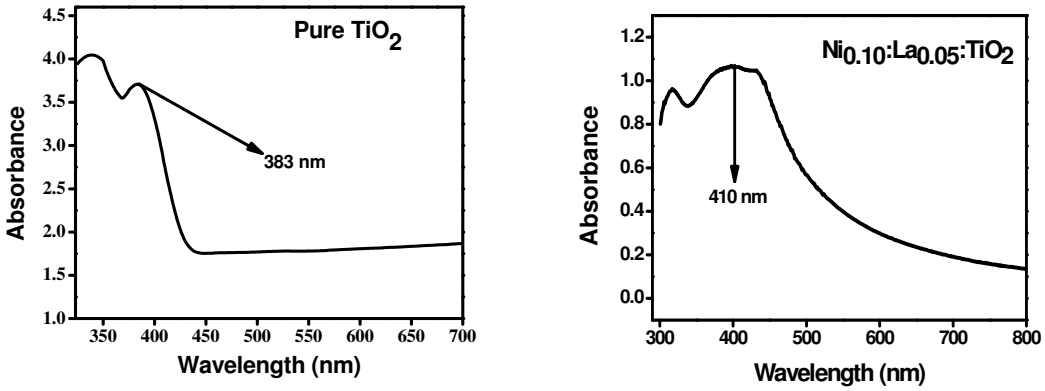

Fig.4.3. UV- spectra of TiO_2 and $Ni_{0.10}$:$La_{0.05}$:TiO_2

4.3.1.3. Band gap energy determination

The band gap of samples was calculated by extrapolation of the $(\alpha h\nu)^2$ versus $h\nu$ plots, where α is the absorption coefficient and $h\nu$ is the photon energy, $h\nu = (1239/\lambda)$ eV. The value of $h\nu$ extrapolated to $\alpha = 0$ gives an absorption energy, which corresponds to a band gap (Eg). From the Figure 4.4 we found an Eg value of 3.2 eV for TiO_2 and 3.0 for

$Ni_{0.10}$:$La_{0.05}$:TiO_2 [48]. The slight decrease in band gap energy in case of $Ni_{0.10}$:$La_{0.05}$:TiO_2 is due to formation of sub-band level between valence band and conduction band caused impregnation of Ni^{2+} and La^{3+} ions in TiO_2 host [49].

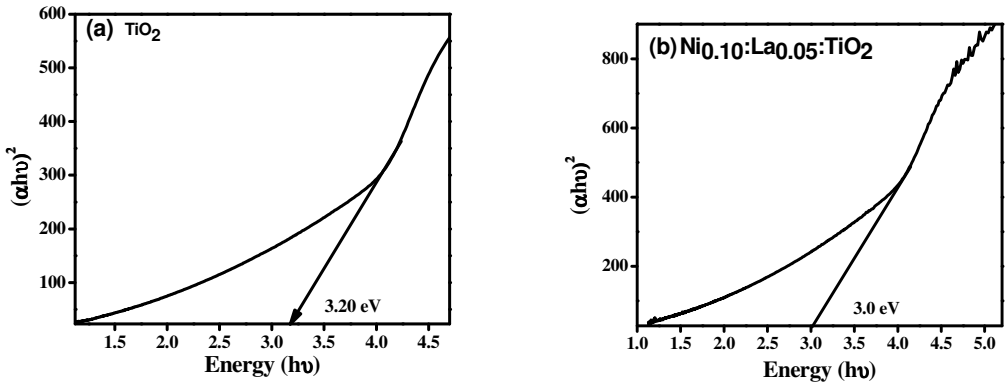

Fig.4.4. Band gap energy of (a) TiO_2 (b) $Ni_{0.10}$:$La_{0.05}$:TiO_2

4.3.1.4. FT-IR spectroscopy

FT-IR spectra of undoped and 10% Ni and 5% La impregnated TiO_2 samples (Figure 4.5) show peaks corresponding to stretching vibrations of the O-H and bending vibrations of the adsorbed water molecules around 3350-3450 cm^{-1} and 1620-1635 cm^{-1}, respectively. The broad intense band below 820, 804, 592 and 456 cm^{-1} is due to Ti-O-Ti vibrations. The shift to the higher wave numbers and sharpening of the Ti-O-Ti band may be due to decrease in size of the catalyst nanoparticles. In addition, the surface hydroxyl groups in TiO_2 increased with the increasing of Ni loading, which is confirmed by increase in intensity of the corresponding peaks. The FT-IR spectra of $Ni_{0.10}$:$La_{0.05}$:TiO_2 show strong band at 1075 cm^{-1}, corresponds to the vibration of Ni–O bond and confirms the penetration of nickel in Titania [50].

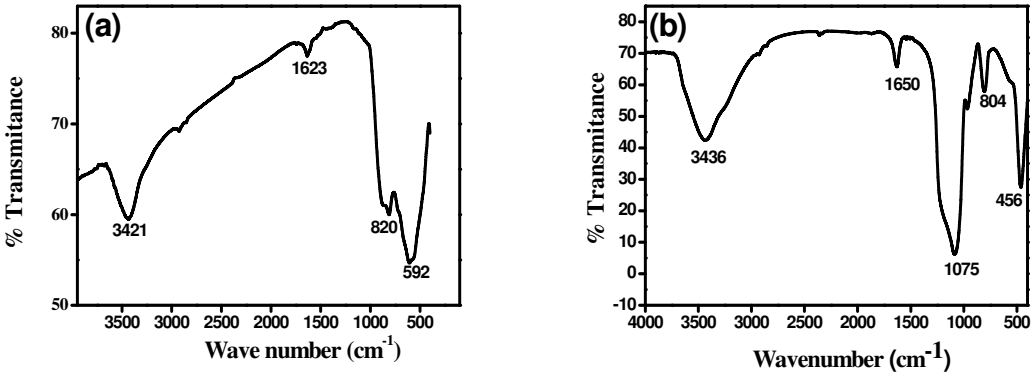

Fig.4.5. FT-IR spectra of (a) TiO_2 (b) $Ni_{0.10}$:$La_{0.05}$:TiO_2

4.3.1.5. Transmission Electron Microscope (TEM) and EDX.

TEM images were clearly displayed the morphology and particle size of neat TiO_2 and Nickel and lanthanum doped TiO_2. From the Fig. 4.6 we find that Nickel and lanthanum doped modified TiO_2 change the size of neat TiO_2 significantly, as shown in Fig. 4.6 (a) and (b).

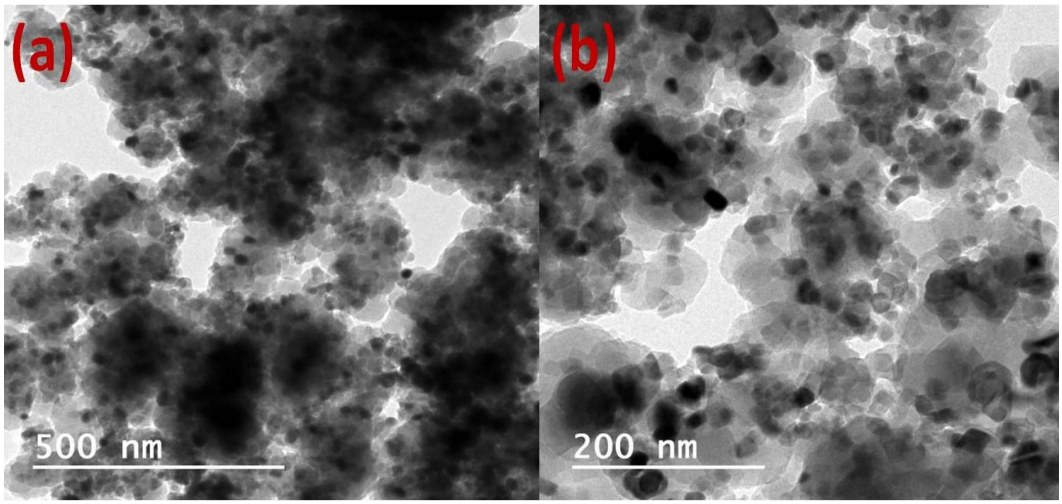

Fig.4.6. TEM image of the (A) TiO_2 (B) $Ni_{0.10}$:$La_{0.05}$:TiO_2

The sizes of both modified and neat TiO_2 are mono disperse about 100–200 nm. Moreover, the crystal lattice line can be clearly found in the TEM images. The

aggregations of both kinds of particles are caused by high surface energy; however, the agglomeration of the modified one is alleviated obviously compared with that of the neat [51].

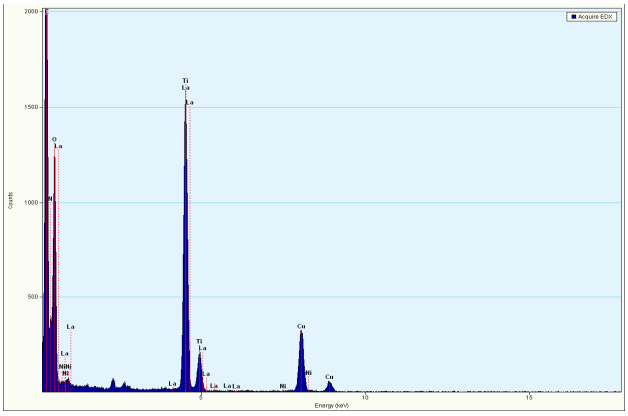

Fig.4.7. EDX image of $Ni_{0.10}$:$La_{0.05}$:TiO_2 nanocomposite

EDX Is an analytical technique used for the elemental analysis or chemical characterization of a sample. Compositional analysis of the nanomaterials can also be obtained by monitoring the X-rays produced by electron-specimen interaction. The formation and composition of crystalline $Ni_{0.10}$:$La_{0.05}$:TiO_2 nanocomposite was justified from EDX measurements. The compositional measurement of $Ni_{0.10}$:$La_{0.05}$:TiO_2 nanocomposite is showing in the Figure 4.7. The presence of La and Ni in the EDX is indicating that the metal ions of Ni and La have been impregnated in the Titania crystal. In the Figure the Cu is also observed this is due to the copper grid used in TEM analysis.

4.3.1.6. Scanning Electron Microscopy (SEM)

The morphology of the samples was investigated by scanning electron microscopy and it resumes the most interesting outcomes. Fig.4.8 (a) and 4.8 (b) clearly show that both the prepared samples are obtained in nanometric dimension. The impregnation of Nickel and lanthanum is indicating that the particle size reduce due the penetration of Nickel and lanthanum in the lattice of titanium dioxide [52].

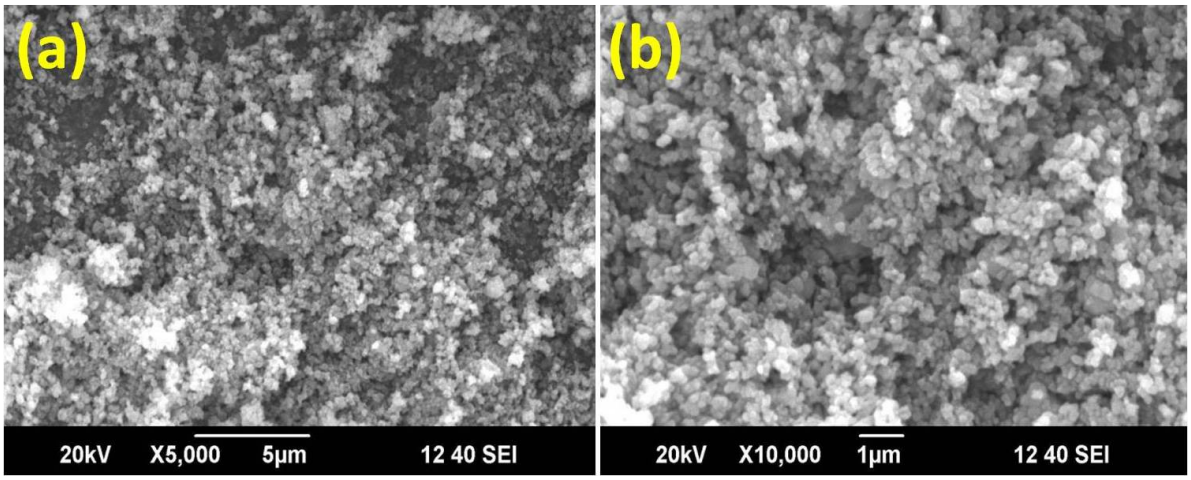

Fig.4.8. SEM image of the (A) TiO_2 (B) $Ni_{0.10}$:$La_{0.05}$:TiO_2

4.3.1.7. Surface Area Analysis (BET)

The specific surface area, pore volume and average pore size of the TiO_2 and $Ni_{0.10}$:$La_{0.05}$:TiO_2 photocatalyst were determine. Figure 4.9 showing the BET adsorption and desorption plots for the pure Titania and Ni, La impregnated Titania. Table 4.2 shown the physical properties of TiO_2 and $Ni_{0.10}$:$La_{0.05}$:TiO_2. The surface area of TiO_2 and $Ni_{0.10}$:$La_{0.05}$:TiO_2 was found 34.72 and 96.58 m2/g. The surface area of $Ni_{0.10}$:$La_{0.05}$:TiO_2 is increased rapidly with impregnation of Ni and La in pure Titania. The TiO_2 modified by Ni and La are fragmented to some extent during thermal treatment, leading to a marked increase of the *BET* surface areas and the average pore radius size and decreasing of the pore volume [53].

Table 4.2. The specific surface area, pore volume and pore radius of the TiO_2 and $Ni_{0.10}$:$La_{0.05}$:TiO_2

Sample	Surface area (m^2/g)	Pore volume (cm^3/g)	Pore radius (nm)
TiO_2	34. 72	11.132	1.21
$Ni_{0.10}$:$La_{0.05}$:TiO_2	96.58	9.9124	1.64

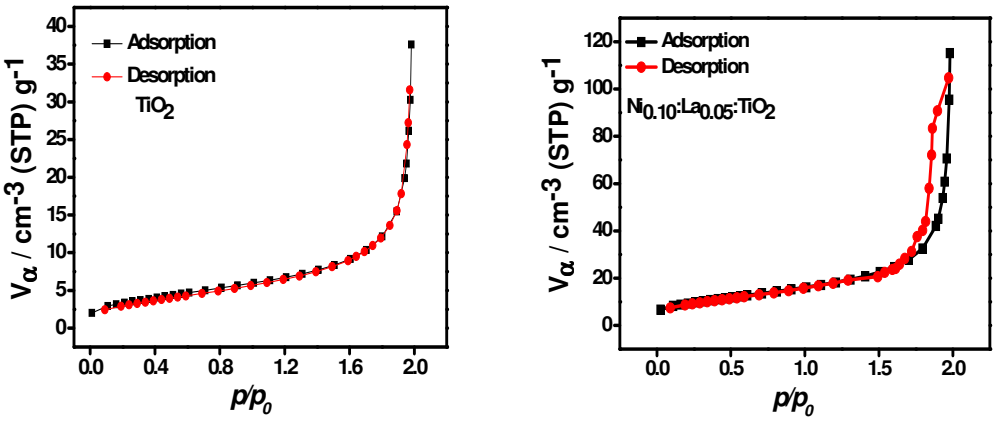

Fig.4.9. Adsorption and desorption plots for Titania and Ni, La Impregnated Titania.

4.3.2. Adsorption study

A control experiment was first carried out under two conditions, vis (i) dye + UV (no TiO_2) (ii) TiO_2 + dye in dark without any irradiation (iii) $Ni_{0.10}$:$La_{0.05}$:TiO_2 + dye in dark without any irradiation (Figure 4.10). It can be seen that under dark conditions, after 20 min the amount of Methyl Green dye adsorbed becomes constant i.e. equilibrium adsorption is achieved.

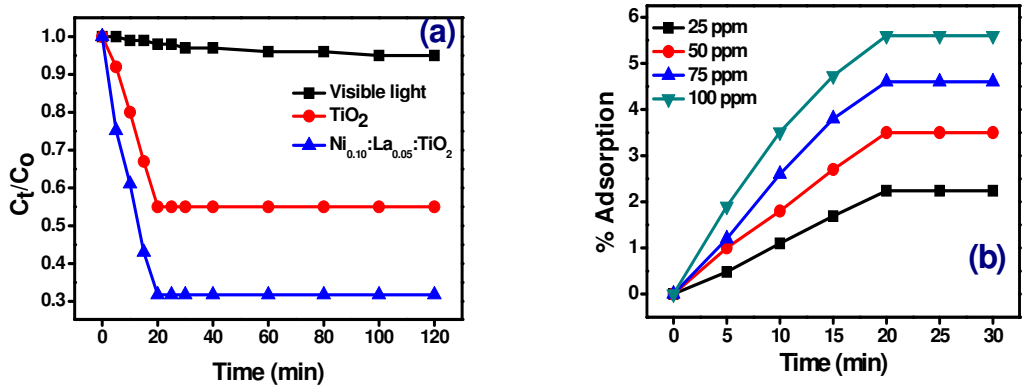

Fig.4.10. (a) change in concentration under dark with TiO_2, $Ni_{0.10}$:$La_{0.05}$:TiO_2 and in visible light (b) under dark with $Ni_{0.10}$:$La_{0.05}$:TiO_2 at different concentrations.

The reaction of Methyl Green in presence of TiO_2 and $Ni_{0.10}$:$La_{0.05}$:TiO_2 nanocomposites and UV irradiation is an example of heterogeneous catalysis. Rate laws in such reactions seldom follow proper law models and hence are inherently more difficult to formulate from the data. It has been widely accepted that heterogeneous catalytic reactions can be analyzed with the help of Langmuir Hinshelwood (LH) Model [54], with the following assumptions being satisfied:

(i). There are limited numbers of adsorption sites on the catalyst and its surface is homogeneous,

(ii). Only one molecule can be adsorbed on one site and monolayer formation occurs

(iii). The absorption reaction is reversible in nature, and

(iv). The adsorbed molecules do not react amongst themselves [55].

According to LH Model, following steps take place in the kinetics mechanism [56] (Adsorption of dye onto the catalyst surface). There are three steps of adsorption, Surface reaction, Desorption of products from the surface.

Step 1:- D (Dye) + C (catalyst) $\longleftrightarrow$ D.C

Step 2:- D.C $\longleftrightarrow$ E.C + Other products

Step 3:- E.C $\longleftrightarrow$ E + C

4.3.3. Photo-degradation of Dyes

The residual concentration of dye in the reaction mixture was measured spectrophotometrically. The results obtained for the degradation of Methyl Green is shown in Fig. 4.11-4.15.

4.3.3.1. Effect of concentration of dye

Effect of dye concentration keeping the catalyst loading concentration constant at 800 g/liter of the dye solution, the effect of varying concentration of the dye was studied on its rate of degradation (from 25 ppm to 100 ppm) as given in Fig. 4.11. In presence of Titania the photodegradation of Methyl green dye was found 18% and 3% at 25 and 100 ppm concentration of dye solution. But in presence of $Ni_{0.10}$:$La_{0.05}$:TiO_2 the

photodegradation was found 98.6 % and 56% at 25 ppm and 100ppm concentration of dye. With increasing concentration of Methyl Green the rate of degradation was found to decrease. This is because as the number of dye molecules increase, the amount of light (quantum of photons) penetrating the dye solution to reach the catalyst surface is reduced owing to the hindrance in the path of light. Thereby the formation of the reactive hydroxyl and superoxide radicals is also simultaneously reduced. Thus there should be an optimum value maintained for the catalyst and the dye concentration, wherein maximum efficiency of degradation can be achieved [34-39, 57].

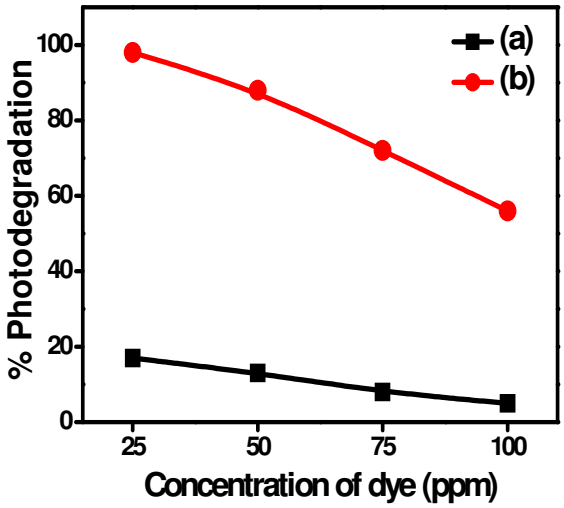

Fig.4.11. Effect of concentration on photocatalytic degradation of Methyl Green with (a) TiO_2 and (b) $Ni_{0.10}$:$La_{0.05}$:TiO_2.

4.3.3.2. Effect of irradiation Time on photodegradation

The effect of irradiation time on the photodegradation of Methyl Green has been studied in presence of $Ni_{0.10}$:$La_{0.05}$:TiO_2. The photodegradation of Methyl Green was increased with increase irradiation time. The photodegradation was found maximum in 50 min irradiation of visible light. Figure 4.12 shows the effect of irradiation time on photocatalytic degradation of Methyl Green. This is because of the interaction of dye

molecule with the surface of photocatalyst. The time of irradiation increase, the interaction of methyl green dye molecule increased with the surface of photocatalyst. Therefore the photodegradation efficiency of photocatalyst was increased [34-36, 58].

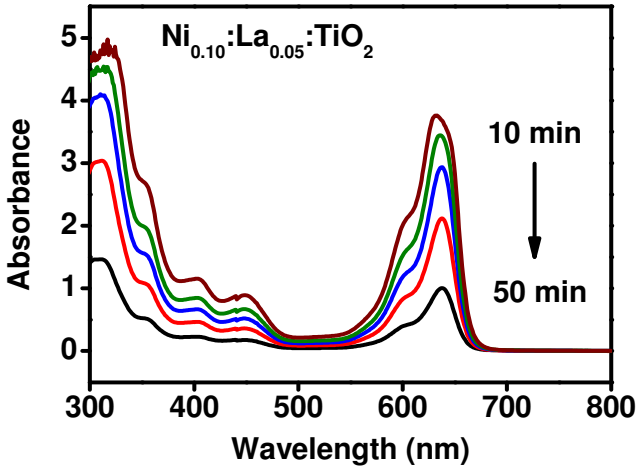

Fig.4.12. Effect of irradiation time on photocatalytic degradation of Methyl Green with $Ni_{0.10}$:$La_{0.05}$:TiO_2.

4.3.3.3. Effect of pH of solution

The photodegradation reaction was also carried out under varying pH from 4 to 9, by adjusting with H_2SO_4 and NaOH, with photocatalyst kept at constant amounts of 800 mg/L in the dye solutions (Figure 4.13). The maximum photodegradation of Methyl Green dye was found 17% and 88% in presence of TiO_2 and $Ni_{0.10}$:$La_{0.05}$:TiO_2 at neutral medium or 7 pH of solution. The reaction of photodegradation was found low rates at acidic and basic ranges of pH. While at pH 7 or neutral medium, the photodegradation was found maximum. This implies that neutral conditions are favourable towards the formation of the reactive intermediates that is hydroxyl radicals is significantly enhanced, which further help in enhancing the reaction rate. There is another region that the Methyl Green is the dicationic dye which has 2+ charges. The surface of photocatalyst has slightly negative which can interact to positive dye molecule easily in the solution. On the

other hand in highly acidic medium conditions for the formation of reactive intermediates is relatively less favourable and hence less spontaneous [40-42, 58].

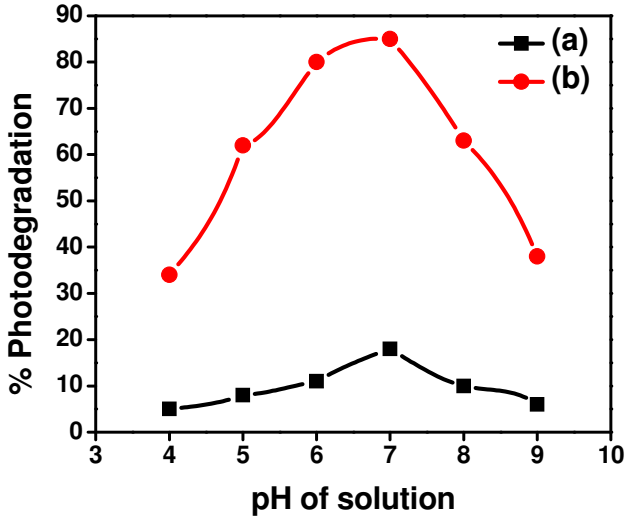

Fig.4.13. Effect of pH on photodegradation of Methyl Green with (a) TiO_2 and (b) $Ni_{0.10}$:$La_{0.05}$:TiO_2.

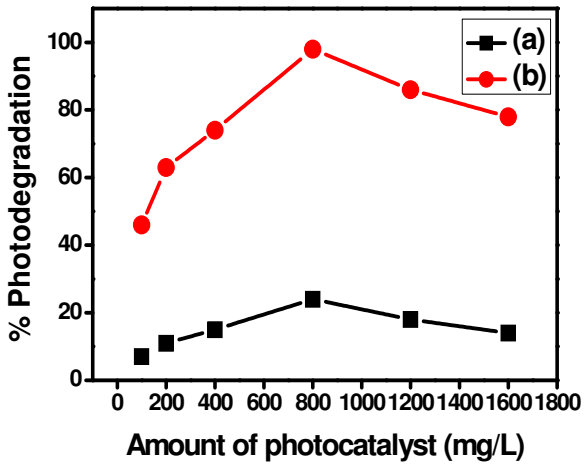

Fig.14. Effect of amount of photocatalyst on photocatalytic degradation of Methyl Green with (a) TiO_2 and (b) $Ni_{0.10}$:$La_{0.05}$:TiO_2.

4.3.3.4. Effect of photocatalyst amount

The effect of photocatalyst amount has been studied by applying the different amount (100 ppm to 1600 ppm) of the photocatalyst. The photodegradation rate was found to increase by increasing the amount of photocatalyst but still a limited amount of photocatalyst, after certain amount of photocatalyst, the photodegradation is decreasing. The maximum photodegradation was found 99.2 and 21 % at 800mg/L amount of photocatalyst in presence of $Ni_{0.10}$:$La_{0.05}$:TiO_2 nanocomposite and TiO_2 respectively. It is clear from the results shown in Figure 4.14, the photodegradation increased rapidly with increase of amount from 100 mg/L to 800mg/L of $Ni_{0.10}$:$La_{0.05}$:TiO_2. We were found that when increase the amount of photocatalyst from 800mg/L to 1600mg/L, the photodegradation of dye rapidly decreased. This is due to the photocatalyst and dye molecule is properly interacting to each other till the 800mg/L amount of photocatalyst. After 800mg/L amount of photocatalyst, the turbidity increased in the solution due to photocatalyst molecules. The light (photon) is not striking on the surface of molecule. Therefore, the interaction between dye molecule and photocatalyst is decreased in some amount. The introduction of Ni^{2+} and La^{3+} ions in TiO_2, the surface area of photocatalyst was increased which increased the photocatalytic activity of Titania [43, 59].

4.3.3.5. Effect of photocatalyst

It is clear from the results shown in Fig.4.11-4.14 that $Ni_{0.10}$:$La_{0.05}$:TiO_2 is effective photo-catalyst for the degradation of Methyl Green (MG) dye than pure TiO_2. However $Ni_{0.10}$:$La_{0.05}$:TiO_2 seems to be more effective as photocatalyst for the degradation of Methyl Green (MG). The prominent degradation of Methyl Green was found in 50 min study in the presence of $Ni_{0.10}$:$La_{0.05}$:TiO_2 in comparison to the prepared TiO_2 [42, 59].

4.3.4. Lowering of electron-hole recombination

Photoluminescence spectra have been used to examine the mobility of the charge carriers to the surface as well as the recombination process involved by the electron-hole

pairs in semiconductor particles. PL emission results from the radiative recombination of excited electrons and holes. In other words, it is a critical necessity of a good photocatalyst to have minimum electron-hole recombination. To study the recombination of charge carriers, PL studies of synthesized materials have been undertaken. PL emission intensity is directly related to recombination of excited electrons and holes. Fig. 4.15 shows the photoluminescence spectra of synthesized photocatalysts. In the PL spectra the intensity of TiO_2 is higher than $Ni_{0.10}$:$La_{0.05}$:TiO_2 indicating rate of recombination of e^-- h^+ is higher in TiO_2 than that of $Ni_{0.10}$:$La_{0.05}$:TiO_2 .The weak PL intensity of $Ni_{0.10}$:$La_{0.05}$:TiO_2 may arise due to the impregnation of Ni in Titania lattice, which for sub band level in band gap region of TiO_2. This delays the electrons- holes recombination process and hence utilized in the redox, reaction leading to improved photocatalytic activity [60].

As hydroxyl radical performs the key role for the decomposition of the organic pollutants, it is necessary to investigate the amount of hydroxyl radicals produced by each photocatalyst. In this study terephthalic acid (TA) has been used as a probe reagent to evaluate $^{\bullet}OH$ radical present in the photoreaction pathway. Fig. 4.16 shows the PL spectra of TiO_2 and $Ni_{0.10}$:$La_{0.05}$:TiO_2 recorded Methyl Green solution in presence of 10^{-3}M Terephthalic solution. OH radical attack Terephthalic Acid, forming 2- hydroxyl terephthalic acid (TAOH) which gives a fluorescence signal at 426 nm. The fluorescent intensity is linearly related to the number of hydroxyl radicals formed by the photocatalysts. Higher the generation of hydroxyl radical, more will be yield of TAOH and hence more intense will be the fluorescence peak. The spectra show that the intensity of peak indicating in presence of $Ni_{0.10}$:$La_{0.05}$:TiO_2 higher generation of more number of hydroxyl radicals compared to TiO_2 [61].

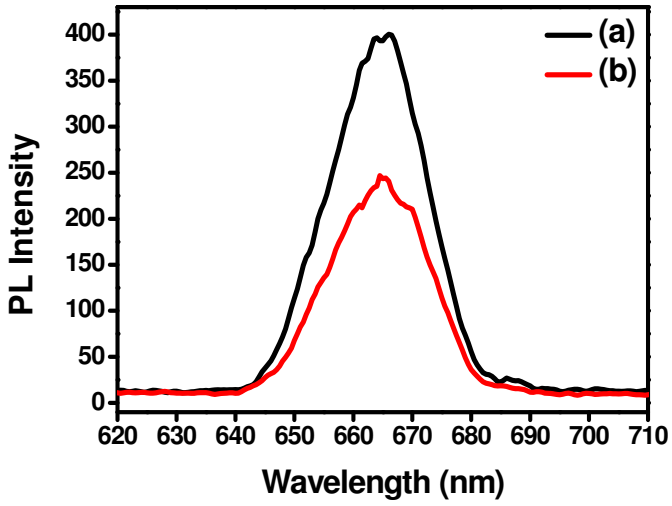

Fig.4.15. Photolumiscence Spectra of (a) TiO_2 and (b) $Ni_{0.10}$:$La_{0.05}$:TiO_2

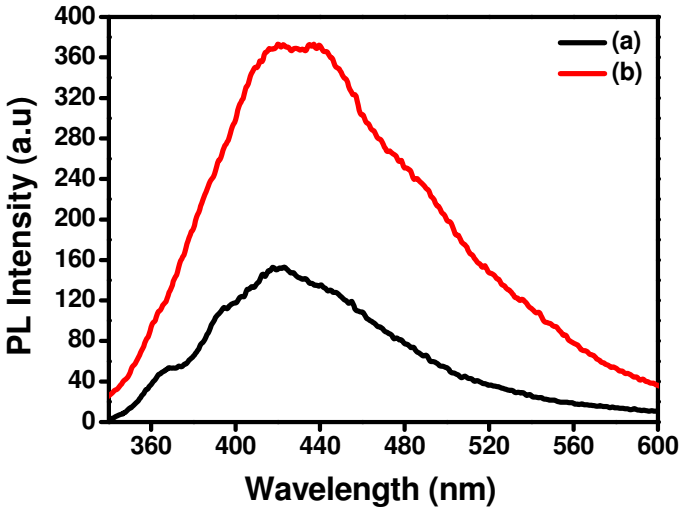

Fig.4.16. PL spectra of (a) TiO_2 and (b) $Ni_{0.10}$:$La_{0.05}$:TiO_2 photocatalyst with terephthalic acid (0.001M) in visible light

4.3.5. Kinetic study

The data plotted in Fig. 4.17 were used for the calculation of the apparent kinetic constants for different reaction conditions. The rate of degradation of organic compounds

in wastewaters can be described by a pseudo-first order Langmuir–Hinshelwood kinetic model [62-63]:

$$\boldsymbol{r = -\frac{dC}{dt} = \frac{CK\,K_r}{1+KC}} \quad \textbf{(6)}$$

where r stands for the rate of degradation, K represents the equilibrium constant for the adsorption of MG on the catalyst surface, and kr denotes the kinetic constant for the degradation reaction at maximum surface coverage. On integrating Eq. (6), we obtain the irradiation time, t, for attaining a concentration C_t of the MG:

$$\boldsymbol{t = \left(\frac{1}{Kk_r}\right)\ln\left(\frac{C_0}{C_t}\right) + \frac{C_0 - C_t}{k_r}} \quad \textbf{(7)}$$

where C_o represents the initial concentration of MG. Therefore at low C_o, the second term in Eq. (7) becomes insignificant and hence can be neglected:

$$\boldsymbol{\ln\left(\frac{C_0}{C_t}\right) = k_rKt = k_{app}t} \quad \textbf{(8)}$$

With k_{app} as the apparent rate constant for the photocatalytic degradation reaction. The almost perfect linearity of the $\ln(C_o/C_t)$ versus t plots for various initial MG concentrations, Fig. 4.17, proves the applicability of the Langmuir–Hinshelwood equation for the photocatalytic degradation of MG [64]. The apparent rate constant, k_{app}, decreases as the initial concentration of MG increases. At too high MG concentrations, a greater amount of dye molecules adsorb on the catalyst surface blocking the photocatalytically active sites on the catalyst, thus reducing the absorption of photons, their interaction with the active sites and therefore inhibiting the photocatalytic degradation process. In addition, increasing MG concentration leads to a larger fraction of the UV irradiation that is absorbed by the dye molecules in the water solution, instead of being absorbed by the catalytically active sites [64-66]. The effect of Temperature on rate constant has been studied. The rate constant was found 0.0050 and 0.0062 min^{-1}in presence of Titania at 30 ^oC and 40 ^oC temperature of reaction. The rate constant is slightly increased with increase of temperature. The rate constant was found 0.0072 and 0.0102 min^{-1} in presence of $Ni_{0.10}$:$La_{0.05}$:TiO_2 nanocomposite at 30 ^oC and 40 ^oC temperature of reaction. The rate

constant of the photocatalysis is increasing with increase of temperature. This is due to the rate of reaction increased with increasing the temperature. The kinetic energy of dye molecule is increase with increase of temperature, which causes the interaction of dye molecule with photocatalyst. Hence the rate of reaction and rate constant are increased with increasing the temperature of reaction.

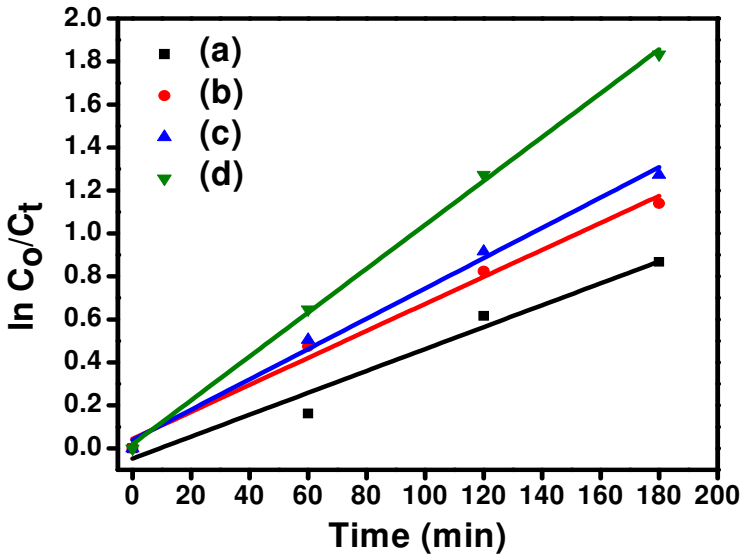

Fig.4.17.The straight line relationship between the ln (C_o/ C_t) and irradiation time indicates photodegradation rate of Methyl Green (50 ppm) can be approximated by a pseudo first order reaction (a) TiO_2 at 30°C (b) TiO_2 at 40°C (c) $Ni_{0.10}$:$La_{0.05}$:TiO_2 at 30°C (d) $Ni_{0.10}$:$La_{0.05}$:TiO_2 at 40°C.

Conclusion

Prepared nanocomposites of $Ni_{0.10}$:$La_{0.05}$:TiO_2 were characterized by X-Ray Diffractometer, SEM, TEM, UV- Vis, FT-IR, Band gap energy and BET. The TiO_2 and $Ni_{0.10}$:$La_{0.05}$:TiO_2 were used as photocatalyst for the degradation of Methyl Green. The particle size was estimated by the Scherrer's and found 76 and 34 nm for TiO_2 and $Ni_{0.10}$:$La_{0.05}$:TiO_2 respectively. The XRD pattern confirmed the presence of anatase and rutile phase in the catalyst. The particle morphology of the photocatalysts was found in

nanodiamension. The surface area of TiO_2 and $Ni_{0.10}$:$La_{0.05}$:TiO_2 were found 34.72 and 96.58 m^2/g. The band gap energy of TiO_2 and $Ni_{0.10}$:$La_{0.05}$:TiO_2 were 3.2 and 3.0 eV. The photocatalytic degradation behaviour of photocatalysts was investigated by considering different parameters such as effect of concentration, effect of amount of photocatalyst, effect of pH, effect of temperature, adsorption, and kinetics. The photodegradation of Methyl Green has been found 90-98 % at 7 pH, 25 ppm concentration of dye, 800 mg/L amount of photocatalyst and 50 min illumination of visible light in presence of $Ni_{0.10}$:$La_{0.05}$:TiO_2 while 10-18 % in presence of neat TiO_2. The photodegradation was following the first order kinetics.

References

[1]. D. F. Duxbury, Chem. Rev., 93, (1993), 381-433.

[2]. T. Inoue, K. Kikuchi, K. Hirose, M. Iiono, T. Nagano, Chem. Biol, 8, (2001), 9-15.

[3]. Green, F. J. The Sigma-Aldrih Handbook of Stains, Dyes, and Indicators; Aldrich Chemical: Milwaukee, WI, (1990).

[4]. T. Geethakrishnan, P. K. Palanisamy, Optik, 117, (2006), 282-286.

[5]. J. Melnick, Pickering, M. Biochem. Int., 16, (1988), 69-75.

[6]. R. Bonnett, Martinez, G. Tetrahedron, 57,(2001), 9513-9547.

[7]. B. P. Cho, T. Yang, L. R.Blankenship, J. D. Moody, M. Churchwell, F. A. Bebland, S. J. Culp, Chem. Res. Toxicol., 16,(2003), 285-294.

[8]. M. Vautier, C. Guillard, J.M. Herrmann, J. Catal., 201, (2001), 46–59.

[9]. S. Yang, X. Yang, X. Shao, R. Niu, L. Wang, J. Haz. Mater., 186, (2011), 659–666.

[10]. C.C. Chen and C. Shinlu, Environ. Sci. Technol., 41, (2007), 4389-4396.

[11]. A. Jain, A. Ashma, K. Marazban, J. Appl. Chem., 2, (2014), 13–25.

[12]. N. Ejhieh, E. Shahriari, J. Ind. Eng. Chem., 20, (2014), 2719–2726.

[13]. M. Nag, P.C. Chen, S. Kumar, Applied Cata. A: General, 433–434, (2012), 75-80

[14]. A. Kumar, G. Pandey, Desalination and Water Treatment, 71, (2017), 406–419.

[15]. P.V. Kamat, K. Vinodgopal, D.E. Wynkoop, Environ. Sci. Technol, 30, (1996), 1660–1666.

[16]. R. Byberg, J. Cobb, L.D. Martin, R.W. Thompson, T.A. Camesano, O. Zahraa, M.N. Pons, Environ. Sci. Pollut. Res., 20, (2013), 3570–3581.

[17]. R. Montan, E. Rivero, Environ. Sci. Pollut. Res., 22, (2015), 784–791.

[18]. D. Choudhury, M. Dey, and A. Choudhury, Int. Nano Letters, 3, (2013), 25.

[19]. G. A. Epling, Chitsan Lin, Chemosphere, 46, (2002),937-944.

[20]. M. Toyoda, T. Yano, B. Tryba, S. Mozia, T. Tsumura, and M. Inagaki, Applied Catalysis B: Environmental, 88, (2009), 160-164.

[21]. X. Chen, & S. S. Mao,Chemical Reviews, 107, (2007), 2891–2959.

[22]. O. Jongprateep, R. Puranasamriddhi, J. Palomas, Ceramics International, 41, (2015), S169-S173.

[23]. H. Lee, Y.K. Park, S.J. Kim, B.H. Kim, S.C. Jung, Journal of Industrial and Engineering Chemistry, 32, (2015), 259-263.

[24]. A. Kumar and G. Pandey, Chemical Science Transactions, 6, (2017), 385-392.

[25]. H. Jia, Z. Zheng, H. Zhao, L. Zhang, and Z. Zou, Materials Research Bulletin, 44, (2009), 1312-1316.

[26]. A. Kumar, G. Pandey, American Journal of Nano Research and Applications, Vol. 5, (2017), 40-48. doi: 10.11648/j.nano.20170504.11

[27]. N. M. Makwana, C. J. Tighe, R.I. Gruar, P. F. McMillan, Materials Science in Semiconductor Processing, 42, (2016), 131-137.

[28]. A. Kumar, G. Hitkari, M. Gautam, S. Singh, G. Pandey, Synthesis, Int. Adv. Res. J. in Sci., Eng. and Tech., 2, (2015), 50-55.DOI 10.17148/IARJSET.2015.21208

[29]. A. M. Ng, P.C. Chen, S. kumar, Applied Catalysis A: General, 433–434, (2012), 75-80.

[30]. M. Hema, A.Y. Arasi, P. Tamilselvi, R. Anbarasan,, Chem. Sci. Trans., 2, (2013), 239–245.

[31]. A. Kumar, G. Hitkari, M. Gautam, S. Singh, G. Pandey, Int. J. of Inn. Res. in Sci., Eng. and Tech. 4, (2015), 12721-12731. DOI:10.15680/IJIRSET.2015.0412097

[32]. B. D. Cullity, S. R. Stock, Elements of X-Ray Diffraction, Third Edition, and New Jersey: Prentice-Hall, Inc. (2001).

[33]. A. Pal, R. Kaur, I. S. Grover, J. of Ind. and Eng. Chem., 33, (2016), 178-184.

[34]. H. Lachheb, E. Puzenat, A. Houas, M. Ksibi, E. Elaloui, C. Guillard, J.M. Herrmann, Appl. Catal. B: Environ., 39, (2002), 75–90.

[35]. Pare, P. Singh,and S.B. Jonnalgadda, Journal of Scientific & Industrial Research, 68, (2009), 724-729.

[36]. W. Baran, A. Makowski, W. Wardas, Chemosphere, 53, (2003), 87–95.

[37]. A. Gnanaprakasam, V.M. Sivakumar, P.L. Sivayogavalli, M. Thirumarimurugan Ecotoxicology and Environmental Safety, 121, (2015), 121-125.

[38]. S. Kaur, V. Singh, Ultrasonics Sonochemistry, 14,(2007), 531-537.

[39]. G.A. Epling, C. Lin, Chemosphere, 46, (2002), 561–570.

[40]. A. Kumar, G. Pandey, Chem. Sci. J. 8, (2017), 164, doi: 10.4172/2150-3494.1000164

[41]. H. B, Hadjltaief, M. B. Zinaa, M. E. Galvez, P. D. Costa, Journal of Photochemistry and Photobiology A: Chemistry, 315, (2016), 25–33.

[42]. M. Vautier, C. Guillard, J.M. Herrmann, J. Catal., 201, (2001), 46–59.

[43]. M.M. Ba-Abbad, A.A.H. Kadhum, A.B. Mohamad, M.S. Takriff, K. Sopian, Int. J. Electrochem. Sci., 7, (2012), 4871–4888.

[44]. S. Kumari, Y.S. Chaudhary, S.A. Agnihotry, C. Tripathi, A. Verma, D. Chauhan, R. Shrivastav, S. Dass, and V.R. Satsangi, Int. J. of Hyd. Ene., 32, (2007), 1299-1302.

[45]. J. Peral, X. Domenech, D.F. Ollis, J. Chem. Technol. Biotechnol., 70, (1997), 117–140.

[46]. J. Zhu, Z. Deng, F. Chen, J. Zhang, H. Chen, M. Anpo, J. Huang, L. Zhang, Appl. Catal. B: Environ., 62, (2006), 329–335.

[47]. J.C. Colmenares, M.A. Aramendia, A. Marinas, J.M. Marinas, F.J. Urbano, Appl. Catal. A: Gen., 306, (2006), 120–127.

[48]. Y. Ao, F.J.D. Xu, X. Shen, C. Yuan, Colloids Surf. A Physicochem. Eng. Aspects, 312, (2008), 125–130.

[49]. K. M. Reddy, S. V. Manorama, A. R. Reddy, Materials, Chemistry and Physics, 78, (2002), 239–245.

[50]. X. Chen, S. S. Mao, Chem. Rev., 107, (2007), 2891−2959.

[51]. A. Sobczynski, A. Dobosz, Pol. J. Environ. Stud., 10, (2001), 195-205.

[52]. G. Tian, K. Pan, H. Fu, L. Jing, W. Zhou, J. Hazard. Mater., 166, (2009), 939−944.

[53]. X. Cheng, H. Liu, Q. Chen, J. Li, P. Wang, Electrochim. Acta, 103, (2013), 134−142.

[54]. H. Freundlich, Ueber die adsorption in loesungen, J. Phys. Chem., 57, (1907), 385–470.

[55]. Langmuir, J. Am. Chem. Soc., 40, (1918), 1361−1403.

[56]. R.W. Matthews, J. Catal., 111, (1988), 264–272.

[57]. M. Vulliet, C.Chovelon, C. Guillard, J.M. Herrmann, J. Photochem. Photobiol. A: Chem., 159, (2003), 71–79.

[58]. U.G. Akpan, B.H. Hameed, Journal of Hazardous Materials, 170, (2009), 520–529.

[59]. K. M. Reza, A.S.W. Kurny, F. Gulshan, Appl Water Sci., 7, (2017), 1569–1578.

[60]. G. K. Pradhan, D. Padhi, and K. Parida, Appl. Mater. Interfaces, 5, (2013), 9101–9110

[61]. T. Tachikawa, S. Tojo, M. Fujitsuka, T. Sekino, and T. Majima, J. Phys. Chem. B, 110, (2006), 29.

[62]. N. Guettaı, H.A. Amar, Desalination, 185, (2005), 439–448.

[63]. N. Jallouli, K. Elghniji, O. Hentati, A. R. Ribeiro, A. M.T. Silva, M. K. sibi, J. of Haz. Materials, 304, 5 ,(2016), 329-336.

[64]. M.D. Murcia, N.O. Vershinin, N. Briantceva, M. Gomez, E. Gomez, E. Cascales, A.M. Hidalgo, Chemical Engineering Journal, 266, (2015), 356-367.

[65]. Z. Bensaadi, N.Y. Mezenner, M. Trari, F.Medjene, J. ofEnvi. Chemi. Eng., 2, (2014), 1371-1377.

[66]. S. Ahmad, R. Bano, S. G. Musharraf, M.A. Sheraz, S. Ahmed, H. Tahir, Q. U. Arfeen, M.S. Bhatti, Z. Shad, S. F. Hussain, J. of Photoche. and Photobi. A: Chemistry, 302, (2015), 1-10.

CHAPTER-5

Photocatalytic degradation of Rose Bengal and Thymol Blue dye under visible light by TiO_2/PAni/GO nanocomposites

Nanocomposites of TiO_2, TiO_2/PAni and TiO_2/PAni/GO were prepared by in situ oxidation polymerization method. The prepared TiO_2, TiO_2/PAni and TiO_2/PAni/GO Nanocomposites were characterized by the XRD, SEM, TEM, BET, UV-Vis, FTIR, Band gap energy and Photolumiscence. The XRD confirmed the presence of Anatase and rutile phase in the prepared photocatalysts. The average particle size was found 68, 15 and 12 nm for TiO_2, TiO_2/PAni and TiO_2/PAni/GO respectively. The SEM and TEM images also confirmed the formation of nanocomposites in the range of ~ 100 nm. The surface area 37.52, 76.68 and 96.24 m^2/g were observed for TiO_2, TiO_2/PAni and TiO_2/PAni/GO Nanocomposites respectively. The Band gap energy of TiO_2, TiO_2/PAni and TiO_2/PAni/GO were calculated by talc plot and obtained 3.0, 2.86 and 1.76 eV respectively. The Photocatalytic degradation of Rose Bengal dye was done at different condition viz concentration of dye, time of illumination, pH and dose of photocatalyst. The maximum photodegradation were found at neutral pH, 6.25 ppm concentration of dye solution, 800 mg/L amount of photocatalyst and 120 min irradiation of visible light. The Photocatalytic degradation of Thymol blue dye was done at the different conditions viz concentration of dye, time of illumination, pH, and the dose of the photocatalyst. The photodegradation of Thymol blue was found 98-99%, 72-93% and 12-17% presence of TiO_2/PAni/GO, TiO_2/PAni and TiO_2 respectively. Kinetics of photodegradation was investigated for Rose Bengal and Thymol blue dye and found first order kinetics The coating of PAni and GO were enhanced the photocatalytic activity of Titania. Hence TiO_2/PAni and TiO_2/PAni/GO are the efficient photocatalyst for the degradation of Rose Bengal B dye than pure TiO_2.

5.1. Introduction

The major source of environmental pollution is the wastewater effluent of textile industries. The textile industries are using the very large amount of chemically stable dyes which causing water pollution. Several investigations reported that about 12% of dyes used in textile industries in each year. During the manufacturing and processing, 20% dyes are lost in environment such as Rose Bengal, Caramine, Rhodamine, Indigo Red, Thymol blue, Red 120, Eriochrome Black-T (EBT), Methylene Blue [2, 3]. Textile industries effluents contain coloured pigments which is causing carcinogenic effect on human being and also causing serious impact on aquatic life. There are lots of dyes used in the textile industries. The xanthene dyes are mostly used in textile industries. Xanthene dyes can be characterized by presence of xanthenes nucleus with aromatic groups as chromophore [4, 5]**.** Rose Bengal is a significant xanthene dye and widely used in textile and photochemical industries whose molecular structure as shown in Figure 1**.** Rose Bengal shows the severe toxic effects on the human health and also affects the corneal epithelium [6]. It is very hazardous for human being because it causes the irritation, itchiness, blistering and reddening. It is also affects on human eyes like eye redness, inflammation, itching etc. [8]. There are several, physical and chemical methods have been studied to remove the organic dyes such as Rose Bengal, Methylene blue etc. from the wastewater. Physical techniques like photo degradation, coagulation**,** flocculation, reverse osmosis, adsorption on the activated carbon, ion exchange method and ultra-filtration, have been used to reduce the toxic effects of dye effluents. Furthermore, various chemical methods like photosensitized oxidation, adsorption, photofenton's reactions are also employed for removal of dyes. These techniques are not effective to remove the trace amount of dye from the waste water. Therefore we need green technology through which we can remove the dyes from the waste water. The photocatalytic degradation is the very advance oxidation process to remove the dye without any side product formation.

Titanium dioxide (TiO_2) is the mostly used photocatalyst due to its non-toxicity, high activity, photo stability, chemical stability, biological inertness, the good absorption, desorption rate of reactants and low cost [4]. TiO_2 photocatalyst has been applied to self-cleaning glasses, antibacterial tiles *etc.* as it has strong oxidizing power

to decompose most organic compounds to CO_2 [5]. Organic compounds such as halogeno-aliphatic hydrocarbons, halogeno aromatic hydrocarbons, organic acids, colouring matters, nitro aromatic hydrocarbons, substituted anilines, multi-ring aromatic hydrocarbons, hydroxybenzenes, surface active agents, and pesticides can be changed into non-toxic, decoloured inorganic compounds and ultimately eliminated as pollutants [6].

It is very interesting fact that TiO_2 absorbs only 5% UV portion of the solar light spectrum. There are two issues namely, limitation of light absorption by TiO_2 in the UV portion of the solar light spectrum and recombination of electron (e-) - hole (h+) pairs. Several researches have been done to synthesized modified nanocomposites for the utilization of solar light [9]. Consequently, hundreds of TiO_2 variants and other oxide/non-oxides have been developed and tested in propose to conquer the recombination process [10]. It is believed that availability of visible light absorbing photocatalysts would largely solve the technological problems photo reactor considerations. Moreover, harnessing sunlight can be considered as a More recently, some groups have used conducting polymers to modify TiO_2 to improve visible light photoactivity and electron transfer performance; e.g., Polyaniline/TiO_2 [11], polypyrrole/TiO_2 [12] and polythiophene/TiO_2 [13]. Many published reports focussed on the preparation and photo catalytic studies on nanocomposites consisting of polyaniline and TiO_2 (PAni/TiO_2) [14-17]. Among these, PAni has several advantageous features over others because of its good environmental stability, ease of synthesis, controllable doping/dedoping chemistry, and reversible electrical properties by controlled charge transfer processes [18, 19].

The incorporation of inorganic nanomaterials into PAni, thereby forming nanocomposite materials, appears to be an effective approach for preparing photocatalytic materials [20]. Some study reported that by adding graphene to PAni, there is an increase in the electric double-layer capacitance as well as charge transfer and charge transport [21].

In this study, the nanocomposites of TiO_2, TiO_2/PAni and TiO_2/PAni/GO were prepared by the co-deposition oxidation method. The prepared materials were characterized by the XRD, BET, TEM, SEM, UV-Vis, Band gap energy,

Photolumiscence spectra, and FTIR. The prepared materials were used as photocatalyst for the photodegradation of Rose Bengal dye in the visible light. The photodegradation of Rose Bengal has been done at different chemical parameters i.e. pH of solution, concentration of dye, amount of photocatalyst, photocatalyst, time of irradiation and recyclability of photocatalyst. The kinetic study of photodegradation has been performed and found the order of reaction.

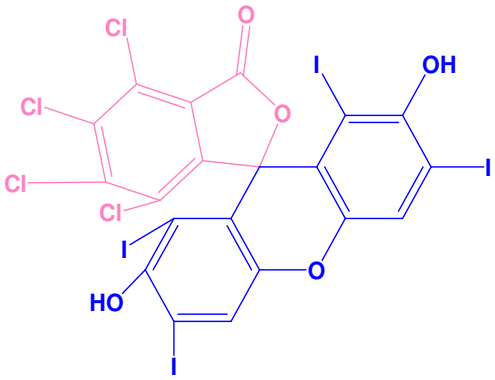

Fig.5.1 Molecular structure of Rose Bengal dye

5.2. Methods and materials

5.2.1 Synthesis of Titanium dioxide

TiO_2 nanoparticles were prepared using H_2O_2 solution added to 10 ml of 1 mol/L ethanol solution of titanium tetra isopropoxide (TTIP). Ethanol was added to the brown coloured solution obtained, and the total volume of the solution was adjusted to 100 ml. The solution was then heated at 120°C for 1hr in a closed vessel. The solution was filter and obtained the solid material, further it was washed with double distilled water 2 to 3 time and dry in oven at 60 °C for 24 h. The obtained solid was calcined at 600°C for 3hr to get white titanium oxide powder [22-23].

5.2.2 Synthesis of TiO_2/PAni nanocomposite

The synthesis of the TiO_2/PAni nanocomposite was done by using aniline, TTIP as the TiO_2 precursor and Ammonium per sulphate as the oxidizing agent. In a typical process, 10 mL of CCl_4 and 4.0 mL of TTIP were placed in a beaker to which 1 mL of aniline were added. The entire system was stirred constantly on an ice bath. To the

above dispersion of aniline, the solution of oxidant (0.5 M APS in 500 mL of 1M HCl) was added drop-wise, which simultaneous initiated the polymerization of aniline and the synthesis of TiO_2. The reaction mixture soon turned into greenish black slurry, which was filtered after 2 hours, and washed sequentially with an excess of water and acetone to remove the excess APS and PAni oligomers. The synthesized TiO_2/Pani nanocomposite was then de-doped with a 1M ammonia solution to neutralize the remaining acid, which converted the TiO_2/PAni nanocomposite to its emeraldine base (EB) form. To render it conductive, the EB of TiO_2/PAni nanocomposite was doped with 100 mL of 1M HCl solution for 12 hours, later filtered and dried in an air oven at 80 °C for 24 hours. Pure PAni was prepared in a similar manner but in the absence of TTIP. [24-25].

5.2.3 Synthesis of TiO_2/PAni/GO nanocomposite

The synthesis of the TiO_2/PAni nanocomposite was done by using aniline, TTIP as the TiO_2 precursor and Ammonium per sulphate as the oxidizing agent. In a typical process, 10 mL of CCl_4, 4.0 mL of TTIP and 60 mg of prepared Graphene oxide were placed in a beaker to which 1 mL of aniline were added. The entire system was stirred constantly on an ice bath. To the above dispersion of aniline, the solution of oxidant (0.5 M APS in 500 mL of 1M HCl) was added drop-wise, which simultaneous initiated the polymerization of aniline and the synthesis of TiO_2. The reaction mixture soon turned into greenish black slurry, which was filtered after 2 hours, and washed sequentially with an excess of water and acetone to remove the excess APS and PAni oligomers. The synthesized Pani-TiO_2 nanocomposite was then de-doped with a 1M ammonia solution to neutralize the remaining acid, which converted the TiO_2/PAni nanocomposite to its emeraldine base (EB) form. To render it conductive, the EB of TiO_2/PAni nanocomposite was doped with 100 mL of 1M HCl solution for 12 hours, later filtered and dried in an air oven at 80 °C for 24 hours.

5.2.4 Characterizations

The prepared TiO_2, /PAni, TiO_2/PAni and TiO_2/PAni/GO nanocomposites were characterized by x-ray diffraction (XRD) patterns in the range of $2\theta = 20–80°$. The size of TiO_2 particles was investigated with transmission electron microscope (TEM). The

morphology of TiO_2, TiO_2/PAni, and TiO_2/PAni/GO nanocomposites were investigated by scanning electron microscopy. Fourier-transform infrared (FTIR) was used for the bonding determination, UV-visible DRS was used for band gap energy determination and Photolumiscence was used for the hydroxyl radical mechanism determination and e^--h^+ recombination determination.

5.2.5 Irradiation procedure

The dye and photocatalyst suspension were stirred in the dark for 30 min to reach adsorption equilibrium with the nanocomposites (TiO_2, PAni, TiO_2/PAni and TiO_2/PAni/GO) surface. Irradiation experiments of dyes were carried out on stirred aqueous solutions contained in a 100 mL beaker. Degradations were performed on 20 mL of aqueous solutions containing the desired concentration of Rose Bengal. The amount of nanocomposites material varies from 100 mg/L to 800 mg/L. Irradiations were carried out using one UV-365 nm, Hanovia lamp (450 W). At any given irradiation time interval, the dispersion was sampled (5 mL), centrifuged, and subsequently filtered through a Millipore filter to separate the TiO_2 particles and take UV- Vis spectra to determine the residual concentration [26].

5.2.6 Determination of Hydroxyl radicals

To determine whether reactive oxygen species involved in the photocatalytic degradation of dyes is hydroxyl radical or not, terephthalic acid photoluminescence probing technique was used. In this, alkaline solution of terephthalic acid, having TiO_2, TiO_2/PAni and TiO_2/PAni/GO nanocomposites was irradiated with visible light. After 30 min of irradiation, sample was withdrawn from the reaction mixture and was centrifuged to separate photocatalyst particles. The photoluminescence spectrum of sample was recorded between 335 and 600 nm at an excitation wavelength of 325 nm and variation in intensity of peak at 425 nm was monitored using Perkin Elmer LS 55 Fluorescence Spectrometer [27].

5.3. Results and discussion

5.3.1 Characterisation

5.3.1.1 X-Ray Diffraction

The XRD patterns of TiO_2, PAni, TiO_2/PAni, TiO_2/PAni/GO nanocomposite are showing in Fig 5.2. The XRD pattern of TiO_2 showing in Fig. 5.2(a) a series of characteristic peaks : 2θ = 25.32° (101), 37.86° (103), 48.06° (200), 55.09° (211) and 62.75° (204) are observed due to the tetragonal anatase phase of TiO_2 (JCPDS file No : 86-1157). Fig.5.2 (b) showing the XRD pattern of PAni, a broad peak corresponding to the periodicity parallel to the polymer chain to (200) plane was observed at 19.26° 2θ [28]. The peak at 2θ ~25° due to the periodicity perpendicular to the polymer chain and other crystal planes at 2θ ~15° was absent, which shows that the as-synthesized PAni is highly amorphous in nature. In the XRD pattern of the TiO_2/PAni nanocomposites (Fig.5.2c) the usual broad peak corresponding to the periodicity parallel to the polymer chain encompassing a slight crystalline small peak at 20° 2θ was not observed. All the peaks corresponding to anatase TiO_2 were also present. In the XRD pattern of the TiO_2/PAni/GO nanocomposites (Fig. 5.2d), all the peaks corresponding to anatase TiO_2 were also present suggesting that the state of TiO_2 did not change during the polymerization process. On the other hand, a slight reduction in the peak intensity and red shift was observed for TiO_2 peaks in the TiO_2/PAni nanocomposite [29]. This might be due to the surface coating of PAni on TiO_2 during the polymerization process and the interactions between the TiO_2 nanoparticles and the PAni chain [30].

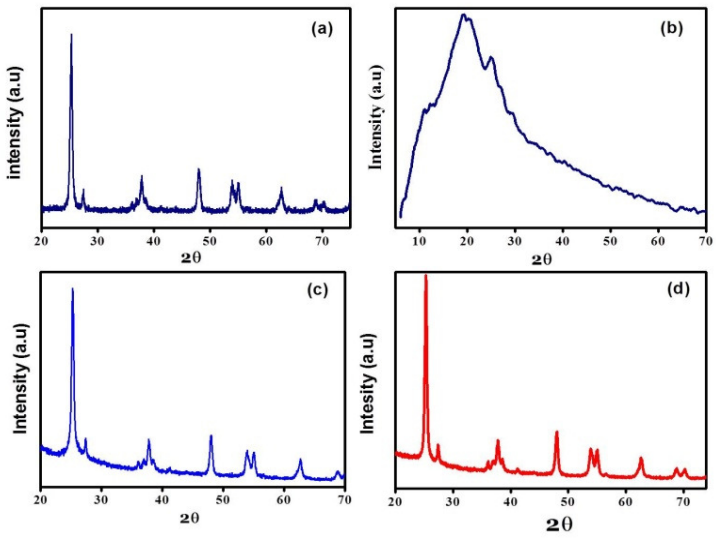

Fig.5.2 XRD Pattern of (a) TiO_2 (b) PAni (c) TiO_2/PAni (d) TiO_2/PAni/GO

5.3.1.2 FTIR

FT-IR spectra of TiO_2, PAni, TiO_2/PAni and TiO_2/PAni/GO are shown in Figure 5.3. In Figure 5.3(a), five peaks are observed due to O-Ti-O bond stretching (3418, 1628, 1502, 1302 and 1231 cm^{-1}) the main characteristic bands of polyaniline were seen in Figure 5.3b. The band at 3439 cm-1 is attributable to N-H stretching. Also the band at 1663 cm^{-1} assigned to N-H bend of a primary aromatic amine. The peaks at 1484 and 1419 cm^{-1} belong to C-C stretch in ring and N-O asymmetric and 1219 cm^{-1} C-O stretching and this confirms the presence of PAni and GO in the TiO_2/PAni/GO nanocomposite. Because titanium is a transition metal, it has intense tendency to form coordination compound with nitrogen atom in PAni Macromolecule. This interaction may weaken the bond strengths of N-H, C=C, and C-O in PAni Macromolecule. These results confirm to the presence of PAni and GO in nanocomposite [31].

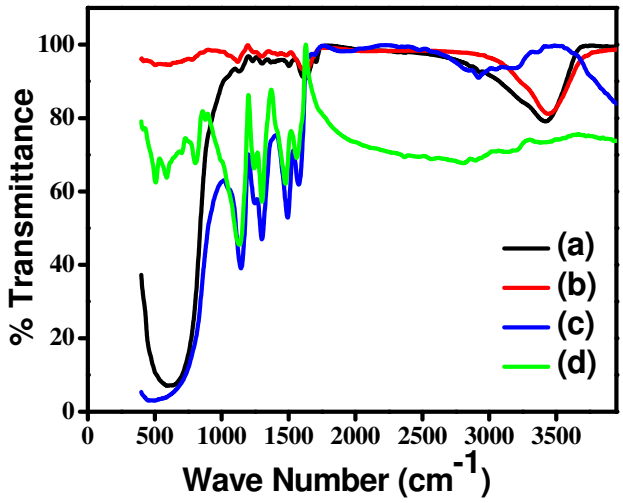

Fig.5.3. FTIR Spectra of (a) TiO_2 (b) PAni(c) TiO_2/PAni (d) TiO_2/PAni/GO

5.3.1.3 Scanning Electron Microscopy (SEM)

The morphology of the prepared nanocomposites was investigated by scanning electron microscopy and it resumes the most interesting outcomes. Fig.5.4 (a, b, c and d) clearly show that all the prepared nanocomposites are obtained in nanodiamension which is agglomerate form. The TiO_2, PAni, TiO_2/PAni and TiO_2/PAni/GO are indicating that the particle morphology is in spherical shape and disc shape. The TiO_2 molecule is agglomerate with PAni to form chips like structures which are partially

spherical and disc shape. The nanocomposites were found to be in nanometer range Fig.5.4 showing the TiO_2/PAni morphology which is in nanodiamension with little change in surface morphology. Fig.5.4 d showing the SEM image of TiO_2/PAni/GO which is in nanodiamension and the surface morphology of TiO_2/PAni/GO has been changed slightly, due to the coating of PAni and GO layer on the TiO_2 lattice. The surface of TiO_2/PAni/GO was observed like disk shape and spherical [32, 33].

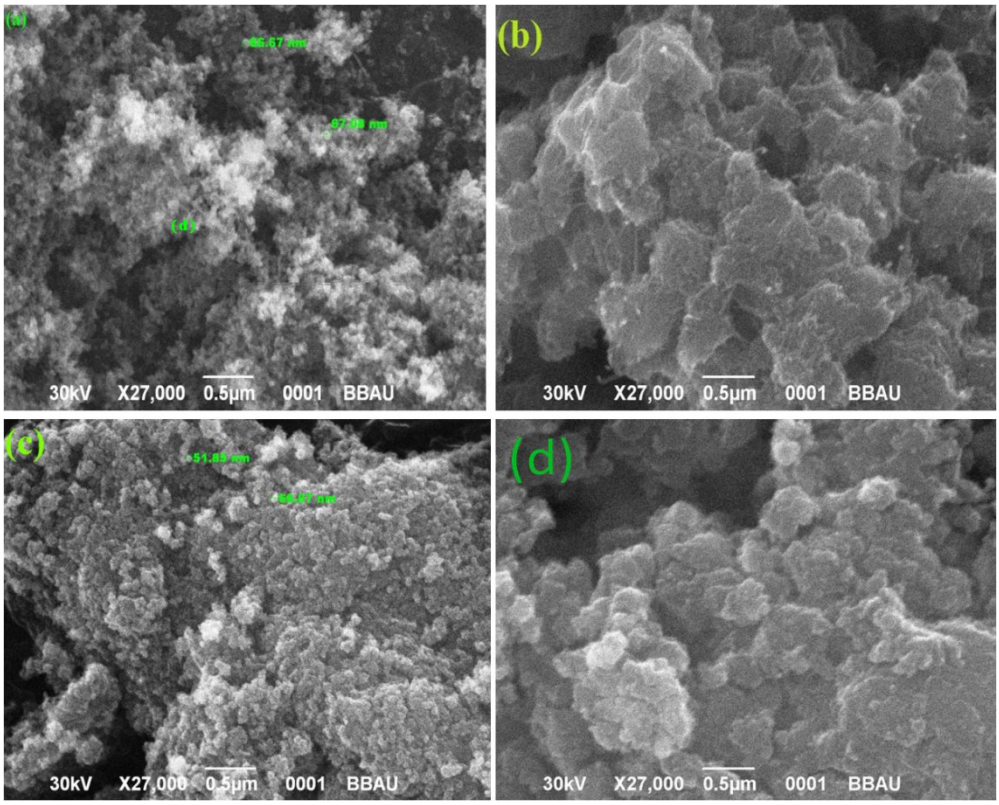

Fig.5.4. SEM images of (a) TiO_2 (b) PAni (c) TiO_2/PAni (d) PAni/TiO_2/GO

5.3.14 TEM analysis

The TEM images of TiO_2, TiO_2/PAni, and TiO_2/PAni/GO are shown in Fig 5. In the TEM of TiO_2 hexagonal crystal lattice structure has been observed (Fig.5.5a). Fig.5.5b showed the TEM image of pure polyaniline. In the TEM images, the spiral chain structure of PAni has been observed. From the TEM images, we find that PAni-modified TiO_2 does not change the size of TiO_2 significantly (Fig.5.5c). The sizes of both modified and TiO_2 are monodisperse about 10–20 nm. Moreover, the crystal lattice line can be clearly found in the TEM images. The aggregations of both kinds of

particles are caused by high surface energy; however, the agglomeration of the modified one is alleviated obviously compared with that of the neat TiO_2 [34, 35]. Generally, PAni synthesized by a chemical oxidative method in hydrochloric acid solution is the emeraldine salt (ES) form (Fig. 5.5), only which is electrically conducting. Anatase TiO_2 nanoparticles were deposited by PAni (ES) so as to avoid TiO_2 particles agglomeration because the positive charges exclude each other.

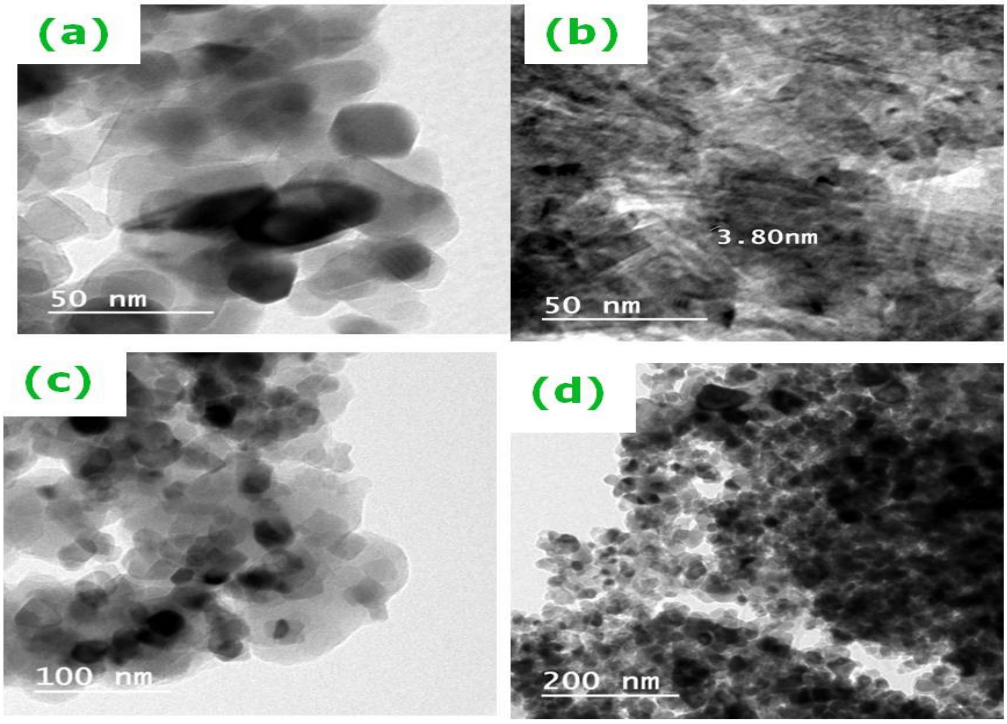

Fig.5.5 TEM images of (a) TiO_2 (b) Pure PAni (c) TiO_2/PAni (d) TiO_2/PAni/GO

5.3.1.5 Brunauer-Emmett-Teller (BET) Surface Area Analysis

Nitrogen adsorption–desorption isotherms were used to determine the structural characteristics and surface area of TiO_2, TiO_2/PAni, and TiO_2/PAni/GO nanocomposite. The N_2 adsorption desorption isotherms of the TiO_2, TiO_2/PAni, and TiO2/PAni/GO nanocomposite were measured at 77 K, as shown in Figure 5.6. The specific surface areas (from BET and Surface area, pore volume and pore radius of the TiO_2, TiO_2/PAni and TiO_2/PAni/GO nanocomposite are showing in Table 5.1. The surface area was found 37.52, 76.68 and 96.24 m^2/g for TiO_2, TiO_2/PAni, and

TiO_2/PAni/GO respectively. There is an increase in pore volume (Vp) of TiO_2, TiO_2/PAni and TiO_2/PAni/GO nanocomposite and pore radius is decreased [36-38].

Table5.1. The specific surface area, pore volume and pore radius of the TiO_2, TiO_2/PAni and TiO_2/PAni/GO

Sample	Surface area (m^2/g)	Pore volume (cm^3/g)	Pore radius (nm)
TiO_2	37. 52	3.132	1.84
TiO_2/PAni	76.68	6.5124	1.64
TiO_2/PAni/GO	96.24	9.5124	1.21

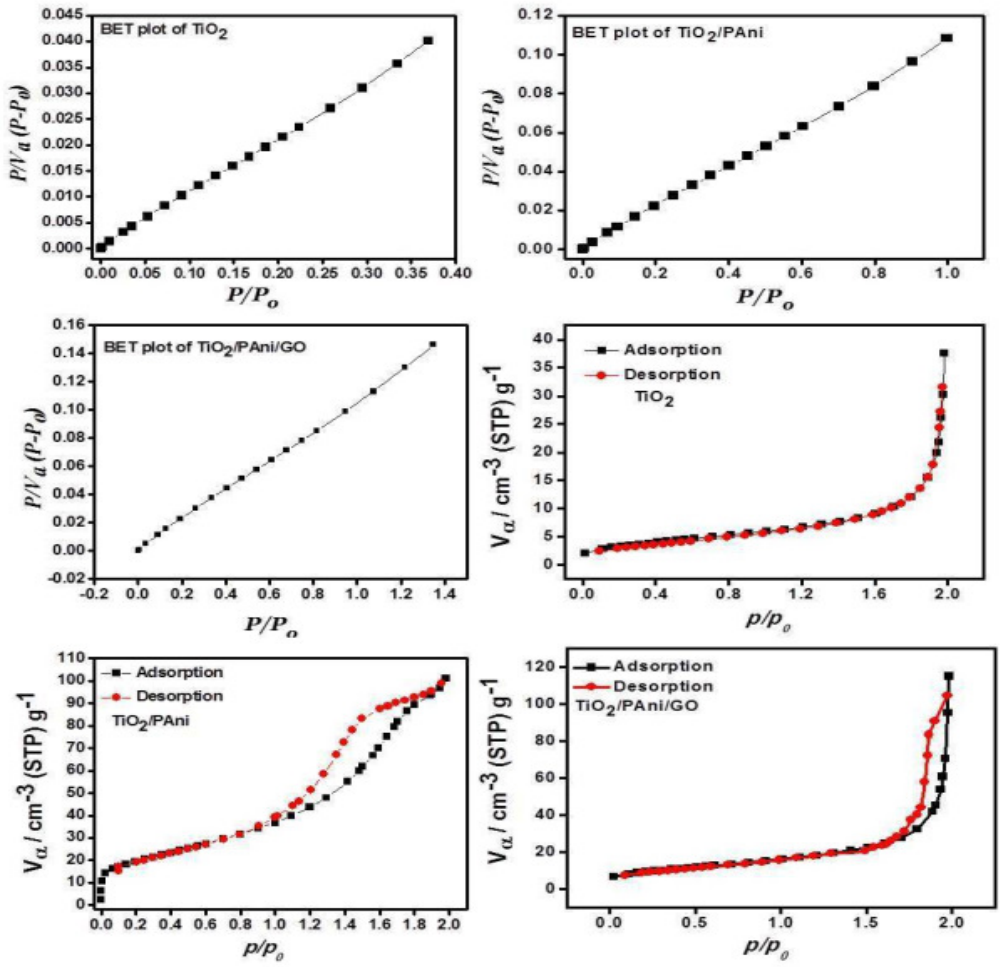

Fig.5.6. BET and Adsorption-desorption plot for TiO_2, TiO_2/PAni and TiO_2/PAni/ GO

From these results, it may be concluded that the high surface area of the TiO_2/PAni/GO nanocomposite may favour rapid electron transport and high ion diffusion, allowing improved photochemical performance. Moreover, the BET surface areas increased remarkably in the TiO_2/PAni/GO nanocomposite, which suggests that TiO_2 is well intercalated in PAni matrix and may also provide direct conduction pathway for electrons. The formation of TiO_2 with PAni by co-deposition oxidation synthesis resulted in the generation of well dispersed TiO_2 in PAni Matrix giving one TiO_2/PAni system with unique set of properties [39].

5.3.1.6. UV- Vis spectrophotometer

The absorption spectrum of TiO_2 consists of a single broad intense absorption around 263 nm (shown in Fig.5.7) in the region of hypsochromic shift. The PAni (Fig.5.7b) showed absorbance in the shorter wavelength region about 225 nm while TiO_2/PAni results showed a red shift in the absorption onset value and the broad peak observed at 287 nm.

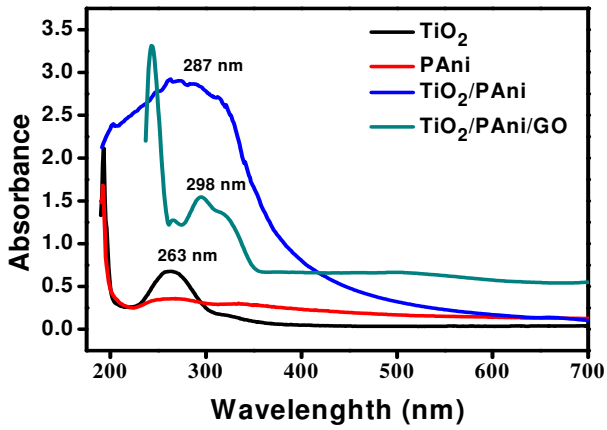

Fig.5.7. UV-Vis spectra of TiO_2, PAni, TiO_2/PAni, TiO_2/PAni/GO

This due to the coating of PAni layer on the surface of Titania [40]. The red shift that is observed at 298 nm in the absorption spectra with the decrease in particle size has been reported in TiO_2/PAni/GO nano hybrid composite. This is due to the coating of PAni and Graphene oxide in the Titania and the Titania completely interacted with PAni and GO.

5.3.1.7 Determination of Optical Band Gap energy of composites

The band gap of TiO_2, TiO_2/PAni, and TiO_2/PAni/GO were determined from absorption spectra and Tauc relation (Eq. (1))

$$\alpha h\nu = B(h\nu - E_{gap})m \quad (1)$$

The band gap energy of prepared materials was calculated by extrapolation of the $(\alpha h\nu)^2$ versus $h\nu$ plots, where α is the absorption coefficient and $h\nu$ is the photon energy, $h\nu = (1239/\lambda)$ eV. The value of $h\nu$ extrapolated to $\alpha = 0$ gives an absorption energy, which corresponds to a band gap (Eg) (showing in Fig.5.8).

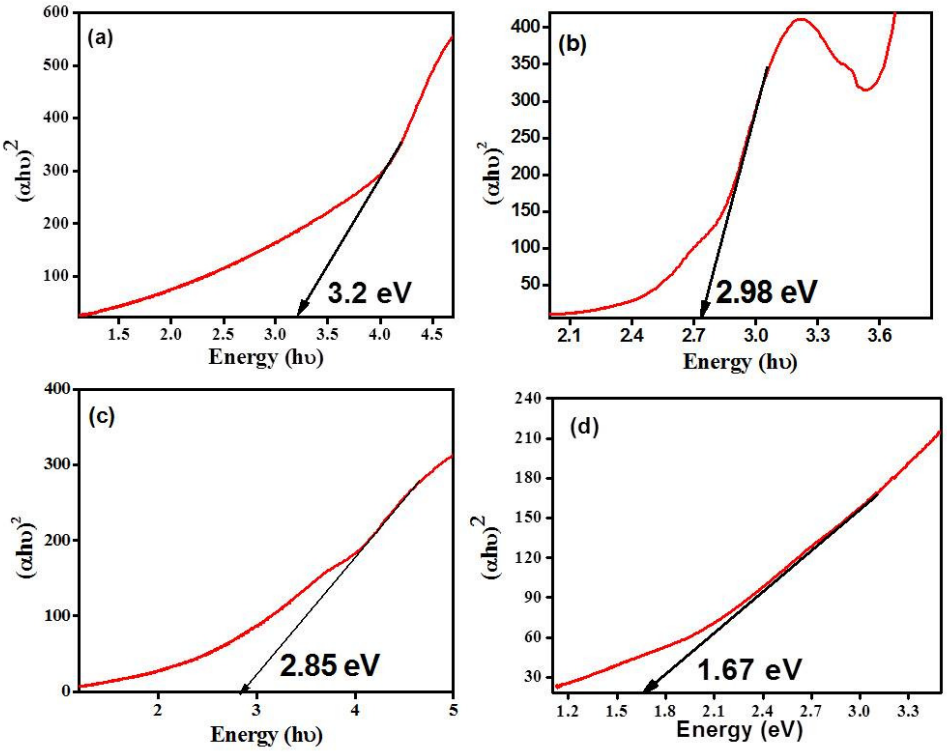

Fig.5.8. Band gap energy of (a) TiO_2 (b) pure Pani (c) TiO_2/PAni (d) TiO_2/PAni/GO

The Band gap energy of TiO_2, pure polyaniline, TiO_2/PAni and TiO_2/PAni/GO were observed 3.2, 2.98. 2.85 and 1.67 eV [41]. The slight decrease in band gap energy in case of TiO_2/PAni is due to formation heterostructures. In case of TiO_2/PAni/GO the band gap energy 1.67 eV was observed due to the coating of PAni and GO on the surface of Titania. In the other word, the PAni and GO form a heterostructures on surface of Titania [42].

5.3.1.8 EDX (Energy Dispersive X-ray Spectrometer)

Low energy secondary electrons, backscattered electrons, and X-rays are generated by primary electron bombardment. The intensity of backscattered electrons can be correlated to the atomic number of the element within the sampling volume. Hence, some qualitative elemental information can be obtained. The analysis of characteristic X-rays (EDX or EDS analysis) emitted from the sample gives more quantitative elemental information. Such X-ray analysis can be confined to analytical volumes as small as 1 cubic micron. It is confirmed the presence of Titania, oxygen, Nitrogen carbon in the prepared sample.

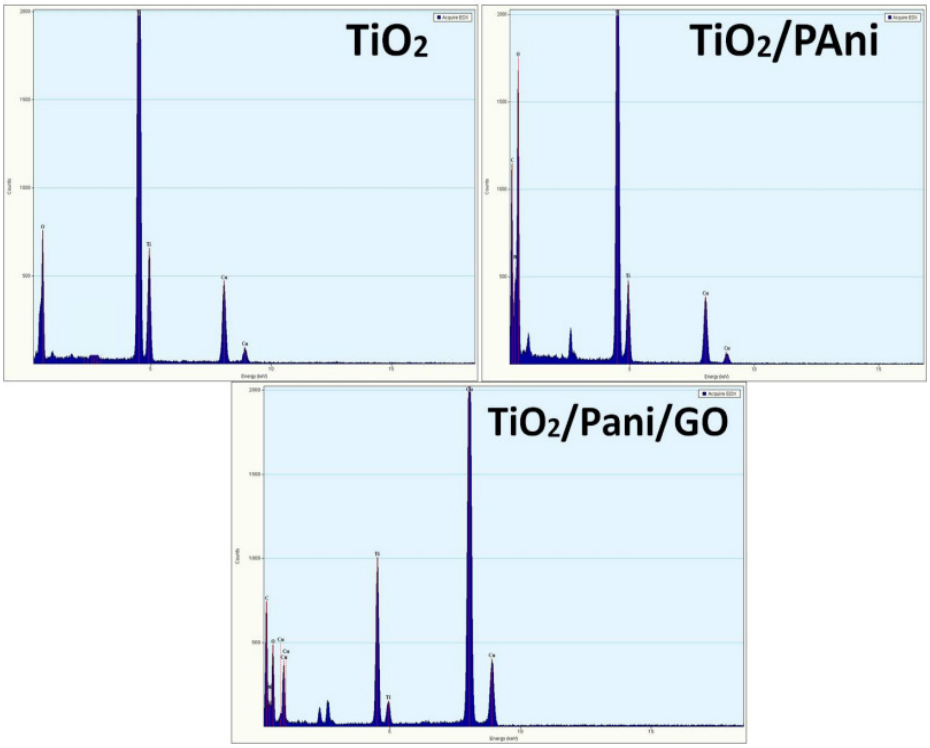

Fig.5.9 EDX Analysis of materials

5.3.2 Photodegradation of Rose Bengal dye

The photo-catalytic degradation of Rose Bengal in the presence of TiO_2, TiO_2/PAni and TiO_2/PAni/GO nanocomposites has been studied. The solutions of dye were prepared in 10:1 (V/V) ratio of water and alcohol. The known amount of photocatalyst 100 mg/L to 1600 mg/L was dispersed in the dye solution. The reaction mixture was illuminated under visible light, while kept continuously under agitation,

for the different time intervals and different concentration. The residual concentration of dye in the reaction mixture was measured spectrophotometrically. The results obtained for the degradation of Rose Bengal is shown in Fig.5.10-5.15.

Photocatalytic degradation efficiencies (η) are obtained by using following equation.

$$\eta = \frac{RB_O - RB_F}{RB_O} X\ 100 \quad (2)$$

where RB_0 is the initial absorbance and RB_F is the final sampled absorbance.

5.3.2.1 Effect of Irradiation time

The effect of the irradiation time on photodegradation of VB dye has been studied in presence of TiO_2, TiO_2/PAni, and TiO_2/PAni/GO nanocomposite. The UV spectrum has been taken for TiO_2, TiO_2/PAni and TiO_2/PAni/GO nanocomposite at different irradiation time (30, 60, 90, 120 and 180 min) (Fig. 4.10). It is interesting to remark that the absorbance decreases with increase of time with photocatalyst. At 120 minutes the photodegradation efficiency observed was 14, 93 and 97 % for TiO_2, TiO_2/PAni and TiO_2/PAni/GO nanocomposite respectively. The Titania was showed very low photodegradation efficiency in visible light. This is due to high band gap energy (3.2 eV) which is not active in visible light region. Whereas TiO_2/PAni and TiO_2/PAni/GO nanocomposite show very high photodegradation efficiency 93 and 97 %, this is due to the formation of sub band in Titania. The coating of PAni and GO decrease the band gap energy of Titania and Titania becomes active in visible light [43].

5.3.2.2 Effect of photocatalyst

The effect of photocatalyst was investigated. It is clear from the results shown in Fig.5.11 that TiO_2, TiO_2/PAni, and TiO_2/PAni/GO nanocomposites are proving as an effective photo-catalyst for the degradation of Rose Bengal (RB) dye. However, TiO_2/PAni/GO seems to be more effective as photo-catalyst for the degradation of Rose Bengal (RB). The prominent degradation of Rose Bengal was found in 120 min study in the presence of TiO_2/PAni/GO in comparison to the prepared TiO_2 and TiO_2/PAni. This is due to the coating of polyaniline of Titania surface which provide the electron

from the HOMO to LUMO. The electrons of HOMO get excited into LUMO which is further jump into the conduction band of Titania [44].

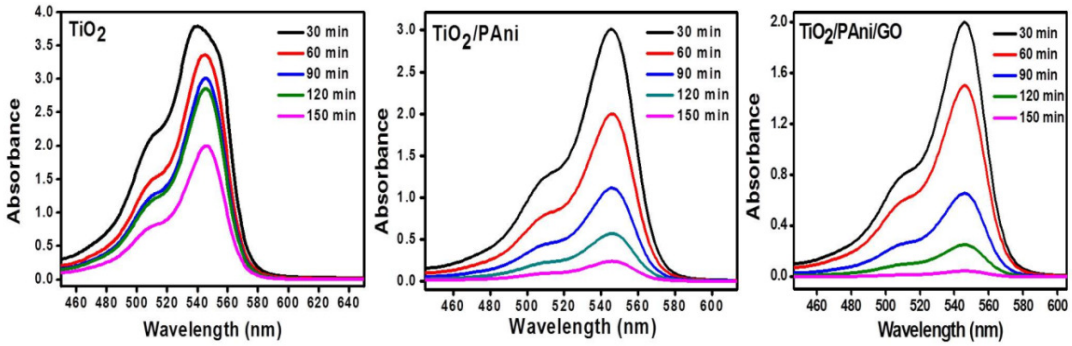

Fig.5.10 UV-Vis spectrum showing the effect of irradiation time on photodegradation with TiO_2, TiO_2/PAni and TiO_2/PAni/GO nanocomposite

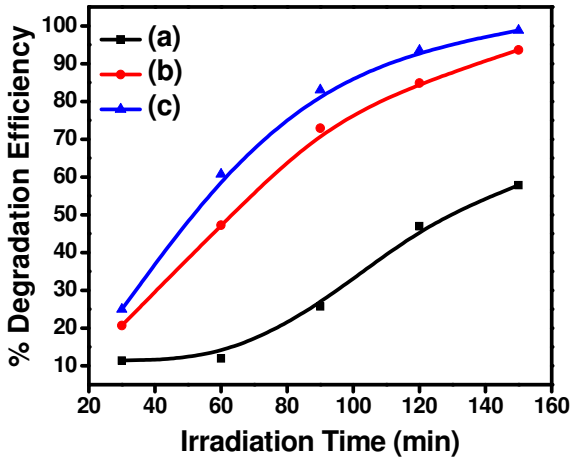

Fig.5.11. Effect of irradiation time on photo-degradation of RB with (a) TiO_2, (b) TiO_2/PAni and (c) TiO_2/PAni/GO nanocomposite

5.3.2.3 Effect of concentration of dye

The effect of dye concentration Keeping the catalyst loading concentration constant at 800 mg/L of the dye solution, the effect of varying concentration of the dye was studied on its rate of degradation (25, 50, 75, 100 and 125 ppm) as given in Fig.5.12. The rate of photodegradation was decrease with increasing concentration of RB. This is because as the number of dye molecules increase, the amount of light (quantum of photons) penetrating into the dye solution to reach the catalyst surface is reduced owing to the hindrance in the path of light. Thereby the formation of the

reactive hydroxyl and superoxide radicals is also simultaneously reduced. Thus there should be an optimum value maintained for the catalyst and the dye concentration, wherein maximum efficiency of degradation can be achieved [45, 46].

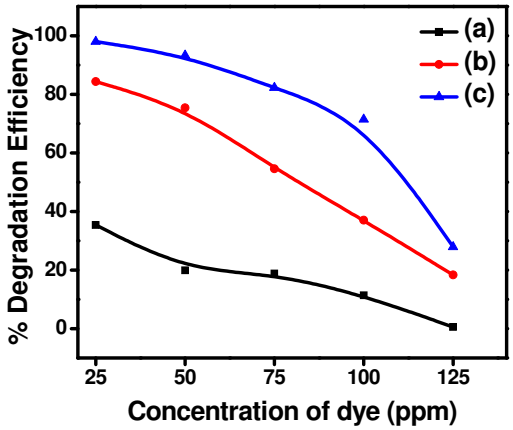

Fig.5.12. Effect of concentration on photo-degradation of RB with (a) TiO_2, (b) TiO_2/PAni and (c) TiO_2/PAni/GO nanocomposite

5.3.2.4 Effect of pH

The photodegradation was carried out under varying pH conditions from (3 to 11), by adjusting with H_2SO_4 and NaOH, with TiO_2 kept at constant amounts of photocatalyst of 800 mg/ L and 25 ppm concentration of dye solutions (Fig.5.13). The photodegradation was found to have highest rates at neutral ranges of pH. While at lower pH it was found to decrease. In the basic condition, the photodegradation rate was found slow and very poor degradation. Hence highly acidic and basic condition is not favourable for the degradation of VB. This implies that neutral conditions are favourable towards the formation of the reactive intermediates that is hydroxyl radicals is significantly enhanced, which further help in enhancing the reaction rate. On the other hand in basic and acidic conditions, the formation of reactive intermediates is relatively less favourable and hence less spontaneous [47-48].

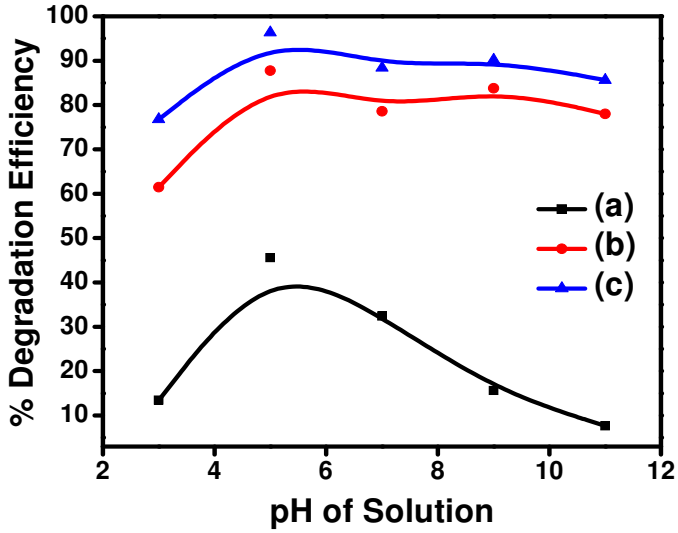

Fig.5.13. Effect of pH of solution on photodegradation of RB with (a) TiO_2, (b) TiO_2/PAni and (c) TiO_2/PAni/GO nanocomposite

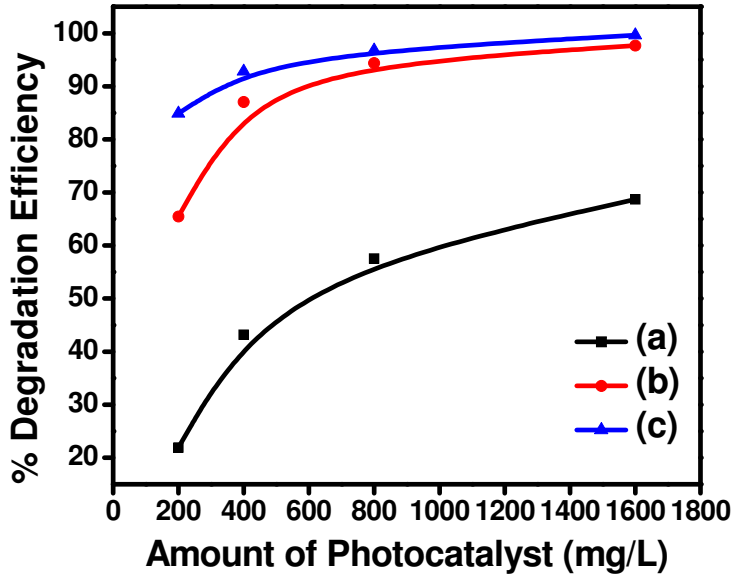

Fig.5.14. Effect of photocatalyst dose on photodegradation of RB with (a) TiO_2, (b) TiO_2/PAni and (c) TiO_2/PAni/GO nanocomposite

5.3.2.5 Effect of photocatalyst amount

It is clear from the results shown in Fig.5.14 that TiO_2, TiO_2/PAni, and TiO_2/PAni/GO nanocomposites are proving as an effective photo-catalyst for the

degradation of Rose Bengal dyes. The photodegradation of Rose Bengal was increasing with increases the amount of photocatalyst. It is observed that TiO_2/PAni/GO is the more effective photocatalyst than TiO_2 and TiO_2/PAni [44]. When the photocatalyst amount increases, the number of active site increase for the reaction of dyes. The amount of photocatalyst increases two times the rate of photodegradation increase about 30% and 60 %, in presence of TiO_2, TiO_2/PAni, and TiO_2/PAni/GO respectively [49].

5.3.3 Recyclability of Photocatalyst

The recyclability of photocatalyst has been studied. The photocatalyst and Rose Bengal mixture was agitated, illuminated with visible light and after desired time, the mixture was centrifuge to remove the photocatalyst. The obtained photocatalyst washed three times with distilled water and finally kept in oven for 24 h at 60 ^{o}C temperature and further it is reuse for the degradation of Rose Bengal. The photodegradation of Rose Bengal by the recyclized Photocatalyst are showing in Fig. 5.15. The result shows that the recyclized photocatalyst efficiency is decreasing due to the loss of some active sites and decrease of collection efficiency of photon [50, 51].

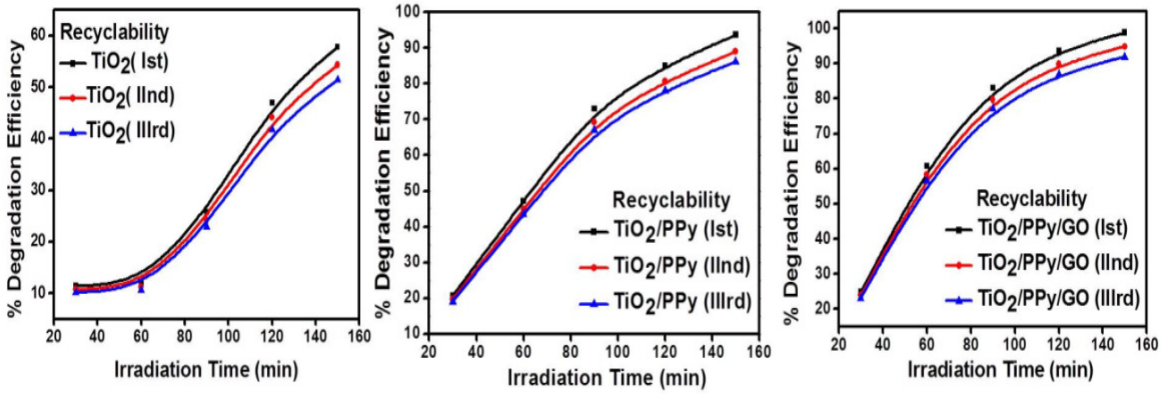

Fig.5.15. Photodegradation of Rose Bengal by Photocatalyst and recyclable Photocatalyst TiO_2, TiO_2/PAni, TiO_2/PAni/GO

5.3.4 Lowering of electron-hole recombination

Photoluminescence spectra have been used to examine the mobility of the charge carriers to the surface as well as the recombination process involved by the electron-hole pairs in semiconductor particles. PL emission results from the radiative

recombination of excited electrons and holes. In other words, it is a critical necessity of a good photocatalyst to have minimum electron-hole recombination. To study the recombination of charge carriers, PL studies of synthesized materials have been undertaken. PL emission intensity is directly related to recombination of excited electrons and holes. Fig. 5.16 shows the photoluminescence spectra of synthesized photocatalysts. It means TiO_2 and TiO_2/PAni with strong PL intensity has high recombination of charge carriers where as TiO_2/PAni/GO has weak intensity.

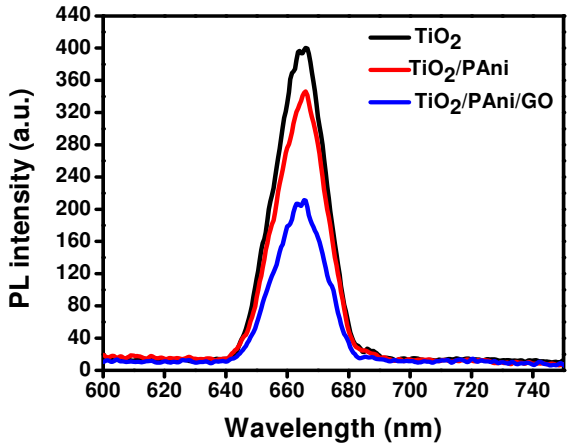

Fig.5.16. Photolumiscence Spectra of TiO_2, TiO2/PAni and TiO2/PAni/GO

The weak PL intensity of TiO_2/PAni/GO may arise due to the coating of polyaniline on Titania lattice. The photo excited electrons were trapped into the graphene oxide. This delays the electrons- holes recombination process and hence is utilized in the redox reaction leading to improved photocatalytic activity [52, 53].

5.3.5 Hydroxyl radical formation

As hydroxyl radical performs the key role for the decomposition of the organic pollutants, it is necessary to investigate the amount of hydroxyl radicals produced by each photocatalyst. Thus, there is a technique to establish the formation of hydroxyl radicals using terephthalic acid (TA) as a probe molecule. In this method, TA was directly attacked by OH radical forming 2- hydroxyl terephthalic acid (TAOH) which gives a fluorescence signal at 426 nm. Fig.5.17 depicts the fluorescent signal of all the photocatalysts after reacting with TA solution. The fluorescent intensity is linearly related to the number of hydroxyl radicals formed by the photocatalysts. It means

higher is the generation of hydroxyl radical, yield of TAOH will be more and hence more intense will be the fluorescence peak. Thus, TiO_2/PAni/GO with highest intensity confirms the generation more number of hydroxyl radicals compared to other photocatalysts. The fluorescence intensity follows the trend (i,e. TiO_2, < TiO_2/PAni < TiO_2/PAni/GO) of photocatalytic performance of all the photocatalyst [54, 55].

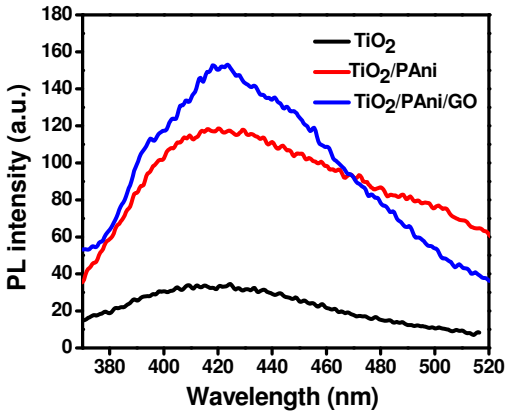

Fig.5.17. PL spectra of photocatalyst with terephthalic acid (0.001M) TiO_2, TiO_2/PAni and TiO_2/PAni/GO

5.3.6 Mechanism of photo-oxidation process

The acceleration of a chemical transformation by the presence of a catalyst with light is called photocatalysis. The catalyst may accelerate the photoreaction by interaction with the substrate in its ground or excited state and/or with a primary photoproduct, depending upon the mechanism of the photoreaction and itself remaining unaltered at the end of each catalytic cycle. Heterogeneous photocatalysis is a process in which two active phases solid and liquid are present. The solid phase is a catalyst, usually a semiconductor. The molecular orbital of semiconductors has a band structure. The bands of interest in photocatalysis are the populated valence band (VB) and it's largely vacant conduction band (CB), which is commonly characterized by band gap energy (E_{bg}). The semiconductors may be photo-excited to form electron-donor sites (reducing sites) and electron-acceptor sites (oxidising sites), providing great scope for redox reaction. When the semiconductor is illuminated with light ($h\upsilon$) of greater energy than that of the band gap, an electron is promoted from the VB to the CB leaving a

positive hole in the valence band and an electron in the conduction band as illustrated in Fig. 5.18.

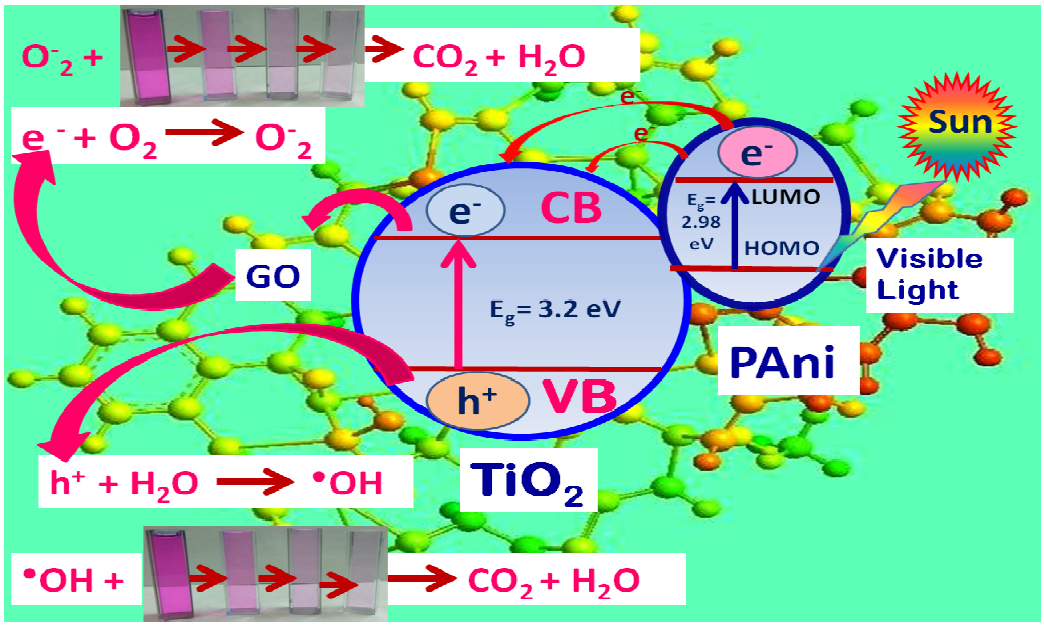

Fig.5.18 Mechanism of photodegradation of Rose Bengal in visible light

If charge separation is maintained, the electron and hole may migrate to the catalyst surface where they participate in redox reactions with absorbed species. Specially, h^+_{VB} may react with surface-bound H_2O or OH^- to produce the hydroxyl radical and e^-_{cb} is picked up by oxygen to generate superoxide radical anion (O_2^-), as indicated in the following equations 3-5; absorption of efficient photons by Titania ($h\upsilon \geq E_{bg} = 3.2$ eV)

$$TiO_2 + h\upsilon \rightarrow e_{cb} + h^+_{dye} \quad (3)$$

Formation of superoxide radical anion

$$O_2 + e_{cb} \rightarrow O_2^- \quad (4)$$

Neutralization of OH^- group into OH by the hole

$$(H_2O \Leftrightarrow H^+ + OH^-)_{ads} + h^+_{dye} \rightarrow {}^\bullet OH + H^+ \quad (5)$$

It has been suggested that the hydroxyl radical ($^\bullet$OH) and superoxide radical anions (O_2^-) are the primary oxidizing species in the photocatalytic oxidation processes [56]. These oxidative reactions would results in the degradation of the pollutants as shown in the following equations 6-7; Oxidation of the organic pollutants via successive attack by OH radicals,

$$R + {}^{\bullet}OH \rightarrow R. + H_2O \quad (6)$$

or by direct reaction with holes

$$R + h^+ \rightarrow R^{\cdot +} \rightarrow \text{degradation products} \quad (7)$$

For oxidation reactions to occur, the VB must have a higher oxidation potential than the material under consideration. The redox potential of the VB and the CB for different semiconductors varies between +4.0 and -1.5 volts versus Normal Hydrogen Electrode (NHE) respectively. The VB and CB energies of the TiO_2 are estimated to be +3.1 and -0.1 volts, respectively, which means that its band gap energy is 3.2 eV and therefore absorbs in the near UV light (λ<387 nm) [61]. Many organic compounds have a potential above that of the TiO_2 valence band and therefore can be oxidized. In contrast, fewer organic compounds can be reduced since a smaller number of them have a potential below that of the TiO_2 conduction band.

Photodegradation of Rose Bengal can be expressed by the following reaction mechanism:

$$TiO_2 \xrightarrow{h\nu} h^+_{VB} + e^-_{CB}$$

$$h^+_{VB} + H_2O \longrightarrow OH^{\bullet}$$

$$RB + OH^{\bullet} \longrightarrow RB^{\bullet}$$

$$RB^{\bullet} \longrightarrow CO_2 + H_2O + NH_3 + \text{other product}$$

The TiO_2/PAni nanocomposite absorbs radiation of energy corresponding to its band gap and generates electron-hole pair. The electron and hole may recombine non-radiatively to release the energy absorbed in the form of heat. The cationic dye RB+ combines with two electrons and a proton to give its reduced form (RBH–). This step is the rate determining step for the photocatalytic degradation of Rose Bengal. The *leuco* form of the dye ultimately degrades to final products containing CO_2 and NH_4.

It is observed that rate constant in the presence of TiO_2/PAni nanocomposite photocatalyst is larger than that in the presence of pure TiO_2 photocatalyst. The electron from the conduction band of TiO_2 may be transferred to the empty PAni states, making the valence band hole of TiO_2 stable, thus enhancing the oxidative efficiency of the

TiO_2 nanoparticles. The same may be the case when an electron is transferred from the trapped states of the nanoparticles. On the other hand, PAni may also absorb light and then energy transfer is possible to the nanoparticles followed by creation of the valence band hole and the conduction band electron adding to the process of creating a strong oxidative -reductive state of the oxide nanoparticles. Other way, by attaching PAni Particles on the surface of TiO_2, it is possible to drive the photogenerated electrons farther away from the TiO_2, thereby achieving more charge separation in these semiconductor particles. As a result, more efficient photocatalyst is obtained. It is already reported that coupled semiconductors exhibit enhanced spatial separation of the photogenerated electrons and holes as a consequence of charge transfer between the two semiconductors [57]. The conduction band of PAni is lower than that of TiO_2 so that the former can act as a sink for the photogenerated electrons. Since the photogenerated holes move in the opposite direction from the electrons, the photogenerated holes in PAni are trapped within the TiO_2 particles.

Thus likelihood of charge carrier recombination is reduced and more charge carriers will be available for production for free radicals through interfacial charge transfer. In all the photodegradation experiments, it is observed that the characteristic absorption band of RB dye decreases but no hypsochromatic shift appears, which indicates that the photodegradation mechanism is favourable to cleavage of the whole conjugated chromophore structure of the RB dye.

5.3.7 Kinetics of photodegradation

For the kinetic study of photocatalytic degradation, a control experiment was first carried out under two conditions, vis (i) dye + Visible light (no catalyst) (ii) catalyst+ dye in dark without any irradiation (Fig.5.19). It can be seen that under dark conditions, the amount of dye adsorbed on the surface of photocatalyst becomes constant after 20 min, where the adsorption equilibrium is achieved with all the nanocomposites [58].

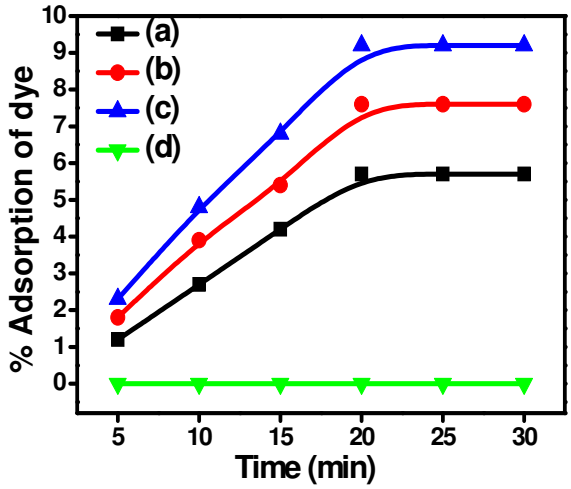

Fig.5.19. % Adsorption under dark condition (a) TiO_2 (b) TiO_2/PAni (c) TiO_2/PAni/GO (d) Dye + visible light without photocatalyst

The Langmuir-Hinshelwood kinetic model [59, 60] is widely used to describe the kinetics of photodegradation of many organic compounds. According to this model, the degradation rate *r* of the dye is described as :

$$\mathbf{r} = -\frac{\mathbf{d[RB]}}{\mathbf{dt}} = -\frac{\mathbf{kK[RB]}}{\mathbf{1+K[RB]}} \qquad \mathbf{(8)}$$

Where *r* is the rate of degradation of RB, *k* is the rate constant, [RB] is the dye concentration, and *K* is the adsorption coefficient. The implicit solution is given in Eq.(9) :

$$\mathbf{ln}\frac{\mathbf{[RB]}}{\mathbf{[RB]_o}} + \mathbf{k}\,(\mathbf{[RB]} - \mathbf{[RB]o}) = -\mathbf{kKt} \qquad \mathbf{(9)}$$

This can be solved explicitly for t by using discrete changes in [RB] from the initial concentration to a zero reference point. The model presented in Eq. (9) yields an exact solution for the degradation of RB. However, when the concentration of RB is very small in the ppm range, a pseudo-first-order model can be assumed, ignoring *K* [RB] in the denominator of eq. (9) leads to Eq. (10),

$$\mathbf{r} = -\frac{\mathbf{d[RB]}}{\mathbf{[RB]}} = \mathbf{kK[RB]} = \mathbf{K'[RB]} \qquad \mathbf{(10)}$$

Integration of eq. (9) yields eq. (10)

$$\mathbf{[RB]} = \mathbf{[RB]}o\ \mathbf{e^{-K\prime t}} \qquad \mathbf{(11)}$$

$$\ln \frac{[RB]}{[RB]o} = kKt = K't \quad (12)$$

Where *k*' is the pseudo rate constant and is in units of time^{-1}.

Figure 5.20 shows the ln [RB_o-RB] *vs.* time plots for TiO_2, TiO_2/PAni and TiO_2/PAni/GO nanocomposite. Samples were dispersed in the same concentration of dye solutions. Pseudo-first-order degradation rate constants *k'* calculated from the slopes of Fig.5.20 [61, 62].

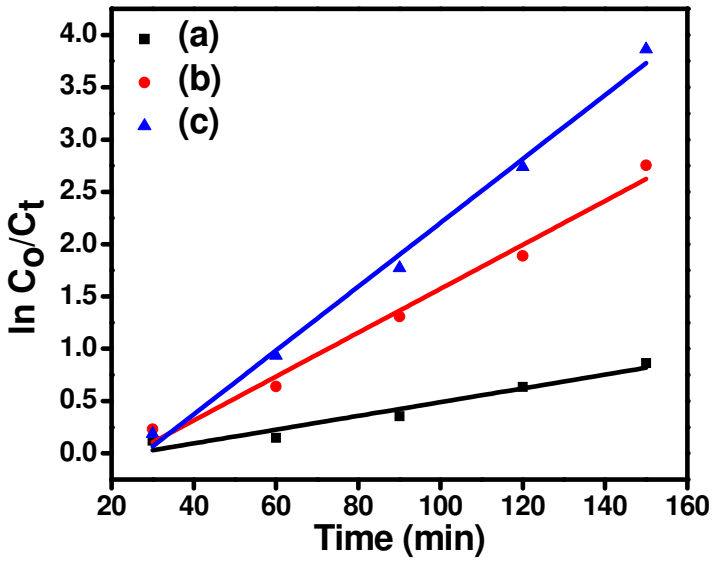

Fig.5.20. kinetics of photodegradation of RB with (a) TiO_2 (b) TiO_2/PAni (c) TiO_2/PAni/GO

5.3.8. Photodegradation of Thymol blue dye

The photo-catalytic degradation of Thymol Blue in the presence of TiO_2, TiO_2/PAni, and TiO_2/PAni/GO has been studied. The solution of dye was prepared in 5:1 (V/V) ratio of water and alcohol. The known amount of photocatalyst was dispersed in the dye solution. The reaction mixture was illuminated under visible light, while kept continuously under agitation, for the different time intervals. The residual concentration of dye in the reaction mixture was measured spectrophotometrically. The results obtained for the degradation of Thymol Blue is shown in Fig 5.21. Photocatalytic degradation efficiencies (η) are obtained by using following equation [43-44].

$$\eta = \frac{TB_O - TB_F}{TB_O} \quad (13)$$

where TB_0 is the initial absorbance and TB_F is the final sampled absorbance for a given time.

5.3.8.1. Effect of concentration of dye

Effect of dye concentration Keeping the catalyst loading concentration constant at 800 mg/litre of the dye solution, the effect of varying concentration of the dye was studied on its rate of degradation (25, 50,75, 100 and 125 ppm) as given in Fig.5.21. The rate of photodegradation was decrease with increasing concentration of TB. This is because as the number of dye molecules increase, the amount of light (quantum of photons) penetrating into the dye solution to reach the catalyst surface is reduced owing to the hindrance in the path of light [45].

5.3.8.2. Effect of photocatalyst amount

The effect of photocatalyst amount is showing in Fig.5.21. The photodegradation of Thymol blue was increased with increase the amount of photocatalyst. It is observed that TiO_2/PAni/GO is the more effective photocatalyst than TiO_2 and TiO_2/PAni. When the photocatalyst amount increases, the number of active site increase for the reaction of dyes. The amount of photocatalyst increases two times the rate of photodegradation increase about 30% and 60 %, in presence of TiO_2, TiO_2/PAni and TiO_2/PAni/GO respectively [46].

5.3.8.3. Effect of Irradiation Time

The effect of irradiation time of visible light was investigated. TiO_2/PAni/GO seems to be more effective as photo-catalyst for the degradation of Thymol Blue (TB). The prominent degradation of Thymol Blue was found in 180 min (Fig.5.21) study in the presence of TiO_2/PAni/GO in comparison to the prepared TiO_2 and TiO_2/PAni. This is due to the coating of polyaniline of Titania surface which provide the electron from the HOMO to LUMO. The electrons of HOMO get excited into LUMO which is further jump into the conduction band of Titania [47].

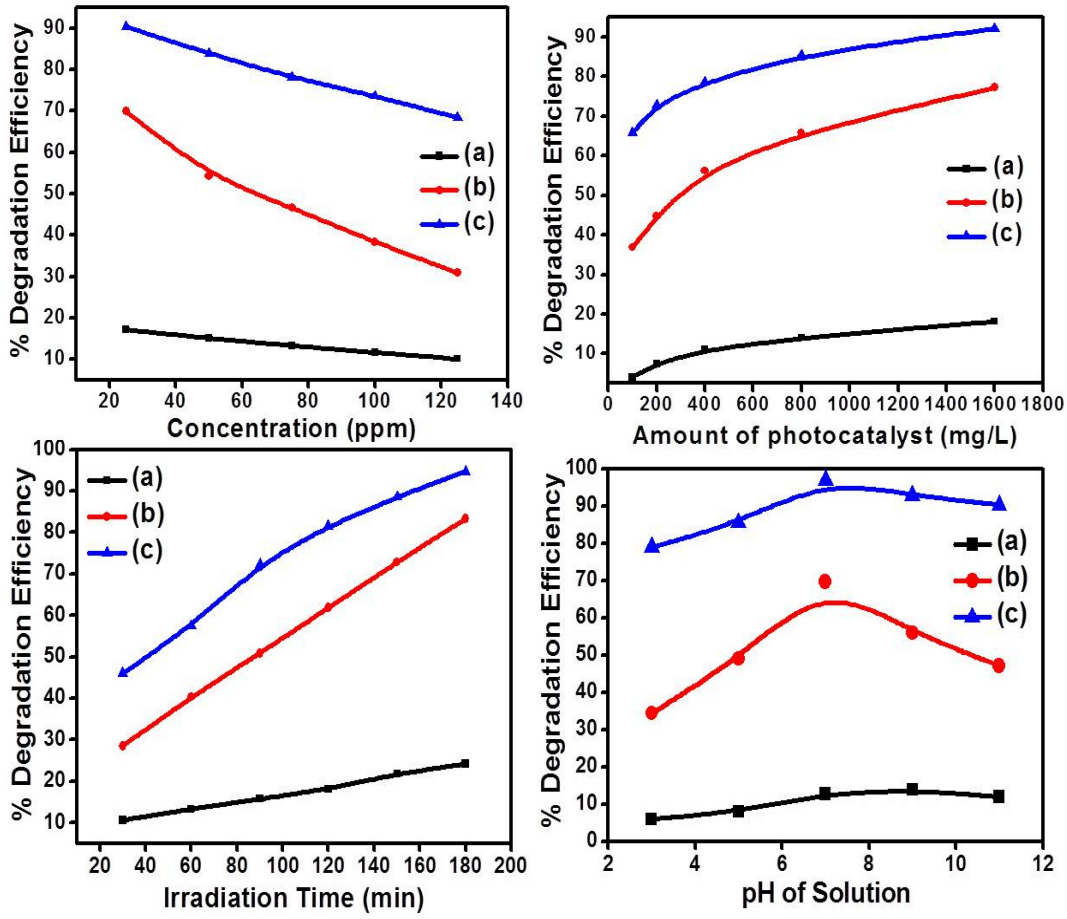

Fig.5.21. Photodegradation of Thymol blue at various conditions with (a) TiO_2 (b) TiO_2/PAni (c) TiO_2/PAni/GO

5.3.8.4. Effect of pH

The photodegradation was carried out under varying pH conditions from (3 to 11), by adjusting with H_2SO_4 and NaOH, with TiO_2, kept at constant amounts of photocatalyst of 800 mg/L and 25 ppm concentration of dye solutions (Fig. 5.21). The photodegradation was found highest rates at neutral ranges of pH. While at lower pH it was found to decrease. In the basic condition, the photodegradation rate was found slow and very poor degradation. Hence highly acidic and basic condition is not favourable for the degradation of TB. This implies that neutral conditions are favourable towards the formation of the reactive intermediates that is hydroxyl radicals is significantly enhanced, which further help in enhancing the reaction rate. On the other hand in basic

and acidic conditions, the formation of reactive intermediates is relatively less favourable and hence less spontaneous [48-49].

5.3.8.5. Recyclability of Photocatalyst

The photocatalyst recyclability has been studied. The photocatalyst and Thymol blue mixture was agitated, illuminated with visible light and after desired time, the mixture was centrifuge to remove the photocatalyst. The removed photocatalyst washed three times with distilled water and finally kept in the oven for 24 h at 60 ^{o}C temperature and further it is reuse for the degradation of Thymol Blue. The photodegradation of Thymol blue by the recyclized Photocatalyst showed in Fig. 5.22. The result shows that the recyclized photo-catalyst efficiency is decreased [51]. The decrease in the efficiency of dye removal for the recyclized catalyst can be attributed to the reduction in the active sites on the surface of the catalyst after one use as well as sticking species that may remain adsorbed on the pores of the catalyst. These observations can lead to reduce the ability of adsorption and consequently reduce its catalytic activity.

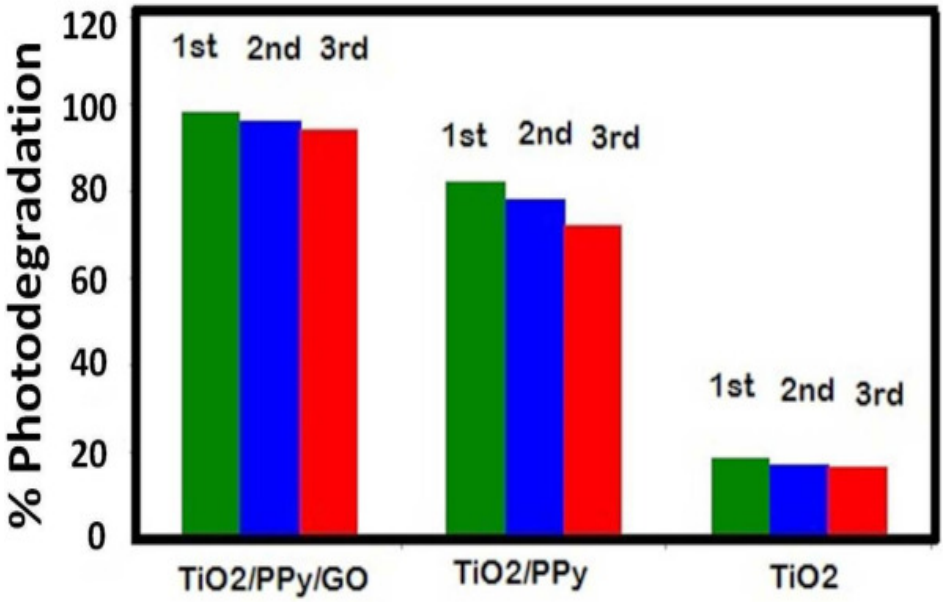

Fig.5.22. Recyclability of Photocatalyst for the degradation of Thymol Blue.

Table 5.2 showing the comparative data of different catalyst used for the degradation of dyes.

Nanomaterials	time	Name of Dye	% Degradation of Dye	References
Titania		RB	20	38
Polyaniline	3	RB	18	39
Graphene Oxide	1h	MO	10	40
TiO2/PAni	3	MG	94.4	41
TiO2/PAni/GO	3h	TB	96	42
ZnO/PAni	4h	MB	99	43
PAni/G	3	RB	56	39

5.3.9. Kinetic study of Photocatalytic degradation of Thymol Blue

For kinetic study of photocatalytic degradation, a control experiment was first carried out under two conditions, vis (i) dye + Visible light (no catalyst) (ii) catalyst+ dye in dark without any irradiation (Fig. 5.23). It can be seen that in under dark conditions, the amount of catalyst adsorbed becomes constant after 20 min, where adsorption equilibrium is achieved. For the kinetic study of bleaching of Victoria Blue and Rose Bengal, the initial concentration of the dyes was varied and the experiments were first conducted in dark for 20 min and then immediately followed by irradiation (Fig. 5.23). The amount of catalyst was kept constant (0.2 g) throughout the experiment. Applying the Langmuir Hinshelwood model for determining the oxidation rate of the photocatalysis of dye:

$$\mathbf{Rate\ (r)} = -\frac{\mathbf{dC}}{\mathbf{dt}} = \mathbf{k\theta} = \boldsymbol{\theta} = \frac{\mathbf{kK_AC}}{\mathbf{1+K_AC}} \qquad \mathbf{(14)}$$

Where k is the rate constant (mg/L min^{-1}), C is the concentration of dye, K_A is the adsorption constant of the dye (L/mg), and t is the illumination time (min).

During the course of reaction, the initial pH, amount of catalyst, and photointensity were kept same. In addition to it, the formation of intermediates may interfere in the rate determination; hence the calculation was done at the begining of irradiation. The rate expression can be written as:

$$\boldsymbol{r_o} = \frac{\boldsymbol{kK_AC_o}}{\boldsymbol{1+K_AC_o}} \qquad (15)$$

Where r_o is the initial rate of degradation of Thymol Blue and C_o is the initial concentration (almost equal to Ceq). When the initial concentration $C_{initial}$ is very small, Co will also be small and Eq. (15) can be simplified as an first-order equation [56-61]:

$$-\frac{dC}{dt} = kK_A C_o = \frac{lnC_o}{C} = kK_A t \quad (16)$$

$$C = C_o e^{-k_f photo\, t} \quad (17)$$

Where $\mathbf{k_{f,\ Photo=}\ k\ k_A}$ The value of $k_{f,\ photo}$ can be determined from the plot of ln C_t/ Co vs. t (Fig.5.24).

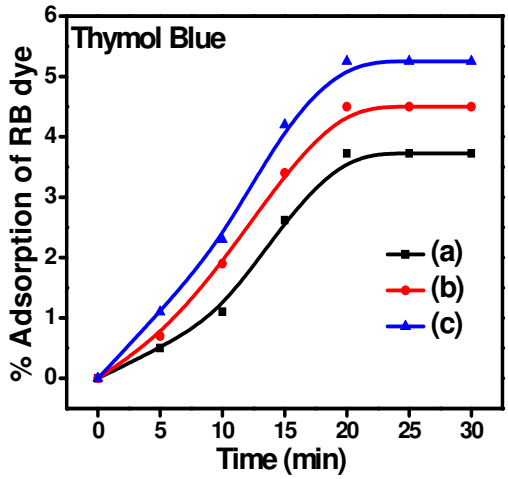

Fig.5.23. % Adsorption of Thymol Blue dye under dark condition in presence of (a) TiO_2, (b) TiO_2/PAni and (c) TiO_2/PAni/GO

The slope of the straight line obtained will be the value of first order rate constant [61]. The Value of apparent rate constant were determine at definite concentrations of dye solution for photocatalysis reaction in presence of TiO_2, TiO_2/PAni and TiO_2/PAni/GO showing in Fig.5.24.

The rate constant values for the photocatalytic degradation of Thymol Blue follow the first order kinetic for the both photocatalyst. This is confirmed that photocatalytic degradation of Thymol Blue follows first order kinetic in presence of TiO_2, TiO_2/PAni, and TiO_2/PAni/GO.

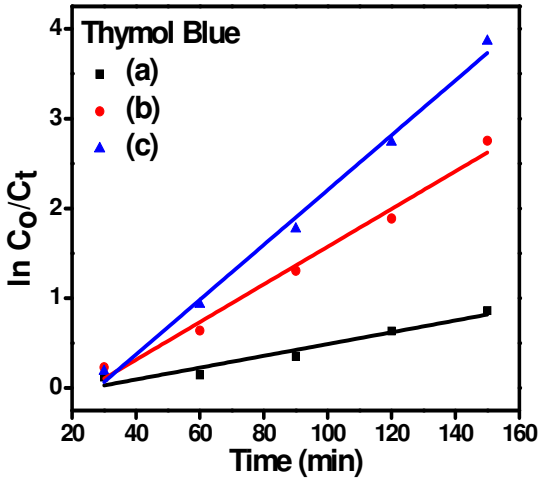

Fig.5.24. Linear first order reaction of Langmuir Hinshelwood kinetics of Thymol Blue dye vs. time (a) TiO_2 (b) TiO_2/PAni (c) TiO_2/PAni/GO

Conclusion

In this work, nanocomposites materials were prepared by the in situ co-deposition oxidative method. Different techniques were used for the characterisation of the TiO_2, TiO_2/PAni and TiO_2/PAni/GO nanocomposite such as XRD, BET, SEM, TEM, FTIR, Photolumiscence, band gap energy and UV spectrophotometer. The XRD confirmed the presence of anatase and rutile phase were observed in the prepared materials nanocomposites. The SEM study confirms that spherical morphology of the nanocomposite. The TEM analysis confirms that the size of nanocomposite. The FTIR characterisation confirms that the TiO_2/PAni/GO molecules are well combined with polyaniline and graphene oxide structure. EDEX confirms about the elements which are present in the prepared sample by x-ray emission spectrum. The surface area 37.52, 76.68 and 96.24 m^2/g were observed for TiO_2, TiO_2/PAni and TiO_2/PAni/GO Nanocomposites respectively. The Band gap energy of TiO_2, TiO_2/PAni, and TiO_2/PAni/GO were calculated by talc plot and obtained 3.0, 2.86 and 1.76 eV respectively. The Photocatalytic degradation of Rose Bengal dye was done at different condition viz concentration of dye, time of illumination, pH, and dose of photocatalyst. The maximum photodegradation were found at neutral pH, 6.25 ppm concentration of dye solution, 800 mg/L amount of photocatalyst and 120 min irradiation of visible light.

Kinetics study was investigated for the photodegradation of Rose Bengal dye and found first order kinetics. The maximum photodegradation of Thymol blue was found in TiO_2/PAni/GO at 25 ppm concentration of dye, 1600 mg/L amount of photocatalyst, pH 7 and 120 min irradiation of visible light. Hence, the photocatalytic activity of Titania has been increased by the coating of PAni and Graphene oxide. The coating of PAni and GO were enhanced the photocatalytic activity of Titania. Hence TiO_2/PAni and TiO_2/PAni/GO is the efficient photocatalyst for the degradation of Rose Bengal dye than pure TiO_2.

References

[1]. Y. Li, Y. Yu, L. Wu, J. Zhi, Applied Surface Science, 273, (2013), 135-143.

[2]. H.M. Moghaddam, S. Nasirian, Applied Surface Science, 317, (2014), 117-124.

[3]. H. Huang, M. Gan, M. Li, L. Yu, H. Hu, F. Yang, Y. Li, C. Ge, Journal of Alloys and Compounds, 630, (2015), 214-221.

[4]. S.H. Nimkar, S.P. Agrawal, S.B. Kondawar, Procedia Materials Science, 10, (2015), 572-579.

[5]. S. Nasirian, H. M. Moghaddam, Polymer, 55, (2014), 1866-1874.

[6]. C. Su, Journal of Hazardous Materials, 322, (2017), 48-84.

[7]. D.C. Clifford, C.E. Castano, J.V. Rojas, Radiation Physics and Chemistry, 132, (2017), 52-64.

[8]. S. Nasirian, H. M. Moghaddam, Int. Journal of Hydrogen Energy, 39, (2014), 630-642.

[9]. L. Su, Y. Li, X. Gan, Composites Part B: Engineering, 43, (2012), 170-182.

[10]. Y. Wu, X. Zhang, S. Li, X. Lv, Y. Cheng, X. Wang, Electrochimica Acta, 109, (2013), 328-332.

[11]. H. Sawada, T. Tsuzuki-ishi, T. Kijima, J. Kawakami, M. Iizuka, M. Yoshida, J. of Colloid and Interface Science, 359, (2011), 461-466.

[12]. C.T. Fleaca, F. Dumitrache, I. Morjan, A.-M. Niculescu, I. Sandu, A. Ilie, I. Stamatin, A. Iordache, E. Vasile, G. Prodan, App. Sur. Sci., 374, (2016), 213-221.

[13]. M.C. Arenas, L. F.R. Núnez, D. Rangel, O.M. Álvarez, C.M. Alonso, V.M. Castaño, Ultra. Sonoche., 20, (2013), 777-784.

[14]. M. R. Karim, K. T. Lim, M. S. Lee, K. Kim, J. H. Yeum, Synthetic Metals, 159, (2009), 209-213.

[15]. S. Xie, M. Gan, L. Ma, Z. Li, J. Yan, H.Yin, X. Shen, F. Xu, J. Zheng, J. Zhang, J. Hu, Electrochimica Acta, 120, (2014), 408-415.

[16]. R. Arora, U. K. Mandal, P. Sharma, A. Srivastav, Materials Today: Proceedings, 2, (2015), 2215-2225.

[17]. B. Wang, C. Liu, Y. Yin, S. Yu, K. Chen, P. Liu, B. Liang, Composites Science and Technology, 86, (2013), 89-100.

[18]. H. Wang, L. Ma, M. Gan, T. Zhou, X. Sun, Wenqin. Dai, H. Wang, S. Wang, Electrochimica Acta, 163, (2015), 232-237.

[19]. S. Kango, S. Kalia, A. Celli, J. Njuguna, Y. Habibi, R. Kumar, Progress in Polymer Science, 38, (2013), 1232-1261.

[20]. S. Chowdhury, R. Balasubramanian, Applied Catalysis B: Environmental, 160–161, (2014), 307-324.

[21]. A. S. Al-Hussaini, R. K. Eltabie, M.E.E. Rashad, Polymer, 101, (2016), 328-337.

[22]. P.T. Patil, R.S. Anwane, S.B. Kondawar, Procedia Mat. Sci., 10, (2015), 195-204.

[23]. C. Lai, G.R. Li, Y.Y. Dou, X.P. Gao, Electrochimica Acta, 55, (2010), 4567-4572.

[24]. S. Bhandari, N.K. Singha, D. Khastgir, Chemical Engineering Journal, In Press, Corrected Proof, Available online 8 November 2016.

[25]. A. Aashish, R. Ramakrishnan, J.D. Sudha, M. Sankaran, G. Krishnapriya, Solar Energy Materials and Solar Cells, 151, (2016), 169-178.

[26]. A. Kumar, A. Bansal, B. Behera, S. L. Jain, S.S. Ray, Materials Chemistry and Physics, 172, (2016), 189-196.

[27]. G.K. Prasad, T. Takei, Y. Yonesaki, N. Kumada, N. Kinomura, Materials Letters, 60, (2006), 3727-3730.

[28]. H. Wang, J. Lin, Z. X. Shen, Journal of Science: Adv. Mat. and Devices, 1, (2016), 225-255.

[29]. L. Zhang, P. Liu, Z. Su, Pol. Degra. and Stability, 91, (2006), 2213-2219..

[30]. J.A.V Albelda, A. Uzunoglu, G. N.C. Santos, L. A. Stanciu, Biosensors and Bioelectronics, 89, (2017), 518-524.

[31]. S. Ameen, M.S. Akhtar, Y.S. Kim, H.S. Shin, App. Cat. B: Env., 103, (2011), 136-142.

[32]. S.C. Tjong, Materials Science and Engineering: R: Reports, 53, (2006), 73-197.

[33]. R. Arora, U.K. Mandal, P. Sharma, A. Srivastav, Procedia Materials Science, 6, (2014), 238-243.

[34]. S. Sultana, M. Rafiuddin, M. Z. Khan, K. Umar, J. of Al. & Comp., 535, (2012), 44-49.

[35]. G. Zhou, D. Wang, F. Li, L. Zhang, Z. Weng, H. Cheng, New Carbon Materials, 26, (2011), 180-186.

[36]. A. Zięba, A. Drelinkiewicz, E.N. Konyushenko, J. Stejskal, Applied Catalysis A: General, 383, (2010), 169-181.

[37]. H. Liang, X. Li, Applied Catalysis B: Environmental, 86, (2009), 8-17.

[38]. X. Tang, M. Tian, L. Qu, S. Zhu, X. Guo, G. Han, K. Sun, X. Hu, Y. Wang, X. Xu, Synthetic Metals, 202, (2015), 82-88.

[39]. X. Wang, S. Tang, C. Zhou, J. Liu, W. Feng Synthetic Metals, 159, (2009), 1865-1869.

[40]. G.A. Epling, C. Lin, Chemosphere, 46, (2002), 561–570.

[41]. M.M. Ba-Abbad, A.A.H. Kadhum, A.B. Mohamad, M.S. Takriff, K. Sopian, Int. J. Electrochem. Sci., 7, (2012), 4871–4888.

[42]. S. Yang, X. Yang, X. Shao, R. Niu, L. Wang, J. Haz. Mater., 86, (2011), 659–666.

[43]. H. Lachheb, E. Puzenat, A. Houas, M. Ksibi, E. Elaloui, C. Guillard, J.M. Herrmann, Appl. Catal. B: Environ., 39, (2002), 75–90.

[44]. A. E. Gary and C. Lin, Chemosphere, 46, (2002), 937-944.

[45]. M. Toyoda, T. Yano, B. Tryba, S. Mozia, T. Tsumura, and M. Inagaki, Applied Catalysis B: Environmental, 88, (2009), 160-164.

[46]. R. Byberg, J. Cobb, L.D. Martin, R.W. Thompson, T.A. Camesano, O. Zahraa, M.N. Pons, Environ. Sci. Pollut. Res., 20, (2013), 3570–3581.

[47]. J.D. Kwon, P.H. Kim, J.H. Keum, J.S. Kim, Sol Energy Mater Sol Cells, 83, (2004), 311–321.

[48]. L. Zhang, P. Liu, Z. Su, Poly. Degra. and Stability, 91, (2006), 2213-2219.

[49]. J. Li, L. Zhu, Y. Wu, Y. Harima, A. Zhang, H. Tang, Polymer, 47, (2006), 7361-7367.

[50]. C. Xiaobo, S.S. Mao, Chem. Rev., 107, (2007), 2891–2906.

[51]. U. Diebold, Surf. Sci. Rep., 48, (2003), 53–229.

[52]. X. Li, Z. Wang, X. Li, G. Wang, Appl. Surf. Sci., 258, (2012), 4788–4793.

[53]. S. Deivanayaki, V. Ponnuswamy, S. Ashokan, P. Jayamurugan, R. Mariappan, Mater. Sci. Semicond. Process., 16, (2013), 554–559.

[54]. A. Katoch, M. Burkhart, T. Hwang, S.S. Kim, Chem. Eng. J., 192, (2012), 262–268.

[55]. S. Deivanayaki, V. Ponnuswamy n, S. Ashokan, P. Jayamurugan, R. Mariappan, Materials Science in Semiconductor Processing, 16, (2013), 554–559,

[56]. E. Kordouli, K. Bourikas, A. Lycourghiotis, C. Kordulis, Catal Today, 252, (2015), 128–135.

[57]. S.K. Kansal, M. Singh, D. Sud, J Hazard Mater, 141, (2007), 581–590.

[58]. E. Vulliet, J.M. Chovelon, C. Guillard, J.M. Herrmann, J. Photochem. Photobiol. A: Chem., 159, (2003), 71–79.

[59]. I.K. Konstantinou, T.A. Albanis, Appl Catal B, 49, (2004), 1–14.

[60]. R.W. Matthews, J. Catal., 111, (1988), 264–272.

[61]. M. Vautier, C. Guillard, J.M. Herrmann, J. Catal., 201, (2001), 46–59.

[62]. R.W. Matthews, J. Catal., 111, (1988), 264–272.

CHAPTER-6

Photocatalytic degradation of Victoria Blue and Rose Bengal dye in visible light by prepared TiO_2/PPy/GO nanocomposite

The present research work describes a proficient method for synthesis of TiO_2/PPy and TiO_2/PPy/GO nanocomposites. These nanocomposites were prepared by one-step *in situ* deposition oxidative polymerization of pyrrole hydrochloride using Ammonium per sulphate (APS) as an oxidant in the presence of ultra fine grade powder of TiO_2 nanoparticles cooled in an ice bath. The obtained nanocomposites were characterized by XRD, TEM, SEM, UV-Vis, FTIR, techniques. The obtained results showed that TiO_2 nanoparticles have been encapsulated by PPy with a strong effect on the morphology of TiO_2/PPy and TiO_2/PPy/GO nanocomposites. The Photocatalytic degradation of Rose Bengal and Victoria blue dye was done at different condition viz concentration of dye, time of illumination, pH and dose of photocatalyst. The maximum photodegradation were found at 7 pH, 20 ppm concentration of Victoria blue and 25 ppm of rose bengal dye solution, 800 mg/L for VB and 1600 mg/L for RB amount of photocatalyst and 120 min irradiation of visible light. Kinetics of photodegradation was investigated for Victoria blue and Rose Bengal dye and found first order kinetics. The coating of PPy and GO were enhanced the photocatalytic activity of Titania. Hence TiO_2/PPy and TiO_2/PPy/GO are the efficient photocatalyst for the degradation of Rose Bengal and Victoria Blue dye than pure TiO_2.

6.1. Introduction

The waste water released from textile and other colouring industries, containing the various dyes have been badly affecting aquatic life and living organism due to their carcinogenic behaviour. Lots of investigations reported that 10-12 % of dyes, such as Rose Bengal, Victoria blue, Thymol blue, Caramine, Indigo Red, Red 120, Rhodamine B, Methylene Blue, Eriochrome Black-T (EBT) etc., have been used every year in textile industries, [1-4]. The major portion (~20%) of these dyes is lost during synthesis and processing operations, which enter into water bodies through effluents, causing water polluted. Rose Bengal (Figure 6.1 a) is a significant xanthene dye used in textile and photochemical industries. It has severe toxic effects on the human health [5-7] and become dangerous in contact with skin, causing itchiness, irritation, reddening and blistering. It also affects to eyes causing inflammation, eye redness, itching etc. [8]. Victoria blue is another triphenylmethane derivatized dye which is extensively used in the textile industry. It has been extensively used as textile dyes for silk, wool, and cotton, in the preparation of inks, in the surface-coating and dyeing of paper [9-11], as colorants in foods, drugs, cosmetics [12], as biological stains, and as anti-infective, antimicrobial and antihelmintic agents [13]. The photocytotoxicity of triphenylmethane dyes is based on the production of the reactive oxygen species and tested extensively with the regard to its photodynamic treatment [14].

In the past several techniques, like coagulation, flocculation, reverse osmosis, adsorption, ion exchange method ultra-filtration and photosensitized oxidation have been used to reduce the toxic dye effluents from wastewater [15-18]. Though methods are fairly effective in removing pollutants, however, the main drawback of these techniques is the formation of the secondary waste product which cannot be treated again and dumped as such [19]. In the recent years, photocatalytic degradation has emerged as an effective technique for complete mineralization of waste water. Titanium dioxide (TiO_2) nanoparticles (NPs) are an excellent photocatalyst because of its low cost, simple preparation, good stability, non-toxicity and better photodegradation ability [20]. It has successfully been used in solar cells [21] photocatalysis [22] and photocatalytic hydrogen production [23]. The bare TiO_2 nanoparticles have the wide band gap, thus has low sunlight energy conversion efficiency and high rate of (e^--h^+) electron-hole recombination capability. Therefore, improvement of the photocatalytic properties of TiO_2 is essential. In order to enhance the

photocatalytic properties of TiO_2, number of manipulations, such as metal or non-metal doping [24], compositing with other semiconductors [25], compositing with conductive materials such as graphene [26] or carbon nanotubes [27], sensitization with organic dyes and conductive polymers, such as polyaniline [28], polythiophene [29], and polypyrrole (PPy) have been tested in the past [30]. Among these routes, the coating of conductive polymers is one of the most effective methods for the generation of good photocatalytic activity [31]. The coating of conductive polymers can reduce the recombination rate of electron-hole (e^--h^+) simultaneously act as sensitizer making effective large band gap semiconductor like TiO_2 [32-33].

Among the various conductive polymers, PPy is one of the most promising coating agents, owing to its good conductivity, high absorption coefficient in the visible part of sunlight, high charge carrier mobility, and good environmental stability [34]. Therefore PPy is suitable conducting polymer and stable photosensitizer to improve the photocatalytic activity of TiO_2 in solar light. In the past TiO_2/PPy nanocomposite has been successively used in solar cells and for the photocatalytic degradation of organic species; however, its use in photocatalytic degradation of organic dyes is rarely reported.

There are many methods of preparing TiO_2/PPy nanocomposite, for example, anodic co-deposition [35], self-assembly techniques [36], photoelectrochemical polymerization [37], and hydrothermal methods [38]. However, in-situ chemical polymerization is a promise method for preparation of TiO_2/PPy owing to its simplicity, good reproducibility, and easy scale up.

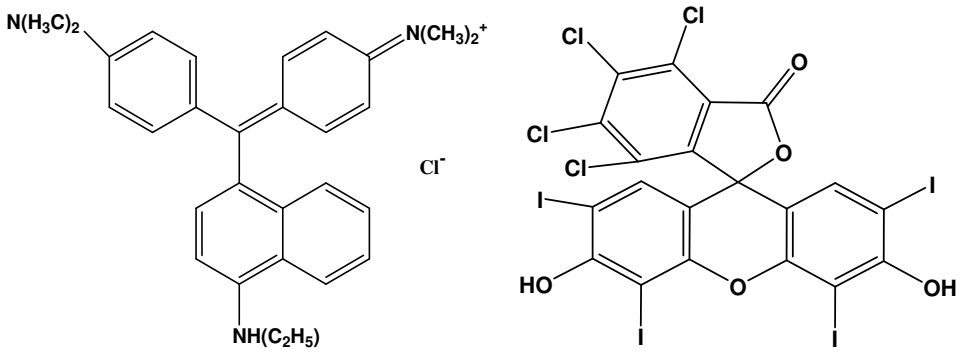

(a) (b)

Fig.6.1. Molecular Structure of dyes (a) Victoria Blue (b) Rose Bengal

In the present study, TiO_2, TiO_2/PPy and TiO_2/PPy/GO nanocomposites have been prepared by one-step *in situ* polymerization of pyrrole in the reaction medium. The photocatalytic degradation of Victoria Blue and Rose Bengal have been studied in the presence of TiO_2, TiO_2/PPy and TiO_2/PPy/GO nanocomposites at the different parameters i.e. concentration of dye, the dose of the photocatalyst, pH of the reaction mixture and irradiation time. The kinetics for the photodegradation process has also been investigated in this work.

Table.6.1. Showing the structure and properties of dyes

Dye	Victoria Blue	Rose Bengal
Structure	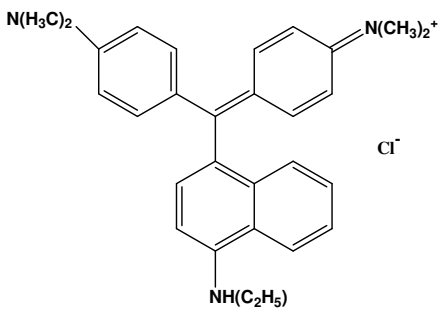	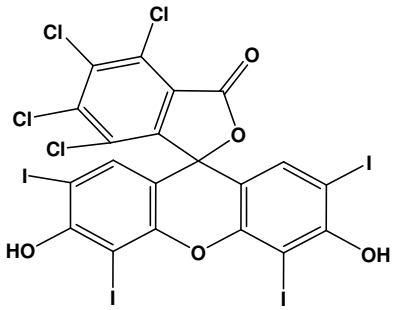
Molar mass:	$[C_{33}H_{40}N_3]Cl.$ 507.5 g/mol	$C_{20}H_4Cl_4I_4O_5$ 973.67 g/mol
λ_{max}	614 nm	547 nm

6.2. Experimental

6.2.1 Materials

Pyrrole monomer, having molar mass of 67 g/mol and density of 0.97 g/cm^3 (Merck India) was triply distilled until a colourless liquid was obtained. The distilled pyrrole was stored at lower than 5 °C temperature in the absence of light. All other chemicals were analytical grade.

6.2.2 Preparation of PPy

1.727 ml pyrrole was dissolved in 50 ml of de-ionized water and stirred for 15 min using a magnetic stirrer. 2.717 ml dilute H_2SO_4 was added slowly using dropper to the pyrrole monomer solution. 2.28 g ammonium per sulphate was dissolved in 50 ml of de-ionised water and slowly added drop - by - drop from a burette to the above prepared solution with constant stirring for half an hour. After stirring for 4 h, the solution was filtered and the residue was washed with double distilled water, methanol and acetone, and dried in oven at 60^{o}C. Subsequently, the product was grinded to get powder of polypyrrole [39].

6.2.3. Preparation of graphene oxide

Graphene oxide was synthesized from graphite powder using a modified Hummer's method. In brief, first, 0.5 g of powdered flake of graphite and 0.5 g of $NaNO_3$ were added into 24 mL of H_2SO_4 and were stirred until dissolved. Then, 3 g of $KMnO_4$ was added slowly, preventing the temperature of the suspension from exceeding 20 °C. After continuous stirring, the mixture for 1 h at 35 °C, 40 ml of distilled water was slowly added to dilute the mixture and the temperature was raised to 90 °C. To reduce the residual permanganate and manganese dioxide to colourless soluble manganese sulphate, 5 ml of 34.5% H_2O_2 was added and the suspension was filtered with distilled water until pH 7.0. The obtained yellow-brown suspension was exfoliated to produce single layer graphene oxide using a sonicator, and the unexfoliated precipitation was removed by centrifugation. Finally, we obtained a brown dispersion of homogeneously exfoliated graphene oxide [40].

6.2.4. Preparation of TiO_2/PPy nanocomposites

TiO_2 nanoparticles, with an average particle size of 50 nm, were prepared by previous reported method [41]. 3.454 ml pyrrole and 5.434 ml dilute H_2SO_4 were stirred with100 ml double distilled water and 1.036 g TiO_2 added in the pyrrole reaction medium. 4.56 g ammonium per sulphate was dissolved in 100 ml of de-ionized water and slowly added drop by drop from a burette to the above prepared solution for half an hour. After stirring for 4 h, the solution was filtered and the residue was washed with double distilled water, methanol and acetone, dried in an oven at 60 ^{o}C and grinded into powder [42].

6.2.5 Preparation of TiO_2/PPy/GO nanocomposites

3.454 ml pyrrole and 5.434 ml dilute H_2SO_4 were stirred with double distilled water. 1.0362 g TiO_2 and 60 mg graphene oxide was added in the pyrrole reaction medium and the mass ratio of TiO_2: PPy: GO was maintain at 8: 17.5: 1. The amount of 4.56 g ammonium per sulphate was dissolved in 100 ml of de-ionized water and slowly added drop by drop using burette to the above prepared solution for half an hour. After stirring for 4 h, the solution was filtered and the residue was washed with double distilled water, methanol and acetone, dried in an oven at 90 ^oC and grinded into powder form [43].

6.2.6. Characterizations

The phase and purity of as-synthesized TiO_2, PPy, TiO_2/PPy and TiO_2/PPy/GO materials were determined by X-ray diffraction (XRD) pattern recorded on analytical X'Pert Pro X-ray diffractometer in the 2θ range 10 to 80° with the step size of 0.025°. The particle size of TiO_2 and morphology of particles was investigated with transmission electron microscope (TEM) images observed on JEOL JEM 200 CX equipment. The morphology of neat TiO_2, PPy, and TiO_2/PPy nanocomposites was investigated by scanning electron microscopy images recorded on JEOL 6490 LB equipment. Diffused Reflectance spectroscopy study was done on Carry 100 spectrophotometer and graphs were used to determine band gap energy of prepared nanocomposites. Photoluminescence spectra (recorded on Perkin Elmer LS 55 spectrofluorometer) were used to study emission behaviour and e^--h^+ recombination determination of the samples.

6.2.7. Determination of the point zero charge of powdered Titania Nanocomposites

The point zero charge (PZC) of the Titania nanocomposites was determined employing the solid addition method using 0.1 mol L^{-1} KCl and 0.002 mol L^{-1} citrimide ($C_{19}H_{42}BrN$) surfactant solutions. Fifty millilitres of KCl and citrimide solution was taken in 100 mL stoppered conical flask. The initial pH values of the solutions were roughly adjusted to be between 2 and 12 by adding either 0.1 mol L^{-1} HCl or 0.1 mol L^{-1}NaOH. The initial pH of the solution was then accurately recorded. One gram of the prepared Titania based nanomaterials was added to each flask. The suspensions were shaken and allowed to equilibrate with intermittent shaking. The final pH of the supernatant liquid was recorded. The difference between the initial and final pH values (pH = pHi − pHf) were plotted against

the initial pH value. The point of intersection of the resulting curve where the change in pH is zero gives the value of the PZC [44].

6.2.8. Irradiation Procedure

The solutions of dyes were prepared in 10:1 (V/V) ratio of water and alcohol. The known amount of photocatalyst was dispersed in the dye solution (20 ml). The desired concentrations of Victoria Blue and Rose Bengal dye (20 mL) were taken in a 100 mL beaker and 1 g of each photocatalyst; TiO_2, PPy, TiO_2/PPy and TiO_2/PPy/GO were mixed to dye solutions and resulting suspensions were stirred on the magnetic stirrer in dark for 30 min to reach adsorption equilibrium. The visible light was irradiation was done by putting xenon lamp (1000 W) vertically on the surface of the reaction medium with constant stirring. After desired time interval, an aliquot of the solution was isolated, centrifuged, filtered through a Millipore filter to separate the photocatalysts and their UV- Vis absorption spectra were recorded to determine the residual concentration.

The % degradation efficiency of the samples was calculated using equation 1 [45-46].

$$\eta\ \% = \frac{A_O - A_F}{A_O} * 100 \quad (1)$$

Where η is the degradation efficiency, A_o is the initial absorbance and A_F is the final absorbance

6.3. Results and Discussion

6.3.1 XRD patterns of nanocomposites

XRD patterns of pure TiO_2, PPy, TiO_2/PPy and the TiO_2/PPy/GO synthesized nanocomposites are presented in Figure 6.2. In the case of pure TiO_2 nanoparticles the main diffraction peaks observed at 25, 38, 48, 55.1 and 63.2 ° are respectively (101), (103), (200), (211) and (204) planes of TiO_2 (JCPDS file No: 86-1157) (Figure 6.2 a). In the XRD pattern of GO obtained via the improved Hummers' method, the (0 0 1) crystal plane of GO was observed, with a spacing of 8.33 A˚ which is typical for GO. In the XRD pattern of pure PPy (Figure 6.2 b) the observance of a broad peak in the 2θ region 20 to 50° revealed that the as-synthesized PPy is amorphous in absence of TiO_2. Broad peaks in the region $15^\circ < 2\theta < 30^\circ$ is revealing that the resulting polypyrrole powders are amorphous in nature.

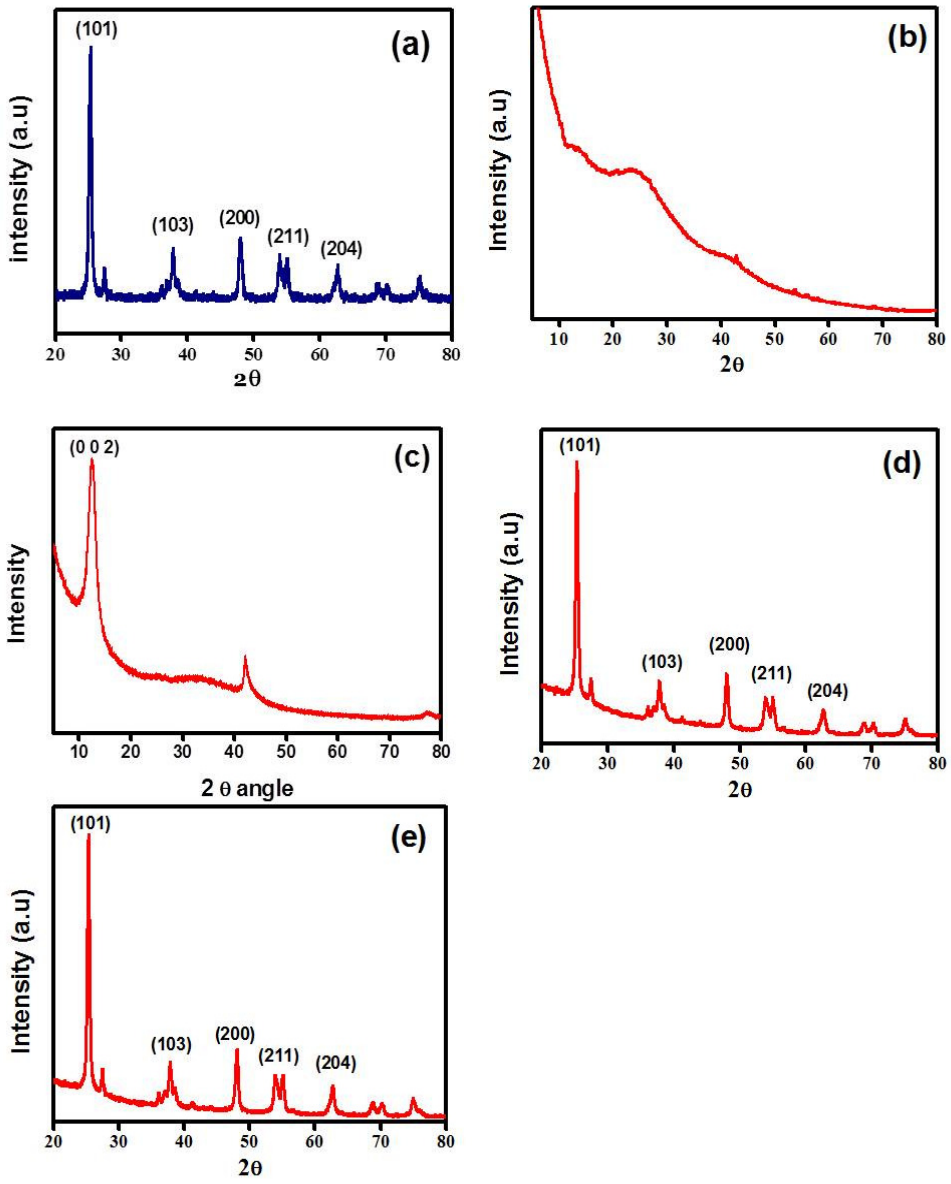

Fig.6.2. X-Ray diffraction of (a) TiO_2 (b) Pure PPy (c) pure graphene oxide (d) TiO_2/PPy (e) TiO_2/PPy/GO

This agrees well with the structure reported in literature [16]. Such broad peak usually indicates short range arrangement of chains. It can be seen from Figure 6.2 c & d that the main peaks of TiO_2/PPy and TiO_2/PPy/GO nanocomposites are similar to those of neat TiO_2 nanoparticles but broad weak diffraction peak of PPy still exists, however, its intensity has been decreased. It implies that when pyrrole is polymerized on TiO_2, each phase maintains its initial structure [47-48].

6.3.2 Determination of Average size of Particles/ Grains in samples

Utilizing the observed X-ray diffraction data of samples, Scherrer's calculations were attempted to know the average size of Crystal in the samples [49]. Although, Scherrer's calculations are only approximate in nature, but definitely provide a first-hand idea of the average size of the Crystal in the samples, which may be quite accurate, provided the size of Crystal is below 100 nm.

$$\mathbf{B} = \frac{0.9\lambda}{t\,Cos\theta} \qquad \mathbf{(2)}$$

The mean size of TiO_2, TiO_2/PPy, and TiO_2/PPy/GO nanocomposites, calculated by Scherrer's Equation, are about 19, 24 nm and 30 nm, respectively. The results of Scherrer's calculations are presented in Table 2. The results suggest average size of the Crystal in the samples lying in nm range.

Table. 6.2. Average size of Crystal in the samples of TiO_2 and TiO_2, TiO_2/PPy, TiO_2/PPy/GO

Sample	Particle Size (nm)
TiO_2	19
TiO_2/PPy	24
TiO_2/PPy/GO	30

6.3.3 SEM and TEM analyses

The morphology and shape of pure TiO_2 nanoparticles, neat PPy, TiO_2/PPy and TiO_2/PPy/GO nanocomposites were characterized by SEM instrument and the obtained pictures are presented in Figure 6.3. As shown in Figure 6.3 b, TiO_2 nanoparticles were aggregated due to their high surface energy. In the corresponding TEM image (Figure 6.4 a) 30±10 nm diameter polygonal prism like structures have been observed. In the SEM image (Figure 6.3 a) and TEM image (Figure 6.4 b), cloud like image of pure PPy has been observed.

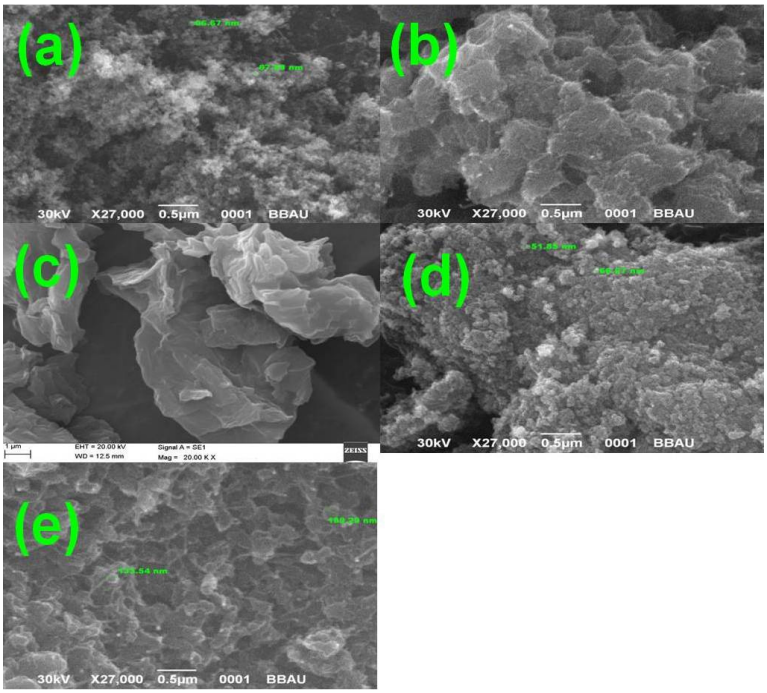

Fig.6.3. SEM images of (a) TiO_2 (b) pure PPy, (c) pure GO (d) TiO_2/PPy (e) TiO_2/PPy/GO nanocomposites.

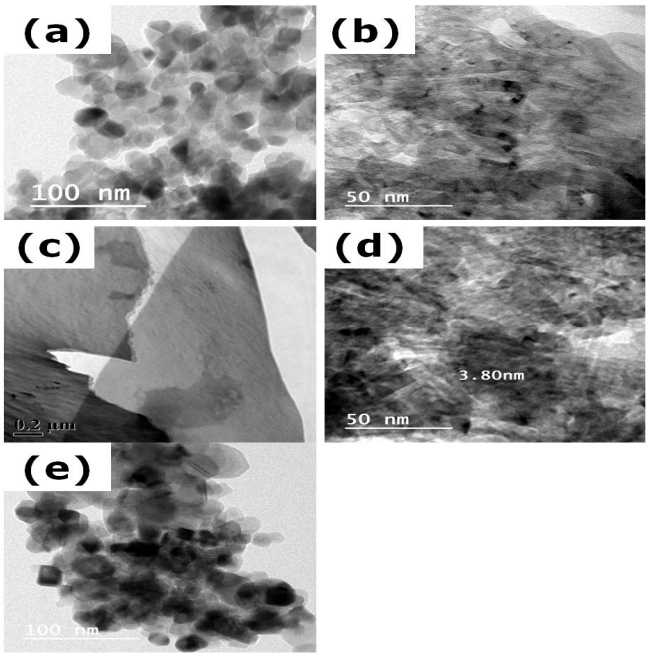

Fig.6.4. TEM of (a) TiO_2 (b) Pure PPy (c) Graphene Oxide (GO) (d) TiO_2/PPy (e) TiO_2/PPy/GO

The SEM and TEM images (Figure 6.3 c and Figure 6.4 c) show that the morphology of TiO_2/PPy composite is similar to pure PPy. In the SEM image (Figure 6.3 d), aggregates

of TiO_2/PPy/GO observed, however in the TEM image (Figure 6.4 d), multi facet polygonal prismatic structures, with diameter 40±15 nm have been observed. Above data indicate that PPy polymerizes in presence of GO. The SEM images help us draw a conclusion that the doping of TiO_2 has a no effect on PPy's morphology, however, presence of TiO_2 along with GO retain the similar structure for TiO_2/PPy/GO as observed in case of pure TiO_2 [50].

6.3.4 Bruner Ernst Teller Surface area analysis

Nitrogen adsorption–desorption isotherms were used to determine the structural characteristics and surface area of TiO_2, TiO_2/PPy, and TiO_2/PPy/GO nanocomposite. The N_2 adsorption desorption isotherms of the TiO_2, TiO_2/PPy, and TiO_2/PPy/GO nanocomposite were measured at 77 K, as shown in Figure 6.5. The specific surface areas (from BET and Surface area, pore volume and pore radius of the TiO_2, TiO_2/PPy and TiO_2/PPy/GO nanocomposite are showing in Table 6.3. The surface area was found 37.52, 76.68 and 96.24 m^2/g for TiO_2, TiO_2/PPy, and TiO_2/PPy/GO respectively. There is an increase in Vp and pore radius of the TiO_2, TiO_2/PPy and TiO_2/PPy/GO nanocomposite respectively [51]. From these results, it may be concluded that the high surface area of the TiO_2/PPy/GO nanocomposite may favour rapid electron transport and high ion diffusion, allowing improved photochemical performance.

Table.6.3. The specific surface area, pore volume and pore radius of the TiO_2, TiO_2/PPy and PPy/TiO_2/GO.

Sample	Surface area (m^2/g)	Pore volume (cm^3/g)	Pore radius (nm)
TiO_2	37. 52	3.132	1.21
PPy	19.83	2.632	1.12
GO	14.86	2.142	1.02
TiO_2/PPy	76.68	6.5124	1.64
TiO_2/PPy/GO	96.24	9.5124	1.84

Moreover, the BET surface areas increased remarkably in the TiO_2/PPy/GO nanocomposite, which suggests that TiO_2 is well intercalated in PPy matrix and may also provide direct conduction pathway for electrons. The formation of TiO_2 with PPy by co-deposition

oxidation synthesis resulted in the generation of well dispersed TiO_2 in PPy Matrix giving one TiO_2/PPy system with unique set of properties [52].

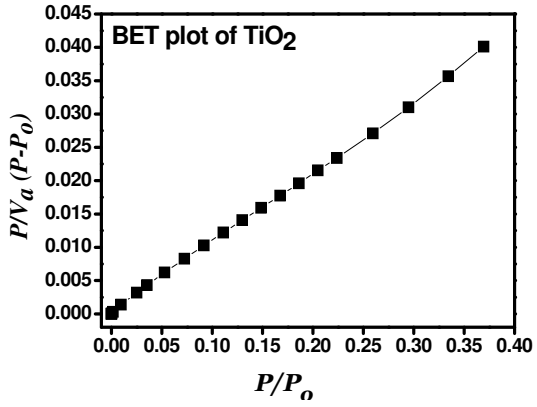

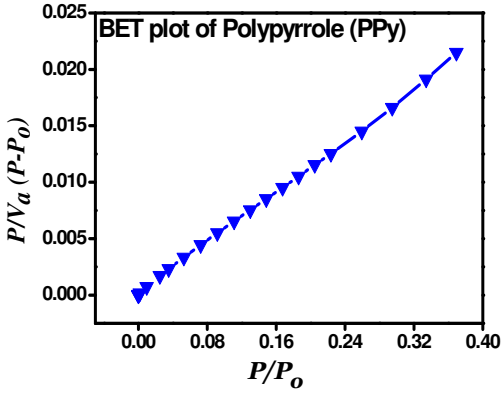

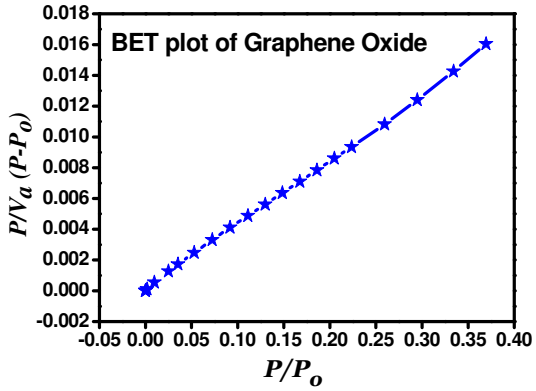

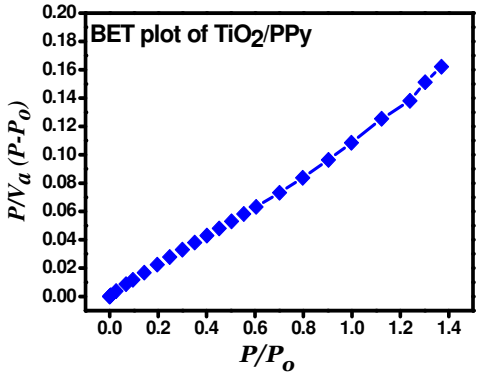

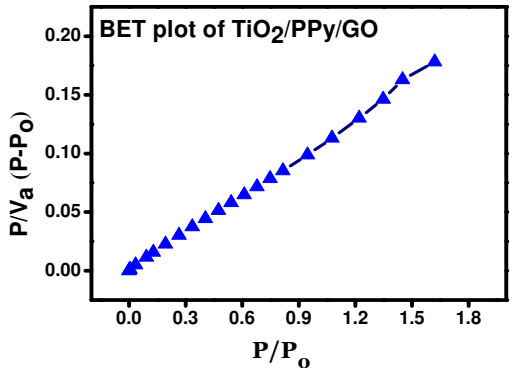

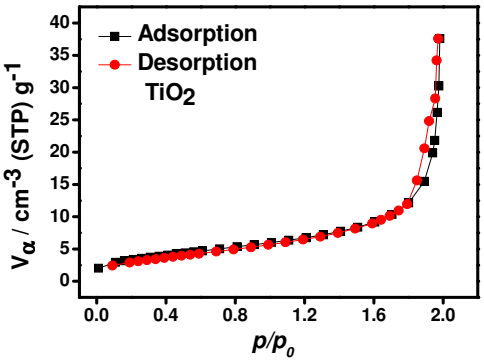

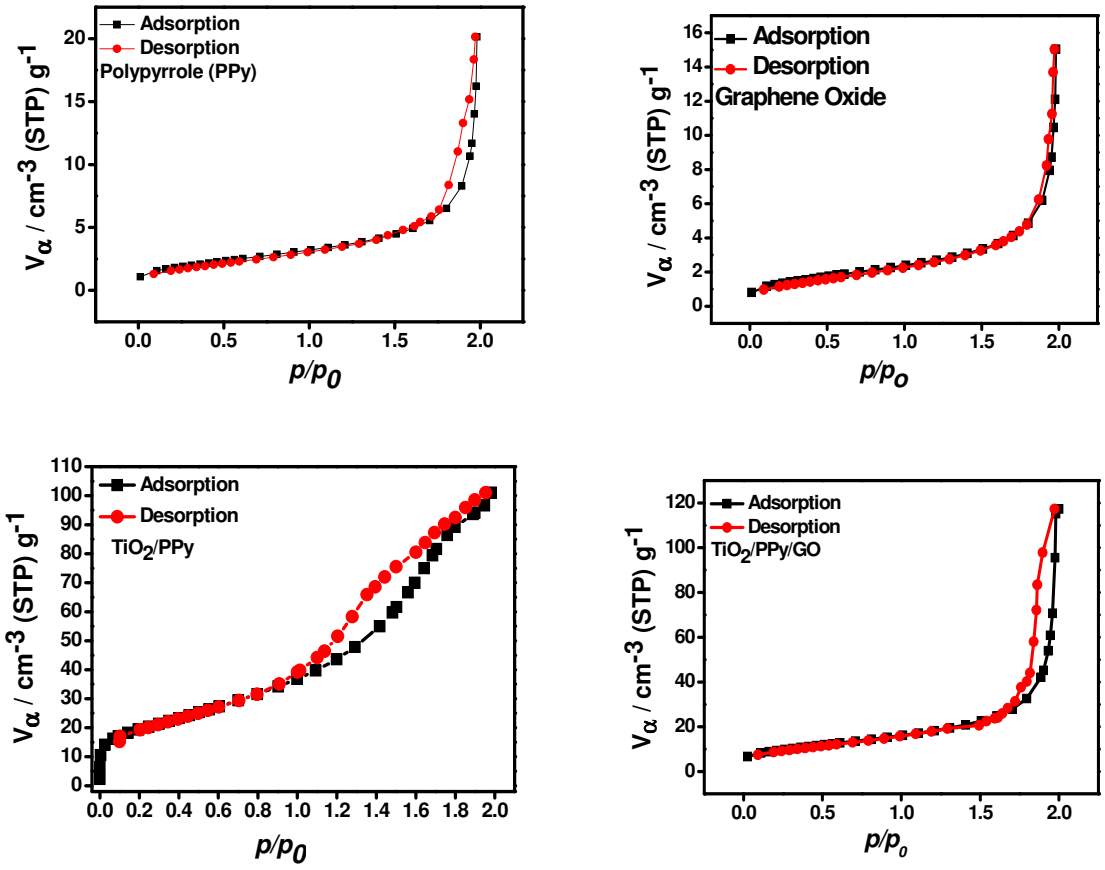

Fig.6.5.BET and Adsorption-desorption plot for TiO_2, PPY, GO, TiO_2/PPy and TiO_2/PPy/GO

6.3.5 UV-Visible spectra of nanocomposites

The prepared nanocomposites aqueous suspensions were used for the UV absorption studies. The absorption spectrum of TiO_2 consists of a single broad intense absorption between 250 to 400 nm due to the charge-transfer from the valence band to the conduction band [53]. The TiO_2 showed absorbance in the shorter wavelength region while PPy, GO, TiO_2/PPy and PPy/TiO_2/GO result showed slight red shift in the absorption edge. The absorption spectrum of TiO_2 consists of a single broad intense absorption around 383 nm (shown in Fig.6.6) in the region of the hypsochromic shift. The TiO_2/PPy results showed a red shift in the absorption onset value and the broad peak observed at 410 nm. This is due to the coating of PPy layer on the surface of Titania [54]. The red shift that is observed at 410 nm in the absorption spectra with the decrease in particle size has been reported in TiO_2/PPy/GO nanocomposite. This is due to the coating of PAni and Graphene oxide in the Titania and the Titania completely interacted with PPy and GO.

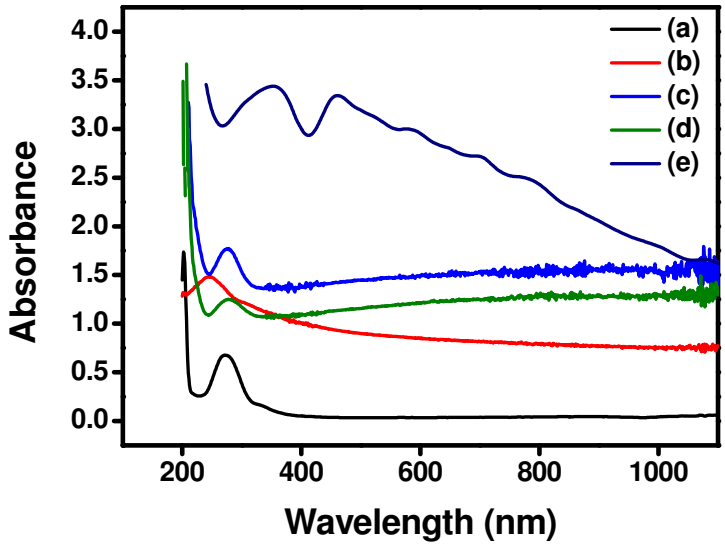

Fig.6.6. UV Visible spectra of nanocomposites (a) TiO_2 (b) PPy (c) GO (d) TiO_2 (e) TiO_2/PPy/GO

6.3.6. Determination of optical band gap of nanocomposites

The UV-Vis spectra of the Titania based nanocomposites have been recorded and data were used to determine band gap values. The band gap of materials was determined by the Tauc relation (Eq. 3)

$$\alpha h\nu = B(h\nu - E_{gap})^{m} \qquad (3)$$

where α is the absorption coefficient, hν is the photon energy and m = 1/2 for direct band gap material shown in Figure 6.7. To describe a direct method for fitting and determination of band gap using Tauc relation [53-54], we can re-write the equation (3) as:

$$\left(\frac{Abs}{\lambda}\right)^{1/m} = B\left(\frac{1}{\lambda} - \frac{1}{\lambda_{gap}}\right) \qquad (4)$$

where λ is the wavelength and *Abs.* the corresponding value of measured absorbance. λ_{gap} can be easily obtained from curve $(Abs./\lambda)^{1/}m$ vs. $1/\lambda$ plot at condition $(Abs./\lambda)^{1/}m = 0$. The band gap value is obtained from relation $E_{gap} = 1239.83/\lambda_{gap.}$ The band gap of samples was calculated by extrapolation of the $(\alpha h\nu)^2$ versus $h\nu$ plots, where α is the absorption coefficient and $h\nu$ is the photon energy; $h\nu = (1239/\lambda)$ eV. The value of $h\nu$ extrapolated to α =

0 gives an absorption energy, which is correspond to a band gap (*Eg*). Figure 6.8 yields an *Eg* value of 3.2 eV for TiO_2, 2.98 eV for pure PPy, 2.65 eV for TiO_2 / PPy and 2.45 eV for TiO_2/PPy/GO [55]. The band gap values of nanocomposites slightly decrease compared to pure TiO_2 because the electrons of pure PPy are excited from the HOMO to the LUMO of PPy whereas holes were left in the HOMO of PPy. The excited-state electrons can be readily injected into the conduction band of TiO_2 [56].

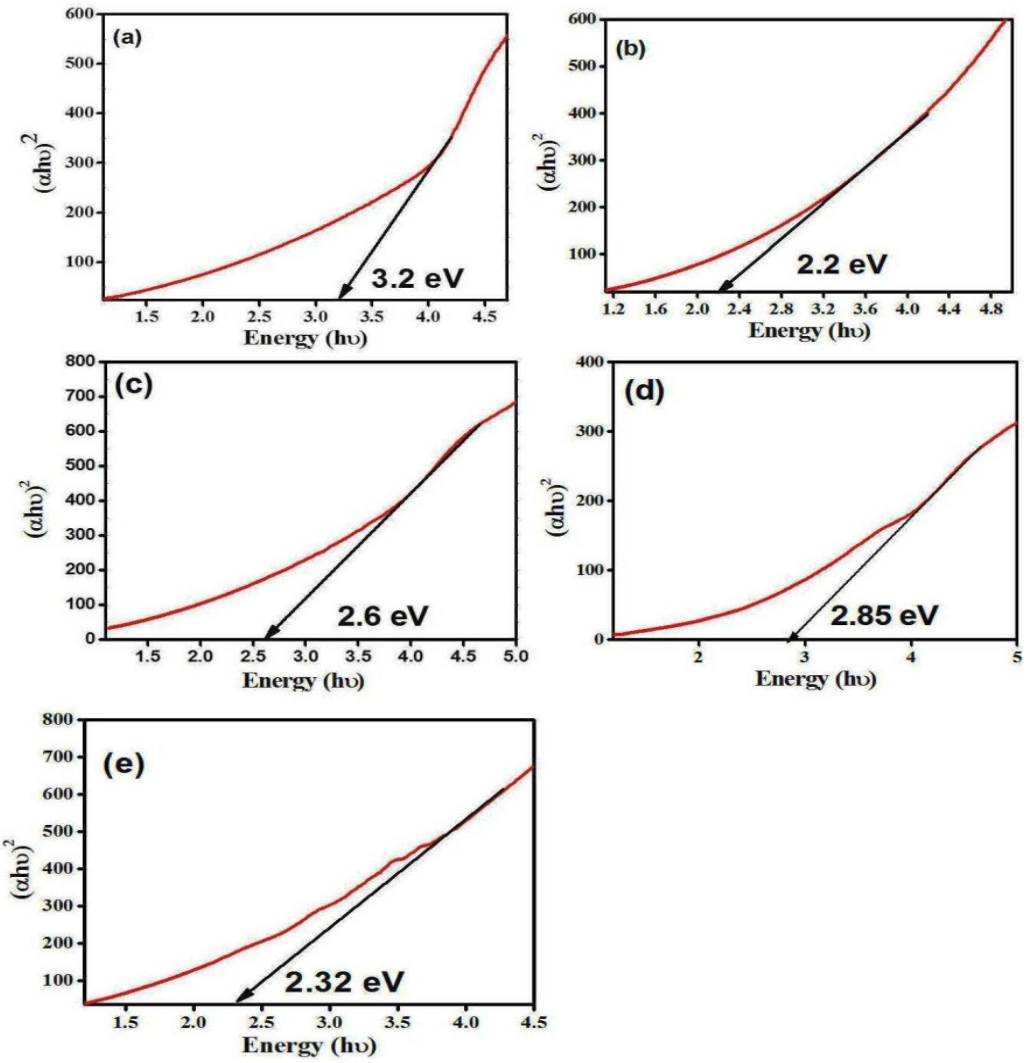

Fig.6.7. Band Gap energy of (a) pure TiO_2 (b) pure PPy (c) Graphene oxide (d) TiO_2/PPy (e) TiO_2/PPy/GO nanocomposites.

6.3.7. Determination of PZC of Nanocomposites

The point zero charge (PZC) of the Titania nanocomposites was determined employing the solid addition method. The point zero charge (PZC) was found 6.4, 6.6 and 6.9 for the TiO_2, TiO_2/PPy and TiO_2/PPy/GO. It is shown in the Fig.6.8.

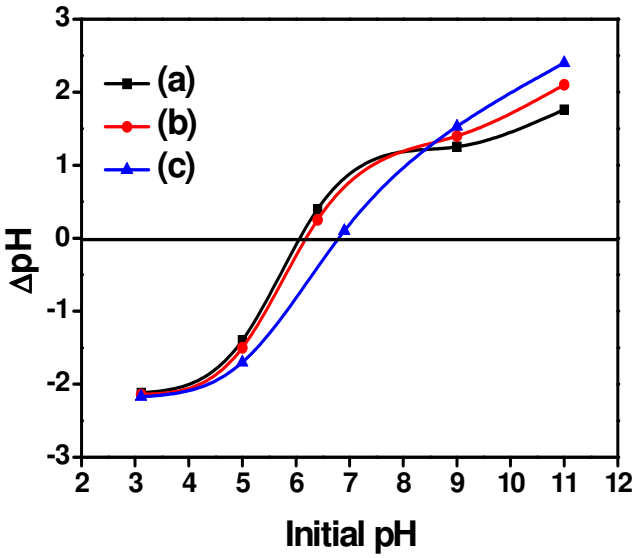

Fig.6.8. Determination of PZC of nanocomposites (a) TiO_2 (b) TiO_2/PPy (c) TiO_2/PPy/Go

6.3.8. Photodegradation

6.3.8.1. Effect of pH

The Photodegradation of dyes are affected by the pH of the solution. The variation of solution pH changes the surface charge of TiO_2 particles and shifts the potentials of catalytic reactions. As a result, the adsorption of dye on the surface is altered thereby causing a change in the reaction rate. Titania has point of zero charge (pzc) at 6.9. Under acidic or alkaline condition the surface of Titania can be protonated or deprotonated according to the following reactions [57]:

$$TiOH + H^+ \rightarrow TiOH_2^+ \quad (9)$$

$$TiOH + OH^- \rightarrow TiO^- + H_2O \quad (10)$$

Thus Titania surface will remain positively charged in acidic medium (pH < 6.9) and negatively charged in alkaline medium (pH > 6.9). Titanium dioxide is reported to have higher oxidizing activity at lower pH, but excess H^+ can decrease reaction rate. TiO_2 behaves as a strong Lewis acid due to the surface positive charge. In other words, the anionic dye acts

as a strong Lewis base and can easily adsorb on the positively charged catalyst surface. This favours the adsorption of the dye under acidic conditions, while in the alkaline conditions this complexation process is not favoured presumably because of competitive adsorption by hydroxyl groups and the dye molecule in addition to the Coulombic repulsion due to the negatively charged catalyst with the dye molecule [58]. The extent of dye adsorption depends on the initial dye concentration, nature of the dye, surface area of photocatalyst and pH of the solution. The pH determines the surface charge of the photocatalyst. Adsorption of the dye is minimum when the pH of the solution is at the isoelectric point (point of zero charge [44]. The surface of the photocatalyst is positively charged below isoelectric point and carries a negative charge above it.

Bubacz et al [59] observed an increase in the rate of the photocatalytic degradation of methylene blue with an increase in pH. According to Ling et al [60], basic pH electrostatic interactions between negative TiO^- and Methylene blue cation leads to strong adsorption with a corresponding high rate of degradation. Ling et al [60] noted that basic pH electrostatic interactions between negative TiO^- and methylene blue cation leads to strong adsorption with a corresponding high rate of degradation. The surface charge properties of TiO_2 were also found to change with a change of pH value due to the amphoteric behaviour of semi conducting TiO_2 (Guillard et al [61], Zielin´ska et al [62], Senthilkumaar et al [63]). Kansal et al [64] also found that the degradation of Reactive Black 5 and Reactive Orange 4 dyes was favored in acidic medium with TiO_2. Tanaka et al. [65] found that positively charged TiO_2 surface adsorbed more Acid Orange 7 at lower pH value, and more decomposition was achieved. The acid black 1 has a sulfuric group in its structure, which is negatively charged. So the acidic solution favours adsorption of dye onto photocatalyst surface as TiO_2 surface is positively charged in acidic solution (Grzechulska and Morawski [66]).

The photodegradation of cationic dyes (Victoria blue) and anionic dye (Rose Bengal) was carried out under varying pH conditions from (2 to 9), by the addition of H_2SO_4 and NaOH, keeping other parameters constant (concentration = 50 ppm, the amount of catalysts = 800 mg/L and irradiation time = 120 min). The results show that degradation of dye Victoria blue is highest in basic medium (at pH = 10) shown in Figure 6.9. Under acidic conditions, it was found difficult to adsorb the cationic VB dye onto the TiO_2 surface. The active •OH radicals, formed in low concentrations, and hence the photodegradation process of VB

remained slow. With higher pH values, the formation of active •OH species is favoured, due to not only improved transfer of holes to the adsorbed hydroxyls, but also electrostatic abstractive effects between the negatively charged TiO_2 particles and the operating cationic dyes. Although the VB dye can adsorb onto the TiO_2 surface to some extent in alkaline media, when the pH value is too high (pH 11), the VB dye molecules will change to a leuco-compound. Our results indicate that the TiO_2 surface is negatively charged, and the VB adsorbs onto the TiO_2 surface through the positive ammonium groups. This is characteristic of heterogeneous photocatalysts, and the results are in agreement with the earlier studies [67].

The photodegradation of Rose Bengal is highest in acidic medium at pH 5 shown in Figure 6.10. This implies that the acidic condition is favourable for the formation of the reactive intermediate hydroxyl radicals for Rose Bengal. This further helps in enhancing the reaction rate. On the other hand in the neutral condition, the formation of reactive intermediate is relatively less favourable and hence not feasible [68]. The rate of photodegradation increases with increases in pH of the solution. At lower pH (3) values, surface of catalyst is negatively charged and dye molecules are positively charged. So dye molecules and catalyst particles will attract to each other. Thus catalytic reaction on the surface of TiO_2 will take place to greater extent. But it is reported to have higher oxidizing activity at lower pH, but excess H^+ can decrease reaction rate of photodegradation of dye. But the maximum photodegradation of Rose Bengal dye was found at pH 5, this is because that decrease in H^+ concentration and adsorption of Rose Bengal (anionic dye) is higher at pH 5, because the force of attraction between catalyst surface and dye molecules will start operating thus resulting in increase in rate of dye degradation [69].

6.3.8.2 Effect of photocatalyst and dose

The effect of photocatalysts and their doses on the degradation of dyes Victoria Blue and Rose Bengal is shown in Figure 6.10 and Figure 6.11. It is clear from the results that the TiO_2, TiO_2/PPy and TiO_2/PPy/Go are effective photocatalyst for degradation of Victoria Blue and Rose Bengal dye; however TiO_2/PPy/Go seems to be the most effective photocatalyst for degradation of Victoria Blue and Rose Bengal. Further photodegradation efficiency of the catalysts follows the trend $TiO_2 < TiO_2$/PPy $< TiO_2$/PPy/GO.

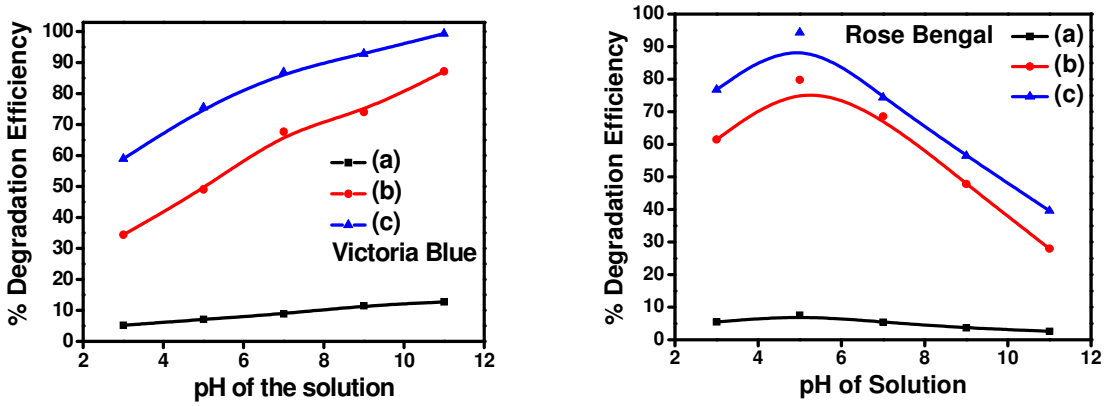

Fig.6.9. Effect of pH on photodegradation efficiency of dyes Victoria Blue and Rose Bengal (a) TiO_2 (b) TiO_2/PPy and (c) TiO_2/PPy/Go

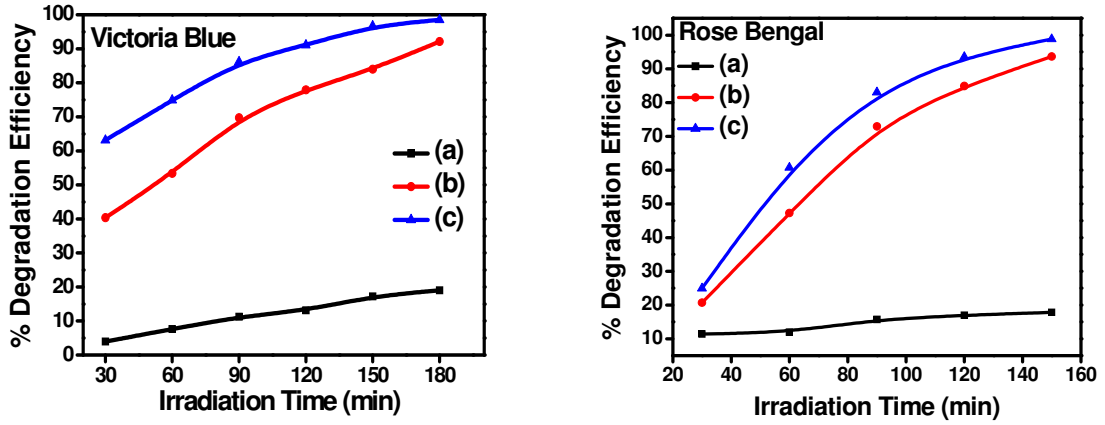

Fig.6.10. Effect of irradiation time on photodegradation efficiency of dyes Victoria blue and Rose Bengal (a) TiO_2 (b) TiO_2/PPy and (c) TiO_2/PPy/GO

The effect of photocatalyst dose on the photodegradation of Victoria Blue and Rose Bengal was studied by applying different concentrations (from 50 mg/L to 800 mg/L) of the photocatalyst is shown in Figure 6.11. Initially (from 50 mg/L to 200mg/L) the rate of degradation of the dyes Victoria Blue and Rose Bengal was very rapid, after that, it became slow and attained plateau at 800 mg/L due to occupancy of all active sites at this concentration. When the PPy is coated in TiO_2, the band gap energy is decreased which enhanced the photo-efficiency, the surface area of photocatalyst also increased the photo-efficiency of the photocatalyst.

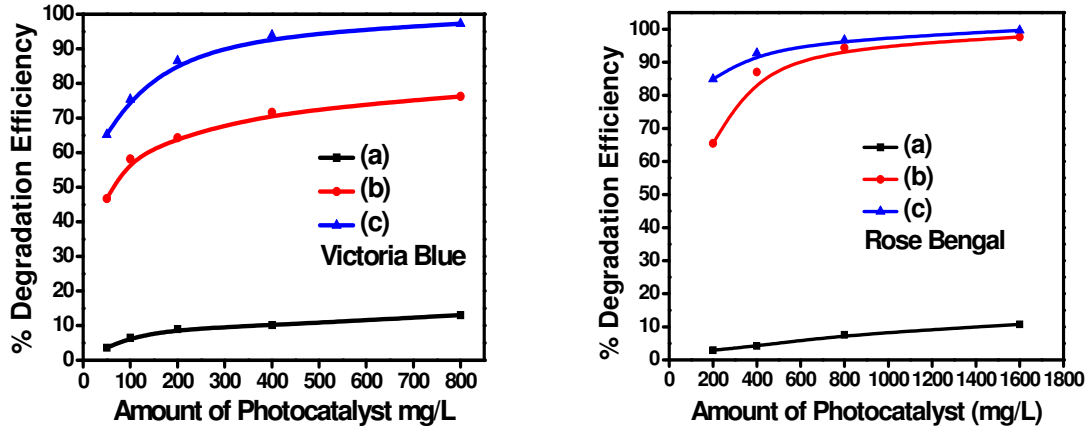

Fig.6.11. Effect of photocatalyst amount on efficiency of dyes Victoria blue and Rose Bengal (a) TiO_2 (b) TiO_2/PPy and (c) TiO_2/PPy/GO

6.3.8.3 Effect of dye concentration

The effect of dyes concentration on photocatalytic degradation was studied in presence of TiO_2 TiO_2/PPy and TiO_2/PPy/GO nanocomposites materials, keeping the amount of catalyst constant. A known concentration of dye solution was prepared in water: alcohol 10:1 (V: V) ratio. The 800 mg/L of photocatalyst was dispersed in the different concentration of dye solution (20, 40, 60, 80 and 100 ppm for Victoria blue and 25, 50, 75, 100 and 125 ppm Rose Bengal) and the reaction mixture was irradiated by visible light. The effect of photocatalytic degradation with time was measured and results are shown in Figure 6.12. The highest photodegradation efficiency (97 %) of both dyes was found in presence of TiO_2/PPy/GO nanocomposite while in presence of TiO_2/PPy and neat TiO_2 it was 86% and 16% respectively. When the concentration of solution increased, the number of dye molecule also increased, therefore, the effective number of photon penetrating the dye reached at the catalyst surface also reduced, owing to hindrance in the path of light, thereby reducing the reactive hydroxyl and superoxide radicals and decreasing the % degradation [67-69].

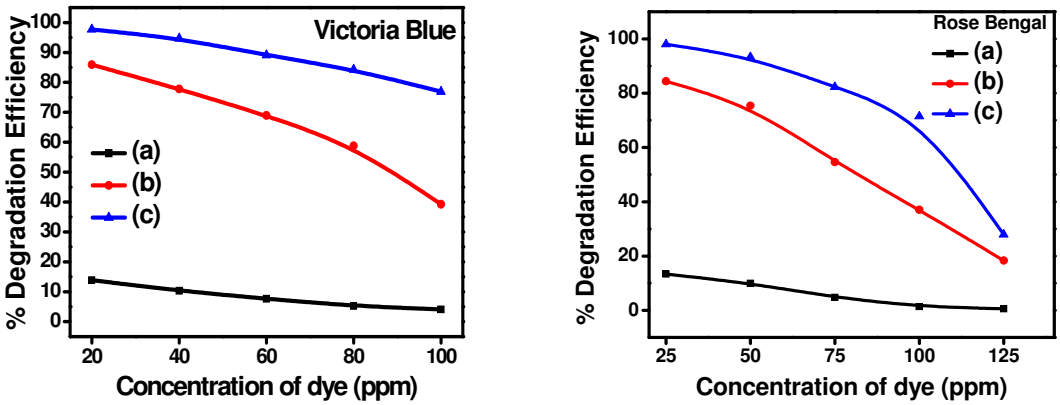

Fig.6.12. Effect of concentration on photodegradation efficiency of dyes Victoria blue and Rose Bengal (a) TiO_2 (b) TiO_2/PPy and (c) TiO_2/PPy/GO

6.3.9. GC-MS of VB and RB photodegradation products

The photodegradation of the Victoria blue and Rose Bengal takes place by irradiating under visible-light in the presence of TiO_2, TiO_2/PPy, and TiO_2/PPy/GO nanocomposite. The photodegraded products of photodegradation of Victoria blue and Rose Bengal have been determined by GC-MS analysis (Fig.6.13 and 6.14). It has been found that MS chromatograph (Fig.6.15 and 6.16) and correspondingly mass chromatographs of Victoria blue and Rose Bengal (after 2 h of irradiation) in the presence of TiO_2, TiO_2/PPy and TiO_2/PPy/GO are almost similar, except in their respective intensities (Fig.6.15 and 6.16). Among the number of degraded products of Victoria blue and Rose Bengal, seven products formed in the photodegradation, shown in mass chromatograph (Fig.6.15 and 6.16) have been identified, as listed in Table 6.4.

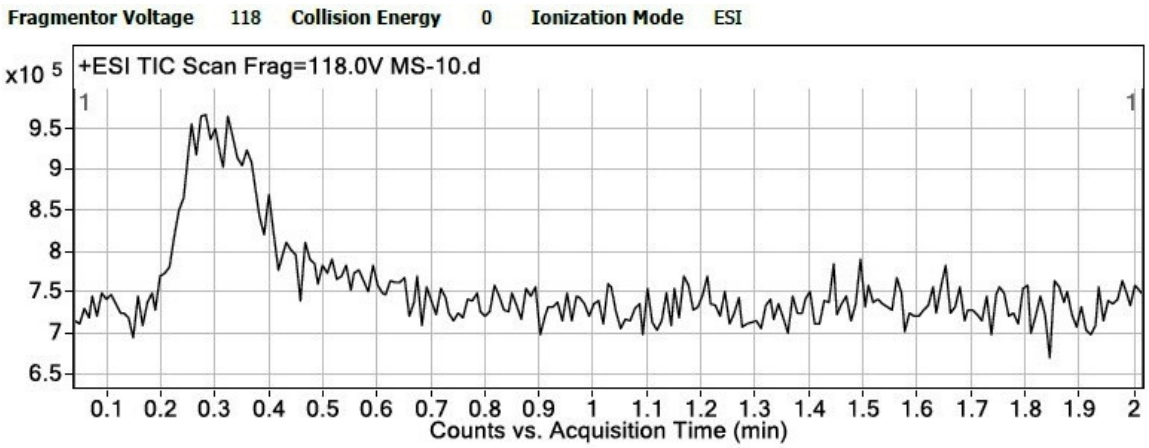

Fig.6.13. GC chromatogram of Victoria blue dye in presence of TiO_2/PPy/GO

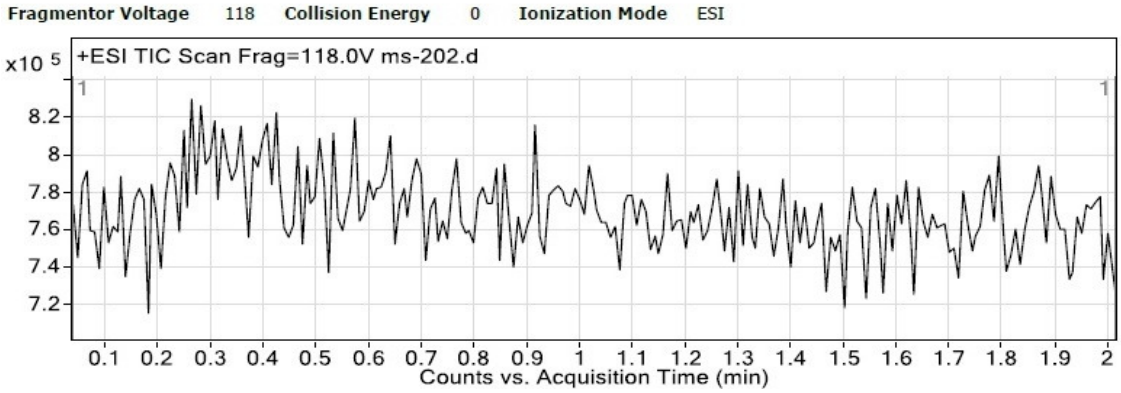

Fig.6.14. GC chromatogram of Rose Bengal dye in presence of TiO_2/PPy/GO

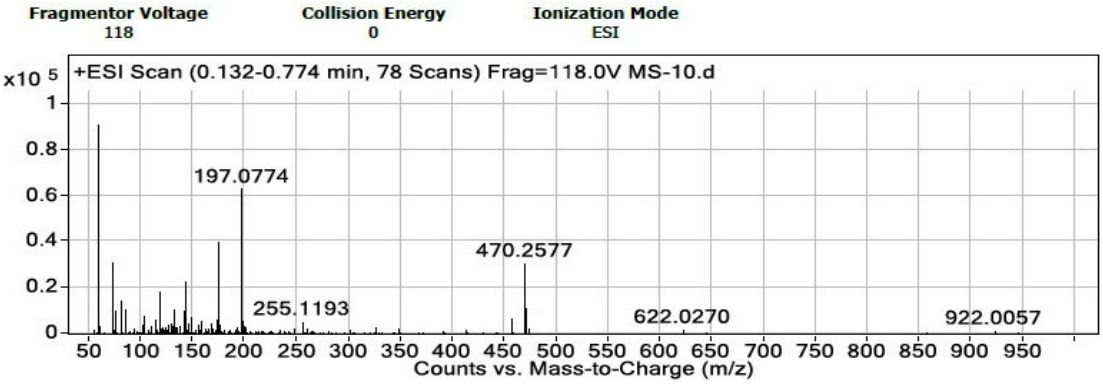

Fig.6.15. Mass Chromatogram of Victoria blue dye in presence of TiO_2/PPy/GO

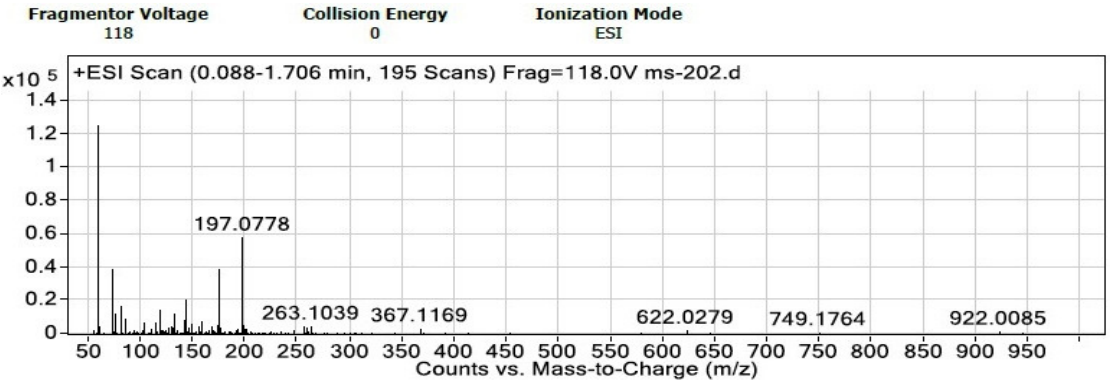

Fig.6.16. Mass Chromatogram of Rose Bengal dye in presence of TiO_2/PPy/GO

The mechanism for the photodegradation of Victoria blue and Rose Bengal using Titania nanocomposites is believed to take place by the photo produced e- and h+, that results into formation of highly oxidative species such as hydroxyl and superoxide radicals, which on reaction with Victoria blue and Rose Bengal results into its decomposition to smaller molecules [70].

Table.6.4 Different intermediate products form in the photodegradation of Victoria Blue dye

	Compound	M+1
[1].	(4-dimethylaminophenyl) (4-methylaminophenyl) (4-ethylaminonaphthyl)methylium	408, 392, 379, 258
[2].	(4-dimethylaminophenyl) (4-aminophenyl) (4-aminonaphthyl)methylium	366, 259, 244, 216
[3].	(4-hydroxymethylaminophenyl) (4-methylaminophenyl) (4-ethylaminonaphthyl)methylium	424, 395, 303, 275
[4].	(4-aminophenyl) (4-aminophenyl) (4-hydroxyethylaminonaphthyl)methylium	382, 260, 232
[5].	(4-hydroxymethylaminophenyl) (4-methylaminophenyl) (4-ethylaminonaphthyl)methylium	424, 303, 275,
[6].	(4-dimethylaminophenyl) (4-hydroxymethylaminophenyl) (4-ethylaminonaphthyl)methylium	424, 395, 317, 288
[7].	(4-aminophenyl) (4-aminophenyl) (4-ethylaminonaphthyl)methylium	36, 336, 273, 245

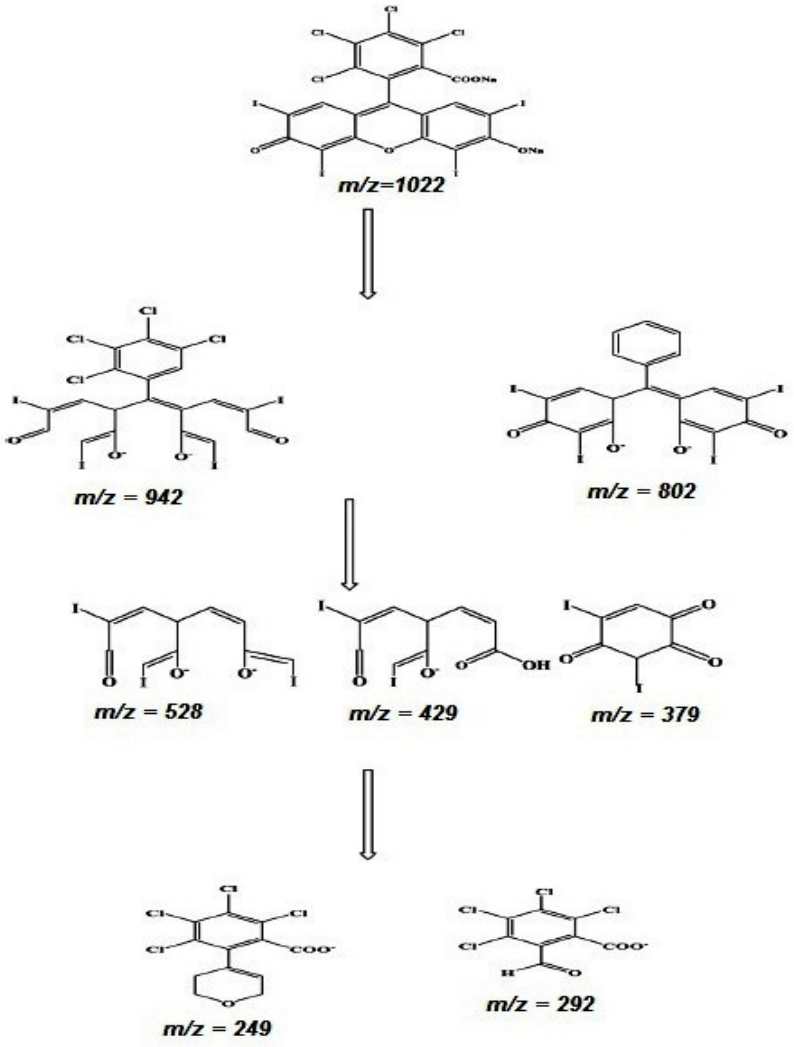

Fig.6.17. Photodegradation Products of Rose Bengal dye identified by mass spectra

The mass spectroscopy has been studied to identify the possible reaction intermediates after 180 min of reaction, as shown in Fig.6. 17. The RB dye solution displays a prominent mass signal at m/z = 1022 in Fig.6. 13 i.e. very close to the formula mass of RB dye. Noticeably,

no mass signals are detected about the formation of the reaction intermediates, which clearly reveal the removal by adsorption. The m/z = 1022 signal is weaken after 180 min of photocatalytic reaction over the TiO2/PPy/GO nanocomposites and multiple mass signals have appeared (Fig.6.17, indicates the formation of reaction intermediates during the photocatalytic degradation. Fig.6.17 depicts the molecular structures of possible reaction intermediates from fragmentations of the main skeleton of RB dye which have the oxy groups in their rings. It is believed that the formations of these reaction intermediates are crucial to determine the degree of degradation of the organic compounds to complete mineralization [71].

6.3.10. Recyclability of Photocatalyst

In order to observe reusability, the photocatalyst recyclability has been studied in this work. The photocatalyst and Victoria Blue and Rose Bengal mixture was agitated, illuminated with visible light and after desired time, the mixture was centrifuged to remove the photocatalyst.

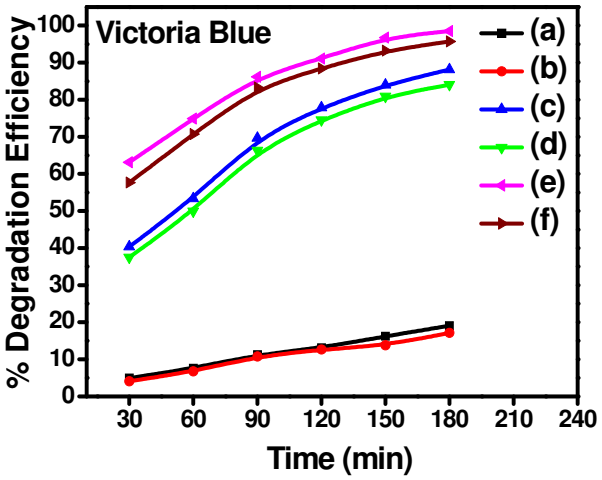

Fig.6.18. Photodegradation of Victoria Blue by Photocatalyst and recyclable Photocatalyst (a) TiO_2 (b) Recyclized TiO_2 (c) TiO_2/PPy (d) Recyclized TiO_2/PPy (e) TiO_2/PPy/GO (f) Recyclized TiO_2/PPy/GO

The obtained photocatalysts were washed three times with distilled water and finally kept in oven for 24 h at 60 ^{o}C temperature and further, it is reused for the degradation of dyes. The photodegradation of Victoria Blue and Rose Bengal by the recyclized

Photocatalyst are showing in Figure 6.18 and 6.19. The results show that the recyclized photocatalyst efficiency is decreased due to the loss of some active sites and decrease of collection efficiency of photon [72].

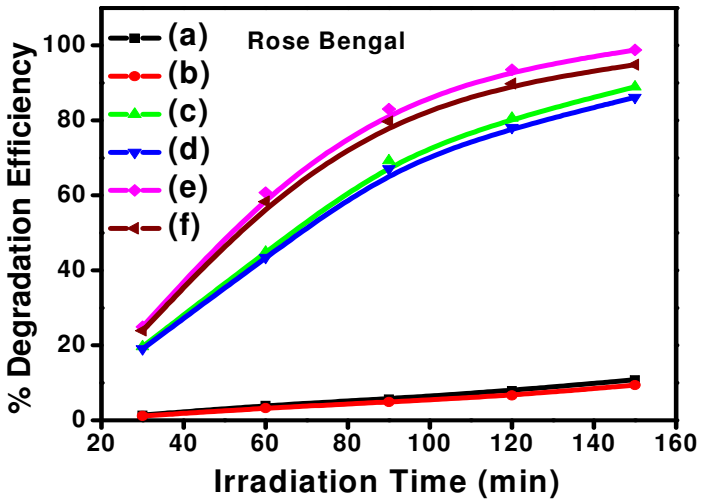

Fig.6.19. Photodegradation of Rose Bengal by Photocatalyst and recyclable Photocatalyst (a) TiO_2 (b) Recyclized TiO_2 (c) TiO_2/PPy (d) Recyclized TiO_2/PPy (e) TiO_2/PPy/GO (f) Recyclized TiO_2/PPy/GO

6.3.11. TOC Analysis of photodegraded dyes

In order to measure the complete mineralization of Victoria blue and Rose Bengal dyes, a TOC analysis was performed. During the initial stage of recirculation in the dark (30 min), the chemisorptions of the dyes on the catalyst surface caused a TOC depletion of 5-8%. The experimental data obtained by using either TiO_2 or TiO_2/PPy and TiO_2/PPy/GO are shown in Figure 6.20. The Blank test of dye (without photocatalyst) is also reported for comparison for photocatalytic activity of nanocomposites, a maximum decrease of the TOC percentage is observed in the presence of the TiO_2/PPy/GO nanocomposites [73].

The TOC analysis of photodegraded Victoria Blue and Rose Bengal dye in presence of TiO_2, TiO_2/PPy and TiO_2/PPy/GO were done. The TOC of Victoria blue is showing in Figure 6.21. The Victoria blue was photodegraded for 3 h in presence of photocatalyst. The TOC of Victoria blue was observed 100, 92, 26 and 4 % for the blank, TiO_2, TiO_2/PPy and TiO_2/PPy/GO. The polypyrrole modified Titania material shows the good photocatalytic

activity. Similarly, The TOC was observed for the Rose Bengal dye shown in Figure 21. The TOC photodegraded Rose Bengal was found 100, 94, 34 and 16 % for blank, TiO_2, TiO_2/PPy and TiO_2/PPy/GO. It means that polypyrrole modified Titania shows the good photocatalytic activity due to formation of heterostructures [74].

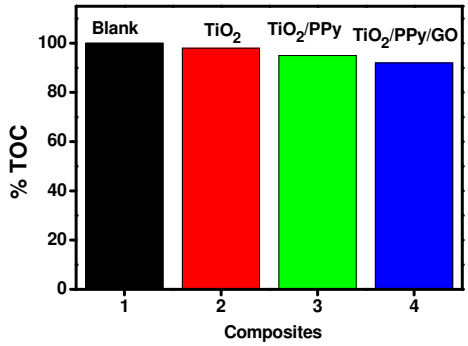

Fig.6.20. % TOC of dye after adsorption (keep in under dark for 30 min)

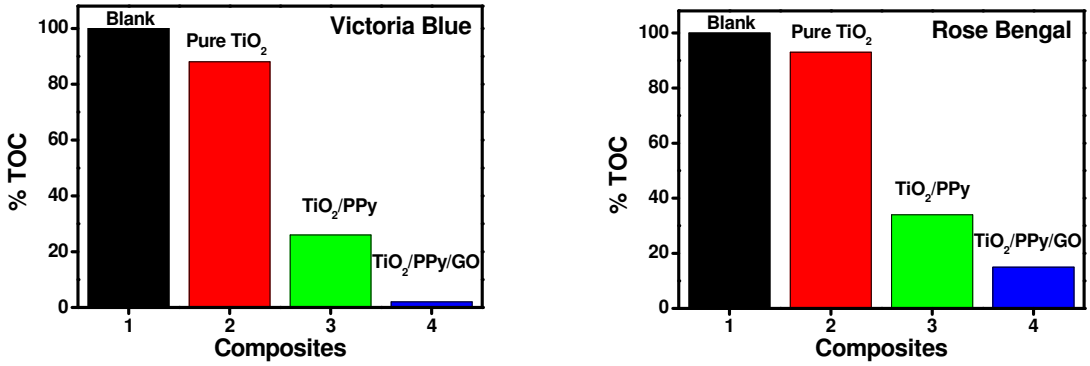

Fig.6.21. % TOC of dyes after photodegradation with TiO_2, TiO_2/PPy, and TiO_2/PPy/GO

6.3.12. Hydroxyl radical formation

To determine whether reactive oxygen species involved in the photocatalytic degradation of dyes is hydroxyl radical or not, terephthalic acid photoluminescence probing technique was used. In this method, alkaline solution of terephthalic acid, having TiO_2, TiO_2/PPy, and TiO_2/PPy/GO nanocomposites was irradiated with visible light. After 30 min of irradiation, a sample was withdrawn from the reaction mixture and was centrifuged to separate photocatalyst particles. The photoluminescence spectrum of the sample was recorded between 335 and 600 nm at an excitation wavelength of 325 nm and variation in the

intensity of a peak at 425 nm was monitored using Perkin Elmer LS 55 Fluorescence Spectrometer.

As hydroxyl radical performs the key role for the decomposition of the organic pollutants, it is necessary to investigate a number of hydroxyl radicals produced by each photocatalyst. Thus, there is a technique to establish the formation of hydroxyl radicals using terephthalic acid (TA) as a probe molecule. In this method, TA was directly attacked by ·OH radical forming 2- hydroxyl terephthalic acid (TAOH) which gives a fluorescence signal at 426 nm. Figure 6.22 depicts the fluorescent signal of all the photocatalysts after reacting with TA solution. The fluorescent intensity is linearly related to the number of hydroxyl radicals formed by the photocatalysts. If the generation of hydroxyl radical is higher, the yield of TAOH will be more and hence more intense will be the fluorescence peak. Thus, TiO_2/PPy/GO with the highest intensity confirms the generation number of hydroxyl radicals compared to other photocatalysts. The fluorescence intensity follows the trend (i,e. TiO_2, < TiO_2/PPy < TiO_2/PPy/GO) of photocatalytic performance of all the photocatalyst [75].

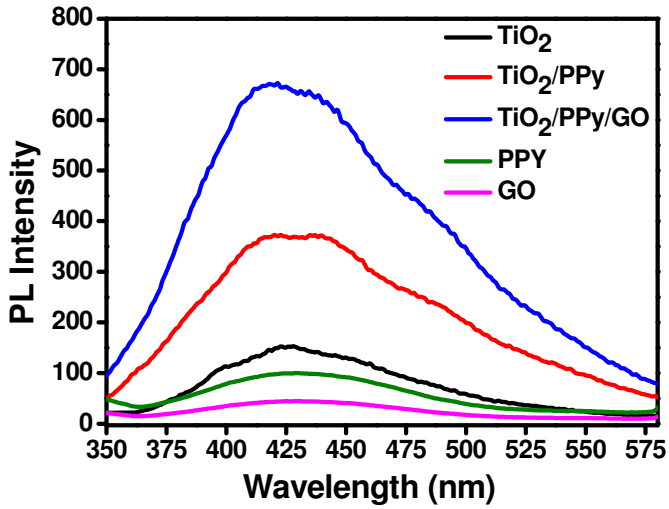

Fig.6.22. PL spectra of photocatalyst with terephthalic acid (0.001M) TiO_2, TiO_2/PPy, and TiO_2/PPy/GO

6.3.13. Lowering of electron-hole recombination

Photoluminescence spectra have been used to examine the mobility of the charge carriers to the surface as well as the recombination process involved by the electron-hole

pairs in semiconductor particles. PL emission results from the radiative recombination of excited electrons and holes. In other words, it is a critical necessity of a good photocatalyst to have minimum electron-hole recombination. To study the recombination of charge carriers, PL studies of synthesized materials have been undertaken. PL emission intensity is directly related to recombination of excited electrons and holes. Figure 6.23 shows the photoluminescence spectra of synthesized photocatalysts. It means TiO_2 and TiO_2/PPy with strong PL intensity have high recombination of charge carriers whereas TiO_2/PPy/GO has weak intensity. The weak PL intensity of TiO_2/PPy/GO may arise due to the coating of polypyrrole on Titania lattice, so that decrease in the band gap of TiO_2/PPy/GO was found which results in the decolourisation of photoexcited electrons. This delays the electrons-holes recombination process and hence is utilized in the redox reaction leading to improved photocatalytic activity [75].

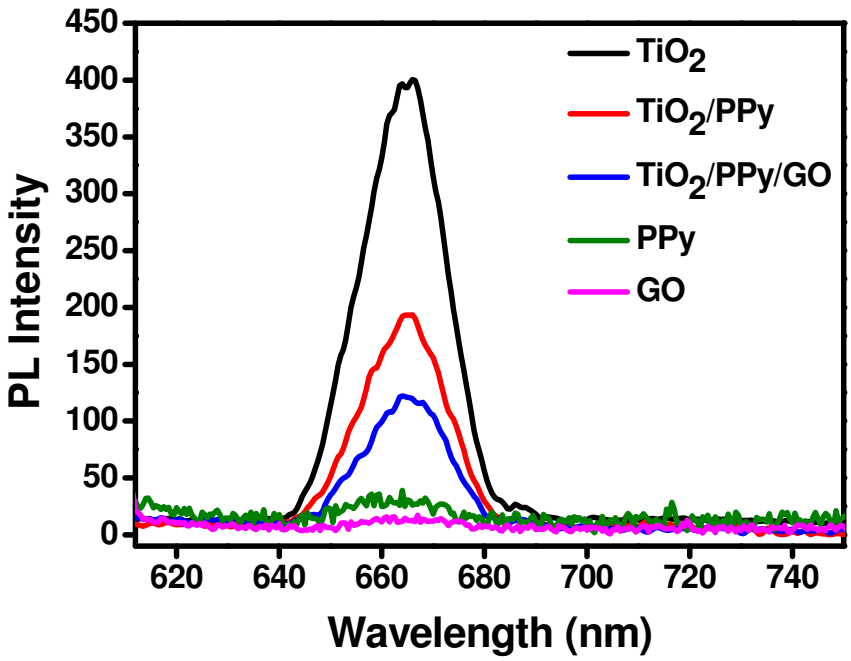

Fig.6.23. Photolumiscence Spectra of TiO_2, TiO_2/PPy, TiO_2/PPy/GO, Polypyrrole (PPy) and Graphene Oxide (GO)

6.3.14. Adsorption of dyes

The Photodegradation of Victoria Blue and Rose Bengal dyes were done under visible light irradiation in presence of TiO_2, TiO_2/PPy and TiO_2/PPy/GO nanocomposites. It is an example of heterogeneous catalysis. Rate laws in such reactions seldom follow proper law

model and hence are inherently more difficult to formulate from the data. It has been widely accepted that heterogeneous catalytic reactions can be analyzed with the help of Langmuir Hinshelwood (LH) Model [76-77], satisfying, the following assumptions (i) there are limited number of adsorption sites on the catalyst and its surface is homogeneous, (ii) only one molecule can be adsorbed on one site and monolayer formation occurs (iii) the absorption reaction is reversible in nature, and (iv) the adsorbed molecules do not react amongst themselves [78-79]. According to LH Model, following three steps take place in the kinetics mechanism [80–81], these steps are of adsorption, surface reaction and desorption of products from the surface.

Step 1: D (Dye) + C (catalyst) ⟷ D.C (Adsorption)

Step 2: D.C ⟷ E.C + Other products (Surface reaction)

Step 3: E.C ⟷ E + C (Desorption)

The Freundlich isotherm [82] is employed, assuming a heterogeneous surface with a non uniform distribution of heat of adsorption over the surface and it may be written as:-

$$q_e = K_F C_e^{\frac{1}{n}} \tag{11}$$

The above equation can be linearized as

$$lnq_e = lnK_F + \frac{1}{n} lnC_e \tag{12}$$

Where q_e (mg/g) is the amount of solute adsorbed per unit weight of adsorbent, C_e (mg/l) is the equilibrium concentration of solute, K_F (mg/g) is the Freundlich constant (which indicate the relative adsorption capacity of the adsorbent) and 1/n is the constant indicate the intensity of adsorption. Since the photocatalyst is covered by both Dye as well as water molecules (C_{water}) by hydrogen bonding, their competition for the active sites cannot be ignored.

Langmuir adsorption model [83] can be applied to the aqueous solutions of dyes with the help of the following expression:

$$q = \frac{q_t}{q_{\max}} = \frac{K_L C}{1 + K_L C + K_{water} + C_{water}} \tag{13}$$

Where q is the fractional sites covered by the dye, q_t is the absorbed quantity of dye at any time, q_{max} shows the maximum quantity of dye that can be adsorbed, K_L is the Langmuir adsorption constant for reactant and K_{water} is the adsorption constant for water.

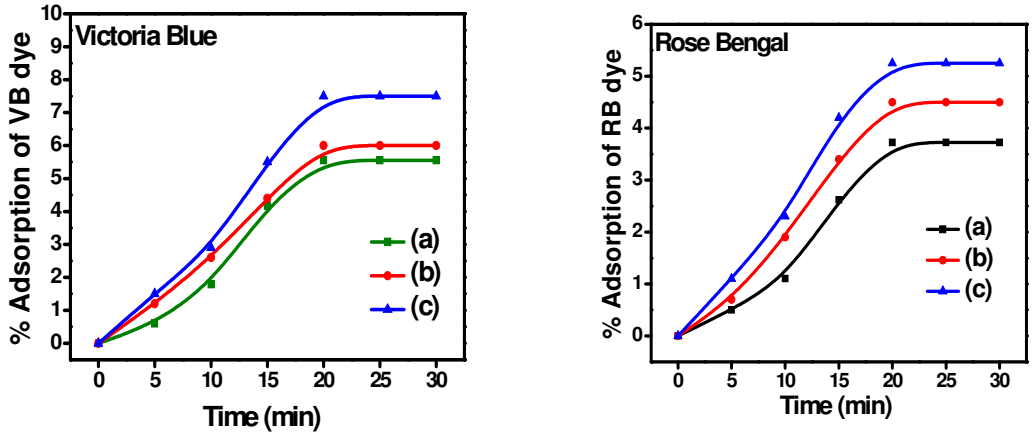

Fig.6.24. % Adsorption of Victoria Blue and Rose Bengal dye under dark condition in presence of (a) TiO_2, (b) TiO_2/PPy and (c) TiO_2/PPy/GO

The value of $C_{water} >> C$, hence C_{water} remains almost same throughout the reaction and the catalyst coverage by water molecules remains almost constant. Thus, we can ignore the quantity K_{water}, C_{water} and rewrite Eq. (13) as:

$$q = \frac{K_L\, C}{1+K_L\, C} \tag{14}$$

The quantity adsorbed at a particular time can also be expressed

$$qt = \frac{(Reactor\ Volume\ )*(Change\ in\ concentration)}{Mass\ of\ catalyst} \tag{15}$$

The equilibrium adsorption quantity q_{eq} can be written as:

$$q_e = q_{Max}\left[\frac{K_L C_e}{1+K_L C_e}\right] \tag{16}$$

where Ce is the equilibrium concentration of the dye. On transforming Eq. (16), a function can be derived as follows:

$$\frac{C_e}{q_e} = \frac{1}{K_L q_{max}} + \frac{C_e}{q_{max}} \tag{17}$$

The intercept on the vertical axis gives $1/K_L q_{max}$ and the reciprocal of slope gives q_{max}.

6.3.15. Kinetic study of Photocatalytic degradation

For kinetic study of photocatalytic degradation, a control experiment was first carried out under two conditions, vis (i) dye + Visible light (no catalyst) (ii) catalyst+ dye in dark without any irradiation (Figure 24). It can be seen that in under dark conditions, the amount of catalyst adsorbed becomes constant after 20 min, where adsorption equilibrium is achieved. For the kinetic study of bleaching of Victoria Blue and Rose Bengal, the initial concentration of the dyes was varied and the experiments were first conducted in dark for 20 min and then immediately followed by irradiation (Figure 6.24). The amount of catalyst was kept constant (0.2 g) throughout the experiment.

Applying the Langmuir Hinshelwood model for determining the oxidation rate of the photocatalysis of dye:

$$\mathbf{Rate\ (r)} = -\frac{\mathbf{dC}}{\mathbf{dt}} = \mathbf{k\theta} = \boldsymbol{\theta} = \frac{\mathbf{kK_AC}}{\mathbf{1+K_AC}} \quad (18)$$

Where k is the rate constant (mg/L min^{-1}), C is the concentration of dye, K_A is the adsorption constant of the dye (L/mg), and t is the illumination time (min).

During the course of the reaction, the initial pH, the amount of catalyst, and photo intensity were kept same. In addition to it, the formation of intermediates may interfere in the rate determination; hence the calculation was done at the beginning of irradiation. The rate expression can be written as:

$$\boldsymbol{r_o} = \frac{\boldsymbol{kK_AC_o}}{\boldsymbol{1+K_AC_o}} \quad (19)$$

Where r_o is the initial rate of degradation of Victoria Blue and Rose Bengal and C_o is the initial concentration (almost equal to Ceq). When the initial concentration $C_{initial}$ is very small, Co will also be small and Eq. (19) can be simplified as first-order equation [84-85]:

$$-\frac{dC}{dt} = kK_AC_o = \frac{lnC_o}{C} = kK_At \quad (20)$$

$$C = C_o e^{-k_f photo\, t} \quad (21)$$

Where

$k_{f,\ Photo=}$ k k_A

The value of $k_{f,photo}$ can be determined from the plot of ln C_t/ Co vs. t (Figure 6.25).

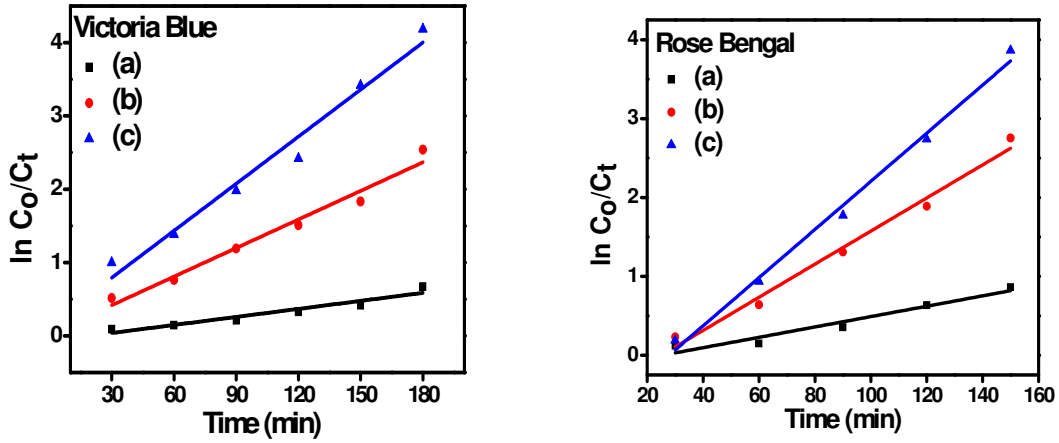

Fig.6.25. Linear first order reaction of Langmuir Hinshelwood kinetics of Victoria Blue and Rose Bengal dye vs. time (a) TiO_2 (b) TiO_2/PPy (c) TiO_2/PPy/GO

The slope of the straight line obtained will be the value of first order rate constant [86]. The Value of apparent rate constant was determined at definite concentrations of dye solution for photocatalysis reaction in presence of TiO_2, TiO_2/PPy and TiO_2/PPy/GO showing in Fig.6.26. The rate constant values for the photocatalytic degradation of Victoria Blue and Rose Bengal follow the first order kinetic for the both photocatalyst. This is confirmed that photocatalytic degradation of Victoria Blue and Rose Bengal follows first order kinetic in presence of TiO_2, TiO_2/PPy and TiO_2/PPy/GO.

6.3.16. Mechanism of photo-oxidation process

The acceleration of a chemical transformation by the presence of a catalyst with light is called photocatalysis. The catalyst may accelerate the photoreaction by interaction with the substrate in its ground or excited state and/or with a primary photoproduct, depending upon the mechanism of the photoreaction, itself remaining unaltered at the end of each catalytic cycle. Heterogeneous photocatalysis is a process in which two active phases, solid and liquid are present. The solid phase is a catalyst, usually a semiconductor. The molecular orbital of semiconductors has a band structure. The bands of interest in photocatalysis are the populated valence band (Victoria Blue and Rose Bengal) and it's largely vacant conduction band (CB), which is commonly characterized by the band gap energy (E_{bg}). The semiconductors may be

photo-excited to form electron-donor sites (reducing sites) and electron acceptor sites (oxidizing sites), providing great scope for the redox reaction. When the semiconductor is illuminated with light (hν) of greater energy than that of the band gap, an electron is promoted from the Victoria Blue and Rose Bengal to the CB leaving a positive hole in the valence band and an electron in the conduction band as illustrated in Figure 6.26 and 6.27.

If charge separation is maintained, the electron and hole may migrate to the catalyst surface where they participate in redox reactions with absorbed species. Specially, h^+ and dyes (Victoria Blue and Rose Bengal) may react with surface-bound H_2O or OH^- to produce the hydroxyl radical and e^-_{cb} is picked up by oxygen to generate superoxide radical anion (O_2^-), as indicated in the following equations 6-8; absorption of efficient photons by Titania

($h\upsilon \geq E_{bg} = 3.2$ eV)

$$TiO_2 + h\upsilon \rightarrow e_{cb} + h^+_{dye} \quad (22)$$

Formation of superoxide radical anion

$$O_2 + e_{cb} \rightarrow O_2^- \quad (23)$$

Neutralization of OH^- group into OH by the hole

$$(H_2O \Leftrightarrow H^+ + OH^-)_{ads} + h^+_{dye} \rightarrow {}^{\bullet}OH + H^+ \quad (24)$$

It has been suggested that the hydroxyl radical ($^{\bullet}OH$) and superoxide radical anions ($O_2^{-\cdot}$) are the primary oxidizing species in the photocatalytic oxidation processes [87-88]. These oxidative reactions would results in the degradation of the pollutants as shown in the following equations 23-24;

Oxidation of the organic pollutants via successive attack by OH radicals

$$R + {}^{\bullet}OH \rightarrow R^{\cdot} + H_2O \quad (25)$$

or by direct reaction with holes

$$R + h^+ \rightarrow R^{\cdot +} \rightarrow \text{ degradation products} \quad (26)$$

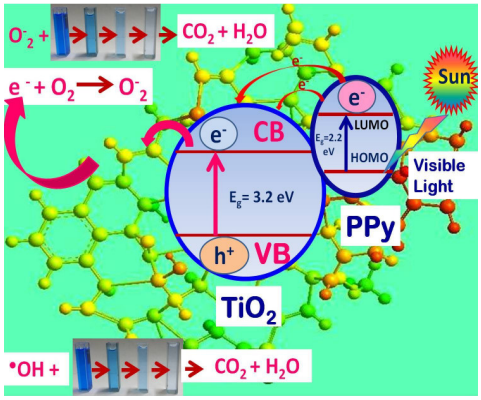

Fig.6.26. Mechanism of Photodegradation of Victoria Blue dye by TiO_2/PPy/GO nanocomposite

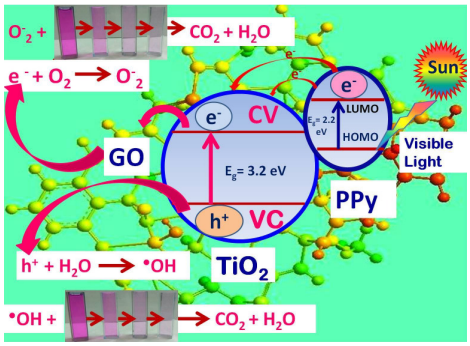

Fig.6.27. Mechanism of Photodegradation of Rose Bengal dye by TiO_2/PPy/GO nanocomposite

Conclusions

The present research work describes a proficient method for synthesis of TiO_2/PPy and TiO_2/PPy/GO nanocomposites. These nanocomposites were prepared by one-step *in situ* deposition oxidative polymerization of pyrrole hydrochloride using Ammonium persulphate (APS) as an oxidant in the presence of ultra-fine grade powder of TiO_2 nanoparticles cooled in an ice bath. The obtained nanocomposites were characterized by XRD, TEM, SEM, and UV-Vis for band gap determination. The obtained results showed that TiO_2 nanoparticles have been encapsulated by PPy with a strong effect on the morphology of TiO_2/PPy and TiO_2/PPy/GO nanocomposites. The Photocatalytic degradation of Rose Bengal and Victoria blue dye was done at different condition viz concentration of dye, time of illumination, pH and dose of the photocatalyst. The maximum photodegradation was found at 7 pH, 20 ppm concentration of Victoria blue and 25 ppm of Rose Bengal dye solution, 800

mg/L for VB and 1600 mg/L for RB amount of photocatalyst and 120 min irradiation of visible light. Kinetics of photodegradation was investigated for Victoria blue and Rose Bengal dye and found first order kinetics. The coating of PPy and GO has enhanced the photocatalytic activity of Titania. Hence TiO_2/PPy and TiO_2/PPy/GO are the efficient photocatalyst for the degradation of Rose Bengal and Victoria Blue dye than pure TiO_2.

References

[1]. J. Kaur, S. Singhal, Physica B, 450, (2014), 49–53.

[2]. M.A. Fox, D.F. Duxbury, Chem. Rev. 93, (1993), 381–433.

[3]. S.K. Kansal, M. Singh, D. Sud, J Hazard Mater 141,11, (2007), 581–590.

[4]. W. Azmi, R.K. Sani, U.C. Banerjee, Enzyme Microb. Technol. 22, (1998) 185–191.

[5]. I.K. Konstantinou, T.A. Albanis, Appl. Catal. B: Environ. 49, (2004), 1–14.

[6]. F. Deng, L. Min, X. Luo, S. Wu, & S. Luo, Nanoscale, 5, (2013), 8703–8710.

[7]. S. Xu, Y. Zhu, L. Jiang, & Y. Dan, Water, Air, & Soil Pollution, 213, (2010), 151-159.

[8]. Y. Park, S. Lee, S. O. Kang, & W. Choi, Chemical Communications, 46, (2010), 2477–2479.

[9]. M. Saquib, M. Muneer, Dyes Pigments 56, (2003), 37–49.

[10]. X. Li, G. Liu, J. Zhao, New J. Chem. 23, (1999), 1193–1196.

[11]. C.C. Chen, C.S. Lu, J. Phys. Chem. C 111, (2007), 13922–13932.

[12]. M. Okano, K. Itoh, A. Fujishima, & K. Honda, Journal of the Electrochemical Society, 134, (1987), 837–841.

[13]. B. Wang, C. Li, J. Pang, X. Qing, J. Zhai, & Q. Li, Applied Surface Science, 258, (2012), 9989–9996.

[14]. X. Chen, & S. S. Mao, Chemical Reviews, 107, (2007),2891–2959.

[15]. A. L. Linsebigler, G. Lu, & J. T. Yates, Chemical Reviews, 95, (1995), 735–758.

[16]. R.J. Davis, J.L. Gainer, G. O'Neal, I.W. Wu, Water Environ Res 66, (1994), 50–53

[17]. S. Mozia, A.W. Morawski, M. Toyoda, M. Inagaki, Desalination 241, (2009), 97–105

[18]. H. Tai, Jiang, Y. Xie, G. Yu, & M. Zhao, Int. J. of Envi. Analy. Chem., 87, (2007) 539–551.

[19]. C. M. Nag, P.C. Chen, S. Kumar, Applied Catalysis A: General, 433–434, (2012), 75-80

[20]. P.V. Kamat, K. Vinodgopal, D.E. Wynkoop, Environ. Sci. Technol, 30, (1996), 1660–1666.

[21]. H. Huang, M. Gan, L. Ma, L. Yu, H. Hu, F. Yang, Y. Li, C. Ge, J. of Alloys and Compounds, 630, (2015), 214-221

[22]. X. Chen, & S. S. Mao, Chemical Reviews, 107, (2007), 2891–2959.

[23]. L. Yuzhen, Y. Yuan, W. Liangzhuan, J. Zhi, Applied Surface Science, 273, (2013), 135-143

[24]. Y. Yang, J. Wen, J. Wei, R. Xiong, J. Shi, and C. Pan, Appl. Mater. Interfaces, 5, (2013) 6201−6207

[25]. M. Vautier, C. Guillard, J.M. Herrmann, J. Catal. 201, (2001), 46–59.

[26]. G. K. Mor, K.Shankar, M. Paulose, O. K. Varghese, & C. A. Grimes, Nano Letters, 6, (2006),215–218.

[27]. T. L. Thompson, & J. T. Yates, Chemical Reviews, 106, (2006), 4428–4453.

[28]. A. Kaur, Y.R. Smith, V.R. Subramanian, Environ. Sci. Technol. 43, (2009), 3260–3265.

[29]. W. Baran, A. Makowski, W. Wardas, Chemosphere 53,(2003), 87–95.

[30]. S. Wei,P. M., Q. Wang, D. Chen, R. Asapu, Y. Mao, N. Haldolaarachchige, D.P. Young, and Z. Guo, J. of The Elec. Soc., 158 (11) K205-K212, (2011), K205.

[31]. R.W. Matthews, J. Catal. 111, (1988), 264–272.

[32]. B. Pare, P. Singh,and S.B. Jonnalgadda, Journal of Scientific & Industrial Research, 68,(2009), 724-729.

[33]. J.L. Gole, J.D. Stout, C. Burda, Y. Lou, X. Chen, J Phys Chem B 108(4) (2004) 1230–1240

[34]. J.D. Kwon, P.H. Kim, J.H. Keum, J.S. Kim, Sol Energy Mater Sol Cells 83 (2004) 311–321

[35]. D. Wang, Y. Wang, X. Li, Q. Luo, J. An, & J. Yue, Catalysis Communications, 9, (2008) 1162–1166.

[36]. H.C. Liang, X.Z. Li, Applied Catalysis B: Environmental, 86,9(2009), 8-17

[37]. C. Ferreira, S. Domenech, & P. Lacaze, J. of Applied Electrochemistry, 31, (2001) 49–56.

[38]. L. Sun, Y. Shi, B. Li, X. Li, & Y. Wang, Polymer Composites, 34, (2013), 1076–1080.

[39]. Z. Guo, K. Shin, A. B. Karki, D. P. Young, R. B. Kaner, H. T. Hahn, J Nanopart Res (2009), 11:1441–1452.

[40]. D.C. Marcano, D.V. Kosynkin, J.M. Berlin, A. Sinitskii, Z. Sun, A. Slesarev, L.B. Alemany, W. Lu and J.M. Tour, *ACS Nano*,(2010), *4* (8), pp 4806–4814

[41]. F. Denga, Y. Li, X. Luo, L. Yang, X. Tu, Colloids,and Surfaces A: Physicochem. Eng. Aspects 395 (2012), 183– 189

[42]. M.C. Arenas, L. F. Núnez, D. Rangel, O.M. Álvarez, C. M. Alonso, V.M. Castaño, Ultrasonics Sonochemistry, 20, (2013), 777-784.

[43]. M. Sedla, M. Mrlik, V. Pavlinek, P. Saha,& O. Quadrat, Colloid and Polymer Science, 290, (2012), 41–48.

[44]. K. Singh, R. Bharose, S.K. Verma, V.K. Singh,93,(2013), 157–165

[45]. H. Lachheb, E. Puzenat, A. Houas, M. Ksibi, E. Elaloui, C. Guillard, J.M. Herrmann, Appl. Catal. B: Environ. 39 (2002), 75–90.

[46]. G.A. Epling, C. Lin, Chemosphere 46 (2002), 561–570.

[47]. B. D. Cullity, S. R. Stock, Elements of X-Ray Diffraction, Third Edition, and New Jersey: Prentice-Hall, Inc. (2001)

[48]. M. Hema, A.Y. Arasi, P. Tamilselvi, R. Anbarasan, Chem. Sci. Trans. 2 (2013), 239–245.

[49]. M.M. Ba-Abbad, A.A.H. Kadhum, A.B. Mohamad, M.S. Takriff, K. Sopian, Int. J. Electrochem. Sci 7 (2012), 4871–4888.

[50]. M. Vautier, C. Guillard, J.M. HerrmannJ. Catal. 201 (2001), 46–59.

[51]. L. Cavigli, F. Bogani, A. Vinattieri, V. Faso, G. Baldi, *J. Appl. Phys. (*2009), *106*, 053516

[52]. S. Yang, X. Yang, X. Shao, R. Niu, L. Wang, J. Hazard. Mater. 186 (2011), 659–666.

[53]. K. M. Reddy, S. V. Manorama, A. R. Reddy, Materials, Chemistry and Physics 78 (2002), 239–245.

[54]. S. Bashir, J. Liu, H. Zhang, X. Sun, J. Guo, J Nanopart Res (2013) ,15:1572.

[55]. J. Guo, Int J Quantum Chem 109 (2009),2714–2721

[56]. A. Achilleos, E. Hapeshi, N. P. Xekoukoulotakis, D. Mantzavinos, and D. Fatta-Kassinos, Chemical Engineering Journal, 161,(2010), 53–59,

[57]. K. M. Reza, ASW Kurny, F. Gulshan, Appl Water Sci (2017) ,7:1569–1578

[58]. E. Vulliet, J.M. Chovelon, C. Guillard, J.M. Herrmann, J. Photochem. Photobiol. A: Chem. 159 (2003), 71–79.

[59]. K. Bubacz, J. Choina, D. Dolat, A.W. Morawski (2010), Pol J Environ Stud 19:685–691.

[60]. Ling CM, Mohamed AR, Bhatia S, Chemosphere 57 (2004), 547–554

[61]. Guillard C, Lachheb H, Houas A, Ksibi M, Elaloui E, Herrmann JM (2003), J Photochem Photobiol A 158:27–36

[62]. Zielin´ska B, Grzechulska J, Kalen´czuk RJ, Morawski AW (2003a) Appl Catal B45:293–300.

[63]. Senthilkumaar S, Porkodi K, Gomathi R, Geetha Maheswari A, Manonmani N (2006), Dyes Pigments 69:22–30.

[64]. S.K. Kansal, N. Kaur, S. Singh, Nanoscale Res Lett 4: (2009), 709–716.

[65]. Tanaka K, Padermpole K, Hisanaga T (2000), Water Res 34:327–333

[66]. Grzechulska J, Morawski AW (2002),Appl Catal B 36:45–51

[67]. E. Vulliet, J.M. Chovelon, C. Guillard, J.M. Herrmann, J. Photochem. Photobiol. A: Chem. 159 (2003), 71–79.

[68]. L. Zhang, W. Zhang, R. Li, H. Zhong, Y. Zhao, Y. Zhang, X. Wang, J. Hazard. Mater. 171 (2009), 294–300.

[69]. D. Chen, A.K. Ray, Appl. Catal. B: Environ. 23 (1999), 143–157.

[70]. S. Ameen, H.-K. Seo, M.S. Akhtar, H.S. Shin, Chemical Engineering Journal 210 (2012), 220–228

[71]. T. Sinha and M. Ahmaruzzaman, Photochem. Photobiol. Sci.,(2016), 15, 1272

[72]. F.D. Mai, C.S. Lu, C.W. Wu, C.H. Huang, J.Y. Chen, C.C. Chen, Separation and Purification Technology 62 (2008), 423–436

[73]. B. Di Credico, I. R. Bellobono, M. D'Arienzo, D. Fumagalli, M. Redaelli, R. Scotti, and F. Morazzon, International Journal of Photoenergy 2015 (2015), Article ID 919217, 13 pages

[74]. M. Vautier, C. Guillard, J.M. Herrmann, J. Catal. 201 (2001), 46–59.

[75]. J. Eriksson, J. Svanfelt, and L. Kronberg, Photochemistry and Photobiology, 86, (2010), 528–532.

[76]. Jie Zhang and Yoshio Nosaka, *J. Phys. Chem. C*,(2014), *118* (20), pp 10824–10832

[77]. R.W. Matthews, J. Catal. 111 (1988), 264–272.

[78]. R. Zepp, D. Crosby D., J. Photochem. Photobiol., A, Lewis Publs., CRC Press, Boca Raton, Florida, Chap. 22 (1994), 317–348.

[79]. S. Yang, X. Yang, X. Shao, R. Niu, L. WangJ. Haz. Mater. 186, (2011), 659–666.

[80]. N. Guettaı, H.A. Amar, Desalination 185 (2005), 439–448.

[81]. M.D. Levant, T. Vermeulen, J Phys Chem 85:3247–3250, (1981),

[82]. E. Kordouli, K. Bourikas, A. Lycourghiotis, C. Kordulis, Catal Today 252, (2015), 128–135

[83]. I.K. Konstantinou, T.A. Albanis, Appl Catal B 49 (2004) ,1–14

[84]. A. F. Júnior, E. C. de Oliveira Lima, A. N. Miguel, P. R. Wells, Journal of Magnetism and Magnetic Materials, 308, (2007), 198-202

[85]. M. A. Abu-Hassan, J. K. Kim, I. S. Metcalfe, and D. Mantzavinos, Chemosphere, vol. 62, no. 5, p, (2006),749.755

[86]. N.M.Mahmoodi, M.Arami, N.Y.Limaee, N.S.Tabrizi, J Colloid Interface Sci295: 159–164, c),

[87]. G. M. Liu, X. Z. Li, J. C. Zhao, S. Horikoshi, and H. Hidaka, Journal of Molecular Catalysis A: Chemical, 153,(2000),221-229

[88]. C. Galindo, P. Jacques, A. Kalt, J. Photochem. Photobiol. A 130, (2000), 35-47

CHAPTER-7

Preparation and Photocatalytic activity of Co:La:TiO_2 nanocomposites for the degradation of Methyl Blue in Visible light

In this study, prepared the nanocomposites of Co:La:TiO_2 by the wet chemical method. Synthesized TiO_2 and Co:La:TiO_2 were characterized by X-Ray Diffractometer, SEM,TEM, UV- vis, FT-IR, Band gap energy and BET. The TiO_2 and Co:La:TiO_2 were used as photocatalyst for the degradation of Methyl Blue. The XRD pattern confirmed the presence of anatase and rutile phase in the catalyst. The particle size was estimated by the Scherrer's and found 68 and 32 nm for TiO_2 and Co:La:TiO_2 respectively. The particle morphology of the photocatalysts was found in nanodiamension. The surface area of the photocatalysts were found 37.52 and 106.68 m^2/g for TiO_2 and Co:La.TiO_2 respectively . The band gap energy of TiO_2 and Co:La.TiO_2 were 3.2 and 3.0 eV. The FT-IR spectra of Co:La:TiO_2 were recorded and found Co bonded with Titania. The photodegradation of Methyl Blue has been found maximum at 5 pH, 25 ppm concentration of dye, 800 mg/L amount of photocatalyst and 180 min illumination of visible light. The photodegradation was following

7.1. Introduction

Photodegradation of dyes, for example, Methylene blue [1] and methyl orange [2] on Titania under UV light illumination is known. However, simulated UV light sources devour a lot of electrical energy and the toxicity of UV light requires safety of the eyes and skin [3-4]. Consequently, the conversion of the light absorption properties of Titania remains an important challenge [5]. Titanium dioxide TiO_2 is a most important nanomaterials which has attracted a great attention due to its unique properties. Titanium dioxide TiO_2 have excellent merits in solar energy transferring and photocatalysis of poison compounds in environment [6]. The chemical inertness and the non-toxicity of TiO_2 have also made it a superior photocatalyst [7-8]. Titania has a large band gap (3.20 eV for anatase TiO_2) and therefore, only a small fraction of solar light can be absorbed [9]. The codoping of metal and non-metal into the Titania has shown affirmative results in extending the photoresponse of Titania into the visible light region and getting better charge separation [10]. This leads to improved photocatalytic activity of codoped Titania compared to single doped and undoped Titania [11]. Variation of Titania with non-metal for example sulphur, nitrogen, phosphorus, carbon, etc., introduces mid-band gap states within the band gap of titania leading to band gap narrowing and visible light absorption [12-13]. The impregnation of metallic species such as palladium, gadolinium, lanthanum, iron, samarium, cobalt, silver, etc., has been found to improve charge separation in titania by acting as electron scavengers [14-16].

Many attempts have been made to sensitize titanium dioxide to the whole visible region, such as doping with transition metals [17], transition metal ions [18], non-metal atoms [19] and organic materials [20]. Introduction of dopant allows Titania to absorb in the visible region but this does not necessarily mean that the doped catalyst has a better photocatalytic activity [21].

In photocatalysis, light is absorbed by an adsorbed substrate. Today, semiconductors are usually selected as photocatalysts, because semiconductors have a

narrow gap between the valence and conduction bands [22]. In order for photocatalysis to proceed, the semiconductors need to absorbed energy equal to or more than its energy gap. When TiO_2 is irradiated by UV light (400 nm or less), electron is excited to generate electron (e^-) hole (h+) pairs. This movement of electrons forms e^-/h^+ or negatively charged electron/positively charged hole pairs [23]. The hole can oxidize donor molecules. In photogenerated catalysis, the photocatalytic activity (PCA) depends on the ability of the catalyst to create electron–hole pairs, which generate free radicals able to undergo secondary reactions [24].

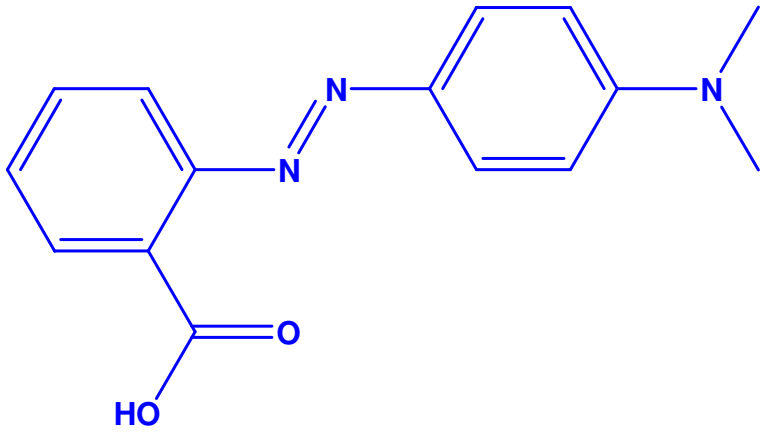

Fig.7.1. molecular structure of Methyl Blue

7.2. Methodology

7.2.1 Synthesis of Titania by wet chemical method.

In this method, both $TiCl_4$ solution (1000 mg/l) and NaOH solution (64.5 g/l) was added drop wise to water with stirring. After the resulting solution reaches pH to 7, the slurry was filtered, and the filter cake of TiO_2 was washed and redispersed in water to prepare 1 M of TiO_2 slurry. Resulting TiO_2 slurry and an aqueous solution of HNO_3 were refluxed at 95^0C for 2 h, cooled to room temperature and neutralized with 28% of aqueous ammonia. Then, it was filtered, washed and calcined at 400 ^{o}C [25, 26].

$$TiCl_4 + 4NaOH + NH_3 \longrightarrow Ti(OH)_4 + 4NaCl$$
$$Ti(OH)_4 \longrightarrow TiO_2 + 2H_2O$$

7.2.2 Synthesis of Co:La:TiO_2 nanocomposite

In this study, Co:La:TiO_2 nanocomposites were prepared by solution impregnation method. In this method, suitable quantity of prepared TiO_2 (2 g) was dispersed in alcoholic cobalt acetate 10% (w/v) and lanthanum nitrate 5% (w/v). The dispersion is agitated continuously for 4 hour at 80 ^oC temperature. After the treatment, the residue was removed through filtration and was sintered for 4 hour in presence of air at 600 ^oC by kipping it in a silica crucible inside the muffle furnace. After sintering and slow anilling to room temperature, content was taken out from furnace and was stored in air tight bottles and was used as photocatalyst [27].

$$TiO_2 + Co(CH_3COO)_2 + La(NO_3)_3 \longrightarrow Co:La:TiO_2$$

7.2.3. Characterization

The physical properties of metal oxide semiconductor nanocomposites that may influence significantly their use as photocatalyst are dependent on nature of crystalline phase present. Thus, phase analysis is an important parameter for this study and the prepared samples were subjected to x-ray diffraction analysis on Powder X-Ray Diffractometer. The observed X-Ray diffractogram of samples were analyzed further to estimate average grain size in the sample by Scherrer's calculation. Since the absorption of light by photocatalyst is the most crucial step in any photocatalysed reaction and is decided primarily by the band gap energy of material. The morphology and size of the Titania particles were analyzed by scanning electron microscopy (SEM) and transmission electron microscopy (TEM).

7.2.4. Photo-degradation of dyes

In this work, the photo-catalytic degradation of Methyl Blue was investigated. A solution of dye in water: alcohol (10:1 V/V) was prepared and in this solution, a suitable quantity of photocatalyst (100 to 800 mg/L) was dispersed. The dispersion was subjected to Visible light irradiation for varying duration and after desired irradiation, the residual concentration of dye in the solution was determine spectrophotometrically by taken out suitable aliquot of dispersion and removal of photocatalyst by centrifugation. For quantitative estimation of dye concentration, initially calibration curve was obtained and it was utilized to measure the concentration in different sample aliquot obtained at different time. A quantitative estimation of dye concentration spectrometric observation when recorded only at the experimental determines λ max value which is 670 nm [28-30].

7.3. Results

7.3.1. Phase identification by X-ray diffraction analysis

The obtained X-Ray diffraction patterns of Titania and Co:La:TiO_2 are shown in Figures 7.2 (a) and (b). The observed pattern of peaks, when compared with the standard JCPDS database, suggested that, in prepared TiO_2 sample, major peaks at 2θ = 25.5 □ 37.2, 48.3, and 54.4, which can be indexed to the (101), (004), (200), and (211) crystal facets of anatase TiO_2 (JCPDS File number: 21-1272). Whereas major peaks at 2θ = 26.9º and 28.2º indicate the presence of rutile phase which can indexed to the (110), (121), respectively. In case of Co:La:TiO_2 sample, the observed XRD pattern indicates not only a change in the peak intensity, compared to TiO_2, but even the absence of some originally observed TiO_2 peaks [31]. This is, probably, due to the change in the crystallinity and grain fragmentation, when the samples were wet impregnated by cobalt and Lanthanum.

7.3.1.1. Determination of Average size of Particles/ Grains in samples

The Scherrer's calculations were attempted to know the average size of particles/grains in the samples [32]. Although, Scherrer's calculations are only approximate in nature, but definitely provide a first-hand idea of the average size of the

particles/ grains in the samples, which may be quite accurate, provided the size of particles/ grains is below 100 nm. The results of Scherrer's calculations are presented in Table 7.1. The results suggest average size of the particles/ grains in the samples lying in nm range.

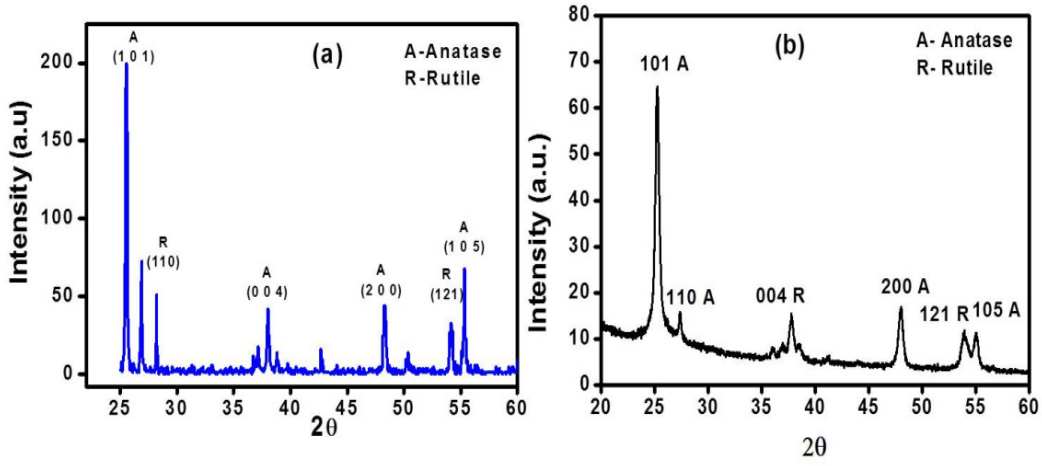

Fig.7. 2. Observed XRD pattern (A) TiO_2 (B) Co:La:TiO_2

Table.7.1. Average size of particles/grains in the samples of TiO_2 and Co:La:TiO_2

Sample	Particle Size
TiO_2	68
Co:La:TiO_2	32

7.3.2. Scanning Electron Microscopy (SEM)

The morphology of the samples was investigated by scanning electron microscopy and it resumes the most interesting outcomes. Fig.7.3 (a) and 7.3 (b) clearly show that both the prepared samples are obtained in nanometric dimension. The doping of cobalt and lanthanum is indicating that the particle size reduce due the penetration of cobalt and lanthanum in the lattice of titanium dioxide [33].

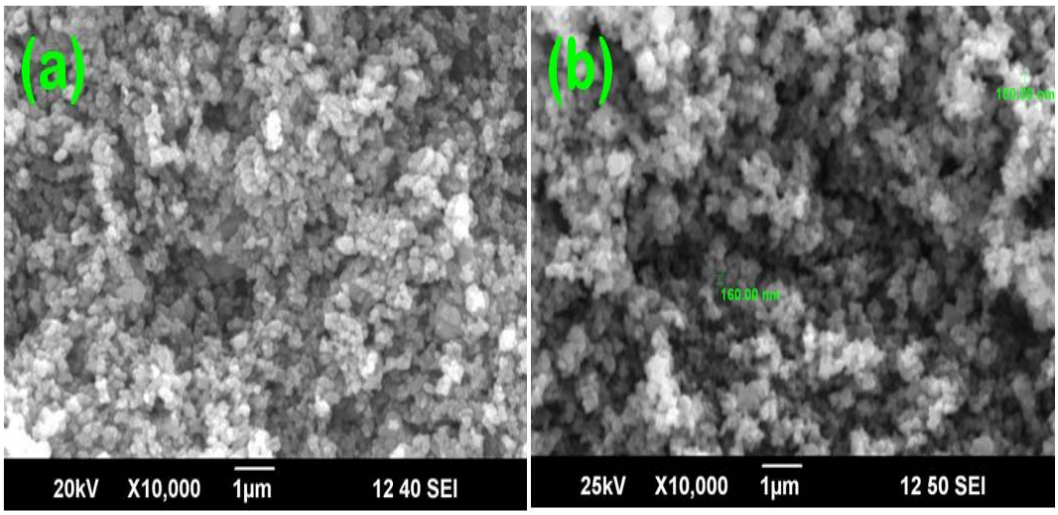

Fig.7.3. SEM image of the (A) TiO_2 (B) Co:La:TiO_2

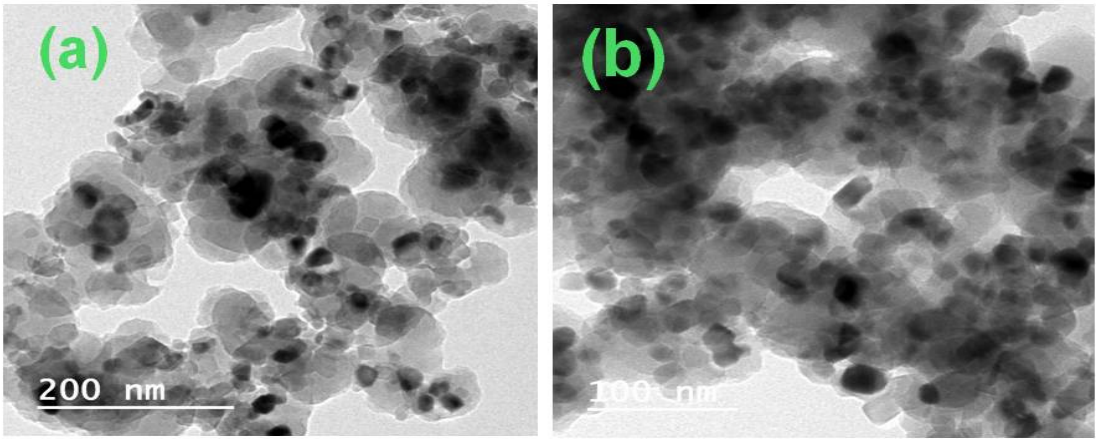

Fig.7.4. TEM image of the (a) TiO_2 (b) Co:La:TiO_2

7.3.3. Transmission Electron Microscope (TEM)

TEM images were clearly displayed the morphology and particle size of neat TiO_2 and Cobalt and lanthanum doped TiO_2. It is observed from the Fig.7.4 that Cobalt and lanthanum doped modified TiO_2 change the size of neat TiO_2 significantly. The sizes of both modified and neat TiO_2 are mono disperse was found 100–200 nm. Moreover, the

crystal lattice line can be clearly found in the TEM images. The aggregations of both kinds of particles are caused by high surface energy; however, the agglomeration of the modified one is alleviated obviously compared with that of the neat [34].

7.3.4. Surface Area Analysis (BET)

Figure 7.5 shown the BET and adsorption and desorption plot for the TiO_2 and Co:La:TiO_2. With the help of Figure 7.5, we can determine the specific surface area, pore volume and average pore size of the TiO_2 and Co:La:TiO_2 photocatalyst. Table 7.2 shown the physical properties of TiO_2 and Co:La:TiO_2. The TiO_2 modified by Cobalt and Lanthanum are fragmentation to some extent during thermal treatment, leading to a marked increase of the *BET* surface areas and the average pore radius size and decreasing of the pore volume [35, 36].

Table.7.2. The specific surface area, pore volume and pore radius of the TiO_2 and Co:La:TiO_2

Sample	Surface area (m^2/g)	Pore volume (cm^3/g)	Pore radius (nm)
TiO_2	37. 52	10.132	1.21
Co:La:TiO2	106.68	9.5124	1.64

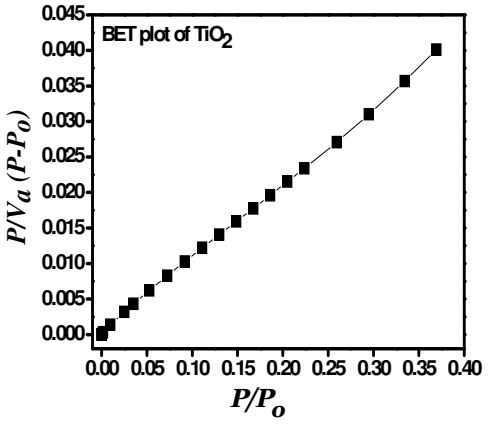

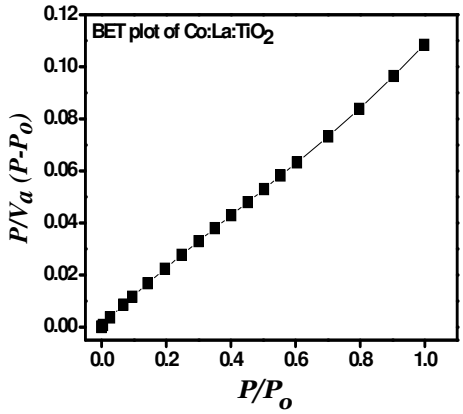

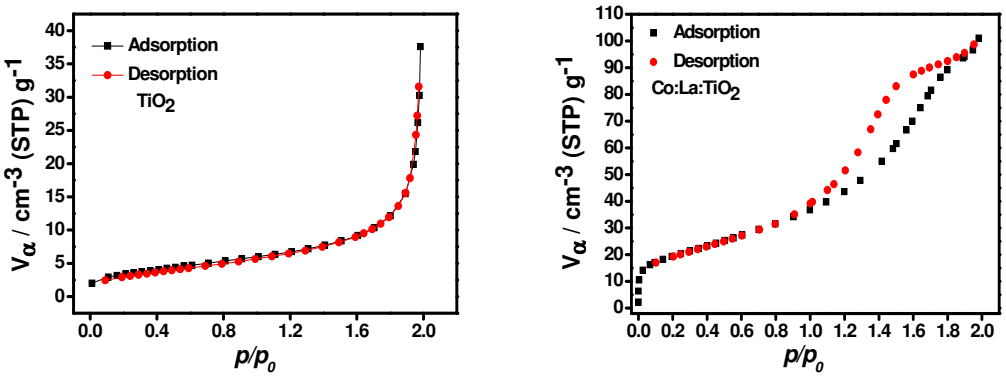

Fig.7.5. BET and Adsorption desorption plot for TiO_2 and Co:La:TiO_2

7.3.5. FT-IR spectroscopy

FT-IR spectra of TiO_2 and 10% Co and % La doped TiO_2 samples (Fig.7.6) show peaks corresponding to stretching vibrations of the O-H and bending vibrations of the adsorbed water molecules around 3350-3450 cm^{-1} and 1620-1635 cm^{-1}, respectively. The broad intense band below 820, 804, 592 and 456 cm^{-1} is due to Ti-O-Ti vibrations. The shift to the higher wave numbers and sharpening of the Ti-O-Ti band may be due to decrease in size of the catalyst nanoparticles.

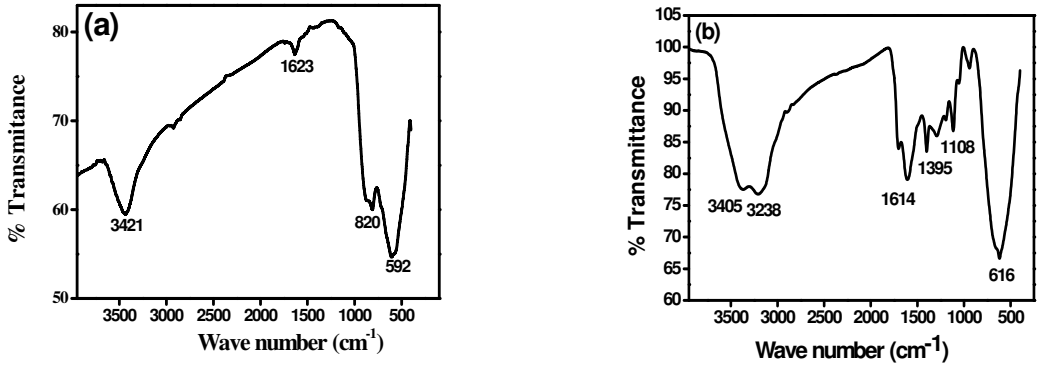

Fig.7.6. FT-IR spectra of (a) TiO_2 (b) Co:La:TiO_2

In addition, the surface hydroxyl groups in TiO_2 increased with the increasing of Co and La loading, which is confirmed by increase in intensity of the corresponding

peaks. The FT-IR spectra of Co:La:TiO_2 show strong band at 616 cm^{-1}, corresponds to the vibration of Co–O bond and confirms the penetration of Cobalt in Titania [37].

7.3.6. UV-Vis spectra

Aqueous suspensions solution of the photocatalysts was used for the UV absorption studies. The absorption spectrum of TiO_2 consists of a single broad intense absorption at 371nm due to the charge-transfer from the valence band to the conduction band. The undoped TiO_2 showed absorbance in the shorter wavelength region while Co:La:TiO_2 result showed a broad peak at 407 nm in the higher wavelength (shown in Fig.7.7). The doping of Co and La ions into TiO_2 could shift optical absorption edge from UV to visible range, but prominent change in TiO_2 band gap was observed [38].

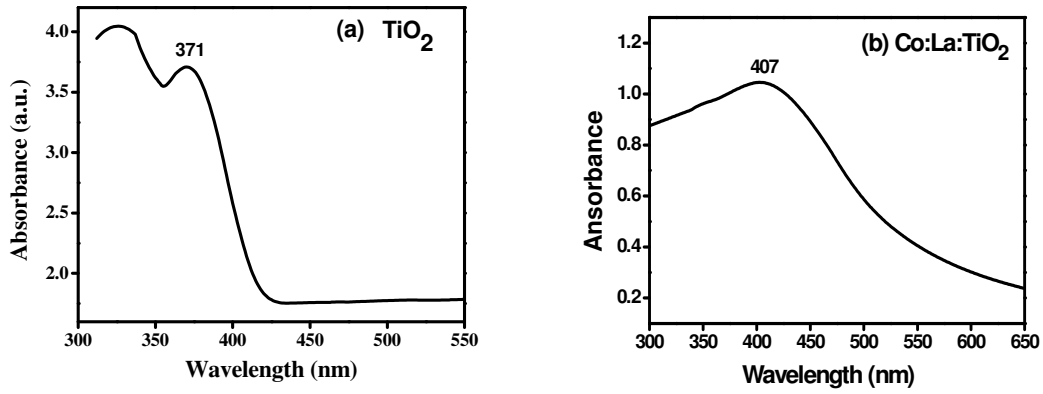

Fig.7.7. UV- spectra of (a) TiO_2 (b) Co:La:TiO_2

7.3.7. Band gap energy determination

The band gap of samples was calculated by extrapolation of the $(\alpha h\nu)^2$ versus $h\nu$ plots, where α is the absorption coefficient and $h\nu$ is the photon energy, $h\nu = (1239/\lambda)$ eV. The value of $h\nu$ extrapolated to $\alpha = 0$ gives an absorption energy, which corresponds to a band gap (Eg). Fig.7.8 yields an Eg value of 3.2 eV for TiO_2 and 3.0 for Co:La:TiO_2 [39]. The slight decrease in band gap energy in case of Co:La:TiO_2, is due to formation of sub-band level between valence band and conduction band caused doping of Co^{+2} and La^{+3} in TiO_2 host.

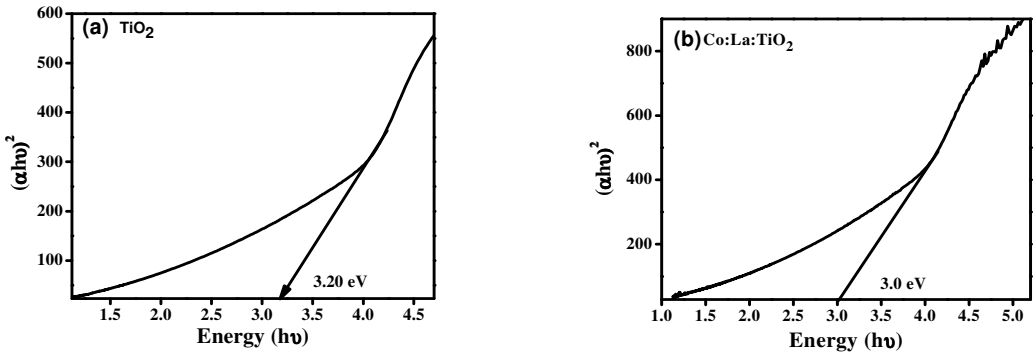

Fig.7.8. Band gap energy of (a) TiO_2 (b) Co:La:TiO_2

7.3.8. Photo-degradation of Dyes

The photo-catalytic degradation of Methyl Blue in the presence of TiO_2 and Co:La:TiO_2 has been studied. The solution of dye was prepared in 10:1 (V/V) ratio of water and alcohol. The known amount of photocatalyst 800 mg/L was dispersed in the dye solution. The reaction mixture was illuminated under visible light, while kept continuously under agitation, for the different time intervals and different temperature. The residual concentration of dye in the reaction mixture was measured spectrophotometrically. The results obtained for the degradation of Methyl Blue is shown in Fig.7.9 - 7.11.

7.3.8.1. Effect of Temperature

The effect of system temperature on photocatalysis has not attracted enough attention. But In present research, it is found that the temperature has a great effect on the photodegradation of Methyl Blue. The photocatalytic efficiency can be increased about 2-3 times if the temperature increased from 30 ℃ to 40 ℃ Because the solar energy include UV light, which can be used to activate the photocatalytic course, which is increase the temperature of photocatalytic system. The experiments showed that Methyl Blue were photodegraded in presence of photocatalyst and Visible light. The Methyl Blue was

efficiently degraded shown in Fig.7.9. The obvious decrease of concentration of dye shows that the TiO_2 and Co:La:TiO_2 can serve as an effective photocatalyst [40].

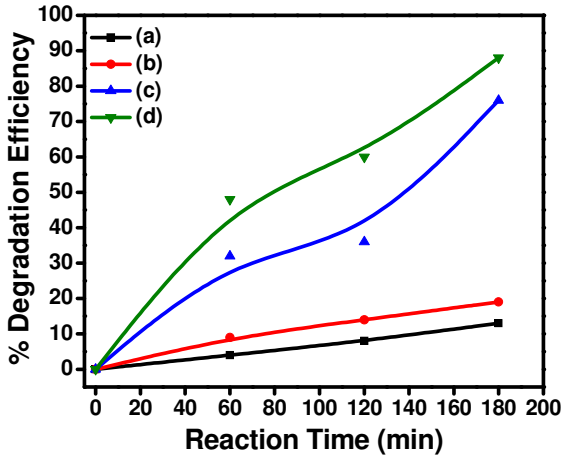

Fig.7.9. Photodegradation of Methyl Blue at initial concentration 50 ppm (a) TiO_2 at 30°C (b) TiO_2 at 40°C (c) Co:La:TiO_2 at 30°C (d) Co:La:TiO_2 at 40°C.

7.3.8.2. Effect of concentration of dye

Effect of dye concentration Keeping the catalyst loading concentration constant at 800 g/liter of the dye solution, the effect of varying concentration of the dye was studied on its rate of degradation (from 25 ppm to 100 ppm) as given in Fig.7.10. With increasing concentration of Methyl Blue the rate of degradation was found to decrease. This is because as the number of dye molecules increase, the amount of light (quantum of photons) penetrating the dye solution to reach the catalyst surface is reduced owing to the hindrance in the path of light. Thereby the formation of the reactive hydroxyl and superoxide radicals is also simultaneously reduced. Thus there should be an optimum value maintained for the catalyst and the dye concentration, wherein maximum efficiency of degradation can be achieved [41].

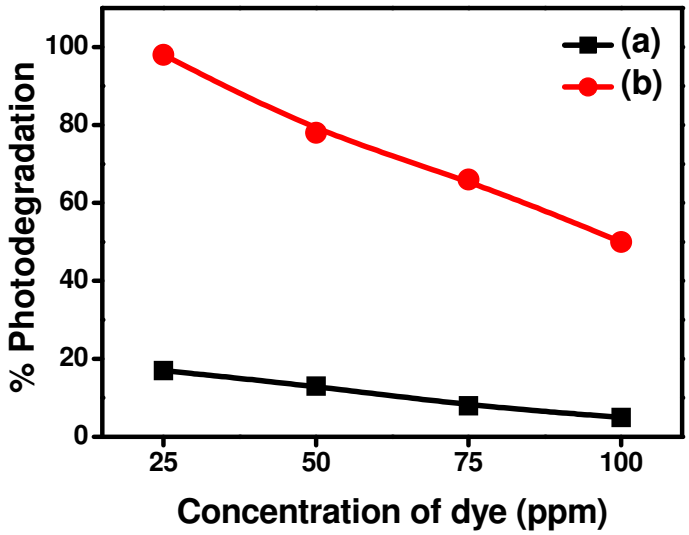

Fig.7.10. Effect of concentration of dye on Photocatalytic degradation of Methyl Blue with (a) TiO_2 (b) Co:La:TiO_2

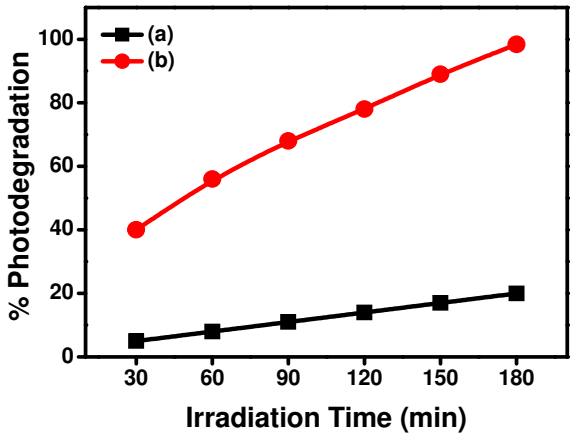

Fig.7.11. Effect of irradiation time dye on Photocatalytic degradation of Methyl Blue with (a) TiO_2 (b) Co:La:TiO_2

7.3.8.3. Effect of irradiation Time on photodegradation

The effect of irradiation time on the photodegradation of methyl blue has been studied in presence of TiO_2 and Co:La:TiO_2. The photodegradation of methyl blue was

increased with increase irradiation time. The photodegradation was found maximum in case of Co:La:TiO_2 for 180 min irradiation of visible light. Fig.7.11 shows the effect of irradiation time on photocatalytic degradation of methyl blue. This is due to the interaction of dye molecule with the surface of photocatalyst as well as the time of irradiation increase the interaction increased. Therefore the photodegradation efficiency of photocatalyst was increased.

7.3.8.4. Effect of pH of solution

The photodegradation reaction was also carried out under varying ph conditions from (2 to 9), by adjusting with H_2SO_4 and NaOH, with TiO_2 kept at constant amounts of 800 mg/ L of dye solutions (Fig.7.12). The reaction was found to have low rates at acidic ranges of pH. While at pH 5 photodegradation was found maximum. This implies that less acidic conditions are favourable towards the formation of the reactive intermediates that is hydroxyl radicals is significantly enhanced, which further help in enhancing the reaction rate. On the other hand in highly acidic medium conditions for the formation of reactive intermediates is relatively less favourable and hence less spontaneous [42].

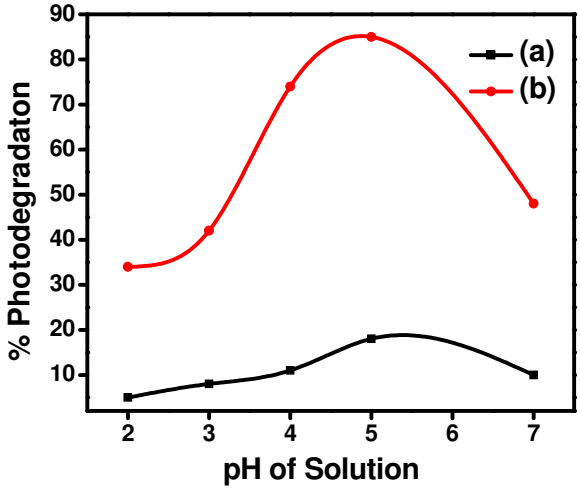

Fig.7.12. Effect of pH (a) TiO_2 (b) Co:La:TiO_2

7.3.8.5. Effect of photocatalyst amount

The effect of photocatalyst amount has been studied by applying the different amount (100 ppm to 800 ppm) of the photocatalyst. The photodegradation rate was found to increase by increasing the amount of photocatalyst. It is clear from the results shown in Fig.7.13, the photodegradation increased rapidly with increase of amount of Co:La:TiO_2. This is due to the fact that introduction of Co^{2+} and La^{3+} the band gap energy decreased up to 3.0 eV which enhance the photocatalytic activity [43].

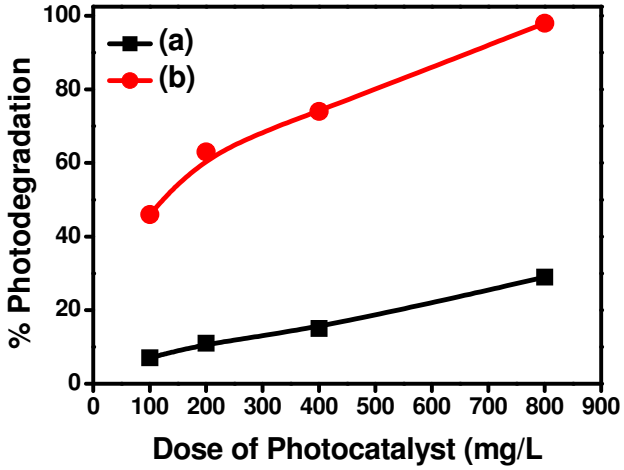

Fig.7.13. Effect of photocatalyst amount on photodegradation of Methyl Blue

7.3.8.6. Effect of photocatalyst

It is clear from the results shown in Fig.7.9-7.12 that both TiO_2 and Co:La:TiO_2 are effective photo-catalyst for the degradation of Methyl Blue (MB) dye. However Co:La:TiO_2 seems to be more effective as photo-catalyst for the degradation of Methyl Blue (MB). The prominent degradation of Methyl Blue was found in 3 hour study in the presence of Co:La:TiO_2 in comparison to the prepared TiO_2 [44].

7.3.9. Recyclability of photocatalyst

The photocatalyst and Methyl Blue mixture was agitated, illuminated with visible light and after desired time, the mixture was centrifuge to remove the photocatalyst. The

obtained photocatalyst was washed three times with distilled water and kept in oven for 24 h at 60 ^{o}C and reused for the degradation of Methyl Blue. The photodegradation of Methyl Blue by the recyclized Photocatalyst are showing in Fig.7.14. The result shows that the recyclized photocatalyst efficiency is slightly decreased probably due to the loss of some active sites and decrease of collection efficiency of photon [45].

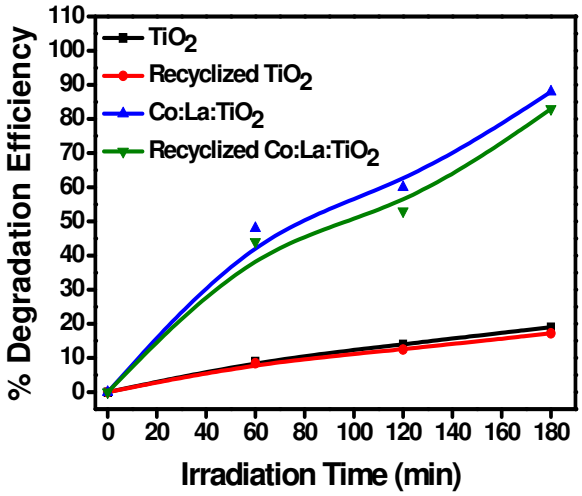

Fig.7.14. Photodegradation of Methyl Blue by recyclable photocatalyst TiO_2 and Co:La:TiO_2

7.3.10. Lowering of electron-hole recombination

Photoluminescence spectra have been used to examine the mobility of the charge carriers to the surface as well as the recombination process involved by the electron-hole pairs in semiconductor particles. PL emission results from the radiative recombination of excited electrons and holes. In other words, it is a critical necessity of a good photocatalyst to have minimum electron-hole recombination. To study the recombination of charge carriers, PL studies of synthesized materials have been undertaken. PL emission intensity is directly related to recombination of excited electrons and holes. Fig.7.15 shows the photoluminescence spectra of synthesized photocatalysts. In the PL spectra the

intensity of TiO_2 is higher than Co:La:TiO_2 indicating rate of recombination of e^-- h^+ is higher in TiO_2 than that of Co:La:TiO_2.The weak PL intensity of Co:La:TiO_2 may arise due to the impregnation of Ni in Titania lattice, which for sub band level in band gap region of TiO_2. This delays the electrons- holes recombination process and hence utilized in the redox, reaction leading to improved photocatalytic activity [46].

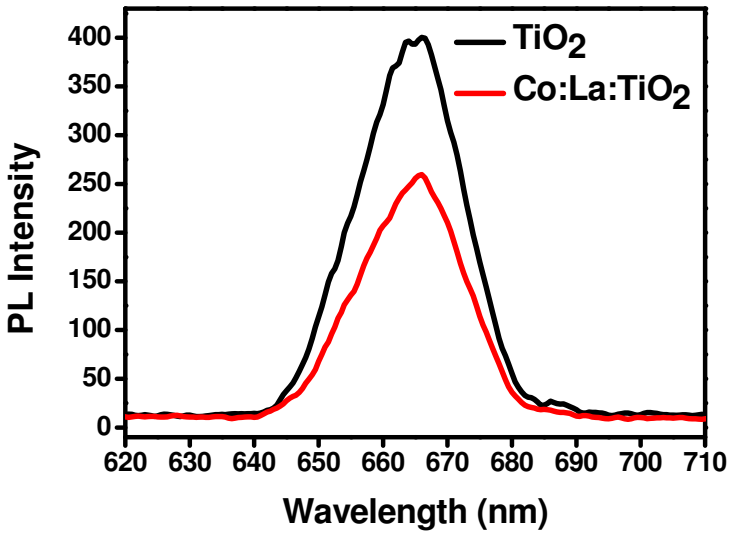

Fig.7.15. Photolumiscence Spectra of (a) TiO_2 (b) Co:La:TiO_2

7.3.11. Hydroxyl radical formation

As hydroxyl radical performs the key role for the decomposition of the organic pollutants, it is necessary to investigate the amount of hydroxyl radicals produced by each photocatalyst. In this study, terephthalic acid (TA) has been used as a probe reagent to evaluate $^{\bullet}OH$ radical present in the photoreaction pathway. Fig.7.16 shows the PL spectra of TiO_2 and Co:La:TiO_2 recorded Methyl Blue solution in presence of 10^{-3}M Terephthalic solution. OH radical attack Terephthalic, forming 2- hydroxyl terephthalic acid (TAOH) which gives a fluorescence signal at 426 nm. The fluorescent intensity is linearly related to the number of hydroxyl radicals formed by the photocatalysts. Higher the generation of hydroxyl radical, more will be yield of TAOH and hence more intense will be the

fluorescence peak [47]. The spectra show that the intensity of peak indicating in presence of Co:La:TiO_2 higher generation of more number of hydroxyl radicals compared to TiO_2.

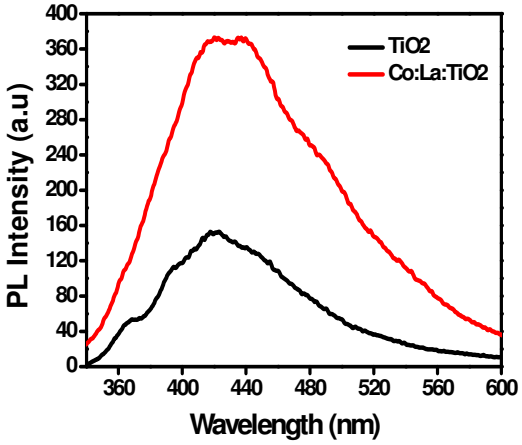

Fig.7.16. PL spectra of photocatalysed Methyl Blue solution in presence of terephthalic acid (0.001M) (a) TiO_2 (b) Co:La:TiO_2

7.3.12. Mechanism of photooxidation process

The photocatalytic mechanism is initiated by the absorption of the photon hv with energy equal to or greater than the band gap of TiO_2 (3.3 eV for the anatase phase) producing an electron hole pair on the surface of TiO_2 nanoparticles. An electron is promoted to the conduction band (CB) while a positive hole is formed in the valence band (VB). Excited state electrons and holes can recombine and dissipate the input energy as heat, get trapped in metastable surface states, or react with electron donors and electron acceptors adsorbed on the semiconductor surface or within the surrounding electrical double layer of the charged particles. After the reaction with water, these holes can produce hydroxyl radicals with high redox oxidizing potential [48-50]. Depending upon the exact conditions, the holes, OH radicals, O^-_2, H_2O_2 and O_2 itself, When the semiconductor is illuminated with light (hυ) of greater energy than that of the band gap, an electron is promoted from the VB to the CB leaving a positive hole (h^+) in the valence

band and an electron (e^-) in the conduction band as illustrated in Fig.7.17. If charge separation is maintained, the electron and hole may migrate to the catalyst surface where they participate in redox reactions with sorbed species. Specially, h^+_{vb} may react with surface-bound H_2O or OH^- to produce the hydroxyl radical and e^-_{cb} is picked up by oxygen to generate superoxide radical anion (O_2^-), as indicated in the following equations 6-8;

Absorption of efficient photons by titania ($h\upsilon \geq E_{bg} = 3.2$ ev)

$$TiO_2 + h\upsilon \rightarrow e_{cb} + h^+_{vb} \quad (6)$$

Formation of superoxide radical anion

$$O_2 + e_{cb} \rightarrow O_2^- \quad (7)$$

Neutralization of OH^- group into OH by the hole

$$(H_2O \square H^+ + OH^-)_{ads} + h^+_{vb} \rightarrow {}^{\bullet}OH + H^+ \quad (8)$$

It has been suggested that the hydroxyl radical ($^{\bullet}OH$) and superoxide radical anions ($O_2^{\cdot -}$) are the primary oxidizing species in the photocatalytic oxidation processes. These oxidative reactions would results in the degradation of the pollutants as shown in the following equations 9-10;

Oxidation of the organic pollutants via successive attack by OH radicals

$$R + {}^{\bullet}OH \rightarrow R^{\cdot} + H_2O \quad (9)$$

or by direct reaction with holes

$$R + h^+ \rightarrow R^{\cdot +} \rightarrow \text{degradation products} \quad (10)$$

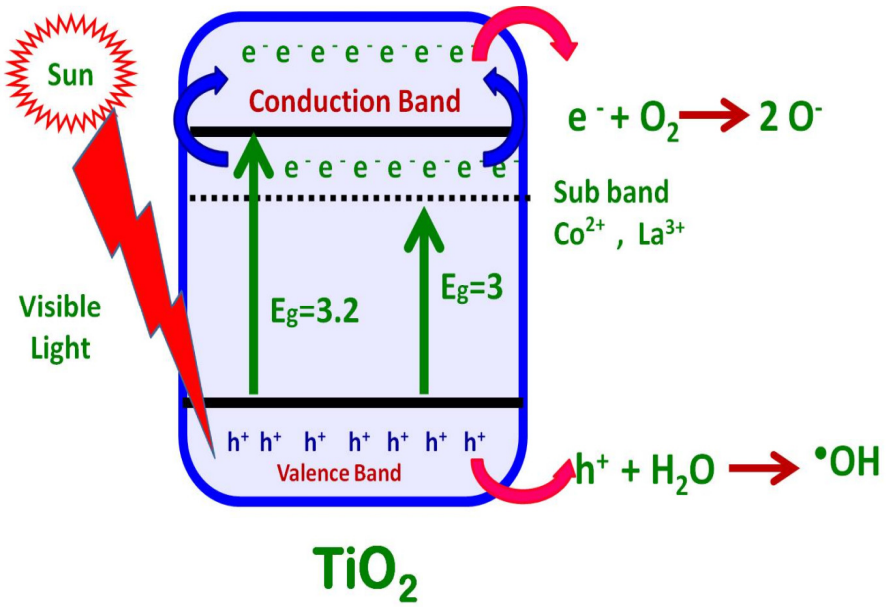

Fig.7.17. Mechanism of photodegradation of Titania and formation of free radical.

7.3.13. Kinetic study

The pseudo-first-order rate constant (k, min^{-1}) for the photodegradation reaction of Methyl Blue was determined through the following relation where k can be calculated from the plot of $\ln(C_o/C_t)$ against time (t), C_o and C_t denote the initial concentration and reaction concentration, respectively.

$$k_1 t = \ln C_o / C_t$$

In addition, the linear feature of plots of $\ln(C_o/C_t)$ versus time (Fig.7.18 and 7.19) indicates that this photocatalytic degradation reactions follow the pseudo-first-order rate law [51-54]. The rate constant of the photocatalysis at 30 ^oC is 0.04260 to 0.0234 min^{-1}. The effect of temperature and concentration are showing in table 7.3.

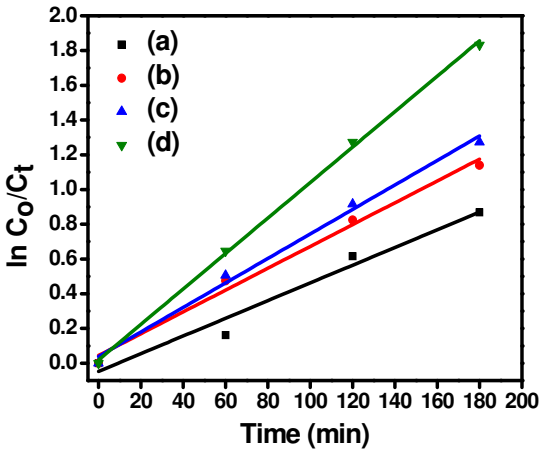

Fig.7.18.The straight line relationship between the ln (C_o/ C_t) and irradiation time indicates photodegradation rate of Methyl Blue (50 ppm) can be approximated by a pseudo first order reaction (a) TiO_2 at 30°C (b) TiO_2 at 40°C (c) Co:La:TiO_2 at 30°C (d) Co:La:TiO_2 at 40°C.

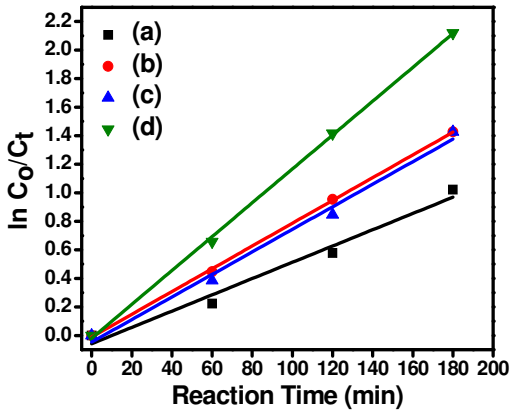

Fig.7.19.The straight line relationship between the ln (C_o/ C_t) and irradiation time indicates photodegradation rate of Methyl Blue (100 ppm) can be approximated by a pseudo first order reaction (a) TiO_2 at 30°C (b) TiO_2 at 40°C (c) Co:La:TiO_2 at 30°C (d) Co:La:TiO_2 at 40°C.

Table.7.3. The effect of concentration and temperature on rate constant

	100 ppm				50 ppm			
	k (min^{-1})	R^2	k (min^{-1})	R^2	k (min^{-1})	R^2	k (min^{-1})	R^2
Sample	30 °C		40 °C		30 °C		40 °C	
TiO_2	0.006	0.969	0.008	0.999	0.005	0.955	0.006	0.986
Co:La:TiO_2	0.008	0.988	0.012	0.998	0.007	0.990	0.010	0.998

Conclusion

Prepared nanocomposites of Co:La:TiO_2 were characterized by X-Ray Diffractometer, SEM, TEM, UV- Vis, FT-IR, Band gap energy and BET. The TiO_2 and Co:La:TiO_2 were used as photocatalyst for the degradation of Methyl Blue. The particle size was estimated by the Scherrer's and found 68 and 32 nm for TiO_2 and Co:La:TiO_2 respectively. The surface area of the photocatalysts were found 37.52 and 106.68 m^2/g for TiO_2 and Co:La.TiO_2 respectively. The band gap energy of TiO_2 and Co:La.TiO_2 were 3.2 and 3.0 eV. The photodegradation of Methyl Blue has been found maximum at 5 pH, 25 ppm concentration of dye, 800 mg/L amount of photocatalyst and 180 min illumination of visible light. The photodegradation was following the first order kinetics.

References

[1]. M.A. Mahmoud, A. Poncheri, Y. Badr, Journal of Science, 105, (2009), 299–303.

[2]. T. Sauer, G. C. Neto, H. J. Jos´e, and R. F. P. M. Moreira, Journal of Photochemistry and Photobiology A: Chemistry, 149 ,(2002), 147–154.

[3]. S. K. Kavitha and P. N. Palanisamy, International Journal of Civil and Environmental Engineering, 3 (2011), 1–6,

[4]. H. Lee, Y.K. Park, S.J. Kim, B.H. Kim, S. C. Jung, Journal of Industrial and Engineering Chemistry, 32, (2015), 259-263

[5]. M.N. Makwana, J. T. Christopher, I. G. Robert, Paul F. McMillan, Materials Science in Semiconductor Processing, 42, (2016) ,131-137

[6]. S. Liu, N. Jaffrezic, C. Guillard, Appl. Surf. Sci. 255, (2008), 2704-2709.

[7]. A. Gnanaprakasam, V.M. Sivakumar, P.L. Sivayogavalli, M. T. Murugan, Ecotoxicology and Environmental Safety, 121 (2015) ,121-125

[8]. D. N. Wang, J. P. Tafen, Journal of theAmerican Chemical Society, 131,(2009), 12290–12297.

[9]. N. Hariprasad, S. G. Anju, E. P. Yesodharan, and Y. Suguna Research Journal of Material Science, 1,(2013), 9–17.

[10]. Z. Zhang, Z. Brown, J.B.M. Goodall, X. Weng, K. Thompson, K. Gong, S. Kellici, R.J.H Clark, J.R.G. Evans, and J. A. Darr, J. Of Alloys and Compounds,476 (2009) ,451-456

[11]. S. Girish Kumar and L. Gomathi Devi, J. Phys. Chem. A, 115, (2011), 13211–13241

[12]. H. Jia, Z. Zheng, H. Zhao, L. Zhang, and Z. Zou, Materials Research Bulletin, 44,(2009), 1312-1316.

[13]. C. G. Silva, W. Wang, J. L. Faria, J. Of Photochemistry and Photobiology A: Chemistry, 181,(2006), 314-324.

[14]. A. G. Epling, Chitsan Lin (2002), Chemosphere, 46, 4, 561-570.

[15]. Yoichi Ishibai, Takashi Nishikawa and Shigeyoshi Miyagishi, Journal of, dispersion science and Technology, (2006), 27, 1093.

[16]. M. Sökmen, A. Özkan, Journal of Photochemistry and Photobiology A: Chemistry 147, (2002), 77–81.

[17]. Y. Badr, M.G. Abd El-Wahed, M.A. Mahmoud,J. Of Hazardous Materials, **154,**(2008), 245-253.

[18]. A. Akyol, M. Bayramoglu, Chemical Engineering, and Processing: Process Intensification, 47 ,(2008),2150-2156.

[19]. A.K. Gupta, A. Pal, C. Sahoo, Dyes and Pigments, 69,(2006),224-232.

[20]. S.A. zakarya, A. Kassim, H.N. Lim, N.S. Anwar & N. M.Huang, sains malaysiana, 39 ,(2010), 975–979.

[21]. B. Rohit, S. Madhulika, D. Bahadur, Dalton Trans 42(19) (2013),6736–6744.

[22]. K. Selvam, M. Muruganandham, I. Muthuvel, M. Swaminathan, J Chem Eng 128 (2007), 51–57.

[23]. R. Ufana, S.M. Ashraf, Chem Eng J 174 (2012),546–555

[24]. D. Zhao, G. Sheng, C. Chen, X. Wang, Appl Catal B: Environ 111 (2012), 303–308.

[25]. C. Hu, Y. Wang, Chemosphere 39 (1999), 2107–2115.

[26]. P.V. Kamat, K. Vinodgopal, D.E. Wynkoop, Environ. Sci. Technol. 30, (1996), 1660–1666.

[27]. G. Liu, T. Wu, J. Zhao, H. Hidaka, N. Serpone, Environ. Sci. Technol. 33, (1999), 2081–2087.

[28]. K. Tanaka, K. Padermpole, T. Hisanaga, Wat. Res. 34, (2000), 327–333.

[29]. Y. Zhu, S. Xu, D. Yi, Reactive & Functional Polymers 70, (2010), 282–287

[30]. B. D. Cullity, S. R. Stock, Elements of X-Ray Diffraction, Third Edition, and New Jersey: Prentice-Hall, Inc. (2001).

[31]. W.Z. Tang, H. An, Chemosphere 31 (1995), 4171–4183.

[32]. W.Z. Tang, H. An, Chemosphere 31 (1995),4157–4170.

[33]. X. Wang, G. Chen, J. Zhang, Catal. Commun. 31(2013), 57−61.

[34]. C.S. Danielle, S.M. Michelle, A.H. Ivo, J.G.Z. Aldo, Chem. Mater. 15(2003), 4658-4665.

[35]. J. Zhao, C. Chen, W. Ma, Topics in Catalysis. 35 (2005), 269-278

[36]. D.S. Wang, J. Zhang, Q.Z. Luo, X.Y. Li, Y.D. Duan, J. Hazard. Mater, 169 (2009), 546-550.

[37]. M.A. Salem, A.F. Al-Ghonemiy, A.B. Zaki, Appl. Catal. B: Environ. 91 (2009), 59-66

[38]. K. Madhusudan Reddy, Sunkara V. Manorama, A. Ramachandra Reddy, Materials Chemistry and Physics 78 (2002), 239–245.

[39]. L. Gu, J. Wang, R. Qi, X. Wang, P. Xu, X. Han, J. Molec. Catal. A: Chem. 357(2012), 19–25.

[40]. K. Vinodopal, D.E. Wynkoop, P.V. Kamate, Environ. Sci, Technol 30 (1996), 1660.

[41]. M. Saquib, M. Muneer, Dyes,and Pigments 56 (2003), 37.

[42]. K. Tanaka, K. Padermpole, T. Hisanaga, Water. Res. 34(2000), 327.

[43]. C. Galino, A. Kalt, Dyes,and Pigments 40 (1998), 27.

[44]. C.Hu, J. C. Yu, Z. Hao, P.K. Wong, Applied catalysis B: Environmental 46(2003), 35.

[45]. I.K. Konstantinou, T.A. Albanis, Appliedcatalysis B: Environmental 49 (2004), 1.

[46]. B. Wang, F. Wu, P. Li, N. Deng, React kinet catal. Lett. 92 (2007) 3.

[47]. M. Neamtu, I. Siminiceanu, A. Yediber, A.Kettrup, Dyes,and Pigments 53(2002), 93.

[48]. E. Baran, B. Yazici, International Journal of Hydrogen Energy, 41 (2016) 2498-2511.

[49]. Q. Sun, Y. Xu, J. Phys. Chem. C 113 (2009), 12387-12394.

[50]. S. Wang, Dyes and Pigments 76(3) (2008) 714.

[51]. E. Vulliet, J.M. Chovelon, C. Guillard, J.M. Herrmann, J. Photochem. Photobiol. A: Chem. 159 (2003), 71–79.

[52]. N. Guettaı, H.A. Amar, Desalination 185 (2005), 439–448.

[53]. D. Chen, A.K. Ray, Appl. Catal. B: Environ. 23, (1999), 143–157.

[54]. I. Langmuir, J. Am. Chem. Soc.40, (1918), 1361–1403.

CHAPTER-8

Summery and Conclusion

Titanium dioxide (TiO_2), commonly known as Titania, is one of the most commonly used photocatalysts. Because of its high oxidative power, stability, and non-toxicity, it promises a broad range of uses as a photocatalysts. Advantage of using TiO_2 as photo-catalyst are: (a) using TiO_2, the process occurs under ambient conditions.(b) using TiO_2, the oxidation of the substrate to CO_2 is complete in most cases and (c) it is comparatively inexpensive and remains quite stable in contact with different substrate. TiO_2 has also played a leading role in the active research for the utilization of solar energy. In this thesis, prepared the different nanocomposites by the doping of metals in Titania and polymer based nanocomposites. The prepared materials were characterized by the XRD, FTIR, UV-Vis, BET, SEM, TEM, PL and LCMS. The Photodegradation of Eriochrome Black T, Acetic Acid, Methyl Green, Victoria Blue, Thymol Blue, Methyl Blue and Rose Bengal have been done. In this study, investigate the effect of different parameters on the photodegradation.

8.1 Summery and Conclusion

Titanium dioxide (TiO_2), commonly known as Titania, is one of the most commonly used photocatalysts. Because of its high oxidative power, stability, and non-toxicity, it promises a broad range of uses as a photocatalysts. Advantage of using TiO_2 as photo-catalyst are: (a) using TiO_2, the process occurs under ambient conditions.(b) using TiO_2, the oxidation of the substrate to CO_2 is complete in most cases and (c) it is comparatively inexpensive and remains quite stable in contact with different substrate. TiO_2 has also played a leading role in the active research for the utilization of solar energy. The TiO_2 based, dye sensitized, photo-electrochemical cells are receiving a great deal of attention as a possible candidate for converting solar energy into electricity on a large scale. Titanium dioxide's photocatalytic characteristics are greatly enhanced due to the advent of nanotechnology. At nano-scale, not only the surface area of titanium dioxide particle increases dramatically but also it exhibits other effects on optical properties and size quantization. An increased rate in photocatalytic reaction is observed as the redox potential increases and the size decreases. In some cases, energy from any ambient light source can be used effectively as the energy source of photo catalysis instead of UV light.

Photo catalyst of solarcoat not only have all the advantages of the traditional photocatalyst but also can disinfect, purify air and eliminate harmful substance in the condition of visible light .therefore, it has incomparable technology and quality advantages of fighting against pollution indoors and outdoors. The strong functions of solar coat photocatalysis will completely eliminate odours of newly-decorated houses and enable people to get rid of the danger caused by epidemic disease. Solar coat of photocatalyst has been widely applied in all kinds of fields and highly affirmed & appraised. The theory of photocatalyst: with the irradiation of light, the TiO_2 on the surface of the ultra strong photocatalyst of solarcoat will take photocatalytic reaction the same as photosynthesis which can produce free radical and ozone with strong function of oxidization. And it can oxidize and decompose various organic compounds and some minerals.

Titanium dioxide, particularly in the anatase form, is a photocatalyst under ultraviolet light. Recently it has been found that titanium dioxide when spiked with nitrogen ions or doped with metal oxide like tungsten trioxide, is also a photocatalyst under visible and UV light. The strong oxidative potential of the positive holes oxidizes water to create hydroxyl radicals. It can also oxidize oxygen or organic materials directly. Titanium dioxide is thus added to paints, cements, windows, tiles, or other products for sterilizing, deodorizing and anti-fouling properties and is also used as a hydrolysis catalyst. It is also used in the Graetzel cell, a type of chemical solar cell.

A detailed study of the synthesis, characterization and photocatalytic activity of titania based nanocomposites have been carried out and presented in the thesis. The organization of whole thesis is given below:

Chapter 1: Introduction and literature review

Chapter 2: Photocatalytic degradation of Eriochrome Black-T by the Ni:TiO_2 Nanocomposites

Chapter 3: Photocatalytic Activity of Co:TiO_2 Nanocomposites and their Application in Photodegradation of Acetic Acid

Chapter 4: The photocatalytic degradation of Methyl Green in presence of Visible light with photoactive $Ni_{0.10}$:$La_{0.05}$:TiO_2 nanocomposites

Chapter 5: Photocatalytic degradation of Rose Bengal and Thymol blue dye under visible light by TiO_2/PAni/GO nanocomposites

Chapter 6: Photocatalytic degradation of Victoria Blue and Rose Bengal dye in visible light by prepared TiO_2/PPy/GO nanocomposite

Chapter 7: Preparation and Photocatalytic activity of Co:La:TiO_2 nanocomposites for the degradation of Methyl Blue in Visible light

Chapter 8: Conclusion and Scope of Further Research Work

The study will broadly follow the scheme as given above. The summary of research work carried out is as follows:

8.1. Introduction and literature review.

In the first chapter, general introduction about the subject, historical background, theories, applications, literature review and objectives of the present study has been presented.

8.2 Photocatalytic degradation of Eriochrome Black-T by the Ni:TiO_2 Nanocomposites

Conventional chemical, biological and adsorption treatments have been applied for the removal of dyes from textile waste water but these processes are insufficient in removing dye contaminants. Photocatalysis is greener approach for the degradation of harmful dye pollutant compounds completely. In the present study TiO_2 and Ni:TiO_2 nanoparticles (NPs) were prepared and their photocatalytic activity was measured against Eriochrome Black T (EBT). The Photo-degradation of Eriochrome Black T was investigated at different condition of concentration and pH in presence of TiO_2 and Ni:TiO_2. The prepared nanoparticles of photocatalyst are characterized by XRD, SEM, EDX, UV-Vis, and BET. The photocatalyst activity was measured by varying pH and concentration of dye solution. Kinetics study was also performed in this investigation.

Table. 1. BET data of TiO_2 and Ni:TiO_2

Sample	Surface area (m^2/g)	Pore volume (cm^3/g)	Pore radius (nm)
TiO_2	2.1522	10.132×10^{-3}	1.21
Ni:TiO_2	46.685	9.5124×10^{-2}	1.64

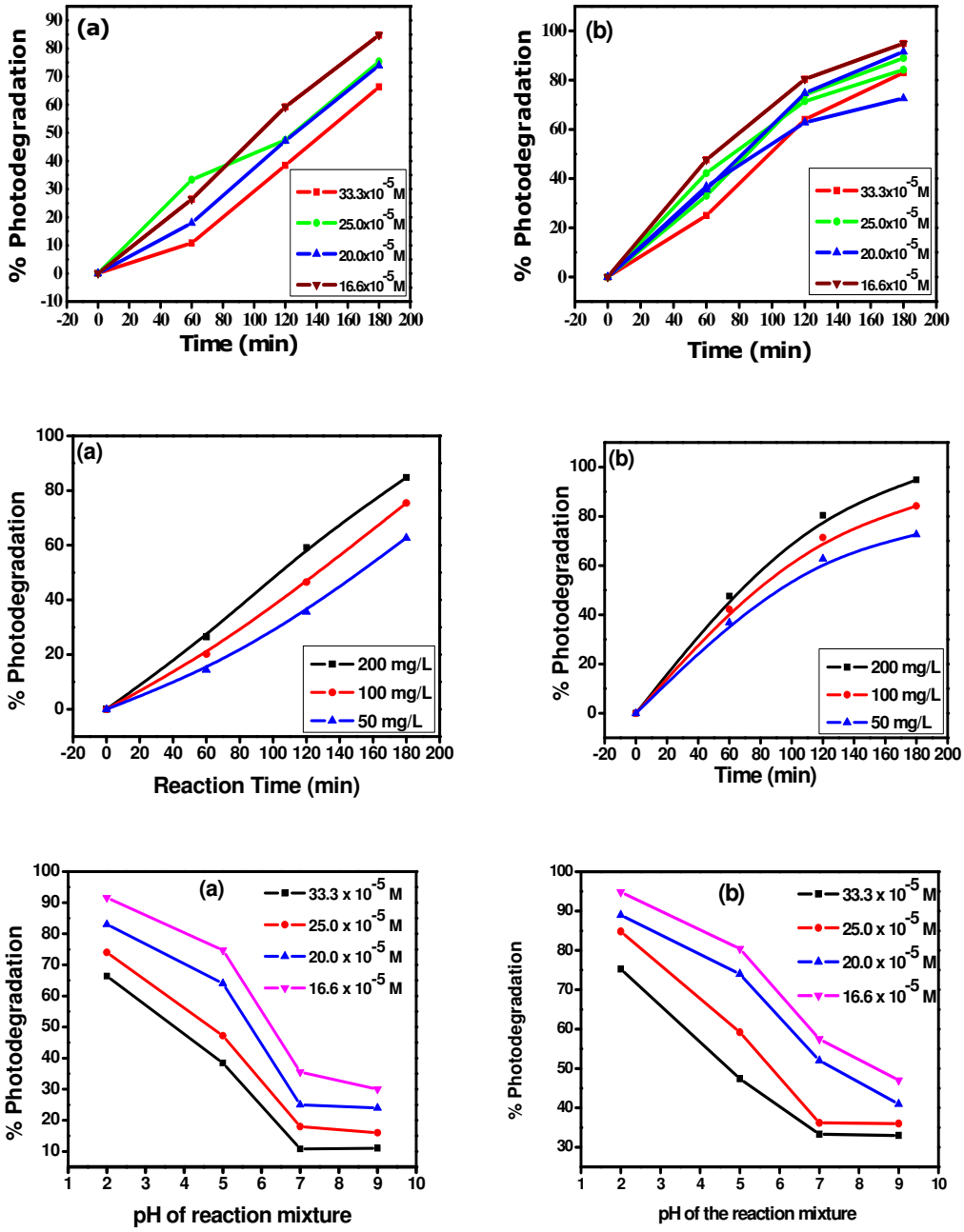

Fig.8.1: Photodegradation of EBT at different parameters such as concentration, time, pH and amount (a) TiO_2 and (b) Ni:TiO_2

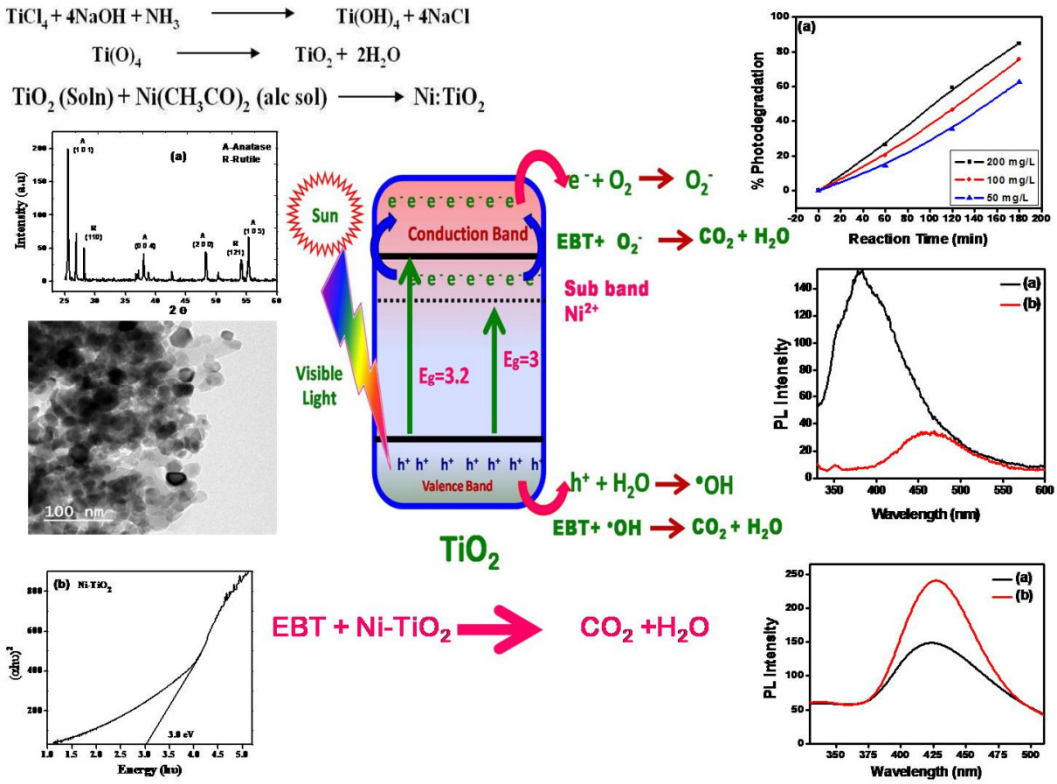

Fig.8.2. Graphical abstract of photodegradation of EBT

8.3. Photocatalytic Activity of Co:TiO_2 Nanocomposites and their Application in Photodegradation of Acetic Acid

The prepared material was subjected to XRD analysis which gives the rutile and Anatase both phases were present in the prepared sample. It is found that in samples sintered at 400 ^{0}C both Anatase and rutile phases were presented and rutile phase was more dominant, while in samples without sintered the exclusive formation of polycrystalline Anatase and rutile phase separately was occurred. Applying the Scherrer's calculations through which particle size was found 35 and 80 nm in case of copper titania and pure titania respectively. The prepared sample of titania and copper titania were subjected to photocatalytic degradation of acetic acid was done. The degradation of acetic acid occurs efficiently. The prominent degradation was found in case of Acetic acid in the presence of nanocomposites Co-TiO_2.

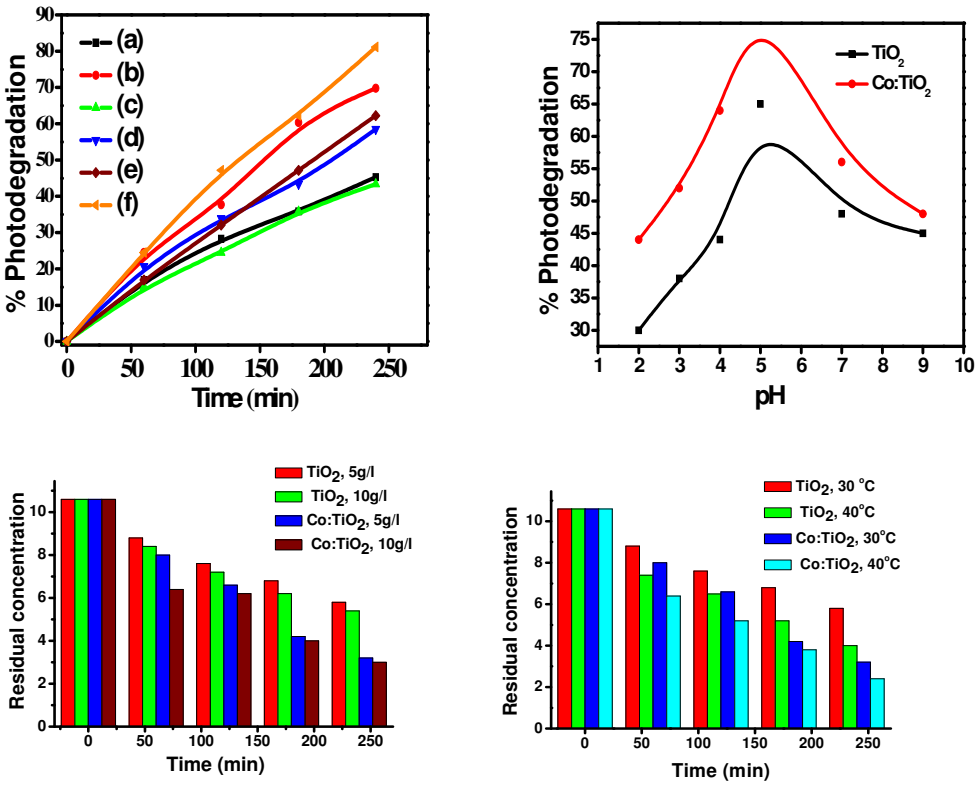

Fig.8.3: Graphical abstract of photodegradation of acetic acid

8.4. The photocatalytic degradation of Methyl Green in presence of Visible light with photoactive $Ni_{0.10}$:$La_{0.05}$:TiO_2 nanocomposites

In this paper, we have done the photodegradation of Methyl green dye in presence of prepared $Ni_{0.10}$:$La_{0.05}$:TiO_2 nanocomposites. The nanocomposites of $Ni_{0.10}$:$La_{0.05}$:TiO_2 was prepared by the solution impregnation method. The characterization of Synthesized TiO_2 and $Ni_{0.10}$:$La_{0.05}$:TiO_2 nanocomposites were done by X-Ray Diffractometer, SEM, TEM, UV- Vis, FT-IR, Band gap energy and BET. The photocatalytic degradation of Methyl Green has been done in presence of TiO_2 and $Ni_{0.10}$:$La_{0.05}$:TiO_2 nanocomposites. The presence of anatase and rutile phase in the nanocomposites has been confirmed by XRD analysis. The photocatalysts particle was found in nanodiamension in morphology. The surface area was observed 34.72 and 96.58 m^2/g for the TiO_2 and $Ni_{0.10}$:$La_{0.05}$:TiO_2 nanocomposites. The band gap energy was observed 3.2 and 3.0 eV for the TiO_2 and $Ni_{0.10}$:$La_{0.05}$:TiO_2 nanocomposites. The photocatalytic degradation behaviour of photocatalysts was investigated by

considering different parameters such as effect of concentration, effect of amount of photocatalyst, effect of pH, effect of temperature, adsorption, and kinetics. The 90-98 % photodegradation of Methyl Green has been found at 7 pH, 25 ppm concentration of dye, 800 mg/L amount of photocatalyst and 50 min illumination of visible light in presence of $Ni_{0.10}$:$La_{0.05}$:TiO_2 while 10-18 % in presence of neat TiO_2. The photodegradation of Methyl Green was following the first order kinetics.

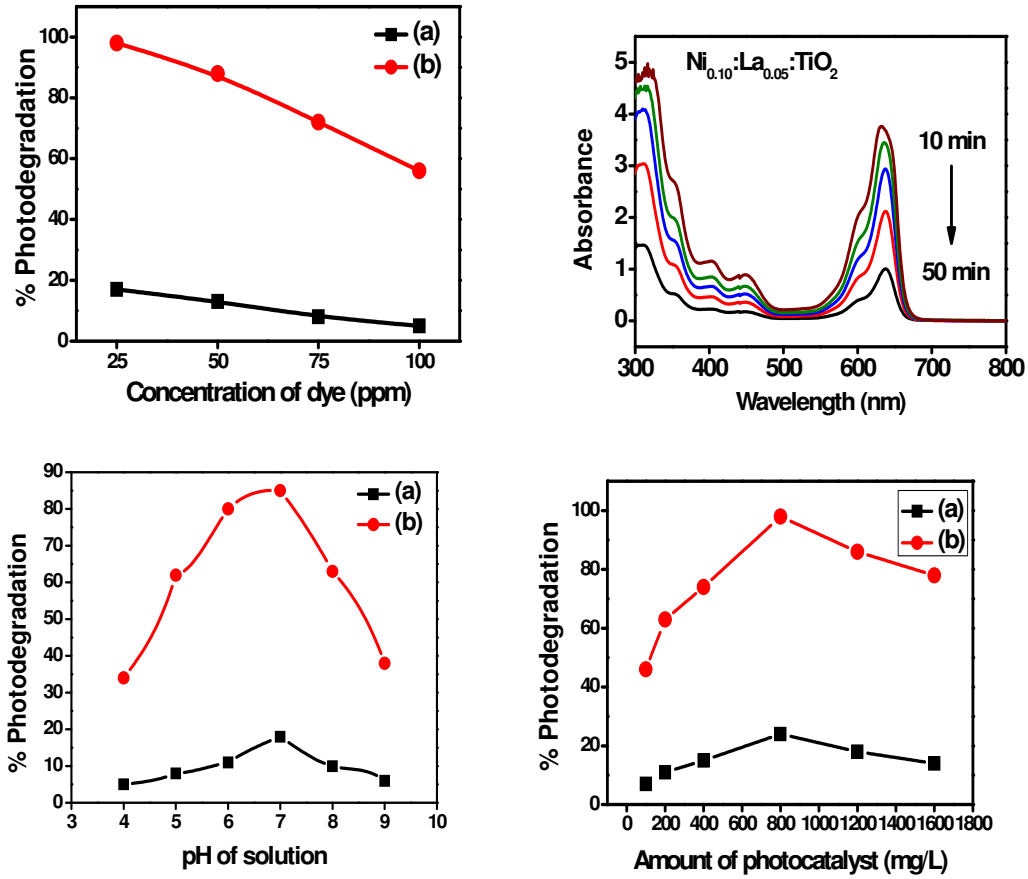

Fig.8.4. Graphical abstract of photodegradation of MG

8.5 Photocatalytic degradation of Rose Bengal and Thymol Blue dye under visible light by TiO_2/PAni/GO nanocomposites

Nanocomposites of TiO_2, TiO_2/PAni, and TiO_2/PAni/GO were prepared by in situ oxidation polymerization method. The prepared TiO_2, TiO_2/PAni, and TiO_2/PAni/GO Nanocomposites were characterized by the XRD, SEM, TEM, BET, UV-Vis, FTIR, Band gap energy and Photolumiscence. The XRD confirmed the presence of Anatase

and rutile phase in the prepared photocatalysts. The average particle size was found 68, 15 and 12 nm for TiO_2, TiO_2/PAni, and TiO_2/PAni/GO respectively. The SEM and TEM images also confirmed the formation of nanocomposites in the range of ~ 100 nm. The surface area 37.52, 76.68 and 96.24 m^2/g were observed for TiO_2, TiO_2/PAni and TiO_2/PAni/GO Nanocomposites respectively. The Band gap energy of TiO_2, TiO_2/PAni, and TiO_2/PAni/GO were calculated by talc plot and obtained 3.0, 2.86 and 1.76 eV respectively. The Photocatalytic degradation of Rose Bengal dye was done at different condition viz concentration of dye, time of illumination, pH, and dose of photocatalyst. The maximum photodegradation were found at neutral pH, 6.25 ppm concentration of dye solution, 800 mg/L amount of photocatalyst and 120 min irradiation of visible light. The Photocatalytic degradation of Thymol blue dye was done at the different conditions viz concentration of dye, time of illumination, pH, and the dose of the photocatalyst. The photodegradation of Thymol blue was found 98-99%, 72-93% and 12-17% presence of TiO_2/PAni/GO, TiO_2/PAni and TiO_2 respectively. Kinetics of photodegradation was investigated for Rose Bengal and Thymol blue dye and found first order kinetics. The coating of PAni and GO were enhanced the photocatalytic activity of Titania. Hence TiO_2/PAni and TiO_2/PAni/GO are the efficient photocatalyst for the degradation of Rose Bengal B dye than pure TiO_2.

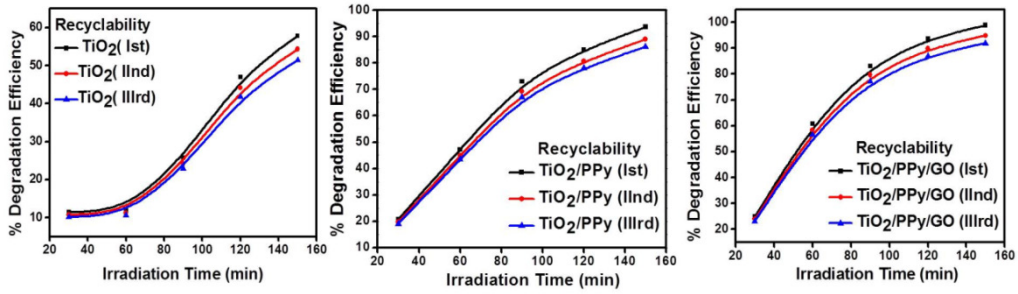

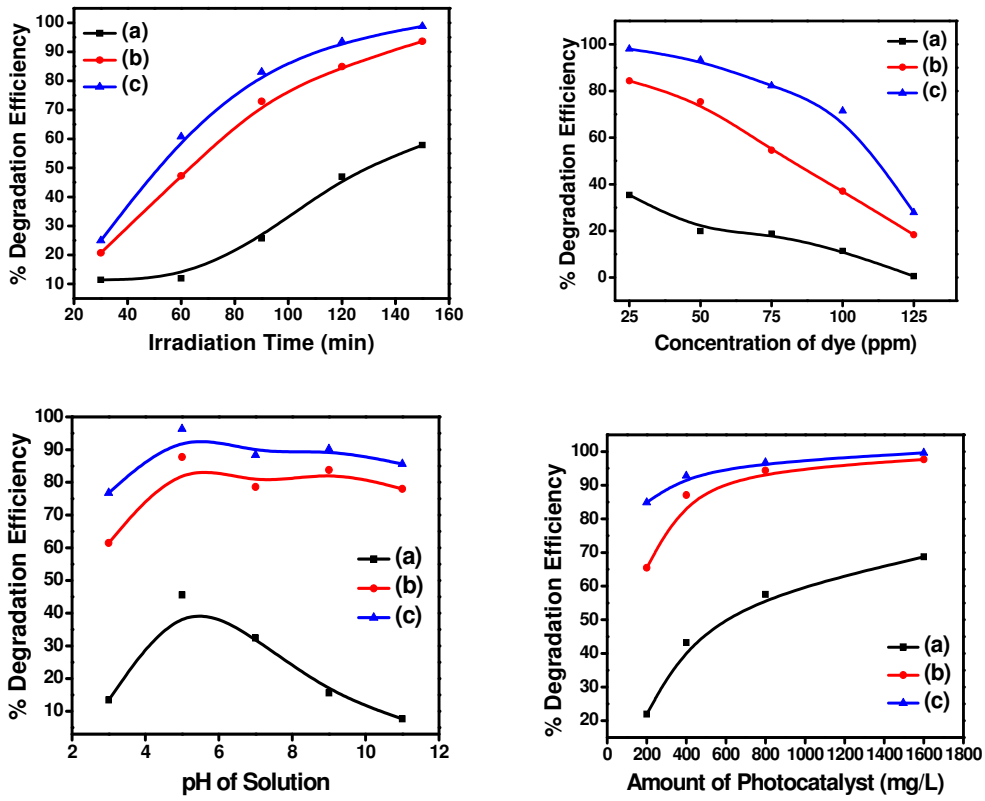

Fig.8.5. Graphical abstract of photodegradation of RB

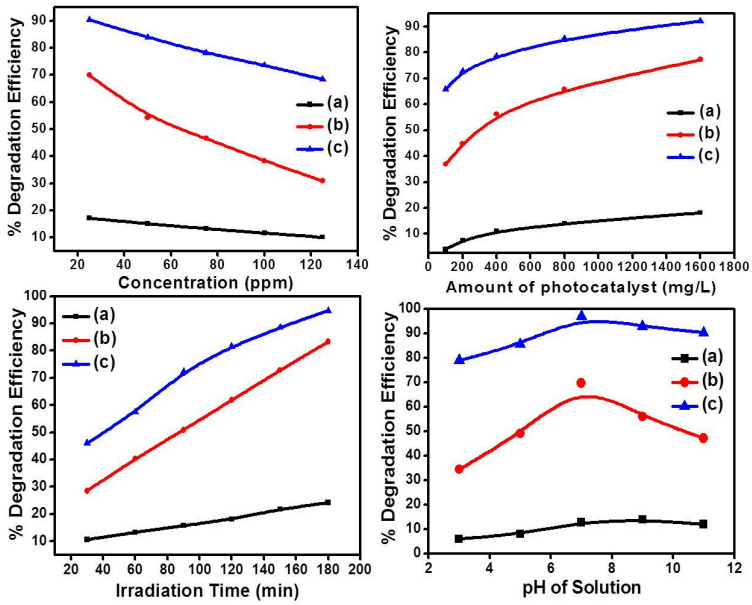

Fig.8.6. Graphical abstract of photodegradation of TB

8.6 Photocatalytic degradation of Victoria Blue and Rose Bengal dye in visible light by prepared TiO_2/PPy/GO through oxidative Polymerization

The present research work describes a proficient method for synthesis of TiO_2/PPy and TiO_2/PPy/GO nanocomposites. These nanocomposites were prepared by one-step *in situ* deposition oxidative polymerization of pyrrole hydrochloride using Ammonium per sulphate (APS) as an oxidant in the presence of ultra fine grade powder of TiO_2 nanoparticles cooled in an ice bath. The obtained nanocomposites were characterized by XRD, TEM, SEM, UV-Vis, FTIR, techniques. The obtained results showed that TiO_2 nanoparticles have been encapsulated by PPy with a strong effect on the morphology of TiO_2/PPy and TiO_2/PPy/GO nanocomposites. The Photocatalytic degradation of Rose Bengal and Victoria blue dye was done at different condition viz concentration of dye, time of illumination, pH and dose of photocatalyst. The maximum photodegradation were found at 7 pH, 20 ppm concentration of Victoria blue and 25 ppm of rose bengal dye solution, 800 mg/L for VB and 1600 mg/L for RB amount of photocatalyst and 120 min irradiation of visible light. Kinetics of photodegradation was investigated for Victoria blue and Rose Bengal dye and found first order kinetics. The coating of PPy and GO were enhanced the photocatalytic activity of Titania. Hence TiO_2/PPy and TiO_2/PPy/GO are the efficient photocatalyst for the degradation of Rose Bengal and Victoria Blue dye than pure TiO_2.

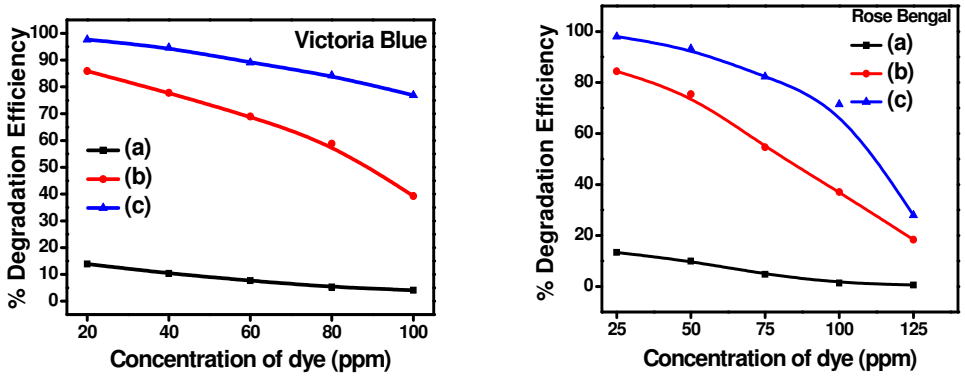

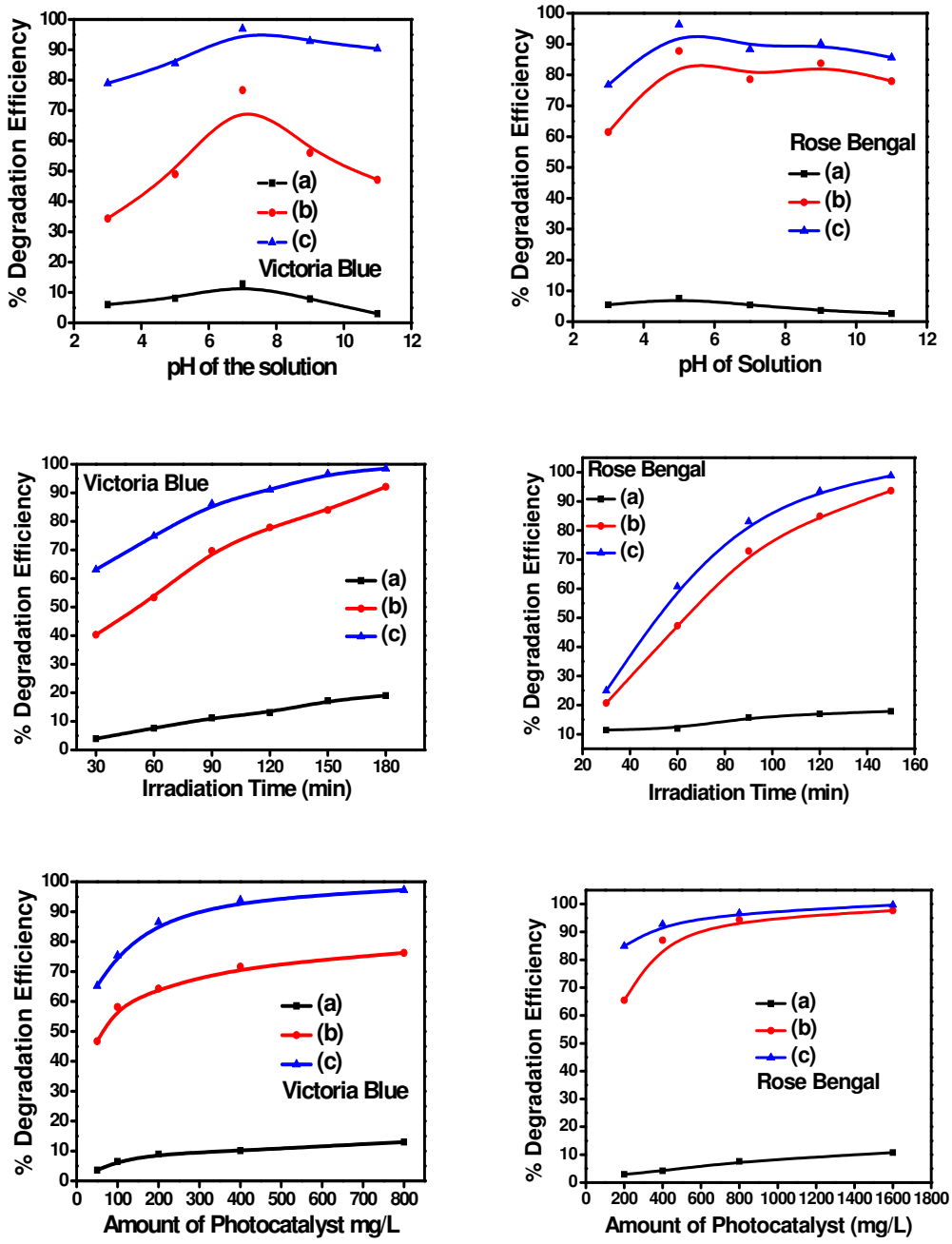

Fig.8.7. Graphical abstract of photodegradation of VB and RB

8.7 Preparation and Photocatalytic activity of Co:La:TiO_2 nanocomposites for the degradation of Methyl Blue in Visible light

In this study, prepared the nanocomposites of Co:La:TiO_2 by the wet chemical method. Synthesized TiO_2 and Co:La:TiO_2 were characterized by X-Ray

Diffractometer, SEM,TEM, UV- vis, FT-IR, Band gap energy and BET. The TiO_2 and Co:La:TiO_2 were used as photocatalyst for the degradation of Methyl Blue. The XRD pattern confirmed the presence of anatase and rutile phase in the catalyst. The particle size was estimated by the Scherrer's and found 68 and 32 nm for TiO_2 and Co:La:TiO_2 respectively. The particle morphology of the photocatalysts was found in nanodiamension. The surface area of the photocatalysts were found 37.52 and 106.68 m^2/g for TiO_2 and Co:La.TiO_2 respectively . The band gap energy of TiO_2 and Co:La.TiO_2 were 3.2 and 3.0 eV. The FT-IR spectra of Co:La:TiO_2 were recorded and found Co bonded with Titania. The photodegradation of Methyl Blue has been found maximum at 5 pH, 25 ppm concentration of dye, 800 mg/L amount of photocatalyst and 180 min illumination of visible light. The photodegradation was following the first order kinetics.

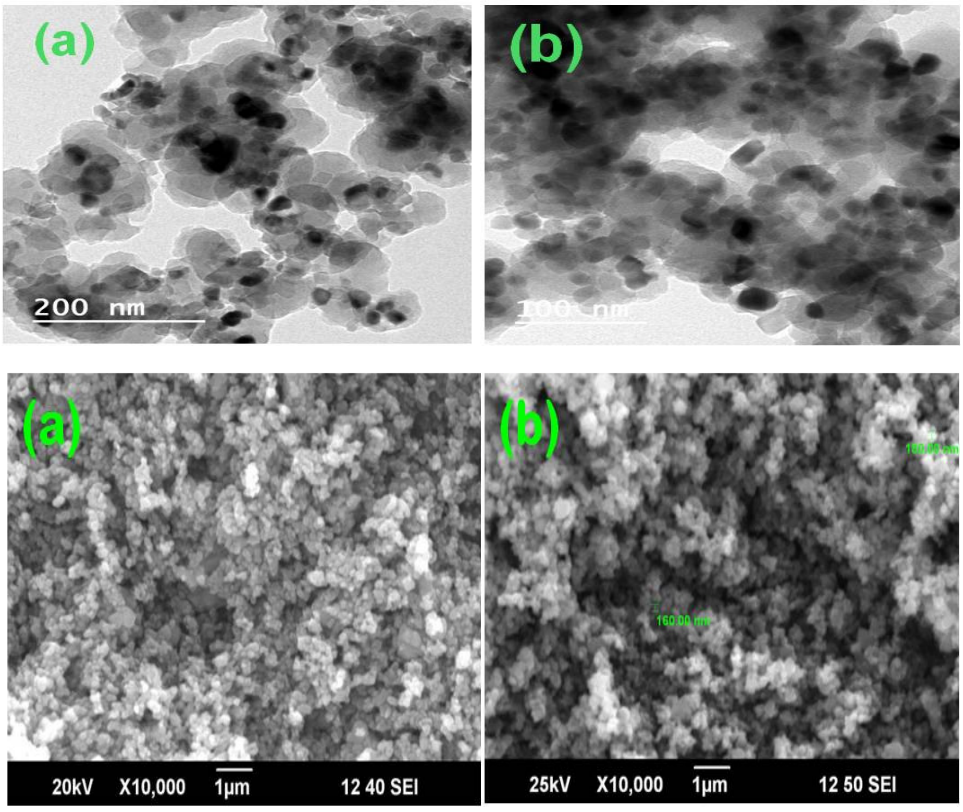

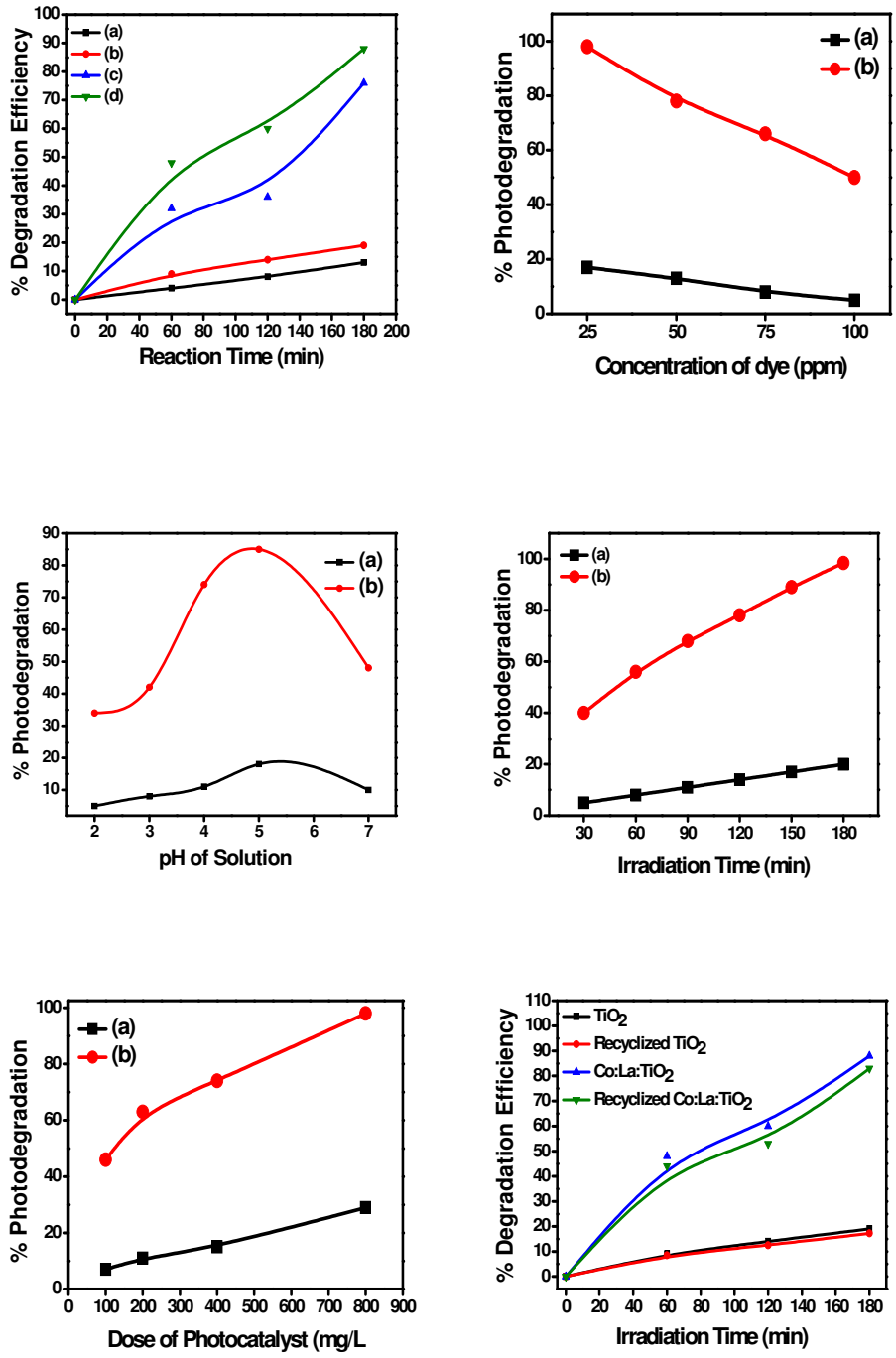

Fig.8.8. Graphical abstract of photodegradation of MB

Future trends

At the present infancy stage of new century future trends for development would include:

- The preparation of photocatalyst material capable of selective photocatalytic degradation of organic pollutants;
- Novel preparation of ternary mixed oxide systems for photooxidative degradation;
- Novel photocatalyst preparations from titanium oxo families since more members of the families became available;
- Preparation of new hybrid nanocomposites of Titania for the photodegradation of organic toxic compound.
- To create the visible light active photocatalyst by the Coating of conducting polymer layer on the surface of Titania.
- Design of more reliable photocatalyst that can be photoactivated by visible and solar light or both.

PUBLICATIONS

[1]. **Azad Kumar**, Gajanan Pandey, Photocatalytic degradation of Eriochrome Black-T by the Ni:TiO_2 nanocomposites, Desalination and Water Treatment, 71 (2017) 406–419.

[2]. **Azad Kumar** and Gajanan Pandey, Photocatalytic Activity of Co:TiO_2 Nanocomposites and their Application in Photodegradation of Acetic Acid, Chemical Science Transaction, 2017, 6(3), 385-392

[3]. **Azad K** and Gajanan P, Photodegradation of Methyl Orange in Aqueous Solution by the Visible Light Active Co:La:TiO_2 Nanocomposite, Chem Sci J 2017, 8:3, DOI: 10.4172/2150-3494.1000164

[4]. **Azad Kumar** and Gajanan Pandey, The photocatalytic degradation of Methyl Green in presence of Visible light with photoactive $Ni_{0.10}$:$La_{0.05}$:TiO_2 nanocomposites, IOSR Journal of Applied Chemistry (IOSR-JAC). 10, 2017, PP 31-44

[5]. **Azad Kumar** and Gajanan Pandey, Comparative Photocatalytic Degradation of Rose Bengal Dye under Visible Light by TiO_2, TiO_2/PAni and TiO_2/PAni/GO Nanocomposites, Int. J. for Research in Applied Science & Engineering Technology (IJRASET), *Volume 6 Issue II, February 2018*

[6]. **Azad Kumar** and Gajanan Pandey, Synthesis, Characterization of Polypyrrole/Titania/GO by Co-Precipitation Method, IJSRSET 4, 1, 693-700

Communicated paper

1) Photocatalytic degradation of Rose Bengal and Thymol Blue dye under visible light by TiO_2/PAni/GO nanocomposites, Fibres and Polymers, Springer
2) Photocatalytic degradation of Victoria Blue and Rose Bengal dye in visible light by prepared TiO_2/PPy/GO nanocomposite, Desalination and water treatment, Taylor and Francis.

Papers in International Conferences

1. 102^{nd} Annual conference 2015 of Indian Science Congress association (ISCA) in Mumbai University Mumbai (Jan 3 to 7).
2. 103^{rd} Annual conference 2016 of Indian Science Congress association (ISCA) in University of Mysore in Mysore, India. (Jan 3 to 7).
3. Kathmandu Symposia on Advanced Materials (KaSAM)-2016, third international conference organized by Nepal Polymer Institute (NPI)**,** October 17-20, 2016.
4. 104^{th} Annual conference 2017 of ISCA in Sri Venkateshwara University, Tirupati (Jan 3 to 7).